

## Dynamical Double Layers

Iizuka, S.; Michelsen, Poul; Rasmussen, Jens Juul; Schrittwieser, R.; Hatakeyama, R.; Saeki, K.; Sato, N.

*Published in:*  
Symposium on Plasma Double Layers

*Publication date:*  
1982

*Document Version*  
Publisher's PDF, also known as Version of record

[Link back to DTU Orbit](#)

*Citation (APA):*  
Iizuka, S., Michelsen, P., Juul Rasmussen, J., Schrittwieser, R., Hatakeyama, R., Saeki, K., & Sato, N. (1982). Dynamical Double Layers. In P. Michelsen, & J. Juul Rasmussen (Eds.), Symposium on Plasma Double Layers (pp. 199-204). Danmarks Tekniske Universitet, Risø Nationallaboratoriet for Bæredygtig Energi. (Denmark. Forskningscenter Risoe. Risoe-R; No. 472).

## DTU Library

Technical Information Center of Denmark

---

### General rights

Copyright and moral rights for the publications made accessible in the public portal are retained by the authors and/or other copyright owners and it is a condition of accessing publications that users recognise and abide by the legal requirements associated with these rights.

- Users may download and print one copy of any publication from the public portal for the purpose of private study or research.
- You may not further distribute the material or use it for any profit-making activity or commercial gain
- You may freely distribute the URL identifying the publication in the public portal

If you believe that this document breaches copyright please contact us providing details, and we will remove access to the work immediately and investigate your claim.

Risø-R-472

RISØ

Risø-R-472 ✓

**Symposium on Plasma Double  
Layers, Risø National Laboratory  
June 16-18, 1982**

**Organized and sponsored by Risø National Laboratory**

**Risø National Laboratory, DK 4000 Roskilde, Denmark  
June 1982**

**SYMPOSIUM ON PLASMA DOUBLE LAYERS**

organized and sponsored by

Risø National Laboratory DK-4000 Roskilde

June 16 - 18, 1982

P. Michelsen, J. Juul Rasmussen, Editors

RISØ-R-472

SYMPOSIUM ON PLASMA DOUBLE LAYERS

organized and sponsored by

Risø National Laboratory DK-4000 Roskilde

June 16 - 18, 1982

P. Michelsen, J. Juul Rasmussen, Editors

Abstract. This report contains papers presented at the "Symposium on Plasma Double Layers". The papers are arranged according to the following subjects: Theory, Laboratory Experiments, Numerical Simulations, and Double Layers in Space.

September 1982

Risø National Laboratory, DK-4000 Roskilde, Denmark

ISBN 87-550-0862-3

ISSN 0106-2840

Risø Repro 1982

## CONTENTS

	Page	
PREFACE .....	11	
 <u>THEORY</u>		
The Theory of Double Layers (Invited).		
Hans Schamel .....	13	
Analytical Double Layers.		
Hans Schamel and Sarbeswar Bujarbarua .....	40	
Formation of Negative Potential Solitary Wave and Double Layer. K. Nishihara, H. Sakagami, T. Taniuti and A. Hasegawa .....		41
Formation of Ion Phase-Space Vortexes.		
H.L. Pécseli, J. Trulsen and R.J. Armstrong .....	47	
Time Evolution of Particle Distributions in a Double Layer. M. Mohan, A.N. Sekar and P.K. Kaw .....		55
Modified Korteweg - de Vries Equation for Propagating Double Layers in Plasmas. S. Torvén .....		59
On the Negative Resistivity of Double Layers.		
M.A. Raadu and M.B. Silevitch .....	60	
Relativistic Effects in Electrostatic Double Layers.		
Michael A. Raadu .....	65	
Theory and Structure of Relativistic Double Layers.		
P. Carlqvist .....	71	
Double Layer Induced Auroral Kilometric Radiation.		
Sarbeswar Bujarbarua and Mitsuhiro Nambu .....	77	

	Page
An Unusual Double Layer Produced by Ponderomotive-Force Effects. J.G. Laframboise .....	78
Electron Diode Dynamics; Limiting Currents; Plasma Diodes. Charles K. Birdsall .....	84
On the Trends in the Non-Linear Development of the Pierce Instability in Laboratory Plasmas. D. Jovanović .....	90
Non-Quasi-Neutral Plasmas of Large Extension. D.K. Callebaut .....	96
A Topological Theory for Solving Plasma Sheath Problems .. and other Problems. Jean-Pierre J. Lafon	107
On the Population of Closed Orbits in Open and Closed Collisionless Gases of Charged Particles Application to Plasma Sheath Problems. Jean-Pierre J. Lafon .....	113
 <u>LABORATORY EXPERIMENTS</u>	
Double Layers in Laboratory Plasmas (Invited). Noriyoshi Sato .....	116
Strong Stationary Space Charge Double Layers in a Magnetic Mirror. R. Schrittwieser, R. Hatakeyama, T. Kanazawa and N. Sato .....	141
Three Dimensional Double Layers in Magnetized Plasmas. D. Jovanović, J.P. Lynov, P. Michelsen, H.L. Pécseli, J. Juul Rasmussen and K. Thomsen .....	147

	Page
Potential Double Layers Formed by Ion Beam Injection Into a Cusped Magnetic Field. Y. Nakamura and R.L. Stenzel .....	153
Double Sheaths Formed by Ion-Beam Reflection in Front of a Langmuir Probe in a Unmagnetized Plasma. A. Skøelv, R.J. Armstrong and J. Trulsen .....	159
Experimental Studies of Electron Scattering Due to Beam-Plasma Interaction near a Double Layer. L. Lindberg .....	164
Electron Temperature Differences Across Double Layers. Chung Chan, Noah Hershkowitz and Karl E. Lonngren .....	170
Double Layer Formation During Current Sheet Disruptions in a Magnetic Reconnection Experiment. R.L. Stenzel, W. Gekelman and N. Wild .....	181
Experiments on Turbulent Potential Jumps in a Long Current-Carrying Plasma. Ch. Hollenstein .....	187
A Potential Double Layer Formed by a Shock Wave in a Plasma, S. Yagura, H. Fujita and E. Yamada .....	193
Dynamical Double Layers. S. Iizuka, P. Michelsen, J. Juul Rasmussen, R. Schrittwieser, R. Hatakayama, K. Saeki and N. Sato .....	199
On the Relation Between Ion Oscillations and Travelling Double Layers in a Positively Biased Single-Ended Q-Machine. G. Popa, M. Sanduloviciu and E. Mravlag .....	205

	Page
Fine Structures of of Potential Formation in a Bounded Plasma with Current. H. Fujita, S. Yagura, E. Yamada, Y. Kawai and N. Sato .....	209
Low-Frequency Oscillations Associated with the Double-Layer in a D.P.-Machine Plasma. G. Popa .....	213
Potential Formation between Two Kinds of Plasmas. R. Hatakeyama, Y. Suzuki and N. Sato .....	219
Observations of Large Amplitude Solitary Pulses in the Current-Limiting Phase of High-Voltage Straight Discharge. Y. Takeda and K. Yamagiwa .....	225
Anodic Instabilities and its Connection with Double Layers. M. Sanduloviciu .....	231
On the Connection between Double Layers and some Periodical Phenomena in the Positive Column of a Glow Discharge in H <sub>2</sub> +N <sub>2</sub> Mixture. D. Alexandroaie and M. Sanduloviciu .....	237
Role of the Double Layers in the Appearance of Self-Sustained Oscillations in a Electric Circuit Including a Magnetized Plasma. S. Talasman and M. Sanduloviciu .....	243
 <u>NUMERICAL SIMULTATIONS</u>	
The Simultation of Plasma Double-Layer Structures. Joseph E. Borovsky and Glenn Joyce .....	249

	Page
<u>DOUBLE LAYERS IN SPACE</u>	
Double Layers in Space (Invited).	
P. Carlqvist .....	255
Formation of Double Layers on Auroral Field Lines.	
R. Lysak, W. Lotko, M. Hudson and E. Witt .....	274
Space Observations Relevant to Laboratory Double Layers, Shocks and Solitons - The Plasmopause and High Latitude Holes. H. Kikuchi .....	279
SUMMARY. L.P. Block .....	280
AUTHOR INDEX .....	282
LIST OF PARTICIPANTS .....	283



PREFACE

This report contains the invited and contributed papers submitted to the Symposium on Plasma Double Layers held at Risø National Laboratory, Roskilde, Denmark on June 16-18, 1982.

The individual papers were limited in length, and to facilitate reproduction and speed up publication the papers were reproduced directly from the authors' manuscripts without editing. The authors' cooperation in conforming to the guide-lines for preparing manuscripts is greatly appreciated.

The Symposium was arranged following a suggestion from Prof. N. Sato, Tohoku University, Sendai, Japan and took place just after the International Conference on Plasma Physics in Gothenburg, Sweden. The aim of the Symposium was to bring together physicists working with problems in connection with double layer and sheath formation in various branches of plasma physics. The interest in double layers and related phenomena has been increasing in recent years since such structures have been found important in a broad range of plasmas from cosmic to fusion.

More than 50 participants from 16 countries took part in the Symposium. Three invited papers covering double layer theory, double layers in the laboratory and in space were presented along with 14 oral contributions and 15 posters. The programme ended with a discussion on the status of double layer research, chaired by Prof. L.P. Block. A summary of this discussion is enclosed in the proceedings. The contributions are divided into the following topics:

1. Theory
2. Laboratory Experiments
3. Numerical Simulations
4. Double Layers in Space

We are grateful to our colleagues in the organizing committee for their help and suggestions of topics and invited speakers. This committee consisted of: S.-I. Akasofu, P. Michelsen, H.L. Pécseli, J. Juul Rasmussen, N. Sato, R.L. Stenzel, and S. Torvén.

Finally, we greatly appreciate the support offered by Risø National Laboratory in making this Symposium possible.

Risø, September 1982.

The Editors.

The Theory of Double Layers \*

Hans Schamel

Institute for Theoretical Physics, Ruhr-Universität Bochum,  
4630 Bochum 1, FRG.

Abstract

Numerical and in some degree laboratory experiments suggest the existence of <sup>at least</sup> two different kinds of time-independent double layers: a strictly monotonic transition of the electrostatic potential, and a transition accompanied by a negative spike at the low potential side (ion acoustic DL). An interpretation of both is presented in terms of analytic BGK modes. The first class of DLs commonly observed in voltage- or beam-driven plasmas needs for its existence beam-type distributions satisfying a Bohm criterion. The potential drop is at least of the order of  $T_e$ , and stability arguments favourize currents which satisfy the Langmuir condition. The second class found in current-driven plasma simulations is correlated with ion holes. This latter kind of nonlinear wave-solutions is linearly based on the slow ion-acoustic mode and exists due to a vortex-like distortion of the ion distribution in the thermal range. During the growth of an ion hole which is triggered by ion-acoustic fluctuations, the partial reflection of streaming electrons causes different plasma states on both sides of the potential dip and makes the ion hole asymmetric giving rise to an effective potential drop. This implies that the amplitude of this second type of double layers has an upper limit of  $1-2 T_e$  and presumes a temperature ratio of  $T_e/T_i \gtrsim 3$  in coincidence with the numerical results.

\* Invited lecture, Symposium on Plasma Double Layers, Roskilde, Denmark, 1982.

## I. Introduction

Electrical double layers (DLs) have been known to appear in a variety of situations in which there are large electric fields or currents. Representing a highly nonlinear state they are of basic interest in general plasma physics as well as in space physics. They are suggested to be the mechanisms for particle acceleration in laboratory and auroral discharges, and are often found in connection with anomalous resistivity.

Historically DLs belong to those phenomena which have been studied actively since the first days of plasma physics (gas discharges). They have been created long time ago in low-current dc discharges<sup>1-3</sup> and have been generated by means of high-current electron beams<sup>4,5</sup>. However, spurious effects such as ionization, particle losses, finite boundaries, etc., not primarily related with DLs, have masked the physics and the understanding of DLs. This has changed considerably in the recent years due to an improvement of diagnostics, of apparatus, of the generation of collision-free plasmas, of radial losses due to stronger magnetic fields, etc. The rapid progress made in this field is expressed in the large number of recent publications and will be reported upon in a separate lecture in this symposium.

A similar development can also be observed in the numerical and analytical treatment of DLs.

Particle simulations dealing with DL formation came up in the late seventies only and since then experience a great deal of attraction in the plasma community. Also this subject will be reported separately. (Later on, we will come back to simulation and laboratory results.)

Analytically, it has been clear for a long time that the stationary, one-dimensional and collision-free nature of DLs suggests a description in terms of appropriate solutions of the Vlasov-Poisson system. It was mainly the use of the wrong method (wrong in the practical sense, not in a strict mathematical one) which rendered a description difficult earlier. One of the intentions of this paper will be to show how an analytical improvement can and could be achieved.

And, last not least, there are now satellite data available which favourize DLs as the mechanism of auroral particle acceleration (see also the review lecture on this subject).

The interaction and mutual stimulation between all four

subprograms has led meanwhile to a considerable degree of understanding of DLs. One is now going to understand under what circumstances DLs are getting formed, what are the basic ingredients of DLs, why are there limits in the potential drop and in other parameters. Details of the stability behaviour are coming up and can be interpreted at least qualitatively; and there are more.

I think it is not an exaggeration if one states that the field of DLs is in a rapidly growing phase, the summit not being in sight.

The aim of this paper will be to report and concentrate on recent theoretical developments rather than to review the theoretical literature. The latter would be an enormous task and I prophylactically apologize to those whose work is not mentioned or adequately represented, and accept that the list of references is rather incomplete.

Section II deals with the definition, the general description and classification of DLs. In Section III the monotonic transition (type-I-DL) is investigated, including comparisons with experiments. The ion acoustic DL (type-II-DL) is considered in Section IV in which an interpretation is offered in terms of an asymmetric ion hole. A scenario of DL formation is presented in Section V in close connection with particle simulations. Conclusions and a summary terminate the paper.

## II. Definition, general description and classification of DLs

### a) The definition

A DL is defined in this paper and commonly understood as a stationary, one-dimensional, collisionless, electrostatic potential structure,

- i) which connects two different, asymptotic uniform plasma potentials, i.e.  $\psi > 0$  where  $\psi \equiv |\phi(x \rightarrow +\infty) - \phi(x \rightarrow -\infty)|$  is the potential drop measured in  $T_e$  units,
- ii) which is due to charge separation, i.e. the spatial extent of the transition layer is measurable in units of the electron Debye lengths  $\lambda_{De}$ ,
- iii) in which the electrostatic energy and particle kinetic energies associated with the coherent structure dominate

over the corresponding energies of fluctuations which are superimposed on the DL.

There is no distinction made at this stage between weak ( $\psi \lesssim 1$ ) and strong ( $\psi \gg 1$ ) DLs which, however, will come out automatically. There may be or may not be an associated electrical current. As we will see, this definition leaves room for <sup>at least</sup> two topologically different classes of DLs. Both are found in reality. Since an electrical double layer is the simplest space-charge distribution giving rise to DLs (Type-I-DL, see later), potential variations of this kind have been called double layers.

From the existence of a stationary potential drop we immediately can deduce the necessity of trapped (reflected) particles. For, free streaming ions entering on the high potential side are accelerated downward whereas free streaming electrons entering on the low potential side are accelerated upward. From the conservation of particle fluxes it follows that the density of this beam ion component decreases and that of the electron beam component increases downward. Thus, starting with equal densities at some intermediate point (the turning point of  $\phi(x)$ ) these densities differ increasingly if one deviates in both directions. To bring the density difference back to zero which is required to get a quasi-neutral state at infinity, there, consequently, must be a trapped ion species at the low potential side and a trapped electron species at the high potential side.

For this reason, DLs are basically a kinetic phenomenon and ask for a Vlasov description. (Simplified descriptions based on fluid theories have been presented elsewhere <sup>6,7</sup>.)

#### b) The general description

To prepare the more detailed constructions of DL solutions which will be presented in the next two sections we first describe the general method of finding solutions with a potential  $\phi(x)$  that varies monotonously between  $\phi_{\min} \leq \phi(x) \leq \phi_{\max}$ , where  $\phi_{\min}$  and  $\phi_{\max}$  are extrema of  $\phi(x)$ . The solution will be valid in  $x_{\min} \leq x \leq x_{\max}$ , where  $x_{\min}$  and  $x_{\max}$  are the extremal points. The method used has been described elsewhere <sup>8,9</sup>. It consists of prescribing the distribution functions and of looking for the special form of  $\phi(x)$ . As pointed out in detail earlier <sup>8,9</sup>, this method has the advantage of providing smooth distributions which cannot be guaranteed by the Bernstein-Greene-Kruskal-me-

We, therefore, look for stationary solutions of the Vlasov-Poisson-system consisting of the electron and ion Vlasov-equation, self-consistently coupled with Poisson's equation. The electron velocity, ion velocity, spatial coordinate, and electric potential are normalized by electron thermal velocity  $v_{the} = (T_e/m_e)^{1/2}$ , ion thermal velocity  $v_{thi} = (T_i/m_i)^{1/2}$ , electron Debye length  $\lambda_{De} = (T_e/4\pi n_0 e^2)^{1/2}$ , and  $T_e e^{-1}$ , where  $T_e (T_i)$  is the thermal energy of untrapped electrons (ions) at the position where trapped electrons (ions) are absent. The Vlasov equations then become in the frame where the potential is at rest

$$\begin{aligned} (v\partial_x + \phi'(x)\partial_v)f_e &= 0, \\ (u\partial_x - \Theta\phi'(x)\partial_u)f_i &= 0, \end{aligned}$$

where  $\Theta = T_e/T_i$ . For convenience, the electron velocity is denoted by  $v$ , the ion velocity by  $u$ . The solution of both equations can be expressed in terms of the constants of motion which are the energy of particles and the sign of the velocity of untrapped particles. Correspondingly, we can distinguish four different distributions

$$\begin{aligned} f_{ef}(v^2/2 - \phi, v_0) & \quad f_{if}(u^2/2 + \Theta\phi, u_0, A), \\ f_{et}(v^2/2 - \phi, \beta) & \quad f_{it}(u^2/2 + \Theta\phi, \alpha, A). \end{aligned}$$

The distinction in free and trapped particles is given by

$$E_e \equiv v^2/2 - \phi \begin{matrix} \geq \\ \leq \end{matrix} - \phi_{\min} \quad E_i \equiv u^2/2 + \Theta\phi \begin{matrix} \geq \\ \leq \end{matrix} \Theta\phi_{\max},$$

where  $E_j (j = e, i)$  are the normalized single particle energies. The upper sign refers to free particles, the lower sign to trapped particles; the energy of the latter being too small to allow a free passage so that at a certain position that depends on the energy the particle velocity becomes zero, and the particle will be reflected (trapped particle). The parameters  $v_0$  and  $u_0$  in the free distribution functions represent a mean drift necessary to describe currents.  $\alpha$  and  $\beta$  are trapped particle parameters which can be varied to describe different situations of trapped particle configurations.  $A$  is a normalization constant and can either be introduced in the ion distribution or in the electron distribution. The separatrix representing the border in phase space between free and trapped particles is given by the equality sign.

The choice of the special form of the distributions suggest-

ed by laboratory and numerical experiments is fixed by the following prescription

1.  $f_{jf}$  ( $j = e, i$ ) is a shifted Maxwellian at the position where the trapped particles are absent, i.e. at  $\phi = \phi_{\min}$  ( $\phi = \phi_{\max}$ ) in the case of electrons (ions).
2.  $f_{jt}$  ( $j = e, i$ ) are symmetric, unshifted Maxwellians in which the "temperatures" are allowed to differ from the free particle temperatures:  $T_{et} = \beta^{-1}T_e$  and  $T_{it} = \alpha^{-1}T_i$ . Also negative temperatures are admitted ( $\alpha < 0, \beta < 0$ ).
3. The distributions are continuous in the entire velocity space.

With this specification which will be commented later on, the densities obtained by a velocity integration will acquire specific forms, the details of which are relegated to Sections III and IV:

$$n_e = n_e(\phi, v_0, \beta) \quad n_i = n_i(\phi, \theta, u_0, \alpha, A).$$

What remains to be solved is then Poisson's equation

$$\phi''(x) = n_e - n_i \equiv -\frac{\partial}{\partial \phi} V(\phi, \dots),$$

where the rhs is now a known function of  $\phi$ . In the latter we have introduced the classical potential  $V$  to point out the analogy with the equation of motion of a classical particle  $\left[ \ddot{x} = -\frac{\partial}{\partial x} V(x) \right]$ .  $V$  is obtained by integrating the densities with respect to  $\phi$

$$V = \int_{\phi_{\min}}^{\phi} d\phi' \left[ n_i(\phi' \dots) - n_e(\phi') \right], \text{ where we assumed that}$$

$V(\phi_{\min}, \dots)$  is zero

$$\left[ \text{or by the equivalent form } V = - \int_{\phi}^{\phi_{\max}} d\phi' [\dots] \text{ with } V(\phi_{\max}, \dots) = 0 \right]$$

and will depend on all the parameters introduced above.

There is a one-to-one correspondence between the shape of the potential  $\phi(x)$  and that of the classical potential  $V(\phi)$  which are related through the "energy law" obtained by integrating Poisson's equation

$$\frac{\phi'(x)^2}{2} + V(\phi, \dots) = 0.$$

It's important to note that charge neutrality at a certain point means that  $\frac{\partial V}{\partial \phi}$  vanishes at the corresponding value of the potential  $\phi$ .

The existence of a solution finally demands that  $V(\phi, \dots)$  vanishes at the second extremum of  $\phi$ , i.e.

$$V(\phi_{\max}, \dots) = 0$$

[ or if the equivalent form was chosen:

$$V(\phi_{\min}, \dots) = 0 ] .$$

This is a non-trivial relation and <sup>15</sup> called nonlinear dispersion relation because it introduces a relation between the drift velocity  $u_0$  which is minus the wave velocity in the ion frame and the wave amplitude.

A uniquely defined solution of the Vlasov-Poisson system is then obtained if it turns out that  $V(\phi)$  is negative in the interval  $\phi_{\min} < \phi < \phi_{\max}$ . With this we are now in a position to consider the following two classes of DL solutions.

### c) The classification

The first class of DLs consists of a strictly monoton transition shown in Fig. 1a together with the corresponding  $V$ . Without loss of generality we take  $\phi_{\min} = 0$ ,  $\phi_{\max} = \psi$ ,  $x_{\min} = -\infty$ ,  $x_{\max} = +\infty$ . The corresponding phase space plots are drawn qualitatively in Fig. 1b, c, where the occupation of the particle trajectories is indicated by the line thickness and increases with it. This kind of DL is found in beam- and voltage driven plasmas. Numerical <sup>13-17</sup> and laboratory <sup>5,18-30</sup> experiments reveal the following characteristic properties:

- I1) The potential structure is correlated with four beam-type distributions. <sup>12,13,16,19-21,31-33</sup>
- I2) The velocities of the drifting species at the entrance, i.e.  $V_{De} = +v_0$ ,  $V_{Di} = -u_0$ , satisfy a Bohm criterion <sup>6,34-36</sup> which for  $\theta = 1$  becomes  $|v_{Dj}| \geq 1$ .
- I3) The Langmuir <sup>6</sup> "condition"  $j_e/j_i = (m_i/m_e)^{1/2}$ , which expresses the ratio of currents, provides the most stable DL <sup>15</sup>. It must, however, not necessarily be satisfied. <sup>24</sup>
- I4) The experimental range of the potential drop is presently given by  $1 \lesssim \psi \lesssim 2000$ . <sup>29</sup> (There seems to be a lower limit of order unity but no natural upper limit.)
- I5) The DL width  $\Delta$  first decreases and then increases with increasing values of  $\psi$  <sup>20,23</sup>. For larger  $\psi$  it scales like  $\Delta \approx 6 \psi^{1/2}$ . <sup>12,13</sup>  $(10 \lesssim \psi \lesssim 100)$
- I6) The temperature ratio  $\theta$  is not a decisive parameter and can deviate from unity in both directions.
- I7) There is usually a hf-turbulence at the high-, and a <sup>27,28</sup> lf-turbulence at the low-potential side associated with. <sup>16,19,25,</sup>

We will see how these features can be understood from an analytical point of view. We will refer to this kind of DL synonymously as Type-I-DL, voltage-driven DL, monotonic transition, strong double layer, or simply double layer.

The second class of DLs found predominantly in current-driven plasmas has in addition a hole at the low-potential side, as illustrated in Fig. 2a. The classical potential  $V$  now consists of two parts, corresponding to two monotonic regions of the potential structure. Consequently, the phase space plots, Fig. 2b, c, show a more complicated pattern. There are, e.g., two separatrices in the ion phase space, one separatrix representing ion trapping in the hole, whereas the other one refers to the reflection of ions at the potential jump, which occurs only once for each ion. Numerical experiments<sup>17,37-41</sup> yield the following results for this second type of double layers:

- II1) There are free and trapped particle distributions involved which are, however, not separated. The ion distribution is strongly skewed with a hole in the trapped region (vortex-distribution).
- II2) The drift velocities can be arbitrary small and do usually not exceed unity.
- II3) The potential drop is weak:  $0 \leq \psi \lesssim 1$ , and covers the range which was excluded for the first type of DL.
- II4) The temperature ratio has to satisfy:  $\Theta \gtrsim 3$ , i.e., it must be such as to support ion acoustic waves.
- II5) The initial drift velocity necessary for a spontaneous DL formation must exceed 0.6.<sup>17</sup>
- II6) The width of the hole is about 10-, the width of the transition is about 50 Debye-length.
- II7) The anomalous resistivity vanishes after the establishment of the DL ("superconducting plasma state"<sup>40</sup>).

Synonyms that can be used for this type-II-DL are: ion acoustic DL, asymmetric ion hole, weak double layer or, more precisely, triple layer, because there are three charged layers involved. Also these characteristic properties can be understood more or less analytically, as we will see.

We now turn to a more detailed discussion of these DLs. First we treat the monotonic transition.

### III. The Monotonic Transition (Type-I-DL)

The distribution functions introduced in Sect. II are spe-

cified in this case by the following set<sup>8,42</sup>

$$f_{ef} = C \exp\left\{-\frac{1}{2}\left[\operatorname{sgn} v(v^2-2\phi)^{1/2}-v_0\right]^2\right\} \quad E_e > 0, \quad (1a)$$

$$f_{et} = C \exp(-v_0^2/2) \exp\left[-\frac{\beta}{2}(v^2-2\phi)\right] \quad E_e \leq 0, \quad (1b)$$

$$f_{if} = AC \exp(u_0^2/2) \exp\left\{-\frac{1}{2}\left[\operatorname{sgn} u(u^2-2\theta(\psi-\phi))^{1/2}+u_0\right]^2\right\} \quad E_i > \theta\psi, \quad (1c)$$

$$f_{it} = AC \exp\left\{-\frac{\alpha}{2}\left[u^2-2\theta(\psi-\phi)\right]\right\} \quad E_i \leq \theta\psi, \quad (1d)$$

where  $E_{e,i}$  are the particle energies defined in Sect. II. Without loss of generality, we will assume that  $\alpha$  and  $\beta$  are positive; the normalization constant  $C$  is given by  $C = (2\pi)^{-1/2}$ . The separatrix in the ion phase space (Fig. 1b) is given by  $E_i = \theta\psi$  or by  $u_s(x) = \pm\sqrt{2\theta(\psi-\phi)}$ , and that in the electron phase space (Fig. 1c) by  $E_e = 0$  or by  $v_s(x) = \pm\sqrt{2\phi}$ ; at  $\phi = \psi$   $f_i$  reduces to a Maxwellian, shifted by  $-u_0$ , and at  $\phi = 0$   $f_e$  is a Maxwellian shifted by  $+v_0$ . Free ions are entering from the right, free electrons from the left. Both distributions are continuous.

The corresponding densities become<sup>8</sup>

$$n_e(\phi) = \exp(-v_0^2/2) \left[ F(v_0^2/2, \phi) + T_+(\beta, \phi) \right], \quad (2a)$$

$$n_i(\phi) = A \left[ F(u_0^2/2, \theta(\psi-\phi)) + T_+(\alpha, \theta(\psi-\phi)) \right]. \quad (2b)$$

In (2)  $F(x, y)$  refers to the free particle contribution and is given by

$$F(x, y) = \exp(y) \operatorname{erfc}(y^{1/2}) + K(x, y), \quad (3)$$

where  $K(x, y)$ , which stands for the drift, is given by

$$K(x, y) = 2\pi^{-1/2} \int_0^{\pi/2} d\varphi x^{1/2} \cos\varphi \exp(-y \tan^2\varphi + x \cos^2\varphi) \operatorname{erf}(x^{1/2} \cos\varphi). \quad (4)$$

Its derivation was first given in Ref.[43] and can be found, e.g., in Ref.[44]. It holds,  $K(x, 0) = \exp(x) - 1$ , and  $K(0, y) = 0$ . The latter equation shows that  $K$  vanishes with the drift. Note, that the sign of the drift velocities does not enter so that distributions, which are symmetrized in  $v$  or  $u$  respectively, corresponding to a current-free situation, would lead to the same density expressions. The results are, therefore, compatible with any particle flux.

The contribution of the trapped particles is denoted by  $T_+(x, y)$  which is defined by

$$T_+(x, y) = x^{-1/2} \exp(xy) \operatorname{erf}(\sqrt{xy}) \quad (5)$$

The subscript  $+$  shall indicate that the trapping parameter  $x$  was chosen to be positive.

Integrating the densities with respect to  $\phi$  gives the clas-

sical potential  $V$  which becomes

$$V(\phi) = A\theta^{-1} \left[ P_+(\theta\psi, \alpha) - P_+(\theta(\psi-\phi), \alpha) + H(u_0^2/2, \theta(\psi-\phi), \theta\psi) \right] \\ - \exp(-v_0^2/2) \left[ P_+(\phi, \beta) - 1 + H(v_0^2/2, 0, \phi) \right], \quad (6)$$

where the integration constant was chosen such that  $V(0) = 0$ , and the new functions are defined by

$$P_+(x, y) = \exp(x) \operatorname{erfc}(x^{1/2}) + 2(x/\pi)^{1/2} (1 - y^{-1}) + y^{-1} T_+(x, y) \quad (7a)$$

$$H(x, a, b) = \int_a^b K(x, y) dy. \quad (7b)$$

In order to get a monotonic transition we must, in addition, demand quasi-neutrality at  $\phi = 0$ , and  $\phi = \psi$ , i.e.  $n_e(0) = n_i(0)$ , and  $n_e(\psi) = n_i(\psi)$ , and thirdly,  $V$  has to satisfy  $V(\psi) = 0$  (non-linear dispersion relation). These are three conditions which together with  $V(\phi) < 0$  for  $0 < \phi < \psi$  restrict the admissible parameter space.

The electron current turns out to be  $j_e = -v_0$ , and the ion current  $j_i = -\sqrt{\frac{m_e}{m_i \theta}} A u_0 \exp(u_0^2/2)$ . Denoting the ratio of both by  $j_e/j_i = (\frac{m_i}{m_e})^{1/2} f$ , we can introduce the new parameter  $f$  instead of one of the drift velocities,  $v_0$  or  $u_0$ , respectively. If  $f$  is set equal to unity, then we say that the Langmuir condition<sup>6</sup> is satisfied.

A variety of solutions was found<sup>4,2</sup> by solving these constraints. First of all, it turned out that no matter how  $f$  was chosen the drift velocities always had to exceed a lower boundary in order to keep  $V$  negative:  $v_0 \geq v_{0c}$ , and  $u_0 \geq u_{0c}$ . These lower bounds depend on  $\psi$  and are found to be always larger than unity, for  $\theta = 1$ . This proves that a Bohm criterion<sup>6,34-36</sup>, derived originally for wall sheaths, is also valid for the monotonic transition.

A similar statement can be made for the trapped particle parameters. Both are limited from below:  $\alpha \geq \alpha_c$ ,  $\beta \geq \beta_c$ , where again the lower bounds depend on  $\psi$  being of order unity. This justifies the choice of positive trapping parameters and proves that four species, beam-like distributions<sup>12,13,16,19-21,31-33</sup> are a prerequisite for the existence of the monotonous transition. A plot of  $f_e$  for the parameters indicated is shown in Fig. 3. Distribution functions like those are usually unstable with respect to two-stream instabilities which are the richer and stronger the larger the drift velocities are. The driven fluctuations will be hf-waves due to mainly electron-electron (e-e) two-stream instabilities sitting at the high potential side, and lf-waves due to

e-i and/or i-i two-stream instabilities at the low potential side<sup>16,25,27</sup>. The turbulence level will be lowest when the drift velocities are smallest. This is exactly the case when  $f = 1$ . This means, that the "Langmuir condition" provides the most stable double layer configuration.

The double layer width  $\Delta$  can be deduced from the depth  $d$  of the classical potential and is given by the relation  $\Delta = \psi d^{-1/2}$ . The latter is obtained by a renormalization of the "energy law"<sup>42</sup>. The investigation of  $\Delta$  shows that it is decreasing up to  $\psi \approx 5$ , and then increasing for higher values of  $\psi$ <sup>23</sup>. For  $\psi > 5$  it scales like  $\Delta \approx 5 \psi^{1/2}$ .<sup>43</sup>

The temperature ratio  $\theta$  is expected not to have an essential influence on the DL properties besides the fact that it will most probably enter in the Bohm criterion ( $u_0 > \theta^{1/2}$ ). More precise statements are missing at the present state because an analytical investigation involving  $\theta \neq 1$  has not been undertaken yet for this kind of distributions. Finally, it has been found that for all DLs that have been constructed the expression  $G \equiv 2 \alpha \psi u_0^{-2}$  was approximately constant ( $G \approx 0.8$ ). This implies, in view of  $u_0 \approx 0(1)$ , that  $\alpha$  must go like  $\psi^{-1}$  as  $\psi$  decreases. Very weak DLs  $\psi \ll 1$  are, therefore, not expected to occur because the trapped ion distribution would then be  $\delta$ -function-like and be subject to strong instabilities. Thus, stability arguments suggest a lower amplitude limit of order unity for this type of DLs. There was, however, no indication for the existence of an upper limit of  $\psi$  in the analytical evaluations.

These analytically obtained features of the monotonic transition, therefore, compare favourably with the properties I1) - I7) listed in Sect. II, and show that the solution presented here is well suited for this strong type of DLs. For a more detailed discussion and comparison with experimental and numerical data I refer to the original paper.<sup>42</sup>

#### IV. The Asymmetric Ion Hole (Type-II-DL)

The second type of DLs turns out to be intimately related to ion holes.<sup>45-47</sup> For this reason we first discuss in some detail the (symmetric) ion hole, develop its characteristic properties and then describe the asymmetric version.

The ion hole together with the phase space diagrammes is plotted in Fig. 4. The potential has a dip and satisfies

$\phi_{\min} \equiv -\psi \leq \phi(x) \leq 0 \equiv \phi_{\max}$ . Adopting the normalization of Section II, we start with the following set of distributions

$$f_{ef} = AC \exp(v_0^2/2) \exp \left\{ -\frac{1}{2} \left[ \operatorname{sgnv} \left( v^2 - 2(\psi + \phi) \right)^{1/2} - v_0 \right]^2 \right\} \quad E_e > \psi, \quad (8a)$$

$$f_{et} = AC \exp \left\{ -\frac{\beta}{2} \left[ v^2 - 2(\psi + \phi) \right] \right\} \quad E_e \leq \psi, \quad (8b)$$

$$f_{if} = C \exp \left\{ -\frac{1}{2} \left[ \operatorname{sgnu} \left( u^2 + 2\theta\phi \right)^{1/2} + u_0 \right]^2 \right\} \quad E_i > 0, \quad (8c)$$

$$f_{it} = C \exp \left[ -\frac{\alpha}{2} \left( u^2 + 2\theta\phi \right) \right] \quad E_i \leq 0, \quad (8d)$$

with the same definitions as in Sects. II and III. Note, that electrons and ions are essentially interchanged in comparison with Sect. III. Again the distributions are well-behaved, being extensions of Maxwellians. The trapping parameters are chosen with a different sign:  $\alpha < 0$  (corresponding to a concave vortex-type, trapped ion distribution) and  $\beta > 0$ .

The densities then become:

$$n_e(\phi) = A \left[ F(v_0^2/2, \psi + \phi) + T_+(\beta, \psi + \phi) \right], \quad (9a)$$

$$n_i(\phi) = \exp(-u_0^2/2) \left[ F(u_0^2/2, -\theta\phi) + T_-(\alpha, -\theta\phi) \right]. \quad (9b)$$

$F$  and  $T_+$  have already been defined, and  $T_-$  is given by

$$T_-(x, y) = 2(\pi|x|)^{-1/2} W(\sqrt{|xy|}) \quad , \quad x < 0, \quad (10)$$

where  $W(x) \equiv \exp(-x^2) \int_0^x dt \exp(t^2)$  is Dawson's integral. At infinity, i.e. at  $\phi = 0$ , the ion density becomes unity, because of  $F(x, 0) = \exp(x)$  and  $T_-(x, 0) = 0$ . Charge neutrality at infinity, therefore, requires

$$A^{-1} = F(v_0^2/2, \psi) + T_+(\beta, \psi), \quad (11)$$

which is a first relation among the parameters. Note that the second charge neutrality condition is absent here in contrast to Sect. III, so that  $v_0$  can be considered as a free parameter. Choosing  $v_0 = 0$  and an isothermal electron state ( $\beta = 1$ ), the electron density then becomes the familiar Boltzmann distribution:  $n_e(\phi) = \exp(\phi)$ .

A classical potential  $V$ , which is obtained by taking the second integral form of Sect. II, becomes

$$V(\phi) = A \left[ P_+(\psi, \beta) - P_+(\psi + \phi, \beta) + H(v_0^2/2, \psi + \phi, \psi) \right] - \theta^{-1} \exp(-u_0^2/2) \left[ P_-(-\theta\phi, \alpha) - 1 + H(u_0^2/2, 0, -\theta\phi) \right], \quad (12)$$

where we used  $V(0) = 0$ , and defined the new function  $P_-$  by

$$P_-(x, y) = \frac{\exp(x) \operatorname{erfc} \sqrt{x + 2(x/\pi)^{1/2}(1 - 1/y) + y^{-1}(\pi|y|)^{-1/2}}}{2W(\sqrt{|xy|})} \quad y \leq 0, x > 0. \quad (13)$$

In the limit  $v_0 = 0$ ,  $\beta = 1$  the electron contribution to  $V$  becomes  $1 - \exp(\phi)$ . (There is a sign error in eqns. (20) and (21) of Ref. 46).

The nonlinear dispersion relation, decisive for the existence of hole solutions, is given by  $V(-\psi) = 0$ , which expresses zero derivative of  $\phi$  at potential minimum.

An investigation of the admissible parameter range, restricted by the further condition  $V < 0$  in  $-\psi < \phi < 0$ , reveals the following results<sup>45-47</sup>:

- The ion hole velocity  $u_0$  is of order unity or less, and decreases with increasing  $\psi$ .
- Ion holes do not exist for  $\Theta = T_e/T_i \leq 3.5$  in the isothermal, current-free limit ( $\beta = 1$ ,  $v_0 = 0$ ). This limit can be lowered somewhat if  $v_0$  is increased or if  $\beta$  is decreased.
- There is an upper limit on  $\psi$  which is nearly one, and independent on  $\Theta$  ( $\Theta > 3.5$ ), for  $v_0 = 0$ ,  $\beta = 1$ . It is increased if  $\beta$  is lowered ( $\psi_{\text{MAX}} \approx 2.5$  for  $\beta = 0.1$ ).
- $\alpha$  has to be strictly negative (ion vortex distribution).
- $n_e$  and  $n_i$  are depressed in the hole region.
- The spatial width  $\Delta$  decreases with  $\alpha$ ; with respect to  $\psi$ , it first decreases and then increases with increasing  $\psi$ .

Expressed in few words, the ion hole needs for its existence a vortex-type ion distribution, it propagates with at most ion thermal velocity and is characterized by depressions of  $\phi$ ,  $n_e$  and  $n_i$ .

Of special interest for the process of DL formation is the limit of small amplitudes:  $\psi \ll 1$ . In this case we can exploit the formulas analytically. Using a small amplitude expansion<sup>8</sup>, we find that the nonlinear dispersion relation  $V(-\psi) = 0$  reduces to

$$-\frac{1}{2} \operatorname{Re} \left[ Z'(v_0/\sqrt{2}) + \Theta Z'(u_0/\sqrt{2}) \right] = \frac{8}{5} \psi^{1/2} \left[ b(\beta, v_0) + \frac{2}{3} \Theta^{3/2} b(\alpha, u_0) \right], \quad (14)$$

where  $Z(z)$  is the Fried-Conte plasma dispersion function and  $b(x, y)$  is defined by

$$b(x, y) = \pi^{-1/2} \left[ 1 - x - y^2 \right] \exp(-y^2/2), \quad x \geq 0. \quad (15)$$

In view of small  $\psi$ , a solution of (14) must be sought in the vicinity of a zero of the left-hand side. The latter is, however,

nothing else but the linear dispersion relation of zero-damped electrostatic modes in the infinite wave-length limit. Zero-damping is artificially introduced by distorting the distribution functions in the resonant region such that the imaginary part of the bracket at the left-hand side of (14) becomes zero. Stix<sup>48</sup> has studied this linear dispersion relation and found two low frequency solutions: the usual ion acoustic branch and a second one called the slow ion acoustic branch. It is this latter branch which is of interest here.<sup>45</sup> Assuming a large temperature ratio,  $\theta \gg 1$ , the solution of (14) is found to be

$$u_0 = 1.305 \left\{ 1 - \frac{1}{2\theta} \operatorname{Re} Z' (v_0/\sqrt{2}) - \frac{8}{5} (\theta\psi)^{1/2} \left[ \frac{2}{3} b(\alpha, 1.305) + \theta^{-3/2} b(\beta, v_0) \right] \right\}. \quad (16)$$

In the current-free, isothermal limit ( $v_0 = 0$ ,  $\beta = 1$ ), where it holds  $b(\beta, v_0) = 0$ , and  $-\frac{1}{2} \operatorname{Re} Z' (v_0/\sqrt{2}) = 1$ , (16) becomes

$$u_0 = 1.305 \left\{ 1 + \frac{1}{\theta} - \frac{16}{15} b(\alpha, 1.305) (\theta\psi)^{1/2} \right\}. \quad (16a)$$

Since  $u_0$  is the phase velocity of the ion hole in the ion rest frame ( $u_0 = \omega/k$ , where  $\omega$  is normalized by  $\omega_{pi}$  and  $k$  by  $\lambda_{De}^{-1}$ ), one easily recovers Stix's result (eq. 72, Chap. 9) in the limit  $\psi \rightarrow 0$ ,  $\theta \rightarrow \infty$ . Hence, ion holes are nonlinear extensions of slow ion acoustic waves.

The classical potential, corresponding to (16a), becomes<sup>45</sup>

$$V(\phi) = -\frac{8}{15} b(\alpha, 1.305) \theta^{3/2} \phi^2 (\sqrt{\psi} - \sqrt{-\phi}), \quad (17)$$

which is shaped properly as one can easily recognize (see Fig. 4a). From (17), it follows that  $b$  must be positive,  $b > 0$ , which implies that  $\alpha < -0.71$ . This means that the ion distribution is of vortex-type. Furthermore, from (16) or (16a) one sees, that  $u_0$  decreases with increasing  $\psi$ , as mentioned earlier.

To summarize, the small amplitude analysis proves analytically that the ion hole is based on the slow ion acoustic mode and demands for its existence a distortion of the ion distribution in the thermal range.

A symmetric ion hole is accomplished now by two identical plasma states on both sides of the hole structure. However, since there are reflected (trapped) particles involved which originate from different asymptotic regions, the plasma states in generality will differ from each other. This is especially true for the electrons. Consequently, the ion hole will respond

with an asymmetric structure, consisting of two different half-ion holes attached at the potential minimum. In particular, the depths of both halves will be affected, so that the most general version will be an asymmetric hole as shown in Fig. 2a. Furthermore, since each part keeps the properties of a hole, all what has been said for the (symmetric) ion hole can also be assigned to the asymmetric one.

If we now compare the properties of ion holes with those of the second type of DLs listed in II1) - II7), we find an almost complete coincidence. (The items II5) and II7) will find an explanation later.) It is, therefore, suggestive to identify both entities. We, therefore, conclude that the asymmetric ion hole provides a natural explanation of ion-acoustic DLs.

With this background, it is now not difficult to sketch a scenario of DL formation.

#### V. A Scenario of Double Layer Formation

This Section deals with the processes involved in the formation of DLs, specialized to the case of the current-driven ion acoustic resistivity. In this case there exist extensive particle simulations<sup>17,38-41</sup> which provide the information needed to illustrate and to understand what is going on during the time development of DLs. The main reference will be the particle simulations of Ref.<sup>40</sup> which are used as guidelines and which will be commented on and interpreted taking into account the analysis developed in the previous sections. Hence, this section mainly refers to the ion acoustic type-II-DL, but also the transition to the monotonic type-I-DL will be discussed as it arises in voltage-driven plasmas. Accordingly, the time-development of a current-driven plasma can be divided into several stages.

##### 1. Ion acoustic turbulence - excitation of slow ion acoustic modes

To start with, we note and remember that DL formation is observed numerically only if  $\theta = T_e/T_i$  is sufficiently high, if the initial electron drift  $v_D$  is of the order of electron thermal velocity, and if the system length  $L$  is sufficiently long. The threshold values are given by  $\theta \geq 3$ ,  $v_D \geq 0.5 v_{the}$ , and  $L \geq 500 \lambda_D$ , and typical parameters, chosen in the simulation,<sup>40</sup> were  $\theta = 20$ ,  $v_D = 0.6$ , and  $L = 1024 \lambda_D$ .

For in this case, the ion acoustic waves are driven fastlv

and strongly and gain a mean fluctuation level of about 20 %, and local values up to 30 % - 40 %.<sup>17</sup> Fluctuations of this amount suffice to trap thermal ions locally, the corresponding trapping velocities  $v_{tri} \equiv \sqrt{2e\phi/m_i}$  being of the order of the ion acoustic speed  $c_s$ . Hence, the ion distribution will be distorted in the thermal range, predominantly at positions where the fluctuations are strongest, and this is essential for the existence of slow ion acoustic modes. Ion Landau damping of the latter is drastically reduced and is offset by electron Landau growth, leading to an amplification of this new mode and subsequently a bifurcation in the frequency spectrum.<sup>40</sup>

## 2. Ion hole formation

Both types of ion acoustic fluctuations are, therefore, coexisting in regions where the distortion has taken place. However, thermodynamically, the system has the tendency to evolve toward a state of maximum entropy which is achieved by the formation of ion phase space holes.<sup>49</sup> Slow ion acoustic modes are, therefore, further growing at the cost mainly of the energy of streaming electrons creating a coherent ion hole pattern. The ion hole will be solitary-like instead of being periodic, due to the local character of the distortion. This readjustment ("self-organization") occurs very fast, the associated anomalous resistivity exceeds the former ion acoustic by one order of magnitude, seen by a strong current reduction. During the convective growth - this is in accordance with the assumption that the ion hole behaves adiabatically - the ion hole, the velocity of which was initially between the ion thermal and the acoustic speed, slows down and comes to rest.<sup>40</sup>

## 3. Electron reflection

The process of ion hole amplification is accompanied by a qualitatively new process, the reflection of streaming electrons.<sup>50</sup> Slowly drifting electrons which could pass the ion hole region before become reflected by the negative potential spike of the hole. Hole depths of 0.2 - 0.4 corresponding to electron trapping velocities of  $0.6 \leq v_{tre}/v_{the} \leq 0.9$  give rise to a substantial electron reflection and an associated current reduction.

## 4. The asymmetric ion hole (type-II-DL)

This electron reflection creates an asymmetry. There will be an electron-rich region upstream, and an ion-rich region downstream. Consequently, the plasma responds by increasing the po-  
(decreasing)

tential at the downstream<sup>(upstream)</sup> side. This increase<sup>(decrease)</sup> is accompanied by new trapping phenomena. Ions moving slowly in the downstream direction will be reflected just as slow electrons moving upstream. The lifting of the plasma potential downstream continues until the charge imbalance is neutralized by these new trapping processes. At the end an asymmetric ion hole is formed distinguished by two distinct asymptotic regions up- and downstream. The different amplitudes of the two half ion holes fitted at the potential minimum are in accordance with the parameter dependency of holes derived in Sect. IV; e. g., a higher value of  $|u_0|$ , as it is observed in the upstream region and which is due to the acceleration of ions, corresponds to a smaller effective amplitude (depth) of the half ion hole upstream. Since the negative potential spike and the corresponding ion vortex distribution are not destroyed during this rearrangement of particles and potentials, the hole character remains preserved, although in asymmetric form. We conclude that the resulting ion acoustic DL is an asymmetric ion hole.

##### 5. The super conducting plasma state

From the preceding we easily understand why a super conducting plasma state<sup>40</sup> expressed by zero resistivity follows the DL formation. The reason is that the current is carried by fast electrons that overcome the potential barrier (= depth of the hole  $\approx 0.2$ ) and thus have velocities larger than approximately  $0.6 v_{the} \approx 6c_s$ . These electrons are off-resonant and do not match the phase velocity of ion acoustic waves. The latter may be present and resonantly interact with slow particles. Since the distribution is more or less symmetrized in this region due to the reflection process mentioned above there may be steady kind of process of absorption and emission of ion acoustic fluctuations which, however, does not affect the current-carrying fast electrons.

##### 6. The monotonic double layer (type-I-DL)

Suppose now that in the presence of an ion acoustic DL an external potential jump is applied across the plasma. The neutral plasma will exclude the applied field and force it to appear solely in the non-neutral DL region.<sup>17</sup> If this jump is several  $T_e e^{-1}$  all the ions moving upstream, being accelerated by the jump, will leave the ion hole region as free particles. The opposite is true for downstream-moving ions. All of them

become trapped by the enlarged potential barrier. The ion distribution, therefore, will assume a configuration like the one indicated in Fig. 1b), i.e., there are two beam-type components upstream and one Maxwellian-type component downstream. The electrons, on the other hand, will just become the mirror image. Downstream-moving electrons will be accelerated and constitute the beam component to the trapped component downstream (Fig. 1c). Thus, the whole configuration becomes favourable to a monotonic transition of the potential. The dip at the low potential side will disappear because an ion hole can no longer be supported by the new ion configuration. This transition from an ion acoustic DL with potential drops of  $\Delta\phi \approx 1 - 2 T_e^{-1}$  to a monotonic DL with  $\Delta\phi \gg T_e^{-1}$  is clearly seen in the simulations of Ref.[17].

#### VI. Conclusions and Summary

In the previous section we have described and interpreted qualitatively the formation of DLs in the presence of current-driven ion acoustic turbulence. The main ingredient was a reflection of electrons due to an ion hole which was excited by a large fluctuation and which gave rise to the formation of an asymmetric ion hole (type-II-DL). An additional voltage drop was shown to cause a further topological change in the potential and to induce a transition to the monotonic DL. The electron reflection was manifest in the reduction (limitation) of the current.

Now this idealized picture may not necessarily be applicable directly to real experiments as other overlapping processes which render the evolution more complex are involved, like particle reflections and accelerations in sheaths, presheaths or grids. It is, however, interesting to note that prior to the formation of DLs an "ion hole" precursor<sup>13,18,51,52</sup>, a negative potential barrier<sup>29,30</sup>, or a current limitation<sup>5,30</sup> have been reported. It is, therefore, suggestive to assume that the picture presented in Sect. V has grasped the essential steps in the formation of DLs. The lack of clear evidence of ion acoustic DLs in laboratories may be attributed to the fact that the devices are mostly voltage-driven so that the electron reflection and the related current reduction caused by some negative barrier directly lead to a monotonic DL. In other devices (e.g. triple plasma devices), beam distributions satisfying a Bohm criterium are produced by pre-acceleration which, provided that appropriate

trapping processes take place, favourize the building-up of a monotonic DL.

In summary, we have reported analytical proofs of the existence of two distinct classes of, in some sense complementary, DL solutions of the Vlasov-Poisson-system. One class consists of a strictly monotonic transition of the potential and needs beam-type distributions, the second class has, in addition, a negative potential spike at the low potential side of the DL and needs distributions which are distorted in the thermal range. The latter ion acoustic type DL has been identified with an asymmetric ion hole. We have, furthermore, derived and described the characteristic properties of both solutions, and have shown by comparison with numerical and experimental results that the analysis presented is well suited for the description of realistic DLs. It turned out that for a correct description the use of smooth, Maxwellian-type distributions was essential, which could only be achieved by using a method different to the Bernstein-Greene-Kruskal method.

Note added in proof :

There are numerical indications of a third type of DLs given by a transition with a hump at the high potential side [Fig. 5]. Electron trapping caused, e.g., by a Buneman-Pierce instability, leads to an electron phase space vortex which slows down as it grows and gives rise to ion trapping and to the formation of an asymmetric electron hole (type-III-DL).

In a recent paper of Temerin et.al. [M. Temerin, K. Cerny, W. Lotko, F. S. Mozer, Phys. Rev. Lett. 48, 1175 (1982)], two possible potential structures for double layers on auroral field lines which are consistent with the data were presented. One of them was appointed to the ion acoustic type-II-DL. We propose here that the alternative second one is an electron acoustic type-III-DL which, in contrast to the first one, does not require a finite temperature ratio.

References

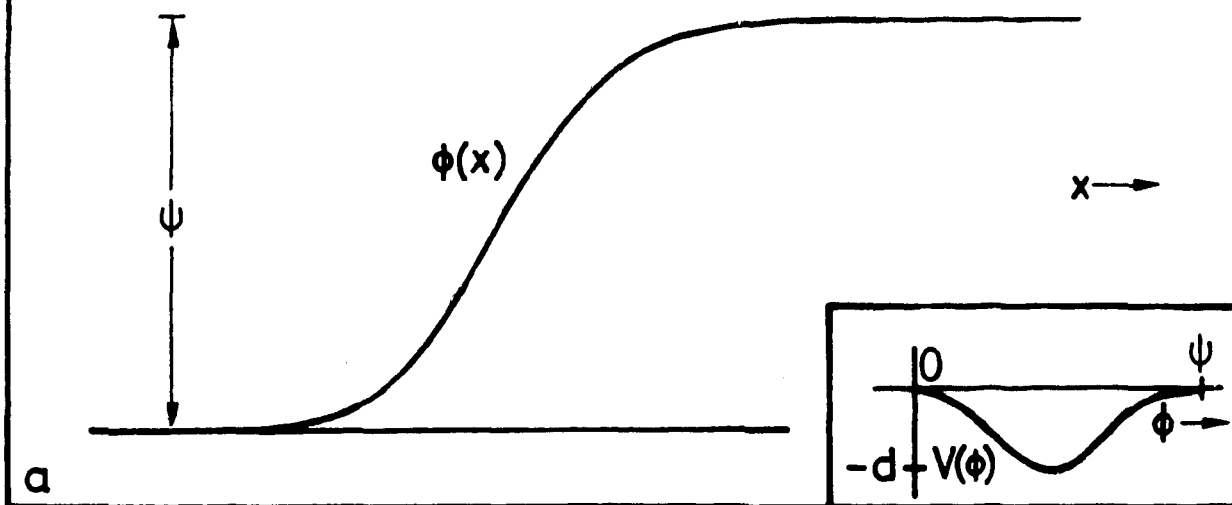
- [1] I. Langmuir, Phys. Rev. 2, 450 (1913), *ibid* 33, 954 (1929),
- [2] L. Tonks, Trans. Electrochem. Soc. 72, 167 (1937),
- [3] M. J. Schönhuber, Z. Angew. Phys. 15, 454 (1963),
- [4] E. Graybill and J. K. Uglum, J. Appl. Phys. 41, 236 (1970),
- [5] E. I. Lutsenko, N. D. Sereda, and L. M. Kontsevoi, Sov. Phys. Tech. Phys. 20, 498 (1976),
- [6] L. P. Block, Cosmic Electrodyn. 3, 349 (1972),
- [7] W. M. Manheimer and I. Haber, Phys. Fluids 17, 706 (1974),
- [8] H. Schamel, Plasma Phys. 14, 905 (1972),
- [9] H. Schamel, J. Plasma Phys. 13, 139 (1975),
- [10] I. B. Bernstein, J. M. Greene and M. D. Kruskal, Phys. Rev. 108, 546 (1957),
- [11] D. Montgomery and G. Joyce, Plasma Phys. 3, 1 (1969),
- [12] G. Knorr and C. K. Goertz, Astrophys. Space Sci. 31, 209 (1974),
- [13] G. Joyce and R. F. Hubbard, J. Plasma Phys. 20, 391 (1978),
- [14] R. F. Hubbard and G. Joyce, J. Geophys. Res. 84, 4297 (1979),
- [15] N. Singh, Plasma Phys. 22, 1 (1980),
- [16] L. E. Johnson, J. Plasma Phys. 23, 433 (1980),
- [17] J. M. Kindel, Ch. Barnes, and D. W. Forslund, Physics of Auroral Arc Formation, AGU Monograph 25, 296 (1981),
- [18] B. H. Quon and A. Y. Wong, Phys. Rev. Lett. 37, 1393 (1976),
- [19] P. Leung, A. Y. Wong, and B. H. Quon, Phys. Fluids 23, 992 (1980),
- [20] P. Coakley, N. Hershkowitz, R. Hubbard, and G. Joyce, Phys. Rev. Lett. 40, 230 (1978),
- [21] P. Coakley and N. Hershkowitz, Phys. Fluids 22, 1171 (1979),
- [22] R. L. Stenzel, M. Ooyama, and Y. Nakamura, Phys. Fluids 24, 708 (1981),
- [23] N. Sato, R. Hatakeyama, S. Iizuka, T. Mieno, K. Saeki, J. J. Rasmussen, and P. Michelsen, Phys. Rev. Lett. 46, 1330 (1981),
- [24] N. Hershkowitz, G. L. Payne, Ch. Chan, and J. R. deKock, Plasma Phys. 23, 903 (1981),
- [25] Ch. Hollenstein, M. Guyot, and E. S. Weibel, Phys. Rev. Lett. 45, 2110 (1980),
- [26] S. Torvén and D. Anderson, J. Phys. D: Appl. Phys. 12, 717 (1979),
- [27] S. Torvén and L. Lindberg, J. Phys. D: Appl. Phys. 13, 2285 (1980),

- [28] J. S. Levine, F. W. Crawford, and D. B. Ilić, Phys. Lett. 65 A, 27 (1978),
- [29] S. Iizuka, K. Saeki, N. Sato, and Y. Hatta, Phys. Rev. Lett. 43, 1404 (1979),
- [30] S. Iizuka, P. Michelsen, J. J. Rasmussen, and R. Schrittwieser, Phys. Rev. Lett. 48, 145 (1982),
- [31] J. G. Andrews and J. E. Allen, Proc. Roy. Soc. Lond. A 320, 459 (1971),
- [32] J. R. Kan, J. Geophys. Res. 80, 2089 (1975),
- [33] S. S. Hasan, and D. ter Haar, Astrophys. Space Sci. 56, 89 (1978),
- [34] D. Bohm, in The Characteristics of Electrical Discharges in Magnetic Fields, edited by A. Guthrie and R. K. Walkering, McGraw-Hill, New York, p. 77 (1949),
- [35] L. P. Block, Astrophys. Space Sci. 55, 59 (1978),
- [36] J. R. Kan and L. C. Lee, J. Geophys. Res. 85, 788 (1980),
- [37] P. H. Sakanaka, Phys. Fluids 15, 1323 (1972),
- [38] J. S. DeGroot, C. Barnes, A. E. Walstead, and O. Buneman, Phys. Rev. Lett. 38, 1283 (1977),
- [39] T. Sato, and H. Okuda, Phys. Rev. Lett. 44, 740 (1980),
- [40] T. Sato, and H. Okuda, J. Geophys. Res. 86, 3357 (1981),
- [41] M. K. Hudson, and D. W. Potter, Physics of Auroral Arc Formation, AGU Monograph 25, 260 (1981),
- [42] H. Schamel and S. Bujarbarua, Report SFB Bochum/Jülich 80-L2-070 (1980) (to appear in Phys. Fluids 1982),
- [43] H. Schamel, Dissertation, University of Munich (1970),
- [44] H. Schamel, Invited Lecture, International Conference on Plasma Physics, Göteborg (1982),
- [45] H. Schamel and S. Bujarbarua, Phys. Fluids 23, 2498 (1980),
- [46] S. Bujarbarua and H. Schamel, J. Plasma Phys. 25, 515 (1981),
- [47] M. K. Hudson, W. Lotko, and E. Witt, preprint (1982),
- [48] T. H. Stix, The Theory of Plasma Waves, McGraw-Hill, New York, 1962, Chap. 9-14,
- [49] T. H. Dupree, Phys. Fluids 25, 277 (1982),
- [50] A. Hasegawa and T. Sato, Phys. Fluids 25, 632 (1982),
- [51] S. Torvén and M. Babić, Proc 12th Int. Conf. on Phen. in Ionized Gases, ed. J. G. A. Hölscher and D. C. Schram (Amsterdam: North-Holland Publ. Co.),
- [52] S. Torvén, Invited Lecture, International Conference on

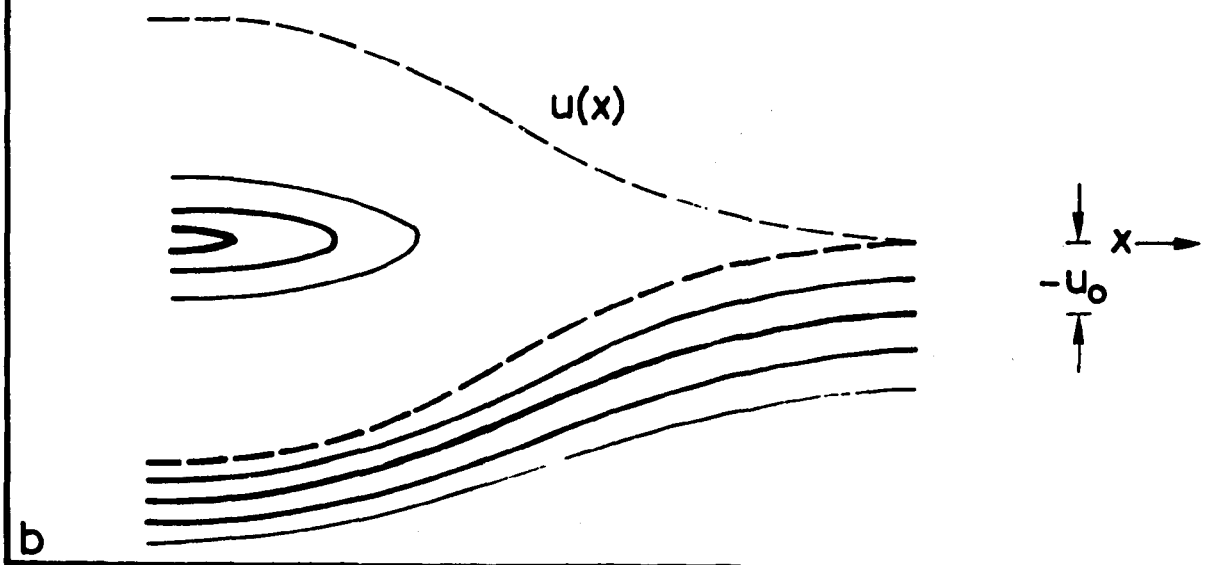
Figure Captions

- Fig. 1a) A qualitative plot of the electrical potential  $\phi(x)$  of a monotonic double layer as a function of  $x$ . The insert shows the corresponding classical potential  $V$  as a function of  $\phi$ .
- b) Ion trajectories are drawn in the ion phase space exhibiting two species of ions. The dashed line marks the separatrix, and the thickness of a contour correlates with the height of the distribution function; free ions are entering into the double layer region from the high potential side with normalized drift velocity  $-u_0$ .
- c) Electron trajectories are drawn in the electron phase space; free electrons enter into the double layer region from the low potential side with a normalized drift velocity  $+v_0$ .
- Fig. 2a) A qualitative plot of the electrical potential  $\phi(x)$  of the ion acoustic double layer as a function of  $x$ . The insert shows the two parts of the classical potential  $V$  corresponding to the two monotonic parts of  $\phi(x)$ .
- b) The ion phase space; further details are found in the text and in the legend of 1b).
- c) The electron phase space.
- Fig. 3 The electron distribution function in the quasi-phase space  $(\phi, v)$ ; the trapped electrons are located around  $v = 0$  on the high potential side  $\phi \leq \psi$ ; the free electrons experience a cooling during their acceleration from  $\phi = 0$  to  $\phi = \psi$ .
- Fig. 4a) A qualitative plot of the electrical potential  $\phi(x)$  of the ion phase space vortex as a function of  $x$ .
- b) The ion phase space.
- c) The electron phase space.
- Fig. 5a) A sketch of  $\phi(x)$  of the electron acoustic double layer as a function of  $x$ .
- b) The electron phase space.
- c) The ion phase space.

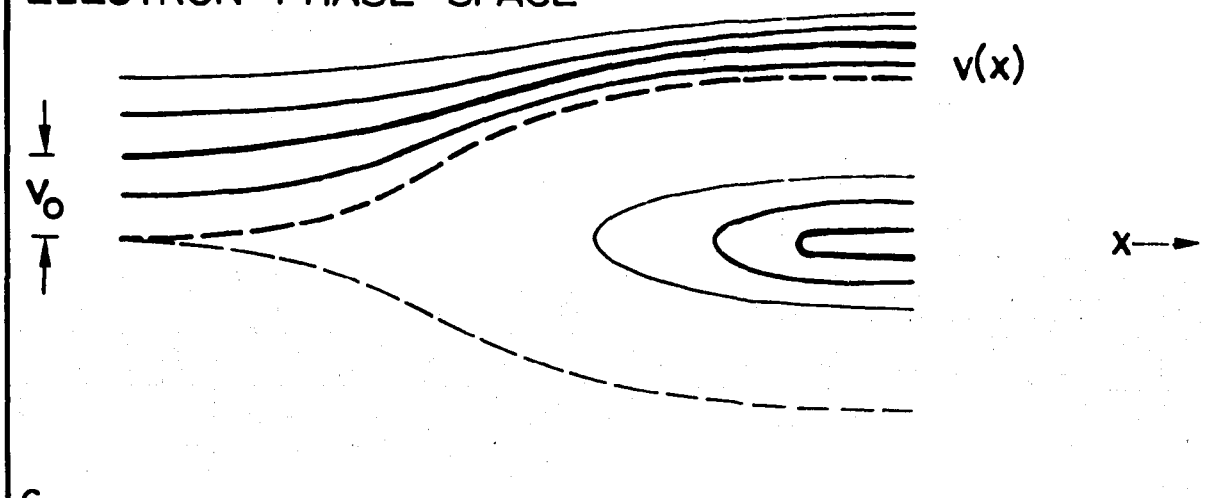
## MONOTONIC TRANSITION (Type-I-DL)



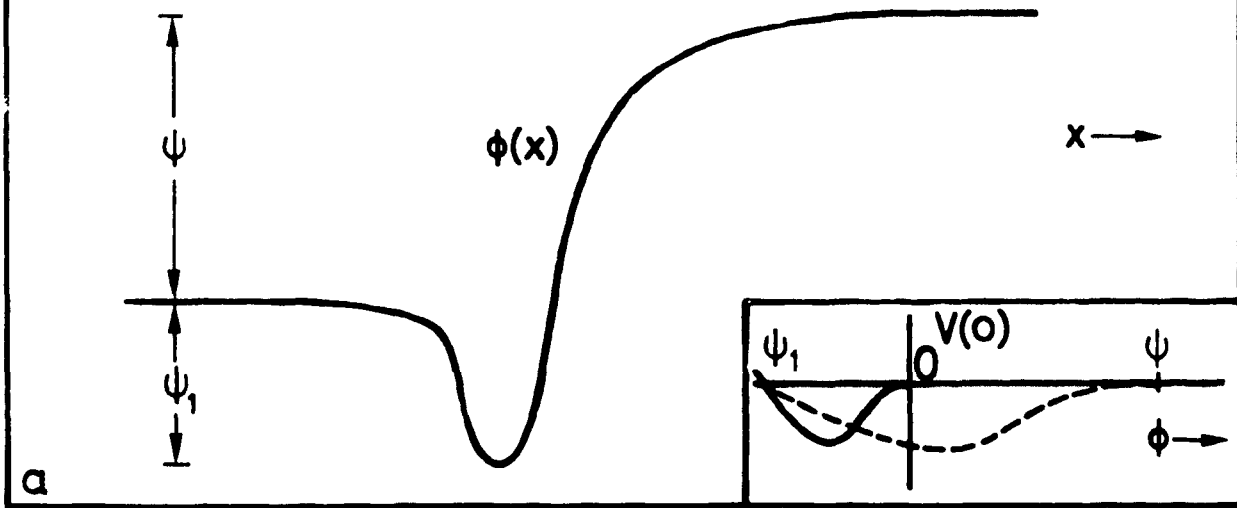
## ION PHASE SPACE



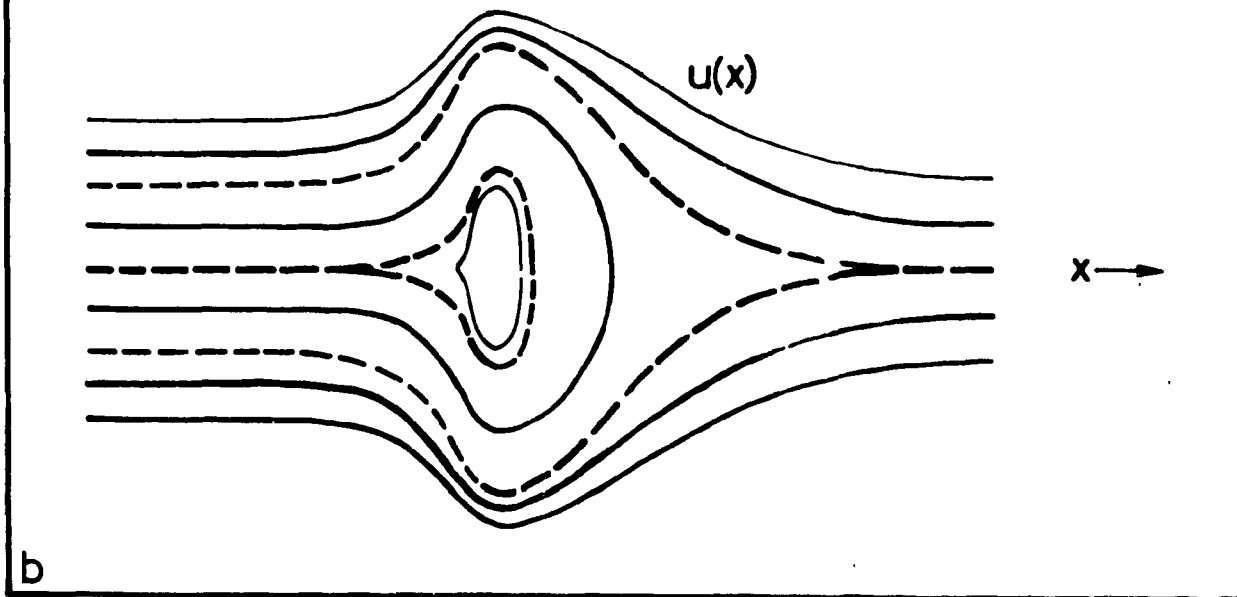
## ELECTRON PHASE SPACE



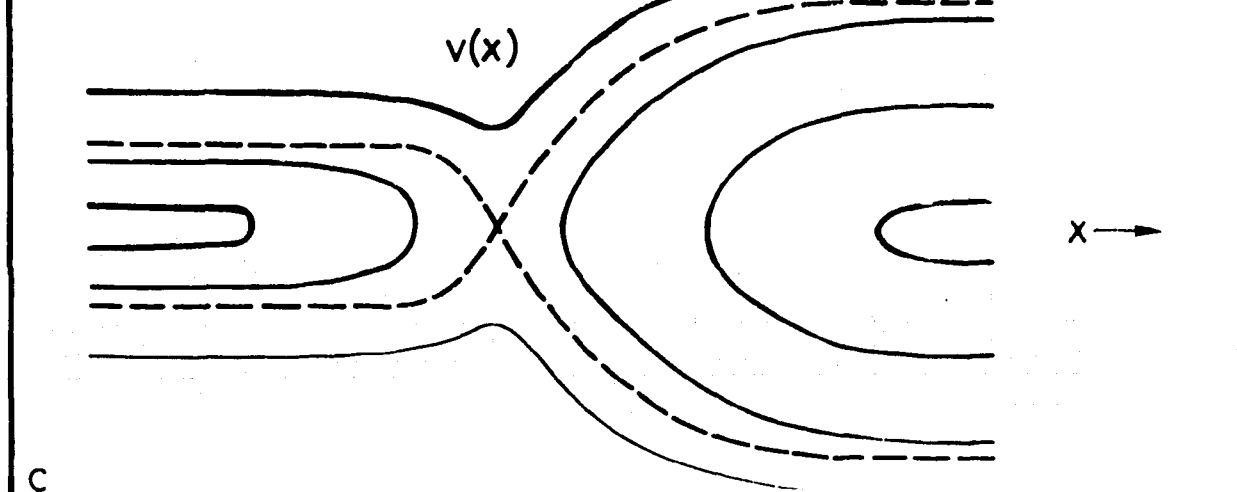
## ASYMMETRIC ION HOLE (Type-II-DL)

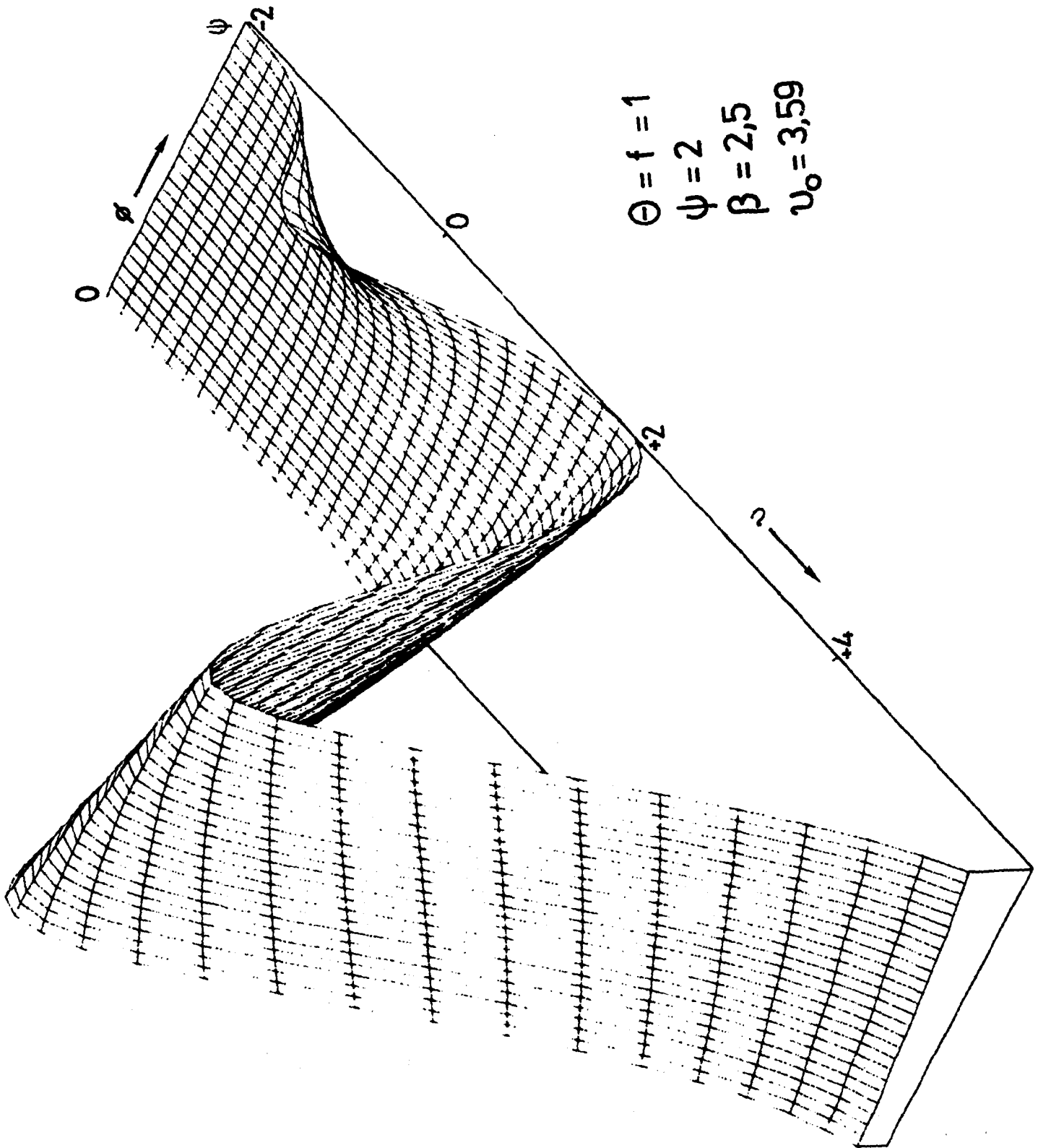


## ION PHASE SPACE

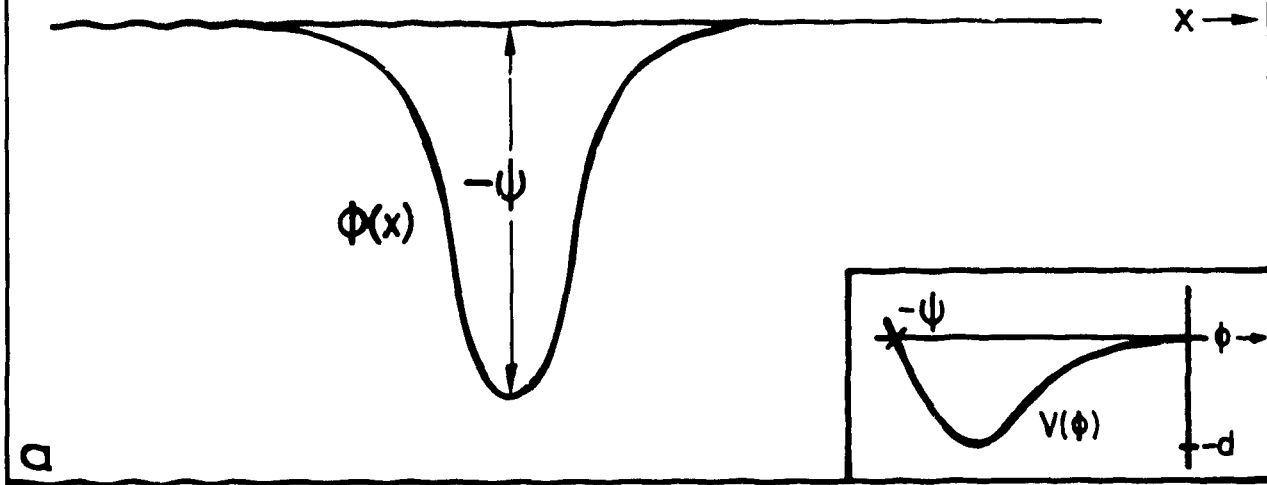


## ELECTRON PHASE SPACE

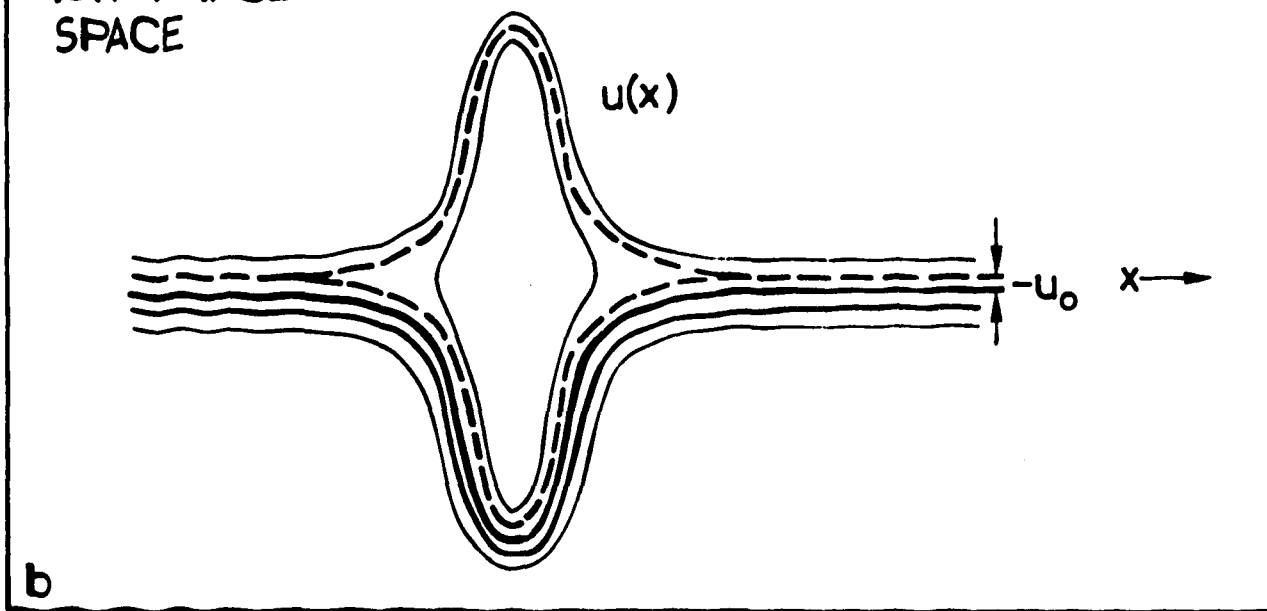




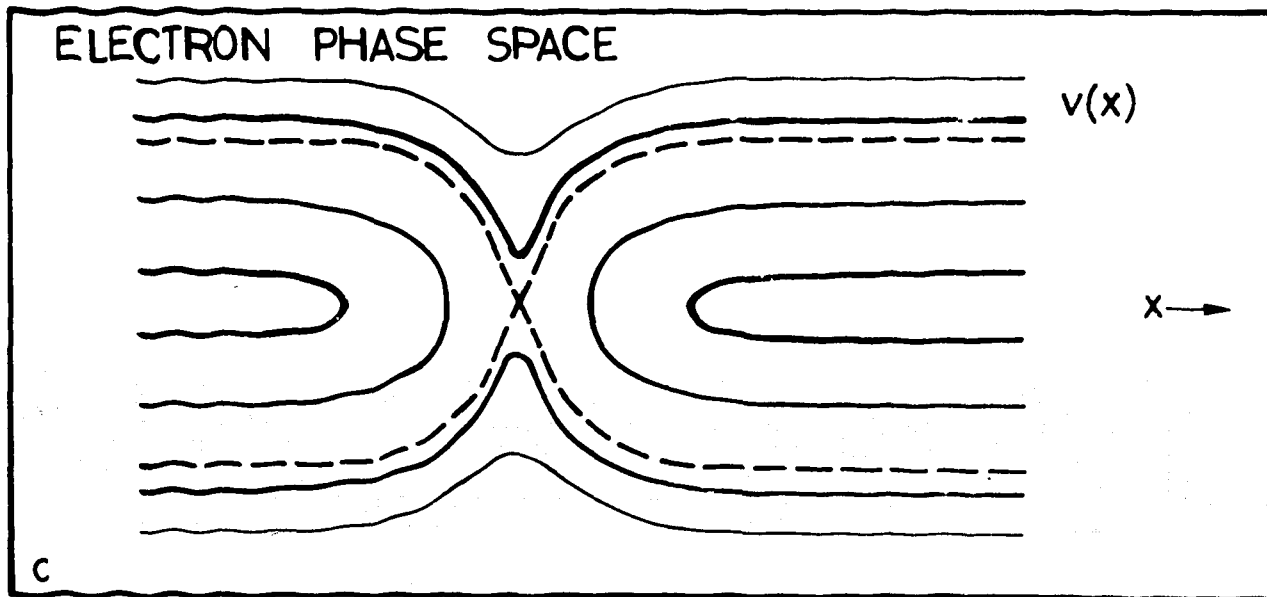
# ION HOLE

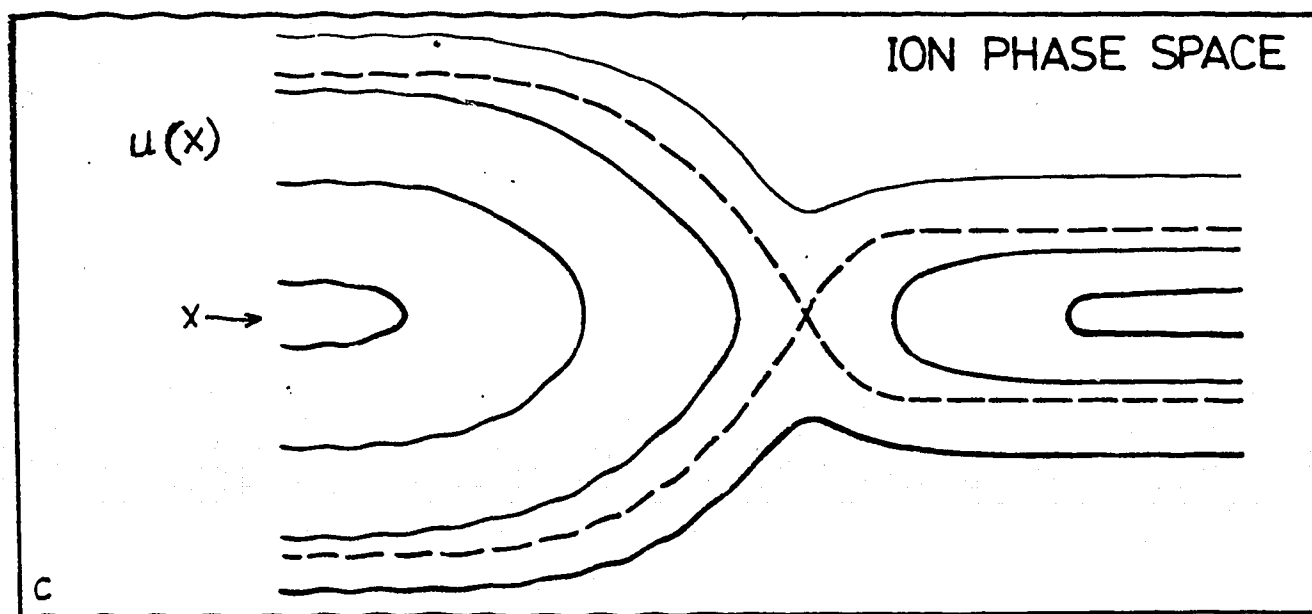
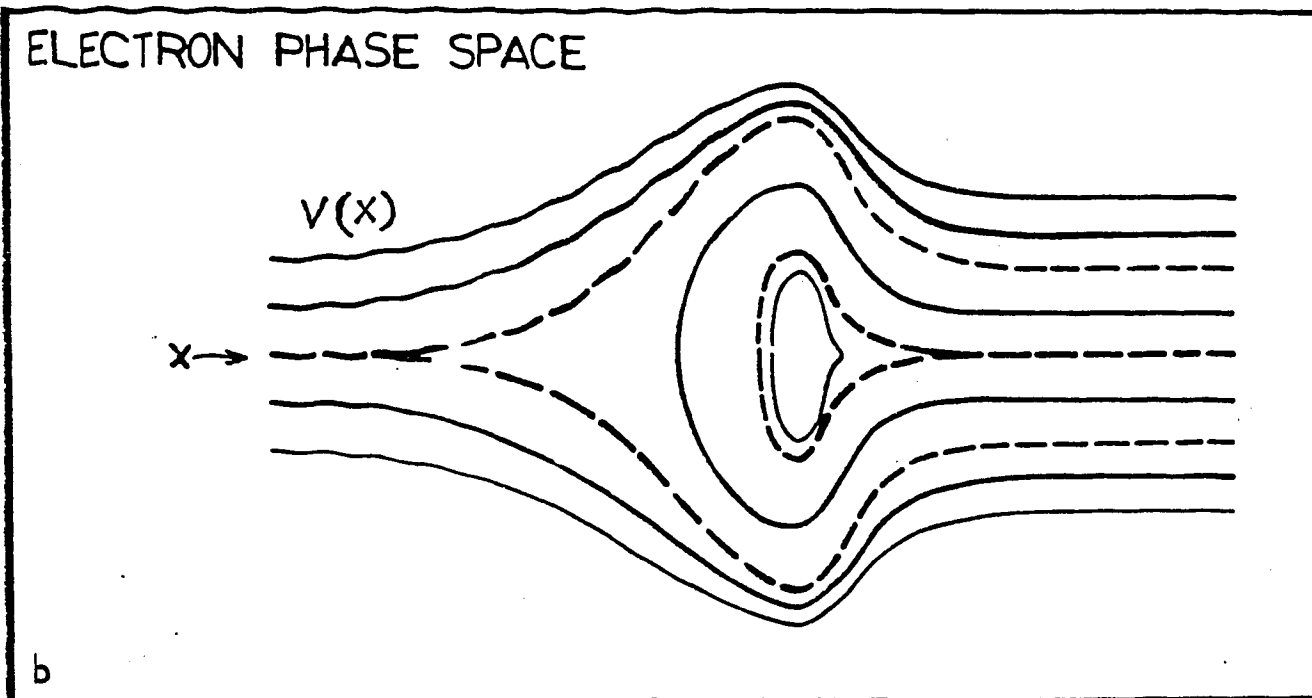
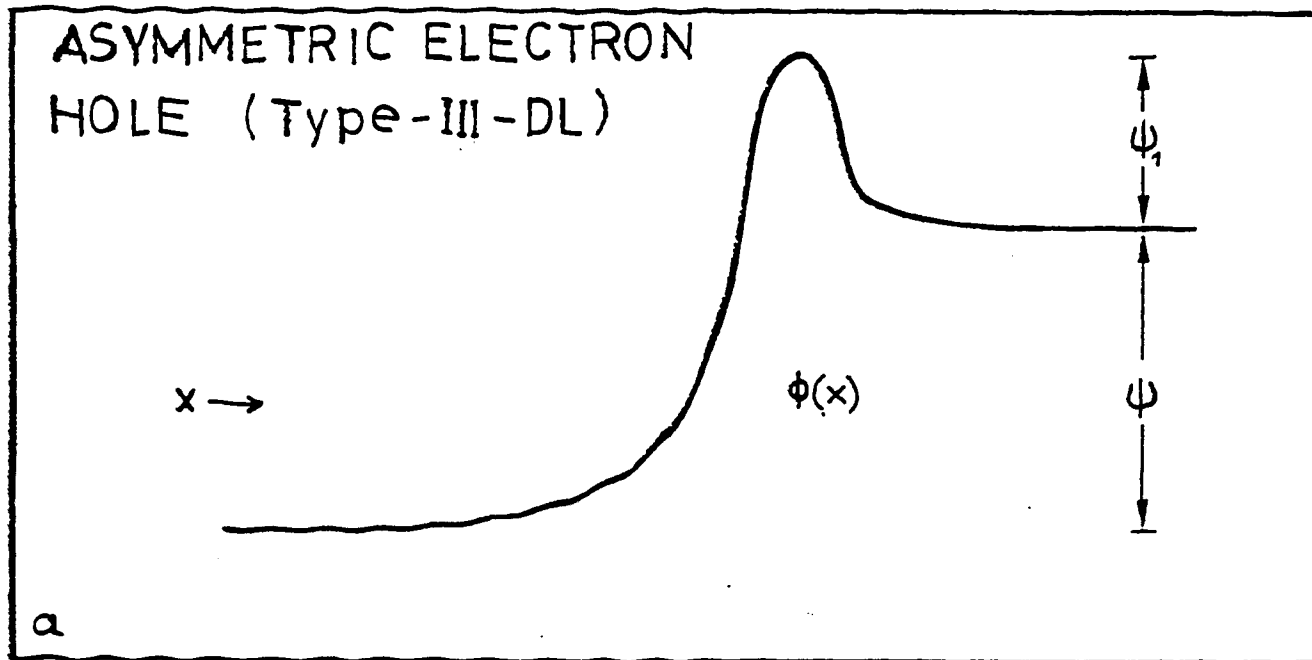


# ION PHASE SPACE



# ELECTRON PHASE SPACE





Title : ANALYTICAL DOUBLE LAYERS

Authors: Hans Schamel<sup>1</sup> and Sarbeswar Bujarbarua<sup>2</sup>

Institution : 1. Theoretische Physik I, Ruhr University,  
4630, Bochum 1, West Germany.  
2. Department of Physics, Dibrugarh Uni-  
versity, Dibrugarh - 786 004, India.

Abstract

Electrostatic Double Layers (DL), one of the most interesting nonlinear entities, have attracted much attention in recent years. However, there is no satisfactory theoretical description of DL because of the use of BGK method, by most of the theoreticians, involving non-physical distributions of the different species of particles. In this paper, we wish to show that acceptable DL solutions can be obtained with the help of an alternative method. The essential of this method is to prescribe the whole set of distributions and to look for the electrostatic potential, the choice of the distributions being fixed by physical considerations. We have thus obtained the lower limits for drift velocities and trapped particle temperatures and a simple relation is established between potential drop, free ion energy and trapped ion temperature. The scaling law for the width of strong double layers is confirmed analytically. It is found that whereas Bohm's criterion is generally valid, the Langmuir condition can be relaxed. Our theoretical results are found to agree quite well with the numerical simulation and experimental works for laboratory plasmas.

Formation of Negative Potential Solitary Wave  
and  
Double Layer

K. Nishihara, H. Sakagami, T. Taniuti\* and  
A. Hasegawa\*\*

Institute of Laser Engineering, Osaka University,  
Osaka 565, Japan

\* Department of Physics, Nagoya University,  
Nagoya 464, Japan

\*\* Bell Laboratories, Murray Hill, New Jersey 07974,  
U.S.A.

Abstract

We present a model of double layer formation in ion acoustic turbulence excited by drifting electrons. It is found, by means of particle simulations, that when the electron drift velocity exceeds  $0.6 v_{te}$ , a negative potential ion acoustic solitary wave first grows until its amplitude reaches to  $e\phi \sim -T_e$  and subsequent reflection of electrons leads to formation of a double layer. The mechanism of the growth of the negative ion acoustic solitary wave is investigated analytically.

Okuda and Sato<sup>1</sup> have discovered in their computer simulation that the ion acoustic wave turbulence which is excited by an electron drift spontaneously generates weak double layers with the potential jump comparable to the electron temperature. Hasegawa and Sato<sup>2</sup> as well as Schamel<sup>3</sup> independently have recognized negative potential spikes are responsible for the formation of the double layer and obtained some stationary solutions. In this manuscript we study dynamical processes of formation of the weak double layers from the ion acoustic turbulence by means of one and two dimensional numerical simulations, as well as of analytical methods.

Initial value problems are solved with certain initial drift of electrons with respect to ions. Figure 1 shows the potential profile obtained in the one dimensional simulation of which para-

meters are  $v_o = 0.6 v_{Te}$ ,  $T_e/T_i = 20$  and  $m_e/m_i = 0.01$ , where  $v_o$  and  $v_{Te}$  are the drift and thermal speeds of electrons. The double layer structure with the preceding negative potential spike is clearly visible. The boundary conditions is periodic hence the potential structure of a double layer is not of an ideal type but is of a triangular shape. In all cases appearance of the negative potential solitary waves are found to be responsible for the formation of double layer as predicted earlier.<sup>3</sup> Parameter surveys of the simulations indicate that there exists a threshold in  $v_o/v_{Te}$  for the formation of the negative potential solitary waves, and it is given by  $v_o/v_{Te} \gtrsim 0.6$ . It is interesting to note that the threshold exists in  $v_o/v_{Te}$  rather than in  $v_o/c_s$ , where  $c_s$  is the ion sound speed.

The reflection of electrons by the negative potential spike also produces anomalous resistivity by reducing the current. The reduction of the initial current is shown in Fig.2 for various values of initial drift speed,  $0.5 v_{Te}$ ,  $0.6 v_{Te}$  and  $0.7 v_{Te}$ . For  $v_o = 0.5 v_{Te}$ , the negative potential spike is not formed hence the reduction of the current is simply due to the excitation of the ion acoustic turbulence. However, when the negative potential spikes are formed corresponding to the cases,  $v_o \gtrsim 0.6 v_{Te}$ , a significantly larger drop in the current is noticeable. The time when the sharp drop of the current occurs coincides the growth of the negative potential (see Fig.3).

The trajectory of the negative potential spike as well as the variation of its peak value are plotted as a function of time in Fig.3. The spike moves initially at the ion acoustic speed (dotted line) and gradually decelerates as its amplitude grows until it stops in the ion frame when the amplitude attains its maximum value. This result indicates that the negative potential spike initially originates from the ion acoustic wave. As will be analytically shown later, the reflection of electrons causes also the deceleration of the negative potential. As the solitary wave decelerates and approaches to halt, the ions are trapped in the potential mainly due to the deceleration of the wave. The deceleration of the wave leads to trap the ions of which relative velocity to the wave is  $\lambda - v \lesssim 3v_{Ti}$ , which is calculated from the observed deceleration, where  $v_{Ti}$  and  $\lambda$  are the ion thermal speed and the wave propagation speed, respectively. The existence of

the trapped ion is seen in its trajectory in phase space in Fig.4. The ion acceleration by the negative potential results in the phase space hole of the ions as shown in Fig.5. The trapped ions form ion rich region near the edge of the solitary wave, near  $\phi \sim 0$  region, while the phase space hole of the ions forms an electron rich region in the center of the potential, leading to the growth of the negative potential. This can be seen in Fig.6 that shows the ion (open circles) and electron (dots) density profiles at different location of the potential. The top side of the curve corresponds to the left side of the potential spike in Fig.1 and the bottom side of the curve corresponds to the right side. The higher density of both electrons and ions in the left side is due to the reflection of the drifting electrons by the negative potential and the trapping of the ions by the deceleration of the wave, respectively.

To prove that the formation of the negative potential solitary wave is not an artifact of the one dimensionality of the model, we also ran two dimensional simulations. A typical result is shown in Fig.7 where the two dimensional profile of potential  $\phi$  is plotted for two different times. At an earlier time (top figure), the ion acoustic turbulence develops in two dimensional directions, however, in a later time (bottom figure) the negative potential solitary wave appears in the one dimensional trough structure perpendicular to the electron drift direction.

We now derive an equation that governs the dynamics of the negative potential solitary wave by taking the electron reflection into account. We use the cold ion fluid and Vlasov electrons. Following Washimi and Taniuti<sup>4</sup>, we introduce the stretched coordinates  $\xi = \epsilon^{1/2}(x - c_s t)/\lambda_{De}$  and  $\tau = \epsilon^{3/2}t\omega_{pi}$ . The dependent variables are expanded on the order of  $\epsilon$ , for example,  $e\phi/T_e = \epsilon\phi_1 + \epsilon^2\phi_2 + \dots$ . Then we can obtain the equation

$$\frac{\partial}{\partial \tau} \phi_1 + v_1 \frac{\partial}{\partial \xi} \phi_1 + \frac{1}{2} \frac{\partial^3}{\partial \xi^3} \phi_1 - \frac{1}{2} \frac{\partial}{\partial \xi} n_{er} = 0, \quad (1)$$

where  $n_{er}$  is the density perturbation corresponding to the reflected electrons. The velocity of the reflected electrons is given by,

$$\frac{1}{2} m_e u^2 - e\phi = \text{constant}. \quad (2)$$

Following the method of Kato et al.<sup>5</sup>, the density can be obtained as

$$n_{er} = 2 \int_0^{u_M} \frac{\partial f}{\partial u} \sqrt{u - 2\phi/m_e} du, \quad (3)$$

where  $u_M = (2 \frac{e}{m_e} (\phi - \phi_M))^{1/2}$  and  $\phi_M = \text{Min}(\phi)$ .

By normalizing  $\bar{u}$  by  $c_s$ , we can obtain

$$\begin{aligned} & \frac{\partial}{\partial \tau} \phi + \phi \frac{\partial}{\partial \xi} \phi + \frac{1}{2} \frac{\partial^3}{\partial \xi^3} \phi \\ & - \frac{1}{\epsilon} \left( \frac{m_e}{m_i} \right)^{1/2} \frac{\partial f}{\partial u} \Big|_{u=c_s} \frac{\partial}{\partial \xi} \left( \sqrt{-\phi_M} \sqrt{\phi - \phi_M} - \phi \ln \frac{\sqrt{\phi - \phi_M} + \sqrt{-\phi_M}}{\sqrt{-\phi}} \right) = 0. \end{aligned} \quad (4)$$

The first three terms are familiar Korteweg - deVries equation, while the last term is the modification due to the electrons reflected by the negative potential. To study the effect of the last term, we solved eq.(4) numerically with and without the last term for an initial condition of a localized potential. Figure 8 shows the comparison of these two cases. It is clearly seen that, while the K-dV equation gives damped solution (left figure), the inclusion of the electron reflection produces a solution which grows and simultaneously slows down. The propagation velocities of the wave are plotted as a function of its amplitude in Fig.9.

To summarize, the dynamical process of formation of a weak double layer is studied both numerically and analytically.

The negative potential solitary wave is decelerated with the increase of its amplitude by the reflection of electrons. On the other hand, ions are trapped by the negative solitary wave mainly due to the deceleration of the wave. The trapped ion form ion rich region near the edge of the solitary wave, while the phase space hole of the ions forms an electron rich region in the center, leading to the growth of the negative potential.

#### References

- 1) T. Sato and H. Okuda, Phys. Rev. Lett. 44, 740 (1980).
- 2) A. Hasegawa and T. Sato, Phys. Fluids, 25, 632 (1982).
- 3) H. Schamel, Physica Scripta, (1982) to be published.
- 4) H. Washimi and T. Taniuti, Phys. Rev. Letters, 17, 996 (1966).
- 5) Y. Kato, M. Tajiri and T. Taniuti, Phys. Fluids, 15, 865 (1972).

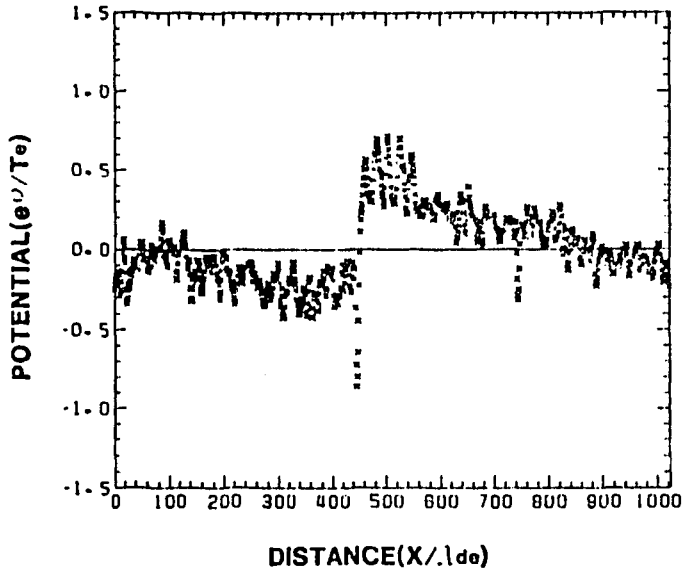


Fig. 1

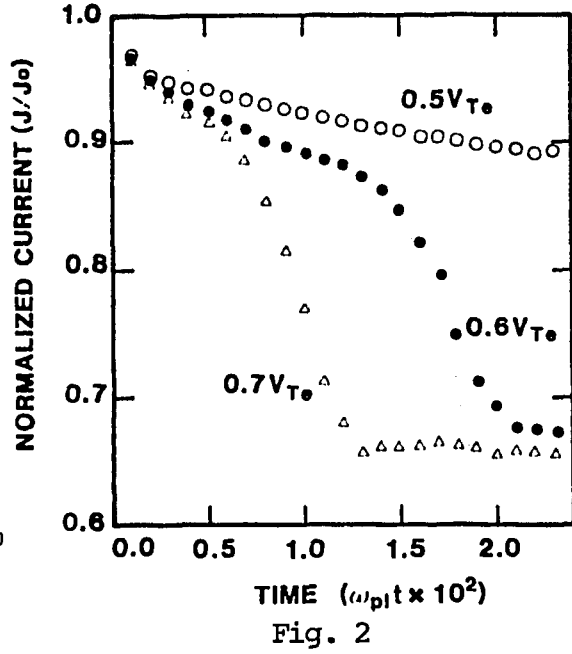


Fig. 2

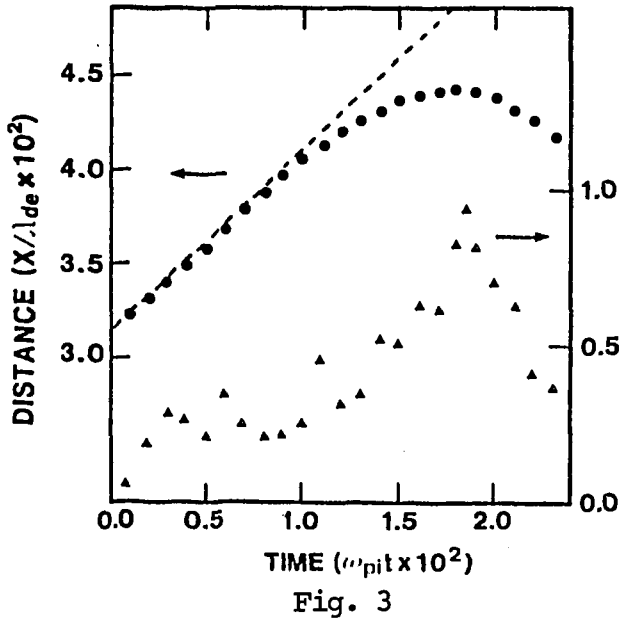


Fig. 3

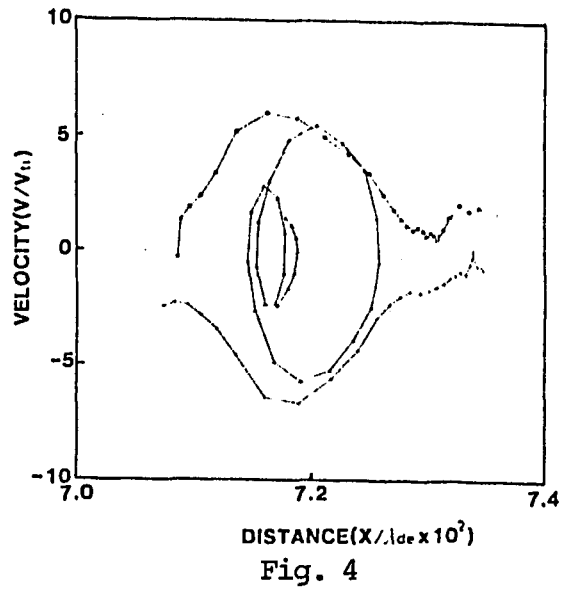
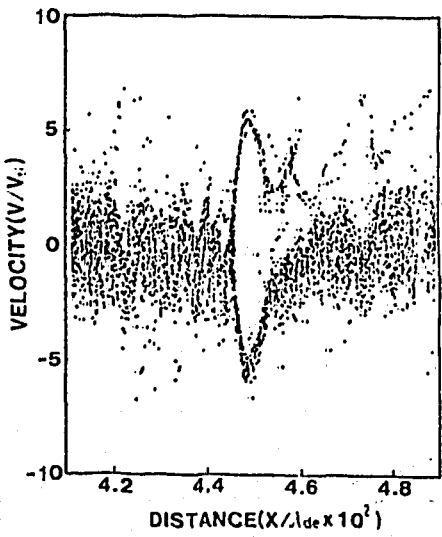


Fig. 4



ION  
Fig. 5

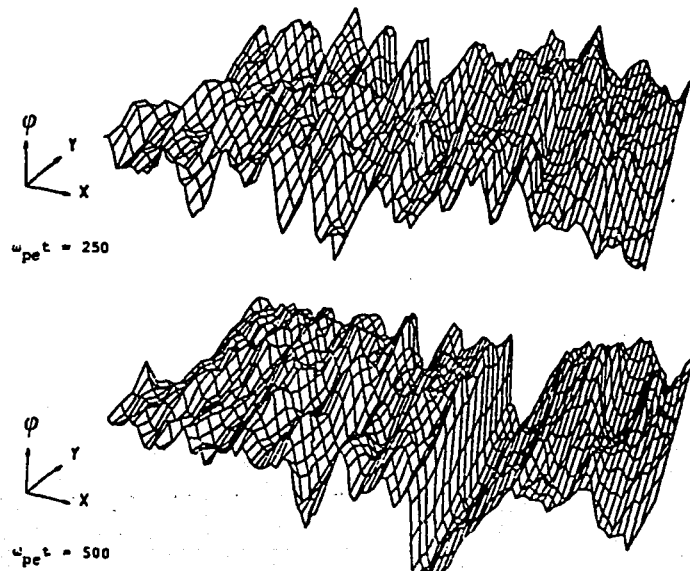


Fig. 7

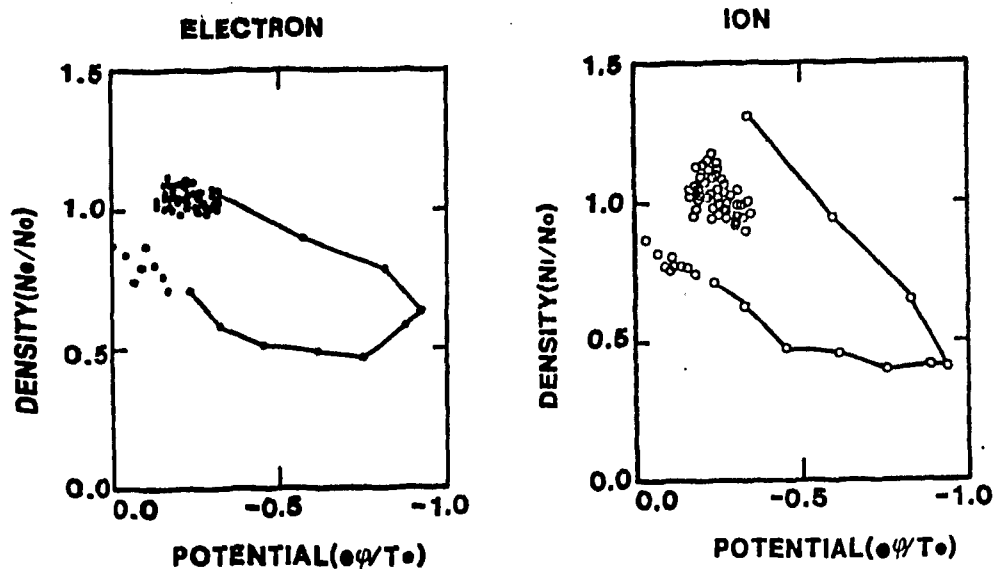


Fig. 6

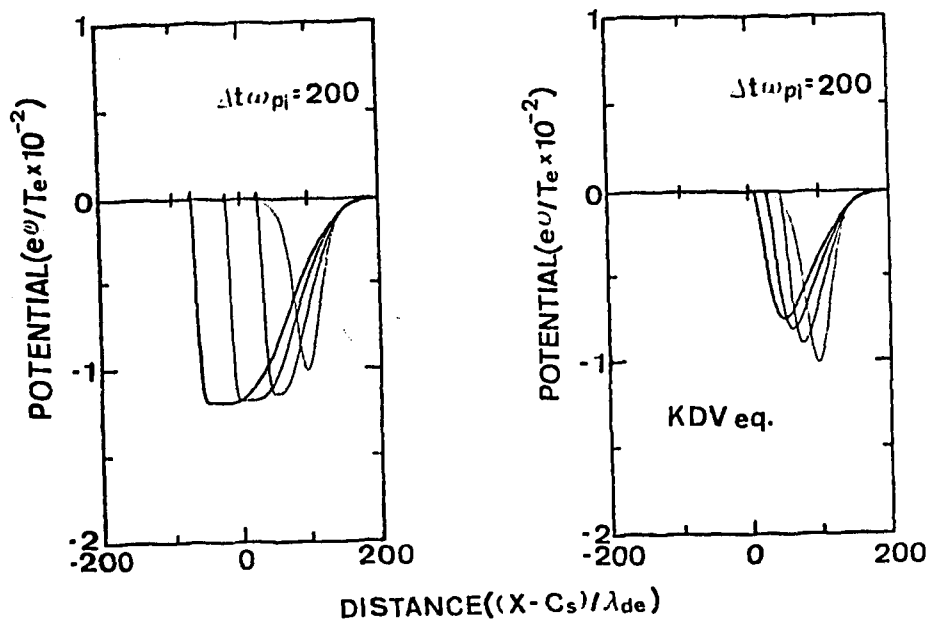


Fig. 8

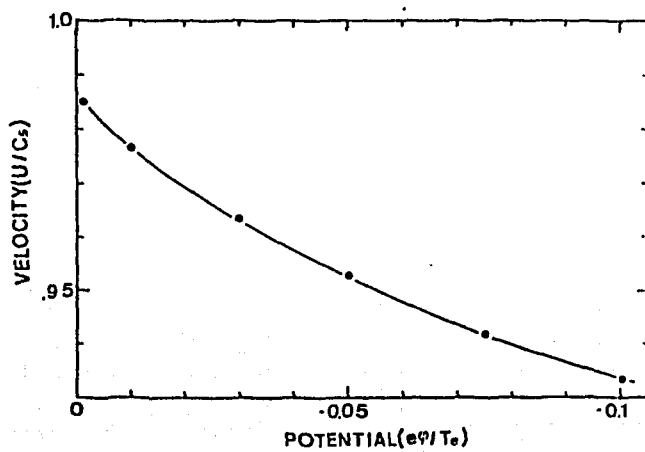


Fig. 9

## FORMATION OF ION PHASE-SPACE VORTEXES

H.L. Pécseli\*, J. Trulsen<sup>†</sup>, and R.J. Armstrong<sup>†</sup>.

<sup>†</sup>The University of Tromsø, P.O. Box 953, N-9001 Tromsø, Norway.

\*Association EURATOM-Risø National Laboratory, P.O. Box 49,  
DK-4000 Roskilde, Denmark.

Abstract. The formation of ion phase space vortexes in the ion two stream region behind electrostatic ion acoustic shocks is observed in a laboratory experiment. A detailed analysis demonstrates that the evolution of such vortexes is associated with ion-ion beam instabilities and a nonlinear equation for their initial evolution is derived. The results are supported by a numerical particle simulation.

1. Introduction. Numerical solutions [1] of the ion Vlasov equation (in one dimension) with the assumption of Boltzmann distributed isothermal electrons demonstrated that ion phase space vortexes may develop in the two stream region behind electrostatic ion acoustic shocks. Similar entities, but in electron phase space [2,3], were previously observed experimentally [4]. A unified analytical description of isolated ion and electron phase space vortexes is given by Bujarbarua and Schamel [5]. Ion phase space vortexes, in particular, seem to play a role in the formation of electrostatic double-layers [6] by creating a localized barrier inhibiting the free flow of the low velocity part of the electron distribution in current carrying plasmas. The subsequent deficit of electrons behind the ion vortex creates a positive potential region which ultimately develops into a double layer like structure. Another interesting aspect is the possibility of unstable plasmas to exhibit self-organizing behaviour by the formation of phase space vortexes [7]. In this work we discuss various properties of ion phase space vortexes.

2. Experimental results. To investigate the problem, considered numerically by Sakanaka [1], we performed a laboratory experiment in a large 0.6×1.2 m Double-Plasma device operated at neutral argon pressure  $\sim 8 \cdot 10^{-5}$  torr. We excited electrostatic shocks in the usual manner [8] by pulsing the driver chamber. Behind the shock we observed the formation of localized density depletions which propagated without significant deformation at a velocity slightly below that of the shock [9]. Using an electrostatic energy analyzer and a boxcar integrator we performed measurements of the ion velocity distribution and demonstrated that the density depletions were indeed associated with ion

phase space vortexes separated from the shock by a region of heated ions, in good agreement with the numerical results [1]. For details see Ref. [9].

**3. Numerical Results.** We developed a particle simulation code [10] for a more detailed investigation of the formation of ion vortexes. Using a "moving slug" i.e. an ion beam of finite extent, we may excite one localized vortex with lifetime exceeding at least 100 ion plasma periods. By slowly varying the electron temperature in the code we may then follow the change in characteristic properties of the vortex, e.g. amplitude, velocity, width etc. This procedure ensures that we do have a phase space vortex to begin with i.e. our results have nothing to do with the excitation efficiency of vortexes for various temperature ratios. The moving slug may represent a burst of well correlated particles often observed both in laboratory experiments and computer simulations. Figure 1 shows the velocity  $U$  and amplitude  $\phi_m$  of one ion vortex, for varying temperature ratio,  $T_e/T_0$ , where  $T_0$  is the initial, unperturbed ion temperature. Note that  $\phi_m \rightarrow 0$  at  $T_e/T_0 \sim 3$  i.e. the ion vortex ceases to exist for small temperature ratios. This observation supports analytical results [5].

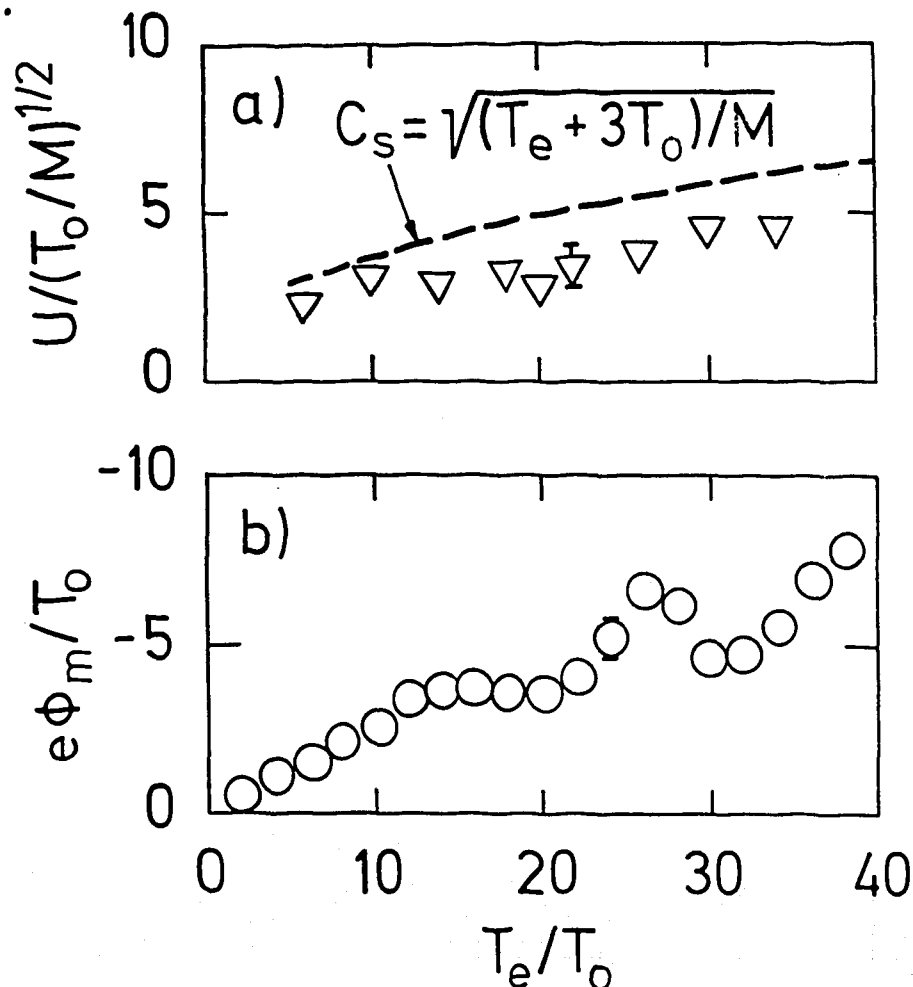


Fig. 1

By introducing the effect of random charge exchange collisions in the code, we demonstrated that the life-time of an ion phase space vortex is roughly one collision period. The code is designed to select ions randomly with a probability proportional to the local density but independent of velocity (corresponding to a constant cross-section for the process). The selected ions are then replaced at the same position but with velocities taken randomly in a Maxwellian distribution, with temperature below that of the initial plasma. The replacement changes the ratio between trapped and untrapped ions associated with the vortex. The resulting configuration will not be an equilibrium solution to the equations and preliminary numerical results seem to indicate that the vortex adjusts itself to the changing conditions by emitting another small vortex before it ultimately damps out.

4. Relation to ion-ion beam instabilities. In order to gain a better understanding of the phenomenon under investigation, we considered a simple cold symmetric ion-ion beam model. Looking for stationary solutions to the problem we obtain the standard form  $\frac{1}{2}(d\phi/dx)^2 + V(\phi) = W$ , with a pseudopotential given by

$$V(\phi) = - (e^\phi + \sigma \sqrt{V_0^2 - 2\phi}) \quad (1)$$

where  $\phi$  is normalized by  $T_e/e$ ,  $x$  by the Debye-length, and  $V_0 > 0$  is the unperturbed ion beam velocity normalized by  $C_s = (T_e/M)^{1/2}$ , the ion sound speed. The coefficient  $\sigma$  is determined through the requirement of overall charge neutrality;  $\lim_{L \rightarrow \infty} (1/2L) \int_{-L}^L \exp(\phi(x)) dx = (\sigma/2L) \int_{-L}^L (V_0^2 - 2\phi(x))^{-1/2} dx$ . Approximately we find  $\sigma = V_0^{\infty}$ . It is readily demonstrated that, for properly chosen  $W$ , solutions  $\phi(x)$  obtained using (1) may have the desired properties characterizing ion phase space vortices, i.e. cusplike spatial structures associated with points where the local ion beam velocity goes to zero. Figure 2 shows pseudopotentials with the approximation  $\sigma = V_0$ . Potential and phase space diagrams corresponding to different values of  $V_0$  and  $W$  are shown schematically. Solitary solutions (i.e. single humped) are found when  $\sigma \exp(-v_0^2/2) > 0.451$ , and they may take the form of two head-on double layers, see Fig. 2c. Note that in the cold ion limit no single vortex solution exists.

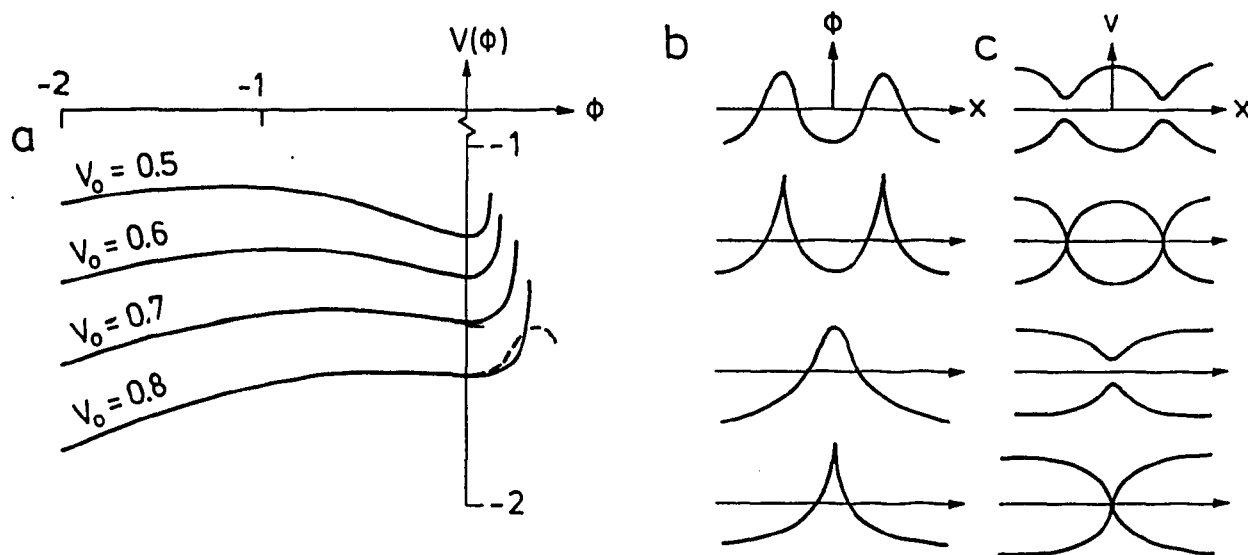


Fig. 2

We found it interesting that the criterion for the existence of bounded (i.e. physically acceptable) solutions for  $\phi(x)$ , namely  $V_0 < 1$ , coincide with the criterion for linear instability for the two ion beams. It thus appears tempting to assume that the stationary solutions derived from (1) represents a final saturated nonlinear stage of this instability. To investigate this conjecture in more detail we derived a nonlinear evolution equation for two counter streaming cold ion beams of equal density.

$$\begin{aligned}
 & \partial_t^4 e^\phi - \partial_x^2 \partial_t^4 \phi - 2V_0^2 \partial_x^2 \partial_t^2 e^\phi + 2V_0^2 \partial_x^4 \partial_t^2 \phi + V_0^4 \partial_x^4 e^\phi \\
 & - V_0^4 \partial_x^6 \phi = - 2V_0 \partial_x^2 \partial_t^2 (V_0^2 - 2\phi)^{\frac{1}{2}} + V_0^5 \partial_x^4 (V_0 - 2\phi)^{-\frac{1}{2}} \\
 & - V_0^3 \partial_x^2 \partial_t^2 (V_0^2 - 2\phi)^{-\frac{1}{2}}
 \end{aligned} \tag{2}$$

This equation retains the correct linear dispersion relation and moreover reproduces (1) with the approximation  $\sigma = V_0$ , for stationary solutions. Equation (2) is derived for the symmetric case where the two beams have the same density. The result will however remain qualitatively the same as long as the beam densities are different but comparable. In deriving (2) we assumed that the temporal evolution of the instability was slow. It is then consistent to ignore  $\partial_t^4 \phi$  and the resulting equation may be integrated twice with respect to  $x$  yielding

$$2\partial_t^2 e^\phi - 2\partial_x^2 \partial_t^2 \phi - V_0^2 \partial_x^2 e^\phi + V_0^2 \partial_x^4 \phi =$$

$$(2/V_0) \partial_t^2 (V_0^2 - 2\phi)^{\frac{1}{2}} - V_0^3 \partial_x^2 (V_0^2 - 2\phi)^{-\frac{1}{2}} + V_0 \partial_t^2 (V_0^2 - 2\phi)^{-\frac{1}{2}} \quad (3)$$

where we assumed  $\phi \rightarrow 0$  for  $x \rightarrow \pm \infty$ . The approximations leading to (3) amounts to ignoring the two stable branches of the linear dispersion relation; after all only the unstable branch leads to finite  $\phi$  for infinitesimal initial perturbations. Some of the properties of Eq. (3) are discussed by Pécseli and Trulsen [7]. Comparison with results of a particle simulation code [7,10] demonstrated that Eq. (3) indeed describes the initial, nonlinear, evolution of the instability very well. The saturation is due to finite temperature effects not included in (2) or (3). They can however easily be included at least quantitatively in the pseudopotential (1) by a simple waterbag model [3,7]. A typical modification of  $V(\phi)$  is shown by the dotted line on Fig. 2. The "cusps" in potential will flatten as  $\phi \rightarrow V_0^2/2$  and now also single vortex solutions are possible. (We emphasize that Eqs. (2)-(3) describe the evolution of a local perturbation of spatially homogenous ion beams, i.e. they are not applicable for e.g. the moving slug problem discussed previously). Some properties of Eq. (3) are demonstrated by Figs. 3a-d. For a linearly unstable case  $V_0 = 0.8$ , Fig. 3a, the perturbation grows and develops potential cusps like those shown on Fig. 2b corresponding to vortex-like structures in ion phase space. A linearly stable case,  $V_0 = 1.2$ , Fig. 3b, will simply give dispersion of the initial perturbation (the symmetry of the problem leads to a break-up of the initial wave packet). For the marginally stable case  $V_0 = 1$ , Fig. 3c, even a small perturbation brings the beams into unstable conditions locally, and the perturbation grows at these positions while not much happens away from these points. Finally, Fig. 3d, we perturb the linearly unstable case  $V_0 = 0.8$  with a wavepacket containing predominantly very short wavelengths which are linearly stable i.e.  $k^2 > (1/V_0^2) - 1$ . This wavepacket will initially disperse like on Fig. 3b, but eventually the growing long wavelength component will dominate, evolving similarly to Fig. 3a, as expected on physical grounds. We thus feel confident that Eq. (3) serves as a useful starting point for more detailed investigations of this particular instability.

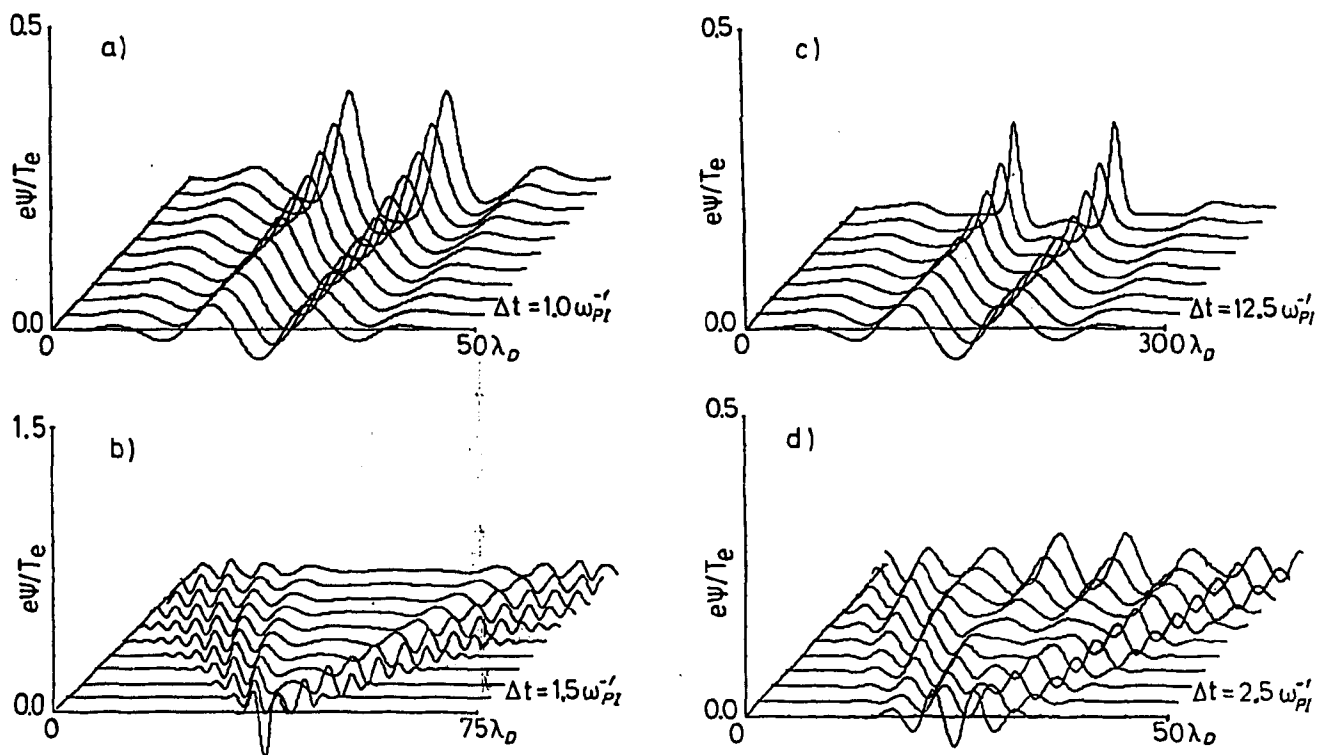


Fig. 3

A comparison with the experimental observations [9] shows that an interpretation as the one suggested here indeed seems fruitful: thus in the experiment a stationary density variation emerges out of an initially noisy two-stream region behind the ion-acoustic shock. The injected beam energy is consistent with the criterion for the two-stream instability and the observed time scales for the evolution agrees with those obtained from the model i.e.  $\sim 10-20 \times (2\pi/\omega_{pi})$ . The strong ion heating in the regions surrounding the ion vortex, was explicitly emphasized in the description of the experimental data, see also Ref. [7].

The analysis outlined hitherto is strictly one dimensional. The selected dimension need not, however, be the direction parallel to the beam velocities, but can be chosen at any angle  $\alpha$  with respect to  $\underline{V}_0$ , resulting in a trivial coefficient  $\cos\alpha$ . Analytical results [11] indicate that ion holes are weakly unstable if the full three dimensional evolution is considered. Their instability seems however to be so weak that it cannot be detected in the laboratory experiment [9], where also other effects are important.

Stable ion phase space vortexes may be a possibility in a strongly magnetized plasma, where we may assume that the ions move essentially along  $\underline{B}$ -field lines. We shall not pursue this problem here, but only mention that the equation (2) can be generalized as

$$\begin{aligned}
& (\partial_t^4 - 2V_O^2 \partial_x^2 \partial_t^2 + V_O^4 \partial_x^4) [e^\phi - \partial_x^2 \phi - \nabla_\perp^2 \phi \\
& - \Gamma (\phi \nabla_\perp^2 \phi + (\nabla_\perp \phi)^2 - \nabla_\perp^2 \phi \partial_x^2 \phi - \nabla_\perp \phi \cdot \partial_x^2 \nabla_\perp \phi - (\nabla_\perp^2 \phi)^2 - \nabla_\perp \phi \cdot \nabla_\perp \nabla_\perp^2 \phi)] = \\
& - 2V_O \partial_x^2 \partial_t^2 (V_O^2 - 2\phi)^{\frac{1}{2}} + V_O^5 \partial_x^4 (V_O^2 - 2\phi)^{-\frac{1}{2}} - V_O^3 \partial_x^2 \partial_t^2 (V_O^2 - 2\phi)^{-\frac{1}{2}}
\end{aligned} \tag{4}$$

where  $\Gamma \equiv (\omega_{pi}/\omega_{ci})^2 \ll 1$ . The ion-cyclotron branch is thus ignored. The properties of a simplified version of Eq. (4) are under investigation.

Saturation mechanisms for the instability differing from the kinetic effects described previously are also considered, and we have derived a model equation based on Eqs. (2)-(4) including such effects. These results will be reported in the future.

5. Conclusions. We may summarize the results of this work as follows: Ion phase space vortexes (or "ion holes") are observed in a laboratory experiment in the two-stream region behind an electrostatic ion acoustic shock [9]. The observed evolution agrees well with the results of one-dimensional numerical results [1,10]. Analytical results based on a simple cold ion beam model indicate that such phase space vortexes represent a natural saturated final stage of ion-ion beam instabilities and a dynamic equation is presented for its initial evolution [7]. The instability is saturated by e.g. particle effects even for very small ion temperatures  $T_i \ll T_e$ , as demonstrated by a numerical particle simulation [10]. These effects can be explained qualitatively by a simple "water-bag" model [7]. We demonstrated that ion vortexes can be excited also by coherent ion bursts [10] and could, using this method in the numerical code, investigate some basic properties of the phase-space structures in question. The relevance of these structures for e.g. double-layer formation in one dimensional systems has already been pointed out [6]. We believe that also some ionospheric observations could be explained in these terms: thus electric field measurements on the S3-3 satellite show frequently occurring small composite spikes of two opposite polarities, see e.g. Fig. 11 in the paper by Carlquist in these proceedings [12] and interpreted there as solitary waves. Such waves would however probably be damped by particle reflection. An interpretation in terms of stable phase space structures thus seems more likely. Note that solitons and ion vortexes are clearly distinguished by the polarity of the associated electric fields, the E-field direction being out of the soliton, but inwards for the vortex.

References

- [1] P.H. Sakanaka, Phys. Fluids 15, 1323 (1972).
- [2] H.L. Berk and K.V. Roberts, Phys. Rev. Lett. 19, 297 (1967);  
H.L. Berk, C.E. Nielsen and K.V. Roberts, Phys. Fluids 13,  
980 (1970); R.L. Morse and C.W. Nielsen, Phys. Rev. Lett.  
23, 1087 (1969).
- [3] M. Kako, T. Taniuti and T. Watanabe, J. Phys. Soc. Jap. 31,  
1820 (1971).
- [4] K. Saéki, P. Michelsen, H.L. Pécseli and J.J. Rasmussen, Phys.  
Rev. Lett. 42, 50 (1979); J.P. Lynov, P. Michelsen, H.L. Pécseli,  
J.J. Rasmussen, K. Saéki and V.A. Turikov, Physica Scripta 20,  
328 (1979).
- [5] S. Bujarbarua and H. Schamel, J. Plasma Phys. 25, 515 (1981).
- [6] A. Hasegawa and T. Sato, Phys. Fluids 25, 632 (1982).
- [7] H.L. Pécseli and J. Trulsen, Phys. Rev. Lett. 48, 1355 (1982).
- [8] H. Ikezi, T. Kamimura, M. Kako and K. Lonngren, Phys. Fluids 16,  
2167 (1973).
- [9] H.L. Pécseli, R.J. Armstrong and J. Trulsen, Phys. Lett. 81A,  
386 (1981).
- [10] J. Trulsen, PICBEAM, a particle-in-cell plasma simulation code  
for phenomena on the ion plasma period timescale. Univ. of  
Tromsø Report (1980).
- [11] H. Schamel, Physics Lett. 89A, 280 (1982).
- [12] M. Tenerin, K. Cerny, W. Lotko and F.S. Mozer, submitted for  
Phys. Rev. Lett. (1982).

Time Evolution of Particle Distributions in a Double Layer

M. Mohan, A.N. Sekar and P.K. Kaw  
Physical Research Laboratory  
Ahmedabad - 380 009 - India.

Abstract :

The time evolution of particle distribution functions in a double layer is studied. By taking a special set of initial distribution functions and the electric field potential, the analysis is carried out numerically using Vlasov and Poisson's equations. The numerical scheme is presented here.

Introduction :

Double layers are shock-like regions in plasma across which very large electric fields exist. These large electric fields are produced by layers of positive and negative charges separated by distances of the order of a few Debye lengths. The plasma within the double layers are far away from being neutral. But when integrated over the whole region, they maintain charge neutrality<sup>1,2</sup>. Such electric fields and charged particles accelerated by them to very high velocities have been detected in many laboratory and magnetospheric plasmas<sup>3,4</sup>.

Double layers as BGK solutions of the Vlasov equation has been studied recently<sup>5</sup>, where it was found that some amount of trapped particles are necessary for their formation and stability.

We are trying to follow the time evolution of particle distribution functions numerically by taking a special set of initial conditions and using the Vlasov and Poisson's equations. In this paper, we give a general outline of our approach.

Time Evolution :

We assume that a potential of the form,

$$\phi = \begin{cases} \phi_0 & x < x_1 \\ \phi_0 \frac{(x-x_2)}{(x_1-x_2)} & x_1 < x < x_2 \\ 0 & x_2 < x < x_3 \\ \phi_0 \frac{(x-x_3)}{(x_4-x_3)} & x_3 < x < x_4 \\ \phi_0 & x_4 < x \end{cases} \quad (1)$$

is created at  $t = 0$ . To be consistent with this, the ion and electron distribution functions at  $t = 0$  are taken to be,

$$f_i(x, u, 0) = \left( \frac{2\pi T_i}{m_i} \right)^{-1/2} \left[ A \delta(x-x_1) + B \delta(x-x_4) + N_0 \right] \cdot \exp \left[ -\frac{m_i u^2}{2T_i} \right] \quad (2)$$

$$f_e(x, u, 0) = \left( \frac{2\pi T_e}{m_e} \right)^{-1/2} \left[ A \delta(x-x_2) + B \delta(x-x_4) + N_0 \right] \cdot \exp \left[ -\frac{m_e (u-u)^2}{2T_e} \right] \quad (3)$$

where

$$A = \frac{\phi_0}{4\pi e(x_2-x_1)} \quad , \quad B = \frac{\phi_0}{4\pi e(x_4-x_3)}$$

and  $u$

is the streaming velocity of the electrons.

Using  $\phi$  given by eq. (1), we solve for the particle trajectories for a small value of time,  $\Delta t$ . Then we have,

$$x = u \cdot \Delta t + \frac{1}{2} \frac{q}{m} \frac{d\phi}{dx} (\Delta t)^2 + x_0 \quad , \quad u = -\frac{q}{m} \frac{d\phi}{dx} \Delta t + u_0 \quad (4)$$

where  $q$  and  $m$  are charge and mass of the particle considered.

Since according to the Vlasov equation,

$$\frac{\partial f}{\partial t} + u \cdot \frac{\partial f}{\partial x} - \frac{q}{m} \frac{d\phi}{dx} \frac{\partial f}{\partial u} = \frac{df}{dt} = 0 \quad (5)$$

the distribution functions do not change along the particle trajectories, we have,

$$f(x, v, \Delta t) = f\left(x - v \Delta t - \frac{1}{2} \frac{qv}{m} \frac{d\phi}{dx} \Delta t^2, v + \frac{qv}{m} \frac{d\phi}{dx} \Delta t, v\right) \quad (6)$$

which we use in the Poisson's equations;

$$\frac{d^2\phi}{dx^2} = 4\pi e \left\{ \int_{-\infty}^{\infty} f_e(x, v, \Delta t) dv - \int_{-\infty}^{\infty} f_i(x, v, \Delta t) dv \right\} \quad (7)$$

and solve for the new form of  $\phi$ . This is used in eq. (4) to find the new trajectories for the next time interval. Then taking the right hand side of (6) as the initial form, we find the new distribution functions. This process is repeated over and over to find the time evolution of the distribution functions.

That part of the distribution functions for which the total energy,  $\omega = \frac{1}{2} m v^2 + q\phi$  is less than  $\phi_c$  correspond to trapped ions or reflected electrons. The time evolution of trapped ion distribution function will be compared with the ones computed using the sudden approximation<sup>6</sup>. The relationship between the stability of a double layer with a given potential drop and the relative streaming between the ions and electrons is also being investigated now.

References :

1. Block, L.P., 1978, Astrophys. and Space Sci. 55, 59.
2. Carlquist, P., 1972, Cosmic Electrodynamics 3 377.
3. Quon, B.H. and Wong, A.Y., 1976, Phys. Rev. Lett. 37 1393
4. Block, L.P., 1975, Physics of the Hot Plasma in the Magnetosphere (ed. Hultquist and Stenflo), 229, Plenum.
5. Knorr, G and Goertz, C.K., 1974, Astrophys. Space Sci. 32 165.
6. Dewar, R.L., 1973, Phys. Fluids, 16, 431.

Modified Korteweg - de Vries Equation for Propagating Double  
Layers in Plasmas

S. Torvén

Department of Plasma Physics, Royal Institute of Technology,  
S-100 44 Stockholm, Sweden

Abstract A modified Korteweg - de Vries equation with a cubic nonlinearity may be used to describe the time evolution of propagating double layers. The asymptotic form of the solution is discussed for a monotonic initial potential profile. The profile may steepen and reach a steady state simultaneously as a number of solitary waves form behind the double layer, resembling the time evolution of experimentally observed profiles. Some physical models, that can be described by this equation, are discussed and necessary conditions on the particle distribution functions are presented.

On the Negative Resistivity of  
Double Layers

By

M.A. Raadu and M.B. Silevitch\*

Royal Institute of Technology, Stockholm, Sweden

\*Permanent Address: Dept. of Electrical Engineering

Northeastern University, Boston, MA 02115, U.S.A.

It is known that large amplitude oscillations can occur in the current flowing through a plasma diode, typically when a constant potential is applied across the device. Burger (J. Appl. Phys. 36, 1938; 1965) suggested via a computer simulation that the oscillation characteristics was a function of the quantities  $\tau_e$  and  $\tau_i$ , namely the respective time for an electron and an ion to cross the electric field region inside the diode. On the rapid time scale  $\tau_e$ , the self consistent equilibrium configuration, was unstable. Norris (J. Appl. Phys. 35, 3260; 1964) had previously arrived at the same conclusion using analytical arguments. In that work, it was concluded that the instability occurred since the diode acted as a negative resistance on the  $\tau_e$  scale. A positive feedback effect forced the system away from equilibrium.

During the later evolution of the system, Burger found that the internal potential structure developed a negative well near the cathode region. This barrier caused current interruption to occur. The system returned to its initial state in a time  $\sim \tau_i$ , and the cycle would then repeat. Recently Iizuka et al (Phys. Rev. Lett., 48, 145; 1982) performed a series of experiments which reproduced the essential features of Burger's simulation.

Silevitch (J. Geophys. Res. 86, 3573; 1981) used the Burger mechanism to suggest an explanation for the flickering aurora phenomenon. He extended the Norris argument and showed by a variational method that a plausible analytic model for a double layer (DL) behaved as a negative resistance on the  $\tau_e$  scale. In this present work we reexamine the Silevitch (1981) results (henceforth referred to as paper 1) by taking a more detailed account of the constraints which are imposed on the various electron distributions which exist within the DL region.

The equilibrium auroral DL model used in paper 1 is taken from the work of Kan and Lee (JGR 85, 788; 1980). The DL potential structure  $\phi(x)$ , varies from  $\phi(x=0) = 0$  to  $\phi(x=d) = \phi_0$ . Moreover, as shown in Figure 4 of paper 1, there are three distinct electron populations associated with the Kan and Lee DL model. These are:

(a) Streaming Electrons Originating at  $\phi(x=0) = 0$

A waterbag velocity distribution is chosen for this population which is simply

$$f_{e1}(\phi) = f_1 = \frac{N_{e1}}{2V_{e1}} \quad , \quad V_L(\phi) < v < V_U(\phi) \quad (1)$$

where  $V_L(\phi) = (2|e|\phi/m)^{1/2}$  and  $V_U(\phi) = [4V_{e1}^2 + V_L^2(\phi)]^{1/2}$ . Here  $N_{e1}$  and  $V_{e1}$  are the density and streaming velocity of the electrons originating at

$x=0$ . Following paper 1 we can easily obtain expressions for the electron density,  $n_{e1}(\phi)$  and its integral  $g_{e1}(\phi) \equiv \int_{\phi=0}^{\phi} n_{e1}(\bar{\phi}) d\bar{\phi}$  at any point  $\phi(x)$  within the DL region. Note that it would be more precise to indicate these quantities as functionals of  $f_{e1}(N_{e1}, V_{e1}, \phi, v)$ .

(b) Trapped degraded primary and secondary electrons originating at  $\phi(x=d) = \phi_0$ .

Again for these particles we use a waterbag distribution  $f_{et}$  of value  $f_t$  centered at  $v=0$  and cut off at  $v = \pm (2|e|\phi/m)^{1/2}$ . Thus,

$$f_t = \frac{N_{et}}{2} \left( \frac{m}{2|e|\phi_0} \right)^{1/2} \quad (2)$$

where  $N_{et}$  is the density of these trapped electrons at  $x=d$ . Again simple expressions for  $n_{et}(f_{et})$  and  $g_{et}(f_{et})$  can be obtained (see paper 1).

(c) Trapped low energy electrons originating at  $\phi(x=d)=\phi_0$ .

A Maxwellian distribution is assumed for this population. It is a full range function characterized by the parameters  $N_{e0} (>> N_{e1})$  and  $kT_{e0} (<< |e|\phi_0)$  which respectively represent the electron density  $n_{e0}$  and thermal energy at  $x=d$ .

If the equilibrium DL structure is perturbed on the  $\tau_e$  time scale then the dynamic resistance of the DL is defined as

$$R_D = \frac{\delta\phi_0}{\delta j} (A)^{-1} . \quad (3)$$

Here  $A$  is the DL cross sectional area and  $\delta j$  ( $\delta\phi_0$ ) represents the electron current density (potential) variations from the equilibrium values

[i.e.  $\phi(x)$  perturbation  $\rightarrow \phi^*(x) = \phi(x) + \delta\phi(x)$ ]. Clearly only the electrons in category (a) contribute to  $j$  and thus,

$$\delta j = \delta(|e|N_{e1}V_{e1}) = |e|V_{e1}\delta N_{e1} + |e|N_{e1}\delta V_{e1} \quad (4)$$

In order to calculate  $R_D$  we need the key result

$$0 = \delta\{g_{e1} + g_{et} + g_{e0}\} \quad (5)$$

This equation is obtained by first multiplying Poisson's equation by  $d\phi/dx$  and then integrating from  $x=0$  to  $x=d$  assuming charge neutrality at both endpoints. Finally, the same procedure is repeated for the perturbed state ( $\phi^*$ ) and the two equations are subtracted keeping only first order terms in the variations like  $\delta\phi$ . It should be noted that to this order in  $\delta\phi$  it is not necessary to impose strict charge neutrality for the perturbed state at  $x=0, d$ . Moreover, a rigorous derivation of (5) would include on the rhs a static ion term  $\delta G_{ion}$  defined by

$$\delta G_i \equiv - \int_{x=0}^d dx n_i(x) \left[ \frac{d\phi^*}{dx} - \frac{d\phi}{dx} \right] \quad (6)$$

where  $n_i(x)$  is the ion density profile in the unperturbed state. In paper 1 this term was neglected. An argument justifying this approximation is presented in the final portion of this paper.

In order to obtain an expression for  $R_D$  we need to specify in detail those constraints that apply during the initial disruption. To illustrate this consider electron population (a). Eq. (4) defines a relation between  $\delta N_{e1}$  and  $\delta V_{e1}$ . Another is needed. For example, in paper 1 it was assumed that  $N_{e1}$  and  $V_{e1}$  were independent and so either  $\delta N_{e1} = 0$  (i.e. strict charge neutrality) or  $\delta V_{e1} = 0$ . Perhaps a more realistic constraint would be to impose the condition  $\delta f_1 = 0$ . This would imply from eq.(1)

$$0 = \delta N_{e1} - \frac{N_{e1}}{V_{e1}} \delta V_{e1} \quad (7)$$

From eqs. (4) and (7) we find

$$\delta N_{e1} = \frac{1}{2} \frac{\delta j}{|e|V_{e1}} \quad , \quad \delta V_{e1} = \frac{1}{2} \frac{\delta j}{|e|N_{e1}} \quad (8)$$

The expression for  $R_D$  is now obtained by expanding eq.(5) as:

$$0 = \left[ \frac{\partial g_{e1}}{\partial N_{e1}} \delta N_{e1} + \frac{\partial g_{e1}}{\partial V_{e1}} \delta V_{e1} + \frac{\partial g_{et}}{\partial N_{et}} \delta N_{et} + \frac{\partial g_{eo}}{\partial N_{eo}} \delta N_{eo} + \Delta \delta \phi_0 \right] \quad (9)$$

where  $\Delta \equiv \frac{\partial g_{e1}}{\partial \phi_0} + \frac{\partial g_{et}}{\partial \phi_0} + \frac{\partial g_{eo}}{\partial \phi_0}$ . Let us first follow paper 1 by

assuming  $\delta N_{e1} = \delta N_{et} = \delta N_{eo} \equiv 0$ . Note that these constraints would not impose strict charge neutrality at  $x=d$ . Using eqs.(4) and (9) we obtain the resistance  $R_1$  given by

$$R_1 = -(\Delta N_{e1} |e|A)^{-1} \frac{\partial g_{e1}}{\partial V_{e1}} \quad (10)$$

If we replace  $\delta N_{e1} = 0$  by condition (7) we find the DL negative resistance  $R_2$  will have the value  $R_2$  where

$$R_2 = (2A|e|\Delta)^{-1} \left[ \frac{\partial g_{e1}}{\partial N_{e1}} \frac{1}{V_{e1}} + \frac{\partial g_{e1}}{\partial V_{e1}} \frac{1}{N_{e1}} \right] \quad (11)$$

For the parameters of the auroral example in paper 1 we find that the two terms in the bracket have roughly the same magnitude and hence  $R_2 \approx R_1$ .

Let us now generalize the constraints on  $\delta N_{et}$  and  $\delta N_{eo}$ . An obvious first step is to assume strict charge neutrality at  $\phi = \phi_0$ . This would imply

$$-\delta n_{e1}(\phi_0) = \delta N_{et} + \delta N_{eo} \quad (12)$$

For simplicity let us also still assume  $\delta N_{e1} = \delta N_{eo} = 0$ . From eqs.(4) and (12) we find that

$$\delta N_{et} = -\{(N_{e1}|e|)^{-1} \frac{\partial n_{e1}}{\partial V_{e1}} \delta j + \frac{\partial n_{e1}}{\partial \phi_0} \delta \phi_0\} \quad (13)$$

the DL negative resistance will now have the value  $R_3$  given by:

$$R_3 = -(N_{e1}|e|A)^{-1} \left[ \Delta - \frac{\partial g_{et}}{\partial N_{et}} \frac{\partial n_{e1}}{\partial \phi_0} \right]^{-1} \left[ \frac{\partial g_{et}}{\partial V_{e1}} - \frac{\partial g_{et}}{\partial N_{et}} \frac{\partial n_{e1}}{\partial V_{e1}} \right] \quad (14)$$

For the parameters of the auroral DL of paper 1 we find that only the  $\partial n_{e1}/\partial V_{e1}$  correction term is important and

$$R_3 \approx \frac{1}{4} R_1 \quad (15)$$

Moreover, if we assumed that it was primarily the low energy population which reacted to maintain charge neutrality (i.e.  $\delta N_{et} = 0$ ,  $\delta N_{eo} = -\delta n_{e1}(\phi_0)$ ), then the resulting negative resistance would be approximately equal to  $R_1$ . A result similar to eq.(15) is obtained if we relax the charge neutrality constraint and assume instead  $\delta f_t = \delta N_{eo} = 0$ .

From the above discussion we conclude that the response of the trapped particle populations will have quite an important effect upon the value of DL negative resistance. According to the theory in paper 1 a smaller value of negative resistance could quench the DL disruption on the  $\tau_e$  time scale. To test this hypothesis we can envisage an experiment which allows the controlled injection of trapped electrons. One could then study the DL disruption characteristics as a function of the trapped electron distributions.

Before concluding this paper we will justify the neglect of  $\delta G_i$  (eq(6)) in eq.(5). The unperturbed electric field of a strong DL structure is primarily nonzero in an interior region of space  $\Delta x (< d)$ . Under the assumption

that the perturbed electric field ( $-\frac{d\phi^*}{dx}$ ) is also confined to essentially the same  $\Delta x$  region we can rewrite eq.(6) as,

$$\delta G_i = \bar{n}_i \int_0^d dx \frac{d}{dx} (\phi^* - \phi) = \bar{n}_i \delta \phi_0.$$

Here  $\bar{n}_i$  is the value of unperturbed ion density in the  $\Delta x$  region. It is given by the expression,

$$\bar{n}_i = \frac{1}{\phi_0} \int_{x=0}^d dx n_i(x) \frac{d\phi}{dx} = \frac{1}{\phi_0} g_i(\phi_0) .$$

For the auroral DL model discussed in paper 1. it can be shown that  $\bar{n}_i \sim 0.1 (\partial g_e / \partial \phi_0)$  and so for this case  $\delta G_i$  can indeed be neglected in eq. (5).

Acknowledgement: The authors would like to thank L. P. Block, C-G Falthammar, L. Lindberg and S. Torvén for their stimulating discussions during the course of this work. For one of us (M.B.S.) this research was supported by AFOSR grant 78-3731.

## RELATIVISTIC EFFECTS IN ELECTROSTATIC DOUBLE LAYERS

Michael A. Raadu

Royal Institute of Technology, Department of Plasma Physics,  
S-100 44 Stockholm 70, Sweden

Abstract: Relativistic effects must be taken into account in calculating the structure of double layers when the potential difference is sufficiently high. In relativistic double layers both ions and electrons are accelerated up to relativistic energies and their dynamics are consequently modified, whereas in the semi-relativistic case only the electron motion is significantly affected. Relationships have previously been derived between double-layer parameters including the effects of relativistic dynamics. For non-zero injection velocities a separate relation is here found between the double layer potential and the boundary parameters. An approximate expression is found for the dependence of the potential difference on the current and thickness of a semi-relativistic double layer.

### 1. Introduction

Much of recent theoretical work on electrostatic double layers (for a review see Carlqvist, 1979) has been devoted to the non-relativistic case. This emphasis is in part due to the stimulus from laboratory studies (cf. Torvén, 1979, for a review of these) and from the evidence which has been obtained for the existence of double layers in the magnetosphere. However in an application to solar flares (Alfvén and Carlqvist, 1967) it was clear that estimates of the current and energy release rates required potential drops of the order  $10^9$  Volts, so that particles must be accelerated up to relativistic energies. Carlqvist (1969) presented an analysis of double layers similar to that of Langmuir (1929) but including relativistic effects. In the strongly relativistic case he found a simple approximate relation between the current, voltage and thickness (ibid). Apart from modifications in the relations between external parameters, there is also a significant modification of the internal structure (Carlqvist, 1969, 1982). The analysis presented here first of all follows that of Carlqvist (1969). An approximate form of the double layer relation for the intermediate, semi-relativistic,

case where only the electrons are relativistic will be derived. Also in a similar treatment to that of Levine and Crawford (1979), but here in the relativistic form, the effects of finite particle injection velocities are calculated.

## 2. The Langmuir Double Layer

Following Langmuir's (1929) treatment of a non-relativistic double layer, the relation between the electron current  $|i_e|$ , double layer thickness  $d$ , and voltage drop  $\phi_{DL}$  may be derived

$$|i_e| d^2 = (4C_0 \epsilon_0 / 9) \sqrt{2e/m_e} \phi_{DL}^{3/2} \quad (1)$$

where the Langmuir relation between the electron and ion currents,  $i_e/i_i = \sqrt{m_i/m_e}$ , holds. The constant  $C_0$ , which Langmuir found to be 1.86, is given by the integral

$$C_0 = \left\{ \frac{3}{4} \int_0^1 \left\{ \sqrt{y} + \sqrt{1-y} - 1 \right\}^{1/2} dy \right\}^2$$

and may be evaluated in terms of elliptic integrals  $\mathbb{E}$  and  $\mathbb{K}$

$$C_0 = 2^{-1/2} \left\{ 4 \mathbb{E}(\sin \pi/8) - (1+2\sqrt{2}) \mathbb{K}(\sin \pi/8/\sqrt{2}) \right\}^2$$

From tables of elliptic integrals  $C_0 = 1.86518$  to five figure accuracy.

## 3. Relativistic Double Layers

The structure of a double layer follows from integrating the Poisson equation

$$\frac{d^2 \phi}{dz^2} = - \epsilon_0^{-1} \sum_j q_j n_j(\phi) \quad (2)$$

where for given distributions of particle velocities the density  $n_j$  of the  $j$ -th component with charge  $q_j$  is a known function of the potential  $\phi$ . A first integration then gives the stress balance equation

$$\sum_j P_j(\phi) - \epsilon_0 E^2/2 = P_0 \quad (3)$$

where  $P_0$  is a constant,  $E$  the electric field and  $P_j$  the total pressure of a particle species. The generalised Langmuir relation for the particle fluxes follows by equating the total stresses at the edges of the double layer ( $\phi = 0, \phi_{DL}$ ) where by definition the electric field  $E$  is assumed to be zero,

$$\sum_j \left\{ P_j(\phi_{DL}) - P_j(0) \right\} = 0 \quad (4)$$

If we now take the special case of cold particle beams with finite injection velocities  $v_j$ , including relativistic effects, the electron (dynamic-) pressure is

$$P_e(\phi) = (|i_e|/c) \sqrt{(\phi + (\gamma_e - 1)u_e)(\phi + (\gamma_e + 1)u_e)}$$

where  $\gamma_e = (1 - v_e^2/c^2)^{-1/2}$  and  $u_e = m_e c^2/e$ . A similar expression holds for the ions but with  $\phi$  replaced by  $(\phi_{DL} - \phi)$ . For zero initial velocity ( $\gamma_e = 1$ ) the expression found by Carlqvist (1969, Equation (5)) may be recovered.

From Equation (4) the relativistic Langmuir condition may now be found

$$\frac{i_e}{i_i} = \frac{\sqrt{(\phi_{DL} + (\gamma_i - 1)u_i)(\phi_{DL} + (\gamma_i + 1)u_i)} - \sqrt{\gamma_i^2 - 1} u_i}{\sqrt{(\phi_{DL} + (\gamma_e - 1)u_e)(\phi_{DL} + (\gamma_e + 1)u_e)} - \sqrt{\gamma_e^2 - 1} u_e} \quad (5)$$

In the non-relativistic case Levine and Crawford (1979) solved this relation to give an explicit expression for the double layer potential  $\phi_{DL}$ . Here for the relativistic case it is only possible to find a cubic equation for  $\phi_{DL}$ . The resulting expression is cumbersome and not immediately useful. It is therefore not given here.

#### 4. Semi-relativistic Double Layers

We now return to the case where the injected particles have negligible velocities. Setting  $\gamma_{i,e} = 1$  in Equation (5) then gives the corresponding relativistic form of the Langmuir condition (cf. Carlqvist, 1969). For a semi-relativistic case where relativistic effects are only significant for the electrons an approximate analysis may be made assuming that the electrons are strongly relativistic ( $P_e \approx |i_e| \phi/c$ ) and that the ions are non-relativistic. Imposing the condition that the electric field is zero at the edges of the double layer Equation (3) then gives

$$\frac{\epsilon_0}{2} \left( \frac{d\phi}{dz} \right)^2 = - \frac{|i_e|(\phi_{DL} - \phi)}{c} + |i_i| \left( \frac{2m_i}{e} \right)^{1/2} \sqrt{\phi_{DL} - \phi}$$

Putting  $\phi = \phi_{DL}(1 - \sin^4 \theta)$  this expression may be integrated across the double layer to give

$$|i_e| d^2 = \left( \frac{\pi^2 \epsilon_0 c}{2} \right) \phi_{DL} \quad (6)$$

with the corresponding Langmuir condition  $i_e/i_i = \sqrt{2m_i c^2/e} \phi_{DL}$  in the semi-relativistic approximation. Notice that the ion current is then given by

$$|i_i| d^2 = (\pi^2 \epsilon_0 / 4) \sqrt{2e/m_i} \phi_{DL}^{3/2} \quad (7)$$

so that in the semi-relativistic approximation the ion current has the same power law dependence on the double layer potential as in the non-relativistic case but is larger by a factor 2.98. The electron current has a weaker dependence on the potential. In the highly relativistic case Carlqvist (1969) finds

$$|i_e| d^2 = \frac{2\epsilon_0 e}{m_i c} \phi_{DL}^2$$

and  $|i_e|/|i_i| \approx 1$ .

## 5. Discussion and Conclusions

A graph of the relationship between  $\phi_{DL}$  and  $i d^2$ , where  $i = |i_i + i_e|$  is the total current, may be found numerically for all regimes (Carlqvist, 1969). In Figure 1 the results of such an integration are compared with the non-relativistic, semi-relativistic and highly relativistic approximations. The semi-relativistic case (dashed curve) is calculated using Equations (6) and (7), giving a stronger dependence of the double layer potential  $\phi_{DL}$  on  $i d^2$ . This is in agreement with the exact calculation, as may also be seen from the graph given by Carlqvist (1969) which shows a steepening in the semi-relativistic range. We conclude that the approximation for this range ( $u_e < \phi_{DL} < u_i$ ) derived here, Equations (6) and (7), gives a good representation of the functional relations.

## References

- Alfvén, H. and Carlqvist, P.: 1967, Currents in the Solar Atmosphere and a Theory of Solar Flares, *Solar Phys.* 1, 220.
- Carlqvist, P.: 1969, Current Limitation and Solar Flares, *Solar Phys.* 7, 377.
- Carlqvist, P.: 1979, Some Theoretical Aspects of Double Layers, Wave Instabilities in Space Plasmas, Astrophysics and Space Science Book Series, Eds P.J. Palmadesso and K. Papadopoulos, D. Reidel Publ. Comp., Dordrecht, Holland, p. 83.

Carlqvist, P.: 1982, On the Physics of Relativistic Double Layers, to appear in Astrophys. Space Sci.

Langmuir, I.: 1929, The Interaction of Electron and Positive Ion Space Charges in Cathode Sheaths, Phys. Rev. 33, 954.

Levine, J.S. and Crawford, F.W.: 1980, A Fluid Description of Plasma Double-Layers, J. Plasma Phys. 23, 223.

Torvén, S.: 1979, Formation of Double Layers in Laboratory Plasmas, Wave Instabilities in Space Plasmas, Astrophysics and Space Science Book Series, Eds P.J. Palmadesso and K. Papadopoulos, D. Reidel Publ. Comp., Dordrecht, Holland, P. 109.

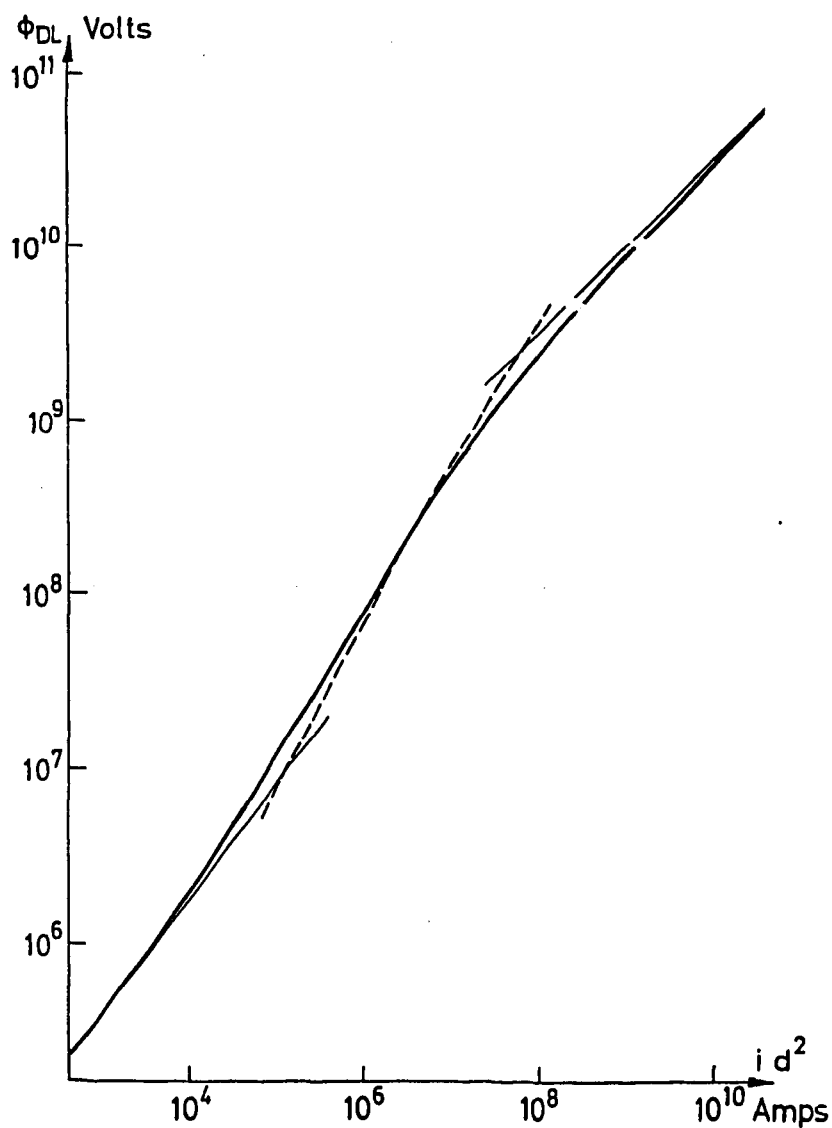


**Figure 1.** The double-layer potential  $\phi_{DL}$  in Volts is plotted as a function of  $id^2$ , where  $i$  is the total current and  $d$  the thickness, for the case of hydrogen ions. The semi-relativistic approximation (dashed curve) gives a fair representation of the exact numerical result (heavy solid curve) in the appropriate range. Straight lines indicate the power law relations for the non-relativistic and highly relativistic regimes.

## THEORY AND STRUCTURE OF RELATIVISTIC DOUBLE LAYERS

P. Carlqvist

Royal Institute of Technology, Department of Plasma Physics,  
S-100 44 Stockholm, SwedenAbstract

A model of a strong, time-independent, and relativistic double layer is studied. The model describes double layers having the electric field parallel to the current as well as a certain type of oblique double layers. From the model the "Langmuir condition" and the potential drop of the double layer are derived. In addition to this the distributions of the charged particles, the electric field, and the potential within the double layer are discussed.

1. Introduction

During the last few decades a considerable number of papers have been published suggesting that double layers may occur in cosmic plasmas. For instance, it has been proposed that double layers may appear in the solar atmosphere (Alfvén and Carlqvist, 1967; Carlqvist, 1969, 1979), in the ionosphere and magnetosphere of the Earth (see e.g. Block, 1978; Carlqvist, 1982a, and references therein), and even in double radio sources (Alfvén, 1978). Among these cosmic double layers the ionospheric and magnetospheric layers are generally considered to be non-relativistic implying that the potential drops of the layers,  $\phi_{DL}$ , are so small that neither ions nor electrons are accelerated to relativistic velocities. The solar and galactic double layers on the other hand are supposed to be relativistic accelerating both ions and electrons to relativistic velocities.

Hence we see that both relativistic and non-relativistic double layers are thought to occur in cosmic plasmas. The theory of non-relativistic double layers has been developed in a number of papers whereas the theory of relativistic double layers has not been so well investigated. It is the aim of the present paper to study a simple relativistic double layer model. By means of this model we shall work out some basic relationships and briefly describe the structure of the relativistic double layer. For a more detailed discussion on relativistic double layers see Carlqvist (1982b).

2. The Model

We consider a simple model of a strong and time-independent double layer with plane geometry (Figure 1). The double layer is confined between two plane surfaces - the cathode boundary at potential  $\phi = 0$  and the anode boundary at potential  $\phi = \phi_{DL}$  (cf. Langmuir, 1929; Carlqvist, 1969). Positive and negative

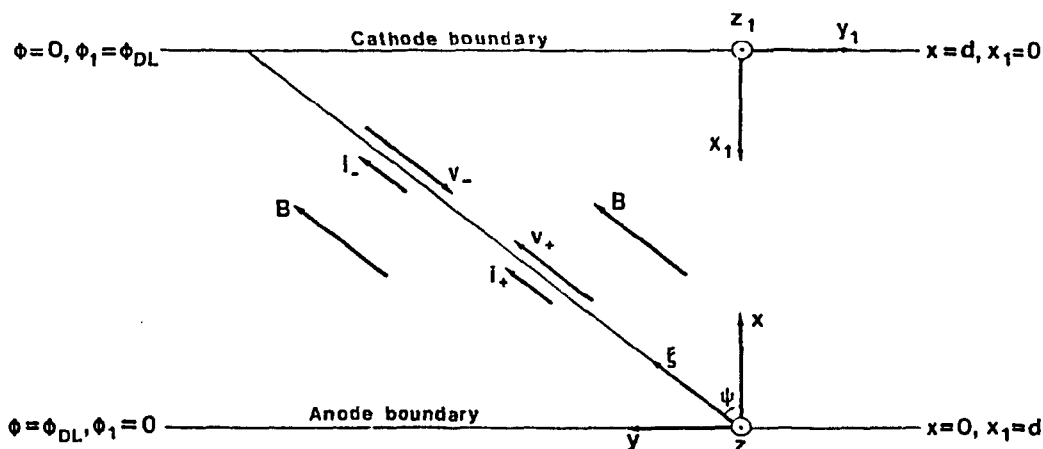


Fig. 1. Model of the double layer.

particles are emitted with zero velocity from the anode and cathode boundaries respectively. It is assumed that the double layer is penetrated by a uniform magnetic field,  $\underline{B}$ , being so strong that both particle species are fully magnetized. Hence, when accelerated by the electric field inside the double layer all the particles are forced to move along the magnetic field lines. The angle between  $\underline{B}$  and the normals of the boundaries is  $\psi$ .

The variation of the potential in the double layer must be consistent with the net space charge of the accelerated particles as described by Poisson's equation. In order to simulate a real double layer surrounded by quasi-neutral plasma as well as possible we assume that the electric field is zero at both the anode and the cathode boundaries. This arrangement ensures that no surface charges exist at the boundaries of the layer and that the layer as a whole is electrically neutral.

For the further analysis we introduce two orthogonal systems of coordinates  $(x, y, z)$  and  $(x_1, y_1, z_1)$  and a  $\xi$ -axis parallel with  $\underline{B}$  in accordance with Fig. 1. To simplify the calculations we also put  $\phi_1 = \phi_{DL} - \phi$ .

### 3. Some Properties of the Relativistic Double Layer

Inside the double layer the positively and negatively charged particles are accelerated by the electric field in opposite directions being aligned with the magnetic field. From the law of conservation of energy we obtain

$$Ze\phi_1 = \frac{m_+c^2}{\left(1 - \frac{v_+^2}{c^2}\right)^{1/2}} - m_+c^2 \quad (3.1)$$

$$e\phi = \frac{m_-c^2}{\left(1 - \frac{v_-^2}{c^2}\right)^{1/2}} - m_-c^2 \quad (3.2)$$

for the positive and negative particles respectively. Here  $Ze$ ,  $m_+$ , and  $v_+$  are the charge, mass, and velocity of the positive particles and  $-e$ ,  $m_-$ , and  $v_-$  are the corresponding quantities for the negative particles while  $c$  is the velocity of light. Using the current densities of the positive and negative particles,  $i_+ = Ze n_+ v_+$  and  $i_- = -e n_- v_-$ , and Equations (3.1) and (3.2) and inserting the densities of the positive and negative particles,  $n_+$  and  $n_-$ , into Poisson's equation we obtain

$$\frac{d^2\phi}{dx^2} = -\frac{e}{\epsilon_0} (Z n_+ - n_-) = -\frac{i_+}{\epsilon_0 c} \cdot \frac{\phi_1 + \phi_+}{(\phi_1^2 + 2\phi_1\phi_+)^{1/2}} + \frac{i_-}{\epsilon_0 c} \frac{\phi + \phi_-}{(\phi^2 + 2\phi\phi_-)^{1/2}} \quad (3.3)$$

where  $\phi_+ = m_+ c^2 / Ze$  and  $\phi_- = m_- c^2 / e$ . It is to be noticed that although the positive and negative particles move parallel or anti-parallel to the  $\xi$ -axis the gradients of the densities of the particles are directed perpendicular to the boundaries. Hence the gradient of the potential must also be perpendicular to the boundaries according to Poisson's equation.

After multiplying both sides of Equation (3.3) by  $2d\phi/dx = -2d\phi_1/dx$  we integrate and get

$$\left(\frac{d\phi}{dx}\right)^2 = \frac{2i_+}{\epsilon_0 c} (\phi_1^2 + 2\phi_1\phi_+)^{1/2} + \frac{2i_-}{\epsilon_0 c} (\phi^2 + 2\phi\phi_-)^{1/2} - C \quad (3.4)$$

where  $C$  is a constant of integration. This equation expresses the momentum balance in the double layer. Since the electric field tends to zero at the two boundaries,  $d\phi/dx = 0$  for  $\phi = 0$  and  $\phi = \phi_{DL}$ , we find from Equation (3.4)

$$C = \frac{2i_+}{\epsilon_0 c} (\phi_{DL}^2 + 2\phi_{DL}\phi_+)^{1/2} = \frac{2i_-}{\epsilon_0 c} (\phi_{DL}^2 + 2\phi_{DL}\phi_-)^{1/2} \quad (3.5)$$

From Equation (3.5) we get the ratio of the current densities usually referred to as the Langmuir condition

$$\frac{i_+}{i_-} = \left( \frac{\phi_{DL} + 2\phi_-}{\phi_{DL} + 2\phi_+} \right)^{1/2} \quad (3.6)$$

For non-relativistic double layers implying,  $\phi_{DL} \ll \phi_- \leq \phi_+$ , the current ratio may be approximated by  $i_+/i_- \approx Z^{1/2}(m_-/m_+)^{1/2}$ . With  $Z = 1$  this expression is the same as the current ratio found by Langmuir (1929) for his non-relativistic and non-oblique ( $\psi = 0$ ) double layer model carrying electrons and singly ionized ions.

For relativistic double layers having potential drops,  $\phi_{DL} \gg \phi_+ \geq \phi_-$ , we obtain from Equation (3.6) the current ratio  $i_+/i_- \approx 1$ . In Fig. 2 the variation of  $i_+/i_-$  with  $\phi_{DL}$  is shown for three different double layers carrying 1)  $\alpha$ -particles and electrons, 2) protons and electrons, and 3) positrons and

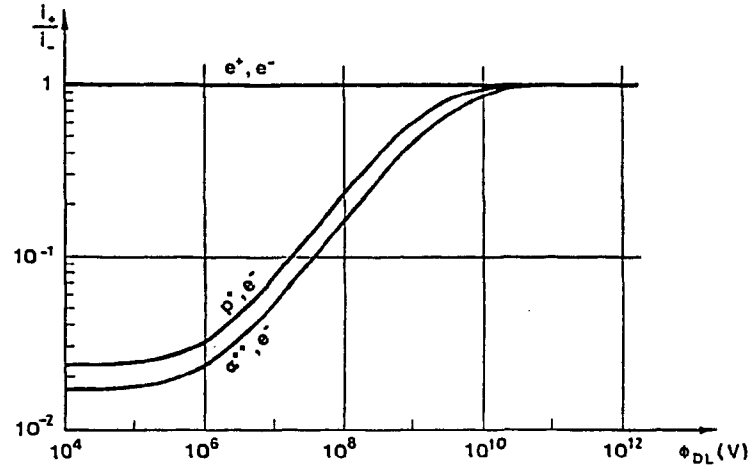


Fig. 2. Current ratio,  $i_+/i_-$ , as a function of potential drop,  $\phi_{DL}$ , for three different double layers.

electrons.

Combining Equations (3.4) and (3.5) we find the general expression for the electric field in the double layer

$$-\frac{d\phi}{dx} = \left\{ \frac{2 i_-}{\epsilon_0 c} \left[ \left( \frac{\phi_{DL} + 2\phi_-}{\phi_{DL} + 2\phi_+} \right)^{1/2} (\phi_+^2 + 2\phi_+ \phi_+)^{1/2} + (\phi_-^2 + 2\phi_- \phi_-)^{1/2} - (\phi_{DL}^2 + 2\phi_{DL} \phi_-)^{1/2} \right] \right\}^{1/2} \quad (3.7)$$

For a relativistic double layer this expression may be simplified and integrated across the layer yielding the potential drop of the layer

$$\phi_{DL} \approx \frac{(\phi_+^{1/2} + \phi_-^{1/2})}{2(\epsilon_0 c)^{1/2}} i^{1/2} d \quad (3.8)$$

where  $i = i_+ + i_-$  is the total current (Carlqvist, 1982b). In the case where the positive and negative charges consist of ions and electrons the potential drop may be approximated by

$$\phi_{DL} \approx \frac{1}{2} \left( \frac{\phi_+}{\epsilon_0 c} \right)^{1/2} i^{1/2} d \quad (3.9)$$

The potential drop of the double layer in the non-relativistic limit,  $\phi_{DL} \ll \phi_- \leq \phi_+$ , may in a similar way be shown to be

$$\phi_{DL} = \left\{ \frac{1}{C_1} \frac{g}{4 \epsilon_0} \left[ 1 + Z^{1/2} \left( \frac{m_-}{m_+} \right)^{1/2} \right] \left( \frac{m_-}{2e} \right)^{1/2} \right\}^{2/3} i^{2/3} d^{4/3} \quad (3.10)$$

(Carlqvist, 1982b), where  $C_1 \approx 1.865$  (Raadu, 1980). Putting  $Z = 1$  this is the same expression as the one derived by Langmuir (1929) for his double layer.

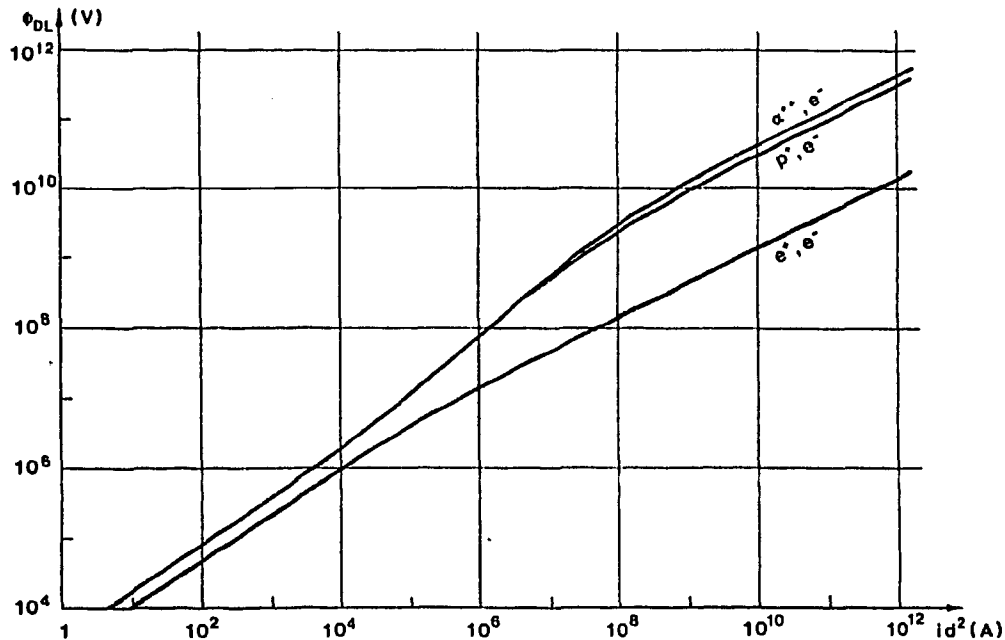


Fig. 3. Potential drop,  $\phi_{DL}$ , as a function of  $id^2$  for three different double layers.

A plot of the potential drop,  $\phi_{DL}$ , as a function of,  $id^2$ , is shown in Fig.3 for three different double layers carrying 1)  $\alpha$ -particles and electrons, 2) protons and electrons, and 3) positrons and electrons. Here Equations (3.8) and (3.10) have been used in the non-relativistic and relativistic regimes respectively, while in the intermediate regime the electric field has been integrated numerically.

It is to be noticed that the angle,  $\psi$ , never enters into the equations derived. This implies that with the model considered all the equations are valid for any value of  $\psi$

#### 4. Structure of Relativistic Double Layers

The relativistic double layer may as regards the distribution of charges,  $Z n_+(x)$  and  $n_-(x)$ , be divided into three principal regions: Two density spike regions close to the boundaries with positive and negative charges and one region in between having low and almost constant charge densities (Fig.4). In the regions of the spikes the particles are accelerated while in the intermediate region the particles move with almost the velocity of light. If the particles consist of ions and electrons the positive spike contains much more charge (absolute value) than the negative spike. The net positive charge of the spikes is balanced by a negative charge distributed evenly in the intermediate region. In this case the electric field decreases nearly linearly from a maximum value close to the anode to almost zero close to the cathode. Hence the potential distribution has a parabolic shape.

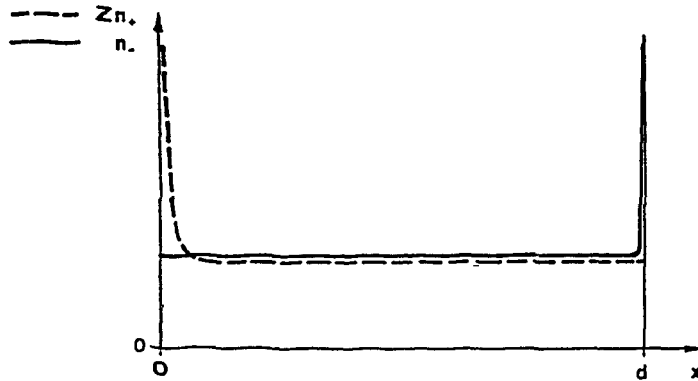


Fig. 4. Distributions of positive and negative charges,  $Zn_+$  and  $n_-$ , as functions of  $x$  in a relativistic double layer.

If on the other hand the particles consist of e.g. positrons and electrons, the charges in the two spikes are equal but of opposite sign and there is no charge in the intermediate region. Now the electric field is constant in most of the double layer so that the potential varies linearly. For this double layer the distributions of charge, electric field, and potential resemble those of a parallel-plate condenser.

#### Acknowledgements

I wish to thank Dr M.A. Raadu for many helpful comments.

#### References

- Alfvén, H.: 1978, *Astrophys. Space Sci.*, 54, 279.  
 Alfvén, H. and Carlqvist, P.: 1967, *Solar Phys.*, 1, 220.  
 Block, L.P.: 1978, *Astrophys. Space Sci.*, 55, 59.  
 Carlqvist, P.: 1969, *Solar Phys.*, 7, 377.  
 Carlqvist, P.: 1979, *Solar Phys.*, 63, 353.  
 Carlqvist, P.: 1982a, in the present volume.  
 Carlqvist, P.: 1982b, to be published in *Astrophys. Space Sci.*  
 Langmuir, I.: 1929, *Phys. Rev.*, 33, 954.  
 Raadu, M.A.: 1980, private communication.

Title: DOUBLE LAYER INDUCED AURORAL KILOMETRIC RADIATION

Authors: Sarbeswar Bujarbarua<sup>1</sup> and Mitsuhiro Nambu<sup>2</sup>

Institution :1. Department of Physics, Dibrugarh University,  
and address            sity, Dibrugarh - 786 004, India

2. College of General Education, Kyushu  
University, Fukuoka 810, Japan

### Abstract

In this paper, we wish to establish a close correlation between Auroral Kilometric Radiation and Double Layers. This correlation has, so far, been ignored by previous theoreticians, although it has been confirmed by experimental observations. Specifically, it will be shown that the enhanced extra-ordinary (X-mode) radiation occurs through the induced bremsstrahlung interaction between auroral beam electrons and double layer potentials. During magnetospheric substorm, the energetic electrons ( $\sim 1$  KeV) are injected from the plasma sheet. The interaction between the high energy electrons and the low energy ( $\sim 1$  eV) background electrons generate double layers for the altitude range 1-3 Earth radii along the auroral field lines. The strong AKR occurs due to the induced bremsstrahlung interaction between double layer potential and beam electrons. Using typical plasma parameters, the growth rate of this radiation is found to be larger than those of all previous proposals.

AN UNUSUAL DOUBLE LAYER PRODUCED  
BY PONDEROMOTIVE-FORCE EFFECTS

J.G. Laframboise

Physics Department, York University  
Toronto, Canada M3J 1P3

ABSTRACT

The 'ponderomotive-force' effect causes strong repulsion of electrons from the region close to an intensely driven antenna in a space plasma. Under certain conditions, the resulting disturbed sheath around the antenna includes a region which has the essential properties of a double layer, but differs in various ways from the more usual types of double layer.

I. INTRODUCTION

When a cylindrical antenna, such as those used for ionospheric sounding from spacecraft, is driven at a large-amplitude RF voltage in a plasma with large enough mean-free-path, electrons near it are strongly repelled from it because of a nonlinear effect of the RF field, called the 'ponderomotive-force' effect. This repulsion arises because of the radial oscillations performed by the electrons in the near field of the antenna. At the innermost end point of such an oscillation (the point nearest the antenna) the outward force due to the near field is stronger than it would be at the same instant at the central point of the oscillation. Conversely, at the outermost end point, the inwardly directed force is weaker. Therefore, there is a net time-averaged force on the electrons, and to a much smaller extent on ions, directed away from the antenna. This force is strong enough to create a region around the antenna which is almost completely depleted of electrons and may therefore contain a net positive time-averaged space charge. In some cases, the total of this positive charge can be larger than the negative time-averaged charge which will reside on the surface of the antenna if the latter has a negative time-averaged voltage offset relative to space. In such cases, this positive region must therefore be balanced by another, negative space-charge region which is located outside of it. We thus obtain the type of charge separation which is characteristic of a double layer.

In this paper, we present numerical sheath solutions, originally obtained by Laframboise et al (1975), which show such behaviour. These solutions have been obtained by replacing the actual time-dependent force

on electrons by its time-average, which is the gradient of a scalar function of position called the 'ponderomotive potential'. The presence of this time-averaged force is therefore equivalent to the existence of an additional term in the static potential as seen by electrons. Therefore, it can be easily incorporated into the self-consistent numerical treatment of a cylindrical electrode (Langmuir probe) in a collisionless plasma, already developed for the time-independent case (Laframboise, 1966a,b). The results which we present here (Sec. III) have been obtained in this way.

## II. THEORY

We assume that after the time-averaging described in Sec. I, the resulting cylindrical sheath is time-independent. We thus exclude the possibility that self-sustaining oscillations, perhaps at some frequency other than that of the imposed RF voltage, may occur in the sheath. We assume cylindrical symmetry, and we therefore exclude flow and magnetic-field effects. We neglect RF (but not electrostatic) forces on ions. We assume that the antenna surface is a perfect absorber of charged particles. We assume that the surrounding plasma is collisionless and Maxwellian, and that ion temperature  $T_i$  = electron temperature  $T_e \equiv T$ . The latter assumption is not essential to our treatment, but is sufficiently applicable to space plasmas for our purposes. We assume that the frequency  $\omega$  of the RF is much larger than the electron plasma frequency  $\omega_{pe}$ , so that the near-field RF electric field amplitude  $E_1$  can be approximated by its vacuum-field limiting form. We consider only cylindrical radii  $r \ll$  RF wavelength  $\lambda$ , so that over most of the antenna length, the instantaneous near field has the same position dependence as the static Coulomb field of an infinite cylinder. These assumptions are generally valid near the upper end of the frequency range used by ionospheric sounding satellites (Rubinstein and Laframboise 1970, Laframboise et al 1975).

It has been shown by a small-amplitude perturbation analysis (Boot et al, 1958) that the time-averaged, 'ponderomotive' force on electrons is

$$-(q^2/4m\omega^2)\nabla(E_1^2) \quad (1)$$

where  $q$  and  $m$  are electron charge and mass. The 'ponderomotive (additional) potential'  $\phi_a$  for electrons therefore is given by

$$\phi_a = (q/4m\omega^2)E_1^2 \quad (2)$$

With our assumptions, the RF electric field has the form

$$\vec{E}_{rf} = \vec{n}_r (c_1/r) \cos \omega t = \vec{E}_1 \cos \omega t \quad (3)$$

Substitution in (2) then yields:

$$\phi_a = (qc_1^2 / 4m\omega^2) / r^2 \quad (4)$$

We now introduce a nondimensional additional antenna potential  $G$  as follows:

$$G = \frac{q\phi_{aA}}{kT} = \frac{q^2 c_1^2}{4m\omega^2 r_A^2 kT} \quad (5)$$

where  $\phi_{aA}$  and  $r_A$  represent additional potential and radius at the antenna surface,  $k$  is Boltzmann's constant, and  $q = -e$ , where  $e > 0$  is the elementary charge. The input parameters for the static sheath calculations (Laframboise 1966a,b) are then three in number: the value of  $G$ , the value of nondimensional antenna static potential  $\chi_A = e\phi_A/kT$ , and the antenna Debye ratio  $r_A/\lambda_D = r_A(e^2 n_\infty / \epsilon_0 kT)^{1/2}$ . Here  $n_\infty$  is electron or ion number density far from the antenna, and  $\epsilon_0$  is the permittivity of free space. As already mentioned, we have eliminated  $T_i/T_e$  as a parameter by assuming  $T_i = T_e$  throughout. Standard antenna theory can be used (Laframboise et al, 1975) to find values of  $G$  for specific cases.

### III. RESULTS AND DISCUSSION

Figure 1 shows numerically-calculated ion and electron density profiles for various values of  $G$  for  $r_A/\lambda_D = 0.5$  and  $e\phi_A/kT = -25$ . Values of  $G$  occurring in spacecraft sounding experiments encompass the range shown (Rubinstein and Laframboise 1970, Laframboise et al 1975). Ponderomotive-force effects evidently cause large changes in these profiles, including enlargement of the sheath to many times the size which it has in the absence of RF. Also visible for  $G=10^3$  and  $10^4$  is a change in the sign of the net space charge from positive at smaller radii to negative at larger radii, verifying the existence of the double-layer behaviour mentioned in Sec. I. As  $r \rightarrow \infty$ , the density profiles approach the asymptotic form (Getmantsev and Denisov, 1962; Rubinstein and Laframboise, 1970, Section 3):

$$n_i = n_e = n_\infty \exp(-\frac{1}{2}Gr_A^2/r^2) \quad (6)$$

Figure 2 shows static potential profiles for conditions corresponding to those of Figure 1. This figure has been plotted logarithmically in radius because doing this causes the potential profiles in the absence of space charge to appear as straight lines. For  $G=10^3$  and  $10^4$ , the transitions from positive to negative net space charge are visible as inflection points in these profiles at values of  $r/r_A$  of about 25 and 50, respectively. The same curves also show barriers of static potential rising to a few times  $kT$  when  $G=10^4$ . These barriers substantially reduce ion collection by the antenna when its static potential is negative (Laframboise

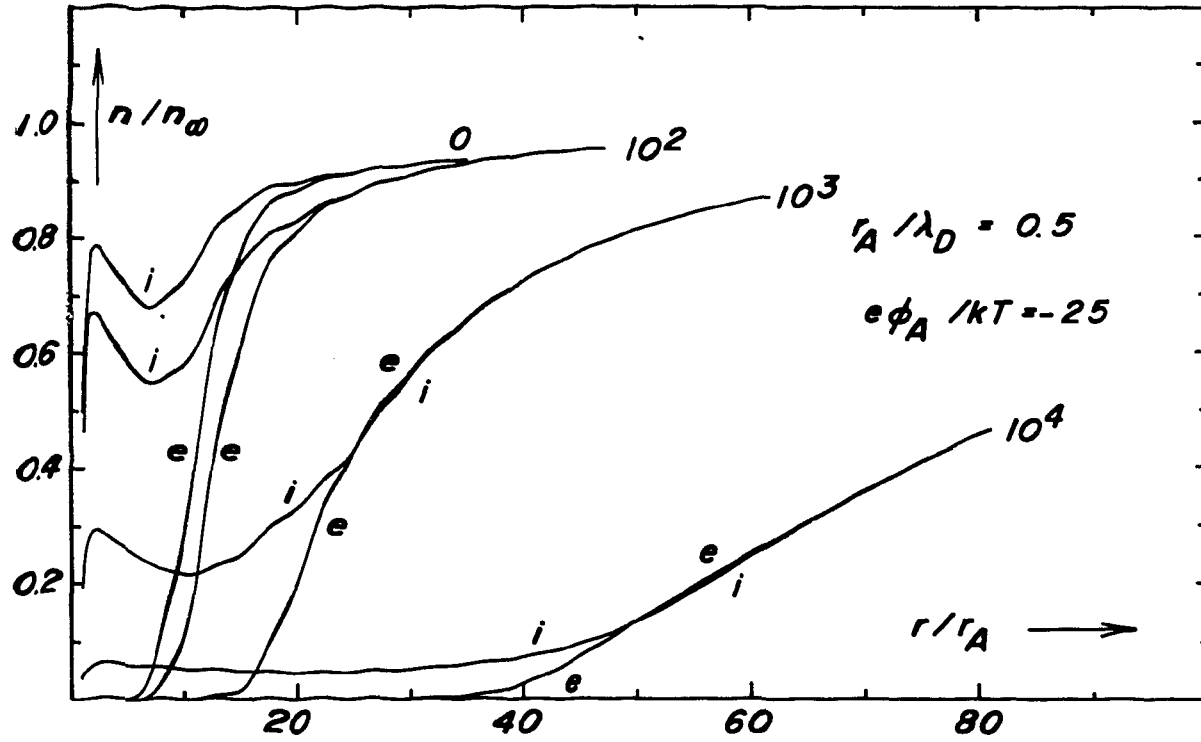


Fig. 1. Ion and electron number densities  $n_i$  and  $n_e$  as functions of radius  $r$  for  $r_A / \lambda_D = 0.5$ ,  $e\phi_A / kT = -25$ , and various values of the radiation strength parameter  $G = q^2 c_l^2 / 4\pi\omega^2 r_A^2 kT$ .

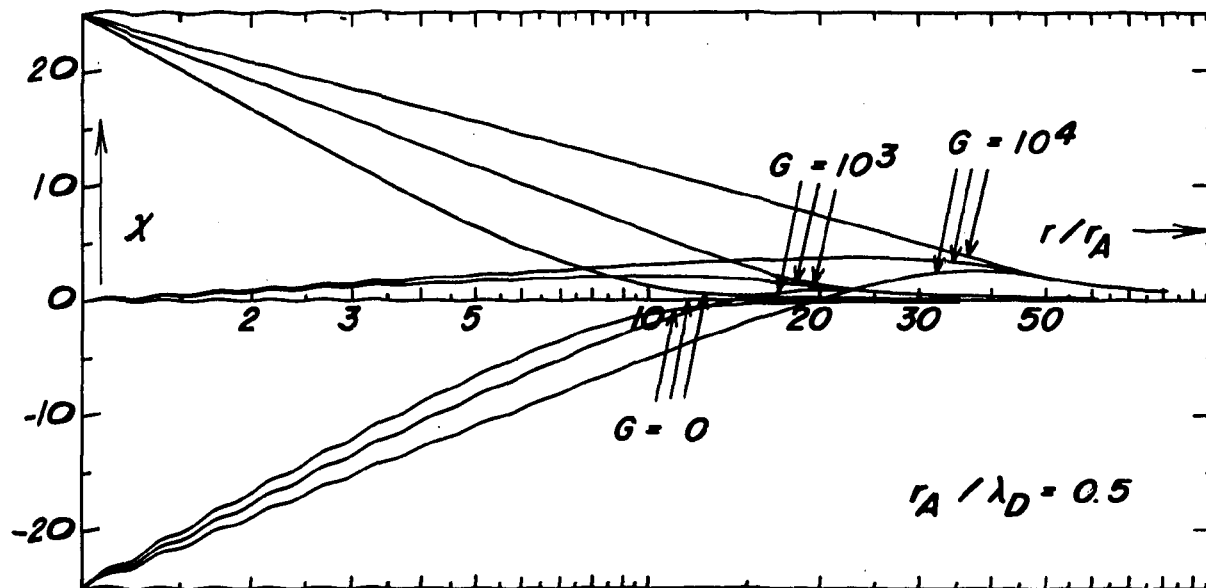


Fig. 2. Dimensionless static potentials  $\chi = e\phi/kT$  as functions of radius  $r$ , for values of antenna static potential  $\chi_A$  of  $-25$ ,  $0$ , and  $25$ , and various values of the radiation strength parameter  $G$ , for  $r_A / \lambda_D = 0.5$ .

et al, 1975, Figs. 12-14).

The double layer structure exhibited in these sheath profiles is clearly an unusual one. This double layer appears to contain only two ambient particle populations instead of the usual four. The electron and ion populations incident onto the double layer from larger radii are both retarded, by the ponderomotive force and by the static electric field, respectively. In the more usual kind of double layer, all momentum carried into or out of it is due to particle motions, but in this double layer, the ponderomotive force provides another source of momentum.

This double layer does in fact have ions entering it from its inner as well as outer boundaries, because ion orbital motion (angular momentum) effects in the cylindrically-symmetric geometry cause reversal of the initially-inward radial motions of many of those ions which penetrate through the double layer to smaller radii. There is a similar effect for electrons, but it is very small because their density near the antenna is very small (Fig. 1). In general, there is no corresponding effect in the more usual planar geometry, although magnetic mirroring of particles on one side of a double layer could produce a similar effect.

Finally, it should be borne in mind that our time-averaged treatment ignores the effects of electron oscillations on all of the sheath profile features shown in Figs. 1 and 2. This approximation is valid in the limit where  $c_1$  and  $\omega$  both increase indefinitely but do so in such a manner that  $G$  remains constant. However, in real situations, in which  $\omega$  is finite, the amplitudes of these oscillations can become comparable in size with these features, especially at smaller radii. For example, in the ionospheric sounding experiment carried by the ISIS II satellite, parameter values at the upper end of its frequency range were (Laframboise et al, 1975):  $r_A = 0.66$  cm,  $\omega/2\pi = 20$  MHz,  $c_1 = 119$  volts, and  $G = 3.52 \times 10^3$ . Corresponding to these values, peak-to-peak amplitudes  $2eE_1/m\omega^2 = 2ec_1/m\omega^2 r$  are 4.0 cm at  $r = 6.6$  cm and 0.8 cm at  $r = 33$  cm. These amplitudes are small enough to indicate that the major features of Figs. 1 and 2 have been realistically modeled. On the other hand, when  $\omega/2\pi = 5$  MHz, then (Laframboise et al, 1975):  $c_1 = 364$  volts,  $G = 5.24 \times 10^5$ , and these amplitudes at the same radii become 1.97 m and 0.39 m, respectively. In order to reliably predict sheath configurations in such cases, it appears that calculations of a more detailed nature will be required.

## ACKNOWLEDGMENTS

We wish to thank the Centre National d'Etudes Spatiales, Toulouse, together with the Centre de Recherches en Physique de l'Environnement, Orléans-La Source, for the provision of very generous amounts of computer time. This work was supported by the Natural Sciences and Engineering Research Council of Canada under grant A-4638.

## REFERENCES

- Boot, H.A.H., S.A. Self, and R.B.R. Shersby-Harvie (1958), Containment of a fully-ionized plasma by radio-frequency fields, *J. Electron. Control*, 4(5), 434-453.
- Getmantsev, C.G. and N.G. Denisov (1962), Concerning an effect during measurement of electron concentration in the ionosphere by the antenna probe method, *Geomagn. Aeron. (USSR)*, 2(4), 575-577.
- Laframboise, J.G. (1966a), Theory of cylindrical and spherical Langmuir probes in a collisionless plasma at rest, in *Rarefied Gas Dynamics*, edited by J.H. deLeeuw, Vol. 2, pp. 22-43, Academic, New York.
- Laframboise, J.G. (1966b), Theory of spherical and cylindrical Langmuir probes in a collisionless, Maxwellian plasma at rest, *UTIAS Rep. 100*, 209 pp., University of Toronto Institute for Aerospace Studies, Toronto, Canada M3H 5T6.
- Laframboise, J.G., J. Rubinstein, and F.H. Palmer (1975), Theory of topside sounder transmission effects on antenna quasistatic sheath impedance, *Radio Sci.* 10(8,9), 773-784.
- Rubinstein, J. and J.G. Laframboise (1970), Plasma sheath around a floating cylindrical antenna at high power, *Can. J. Phys.*, 48(16), 1882-1893.

## ELECTRON DIODE DYNAMICS; LIMITING CURRENTS; PLASMA DIODES

Charles K. Birdsall  
EECS Dept., Cory Hall, University of California  
Berkeley, CA 94720 U.S.A.

Abstract

This paper is intended to complement the papers on double layers, in bringing out the work in the past on virtual cathodes and on limiting currents. The view is that a double layer might be considered to be a virtual cathode for electrons adjacent to a virtual anode for ions, coupled by the shared fields and passing particles. In this view, the formation of a double layer is taken to be the onset of current limiting.

Introduction

It is possible to view double layers as some form of back-to-back virtual cathode and virtual anode, with electrons largely reflected by the former and ions by the latter. The passing particles form the current and are controlled by the fields in the double layer. It may be possible to learn something about double layers by reviewing some of what is known about virtual cathodes. This is one purpose of this paper.

The studies of virtual cathodes show that they are almost always in motion, with the potential minimum oscillating at something like the plasma frequency, both in position and in potential. For cold beams of electrons, this behavior is so pronounced as to make the time average of the time-dependent results (in simulations) quite different from those predicted by time-independent analysis. Hence, we will concentrate in the time-dependent analyses and simulations. For warm beams, the differences are smaller.

### Model

The model most commonly used is one-dimensional (1d), bounded at the two ends,  $x = 0$ ,  $x = L$ , by planar grids, which may or may not be connected to external circuits, as shown in Figure 1

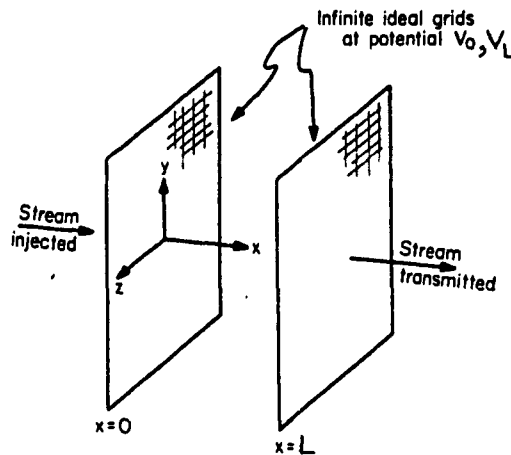


Figure 1. Planar diode model.

Let us use this model to demonstrate a number of results.

### Child's Law Diode

The planar electron diode, with a cathode emitting electrons from rest at the cathode at  $x=0$  where  $\phi=0$  produces a current density at the anode at  $\phi=V_L$  as found by Child (1911), given by

$$J = -(4/9)e_0(-2q/m)^{1/2}v_L^{3/2}/L^2, \text{ or } w_{pL}L/v_L = (2/9)^{1/2} = 0.4714$$

or a current for a beam radius of  $R$ , given by

$$I/v_L^{3/2} = -2.33 \times 10^{-6} \pi R^2/L^2$$

where this quantity is called the perveance, a geometric factor. Physically, the cathode is a copious emitter, injecting  $-J_e$  which greatly exceeds the current transmitted, unless  $V_L$  is raised so high as to collect all charge emitted. Langmuir (1923) solved the same model but with a cathode emitting electrons with a half-Maxwellian velocity distribution, with temperature that of the cathode,  $T$ ; the new feature was the separation of the diode into the  $\alpha$  region with charge flowing out and back to the cathode and the  $\beta$

region, with charge flowing just to the anode, with a potential minimum at the common boundary, as shown in Figure 2.  $x_{min}$  is about a Debye length.

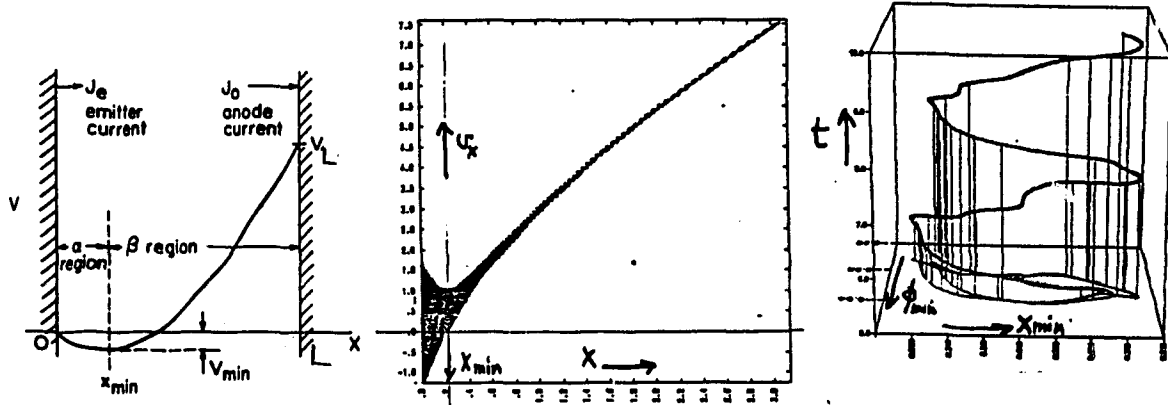


Figure 2 (a) Langmuir warm emitter, with two-directional flow in  $\alpha$ , one in  $\beta$ ; (b)  $v_x-x$  phase space, with both flows, for  $eV_L/KT \gg 1$ ; (c) time history of the minimum potential and position with period about  $w_{p,min}$

For the case where the diode is shorted, with both electrodes at  $\phi=0$ , the phase-space appears as in Figure 3. Note that there are "critical" particles which just reach  $x_{min}$  and must decide to go on or turn back, known for a long time to be crucial in noise properties of beams (see Birdsall and Bridges 1966, Ch.6).

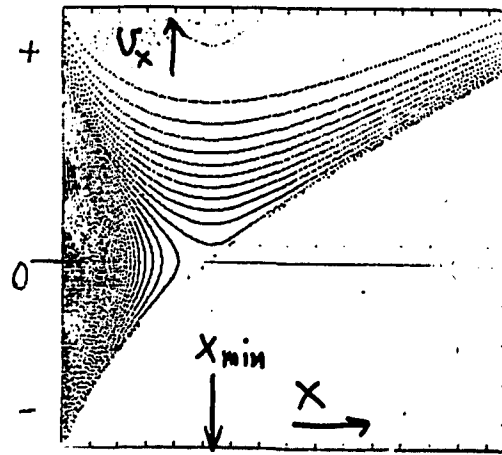


Figure 3

Llewellyn (1941) systematized perturbation analyses for electron diode regions, producing equivalent circuits with admittance  $1/z = y = g + jb$ , such as shown in Figure 4(a), with results for the Child's Law diode in (b).

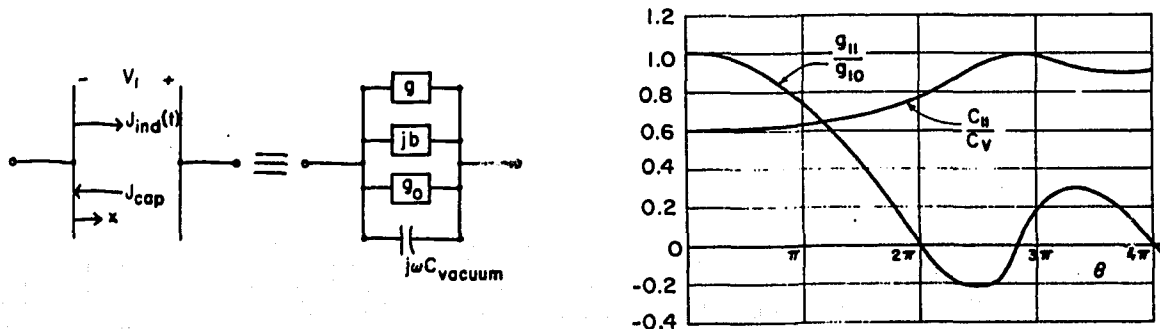


Figure 4 (a) possible equivalent circuit for diode; (b) elements of such a circuit vs. transit angle  $\theta = \omega T$ , where  $T = L/3v_L$ , the transit time.

Note that the conductance can be negative for transit angles  $2\pi < \omega L \leq 3\pi$ ; that is, the diode is unstable and will produce oscillations starting from noise. His methods and extensions are given in Birdsall and Bridges (1966).

Fay, Samuel, and Shockley (1938) and Salzberg and Haeff (1938) solved the electron diode behavior for injection of a cold beam at velocity  $v_0$ . For example, with  $V_0 = V_L$ , they found that the transmitted current  $J_T$  equalled that injected,  $J_I$ , up to  $J_I = 8J_{Child}$ , with unidirectional flow; for larger injection, they postulated two-directional flow and found new virtual cathode solutions with less than half as large  $J_T$ , as shown in Figure 5, with

an arrow indicating the possible connection between the two solutions (making a hysteresis loop), sometimes called the "6L6 effect" after a misbehaving power tetrode. At the maximum current  $\omega_p L / v_L = (16/9)^{1/2} = 1.33$ .

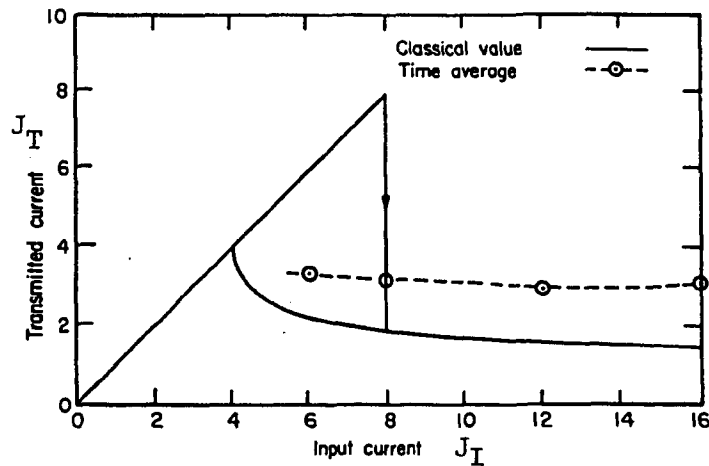


Figure 5

Birdsall and Bridges (1961, 1963, 1966 in Chap. 6) found instability at  $8J_{Child}$  from Llewellyn's equations and using particle simulations, showed that after initial pure exponential growth in time, there is an oscillating  $\phi_{minimum}$  and oscillating  $J_T$  with time average twice that from the above analyses, as shown dashed in Figure 5. For warm beam injection, the oscillation amplitude is smaller and the instability less violent, like Figs. 2, 3.

Pierce (1944) analysed injection of a cold beam into a short-circuited diode with a background of immobile ions for neutralization, finding instability at  $\omega_p L / v_0 = \pi$ , about 5.6 times the current for instability of the unneutralized electron diode; adding finite ion mass, Pierce (1948) found

electron-beam-caused growth in space (complex  $k$ ) a little below  $w_{pi}$  and Buneman (1958) solved the same dispersion relation for complex  $w$  (hence the name Buneman instability). Pierce (1950) applied his 1948 results to his 1944 diode work, finding the same point of marginal stability. Frey and Birdsall (1965, 1966) also used mobile ions for the neutralized diode (and drift tube) and found the surprising result of no instability, a mistake that was corrected by Faulkner and Ware (1969) who found both the diode and beam-ion instabilities (their ion waves), also making ties to arc-starvation.

Birdsall and Bridges (1961) postulated that the low frequency oscillations (at about ion transit periods) observed in plasma diodes (Cs filled thermionic converters) were triggered by limiting electron currents, with high frequency oscillations (near  $w_p$ ) which lowered the average potential making a well as seen by the ions; these would then quench as the ions sloshed and filled the well (with  $w_{pi}$  or ion transit time oscillations). Cutler (1964) observed a sequence of electron-then-ion plasma oscillations experimentally in a plasma diode. Burger (1964, 1965) and Cutler and Burger (1966) provided considerable experimental and simulation results on the sequence and on  $\omega$ -time scale oscillations observed in plasma diodes near electron saturation current.

In studying sheath formation near a floating wall, Birdsall (1982) observes much of the above physics in simulations, such as initial wall charging (electron) current, followed by nearly equal electron and ion fluxes, a drop in  $\phi(x)$  (at  $w_p t = 20$ , the maximum drop has occurred,  $e\phi/KT_e$  of about -2 or -3 for  $m_i/m_e$  of 100 to 400) rising later, a drop in  $n_e(x)$  and  $n_i(x)$  near the wall, ion acceleration to about  $v_s$  or  $2v_s$  (over the whole range of  $T_i/T_e$ , small to large); the somewhat new results are large oscillations of  $\phi_{wall}$  at  $w_p$ , with the ion acceleration region moving away from the wall at speed  $v_s$ , with the plasma eventually disappearing (no source is

present, yet). An object is to see whether electrons are collected in bunches, over short intervals, with ion collection over longer periods, producing both high and low frequency oscillations, still with zero net time average flux. Another object is to resolve the differences between time independent analyses and these time-dependent results.

### Acknowledgments

I am grateful to the conference leaders for admitting my late paper, to my hosts this sabbatical year, Dr. T. Kamimura at I.P.P. Nagoya, Japan, and Profs. R.W. Gould and W.B. Bridges at Calif. Inst. Tech, Pasadena, CA. Figures 1,2a,4a,b,5 are from Birdsall and Bridges(1966);2b,c from Rousset, U.C. Berkeley, unpublished, with thanks.

### References

- 1911 Child, C.D., Discharge from hot CaO, Phys. Rev. Ser.I 32 492-511  
 1923 Langmuir, I., The effect of space charge and initial velocities on the potential distribution and thermionic current between parallel plane electrodes, Phys. Rev. 21, 419-435.  
 1938 Fay, C.E., A.L. Samuel and W. Shockley, On the theory of space charge between parallel plane electrodes, Bell Syst. Tech., 17, 49-79, January  
 Salzberg, B. and A.V. Haeff, Effects of space charge in the grid-anode region of vacuum tubes, RCA Rev.2,336,Jan.  
 1941 Llewellyn, F.B., Electron Inertia Effects, Cambridge Univ. Press, London and New York.  
 1944 Pierce, J.R., Limiting stable current in electron beams in the presence of ions, J. Appl. Phys. 15, 721-726, Oct.  
 1948 Pierce, J.R., Possible fluctuations in electron streams due to ions, J. Appl. Phys. 19, 231-236, March.  
 1950 Pierce, J.R., Note on stability of electron flow in the presence of positive ions, J. Appl. Phys., 1063, Oct.  
 1958 Buneman, O., Instability, turbulence, and conductivity in current carrying plasma, Phys. Rev. Lett. 1, 8-9, July 1.  
 1961 Birdsall, C.K. and W.B. Bridges, Space-charge instabilities in electron diodes and plasma converters, J. Appl. Phys., 32, 2611-2618 Dec.  
 1963 Bridges, W.B. and C.K. Birdsall, Space charge instabilities in electron diodes, II, J. Appl. Phys. 34, 2946, Oct.  
 1964 Cutler, W.H., High-frequency oscillations in a thermal plasma, J. Appl. Phys., 35, 464-465.  
 Burger, P., Nonexistence of dc states in low-pressure thermionic converters, J. Appl. Phys. 35, 3048.  
 1965 Burger, P., Theory of large-amplitude oscillations in the one-dimensional low-pressure cesium thermionic converter, J. Appl. Phys., 36, 1938-1943, June  
 Frey, J. and C.K. Birdsall, Electron stream instabilities with elastic collisions, J. Appl. Phys. 36, 2962, Sept.  
 1966 Frey, J. and C.K. Birdsall, Instabilities in a neutralized electron stream in a finite-length drift tube, Jour. Appl. Phys., 37, 2051-2061, April  
 Birdsall, C.K. and W.B. Bridges, Electron Dynamics of Diode Regions, Academic Press, New York.  
 Cutler, W.H., and P. Burger, Oscillations in the thermal cesium plasma diode, J. Appl. Phys., 37, 2867, June.  
 1969 Faulkner, J.E. and A.A. Ware, The effect of finite ion mass on the stability of a space-charge-neutralized diode, J. Appl. Phys., 40, 366, June.  
 1982 Birdsall, C.K., Sheath formation and fluctuations with dynamic electrons and ions, Int. Conf. Plasma Physics, Göteborg, Sweden, June.

ON THE TRENDS IN THE NON-LINEAR  
DEVELOPMENT OF THE PIERCE INSTABILITY  
IN LABORATORY PLASMAS

D. Jovanović  
Institute of Physics, P.O. Box 57  
Beograd, Yugoslavia

Abstract

The influence of the weak nonlinearities to the Pierce instability is investigated by means of perturbation theory. It is shown that the electron beam is decelerated due to the energy transfer to the electric potential, leading to the decrease of the wavelength and the enhancement of the potential close to the beam inlet boundary. The connection of this effect with the formation of double layers is discussed.

It has been proposed [2,3] that the virtual cathode and/or double layer represent the final (saturated) stage of the potential well growing due to the Pierce instability [1] in a plasma filled diode. However, the actual mechanism of the transition from linear to the saturated regime has not been clarified. The authors of [4] claim that in the process of the formation of electron and ion holes, the strongly unstable front of the beam during its transition time between the electrodes gives rise to the particle trapping, possibly leading to the double layer formation. In the case of the heavy ion background penetrated by an electron beam, treated here, the characteristic time of the potential growth  $1/\gamma$  is much larger than the beam transition time, and the hydrodynamic description is applicable [1]. It will be shown below that the group velocities of both linear and nonlinear Pierce field are less or equal to the beam velocity, and no special treatment of the transient phenomena are necessary, since the conditions in front of the wave front do not affect the wave.

We shall consider a short circuited diode of the length  $L$  filled by cold, collisionless plasma consisting of heavy ions penetrated by an electron beam of the infinite width. The

beam is injected at  $z=0$ , with the velocity  $u$  along the  $z$  axes and the density  $n_{be_0}$ . From the standard set of hydrodynamic and Maxwell equations we obtain the equation for the first and second order perturbation of the electric field  $E_1, E_2$ :

$$ik \cdot \epsilon \cdot E_1 = 0 \quad (1)$$

$$ik \cdot \epsilon \cdot E_2 = \frac{k}{\omega} \cdot j_{NL} + E_2(z=0) \quad (2)$$

where  $\epsilon = 1 - \frac{\omega_{be}^2}{(\omega - ku)^2}$  ( $\omega_{be}^2 = \frac{n_{be_0} \cdot e^2}{m_e \cdot \epsilon_0}$ ) is the dielectric constant, and  $j_{NL}$  is the non-linear current

$$j_{NL} = \int_0^{\infty} dt dz \cdot e^{i(\omega t - kz)} \left( -\frac{m}{e} \cdot i\omega(1-\epsilon) \cdot V_1 \frac{\partial V_1}{\partial z} + \frac{\omega}{\omega - ku} \cdot \frac{en_1 V_1}{\epsilon_0} \right) \quad (3)$$

$V_1, n_1$  being the first order perturbations of the velocity resp. electron density. (1) together with the boundary conditions

$$V_{be}(z=0) = n_{be}(z=0) = E_{||}(z=0) = E_{||}(z=L) = 0 \quad (4)$$

$$\int_0^L E \cdot dz = 0 \quad (5)$$

gives the Pierce field

$$E_1 = e^{\gamma t} \cdot (A_0 + A_1 e^{i k_0 z}) + c.c. \quad (6)$$

$$A_0 = \frac{A}{k_0} \cdot \frac{\gamma}{2(i\gamma - k_0 u)^2}$$

$$A_1 = \frac{A}{k_0}$$

$$k_0 = \frac{1}{u} (i\gamma + \omega_{be})$$

A is an arbitrary real constant, and  $\gamma$  is the growth-rate found from the dispersion relation

$$\frac{i\gamma^2}{(i\gamma - k_0 u)^2} \left( \frac{1}{k_0} - \frac{1}{k_0^*} \right) + \frac{e^{ik_0 L}}{k_0^2} - \frac{e^{-ik_0^* L}}{k_0^{*2}} = \frac{1}{k_0^2} - \frac{1}{k_0^{*2}} \quad (7)$$

Solution (6) is marginally stable ( $\gamma=0$ ) for the critical length of the system

$$L_c = n \pi \cdot \frac{u}{\omega_{be}} \quad n = 1, 2, \dots \quad (8)$$

and becomes unstable for  $L > L_c$ .

Introducing (6) into (3) we find the non-linear current:

$$\begin{aligned} j_{NL} = & -\frac{e}{m} \cdot i\omega(1-\epsilon) \cdot \left\{ \frac{-ik_0}{\omega - 2i\gamma} \cdot \left[ \frac{1}{k - k_0} \cdot \frac{A_1}{i\gamma - k_0 u} \cdot \frac{A_0 + A_0^*}{i\gamma} + \right. \right. \\ & + \left. \frac{1}{k - 2k_0} \cdot \left( \frac{A_1}{i\gamma - k_0 u} \right)^2 + \frac{1}{k - (k_0 - k_0^*)} \cdot \left| \frac{A_1}{i\gamma - k_0 u} \right|^2 \right] + c.c. \left. \right\} - \\ & - \frac{e}{m} \cdot \frac{\omega \omega_{be}}{\omega - ku} \cdot \left\{ \frac{-ik_0}{\omega - 2i\gamma} \cdot \frac{i}{i\gamma - k_0 u} \cdot \left[ \frac{1}{k - k_0} \cdot \frac{A_1}{i\gamma - k_0 u} \cdot \frac{A_0 + A_0^*}{i\gamma} + \right. \right. \\ & + \left. \frac{1}{k - 2k_0} \cdot \left( \frac{A_1}{i\gamma - k_0 u} \right)^2 - \frac{1}{k - (k_0 - k_0^*)} \cdot \left| \frac{A_1}{i\gamma - k_0 u} \right|^2 \right] + c.c. \left. \right\} \quad (9) \end{aligned}$$

$j_{NL}$  is purely growing, due to the singularity  $(\omega - 2i\gamma)^{-1}$ , and the constant of integration  $E_2(z=0, t)$  will have the same time variation. It can be seen from (2) and (9) that the second-order electric field need have the form

$$E_2(z, t) = \sum_n E_2^{(n)} \cdot e^{2\gamma t + ik_n \cdot z} \quad (10)$$

where the summation is performed over all the possible wavenumbers. There are five modes:

$$k_1 = 0$$

$$k_2 = k_0 - k_0^* = i \cdot \frac{2\gamma}{u}$$

$$k_3 = k_0 = \frac{1}{u} (i\gamma + \omega_{be})$$

$$k_4 = 2k_0$$

$$k_5 = k(\omega = 2 \cdot i\gamma) = \frac{1}{u} (2i\gamma + \omega_{be}) \quad (11)$$

and the corresponding complex-conjugates.

One can see that all the modes (11) have the group velocity equal to  $u$ , except  $k_3$  with  $v_{gr} = \frac{1}{2} \cdot u$ . The first two modes have no  $z$ -oscillating character, and the corresponding components of  $V_2(z,t)$ ,  $n_2(z,t)$  can be recognised as the perturbations of the beam velocity and density resp., while the other modes are higher space harmonics. Adopting  $E_2(z=0)$  in agreement with the boundary conditions (4), the perturbation of the beam velocity and density are:

$$\delta u = 2u \cdot \left( 2\pi \frac{e}{m} \frac{|A_1|^2}{u \cdot \omega_{be}} \right)^2 \cdot e^{2\gamma t} \cdot \left( e^{-\frac{2\gamma}{u} \cdot z} - 1 \right) \quad (12)$$

$$\delta n_{be} = n_{be_0} \cdot \left( \frac{2\gamma}{\omega_{be}} \right)^2 \cdot \left( 2\pi \frac{e}{m} \cdot \frac{|A_1|^2}{u \cdot \omega_{be}} \right)^2 \cdot e^{2\gamma t} \cdot \left( e^{-\frac{2\gamma}{u} \cdot z} - 1 \right)$$

The density perturbation is negligibly small, since the surplus of electrons obtained by the beam deceleration is "stored" as the Pierce field related density, rather than becoming "free" background electrons.

The non-linear development of the electric potential can be described by the substitution of (12) into initial hydrodynamic and Maxwell equations. If  $\gamma \ll \omega_{be}$ , the WKB method can be applied, and after some algebra we obtain the expression for the electric potential consisting of a component with the wave-like  $z$  - variation:

$$\phi(z, t) = e^{\gamma t} \cdot \frac{iA_1}{k_0} \cdot e^{ik_0[z - \frac{u}{2\gamma} \cdot e^{2\gamma(t-t_0)} \cdot (e^{-\frac{2\gamma}{u} \cdot z} - 1)]} \quad (13)$$

$$t_0 = -\frac{1}{\gamma} \cdot \ln(2\sqrt{2} \cdot \pi \cdot \frac{e}{m} \frac{|A_1|}{u \cdot \omega_{be}})$$

and the non-linear analog of  $A_0 \cdot z$  in (6) which scales as  $\frac{\gamma^2}{\omega_{be}^2} \cdot z$  and can be neglected.

The potential (13) is plotted in Fig 1 together with the perturbed beam velocity profile in the initial moment (dashed line) and for an almost stopped beam  $t-t_0 = -0.25$  (solid line). In the latter case the wave structure is retained, but it is "compressed" in the vicinity of  $z=0$  (beam inlet side) and more heavily damped at larger distances. The effective wave-number, from (13) is

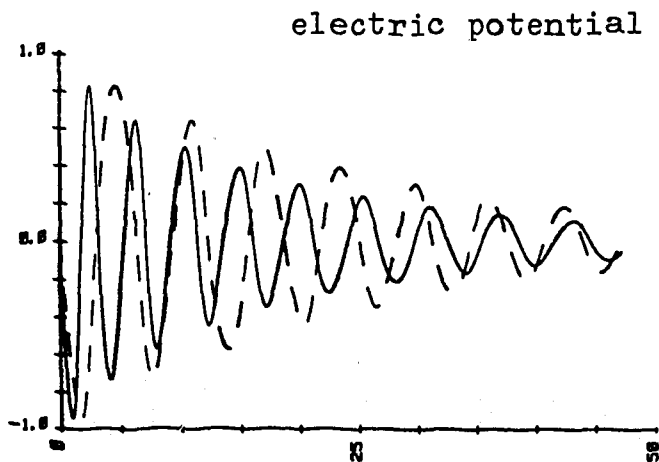
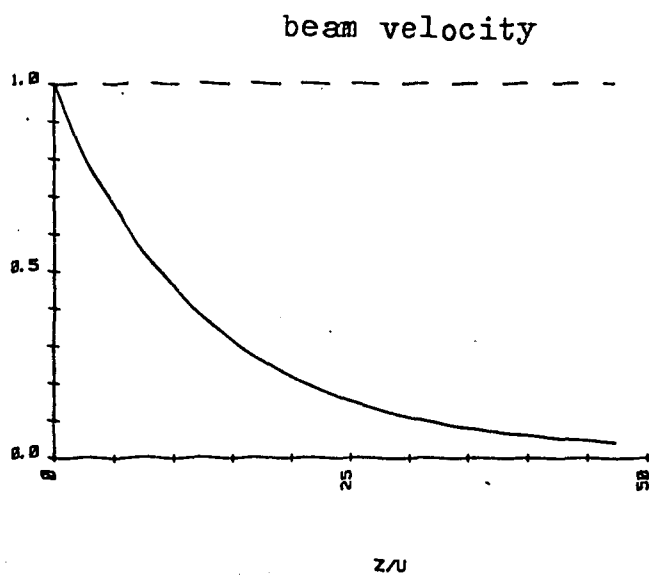
$$k_{eff}(z \ll u/2\gamma) = k_0(1 + \exp(2\gamma(t-t_0))) \quad \text{and}$$

$$k_{eff}(z \rightarrow \infty) = k_0.$$

These results are obtained by assuming immobile ions, being valid on a time scale short compared with the ion motion time. On a longer scale, the potential would be further deformed by the particle trapping, leading to the broadening of the potential minimum nearest to  $z=0$ , further suppression of the other potential well, probably leading to the double layer formation observed in [2].

References

- [1] J.R.Pierce, J.Appl.Phys. 15, 721, (1944)
- [2] S.Iizuka, K.Saeki, N.Sato, Y.Hatta, Phys.Rev.Lett. 43, 1404 (1979)
- [3] M.V.Nezlin, A.M.Solntsev  
Sov.Phys. J.E.T.P. 26, 290, (1968)
- [4] S.Bujarbarua, H.Schamel  
J.Plasma Phys. 25, 515, (1981)



Symposium on Plasma Double Layers, Risø National Laboratory,  
Roskilde, Denmark, June 16-18, 1982.

## NON-QUASI-NEUTRAL PLASMAS OF LARGE EXTENSION

D.K. CALLEBAUT

Phys. Dept. U.I.A., Universiteitsplein 1, B-2610 Antwerpen.  
Belgium.

### Abstract.

A steady state chasma has been studied before by the author and coworkers experimentally and theoretically. The theory was based on a type of nonlinear singular integrodifferential equation, which was solved exactly for the case of constant beam density and constant ion production, even in the 3 dimensional case; it can be solved by approximation in other cases.

The same results, except for a shift in some parameters, can be obtained from an ordinary mhd description yielding a nonlinear second order differential equation, which is more straightforwardly solvable e.g. by series developments than the previous singular integrodifferential equation. Moreover the fluid approach is much better suited for perturbation analysis.

A model of a double layer around the magnetosphere is sketched. It is due to the solar wind and is based on the

difference in electron and ion gyration radii. Although a very rough model it may provide the power station for the currents flowing around the magnetosphere, for the (series of) double layers observed above the ionosphere, for the kilometric radiation, etc.

1. Introduction: laboratory example of chasma<sup>1)</sup>

Consider plane-parallel electrodes. The applied h.f. field between them had 80 MHz and 3000 MHz in typical examples. The gas pressure between the electrodes is below the breakdown pressure. Suppose an ionizing beam (ions, electrons or photons) passes through this gas, either perpendicular (e.g. through holes or consisting of secondaries as in the multipactor effect or secondary electron resonance discharge) or parallel to the electrodes. The electrons created in the ionizations are quickly swept away by the h.f. field towards the electrodes. The created ions however accumulate and thus form an ion potential. Due to their own repulsion these ions are pushed to the electrodes and ultimately a steady state may result. The original beam and the steady state ions in motion towards the electrodes form a non-quasi-neutral plasma or a charged plasma, but since both denominations are in fact *contradictiones in terminis*, it is called a chasma. It is clear that the Debye length (if such a quantity can still be defined for a chasma) can be much smaller than the distance ( $2d$ ) between the electrodes. Another example of a chasma occurs in the experiment of Malmberg and O'Neil<sup>2)</sup>,

which has also fascinating properties, although the densities are usually lower than those in the present example.

To determine the total potential  $\varphi(x)$  and the ion density  $\rho_i$  Poissons equation is used. Some reasoning shows that

$$\rho_i = \int_0^x \frac{P(x') dx'}{v(x, x')} \quad (1)$$

in which  $P(x')$  is the ion production at  $x'$  and  $v(x, x')$  is their velocity when arriving at  $x$ . Using the conservation of energy, one obtains in the 1 dimensional case for once ionized ions with zero initial velocity:

$$\frac{d^2\varphi}{dx^2} = A(x) + \int_0^x \frac{B(x') dx'}{\sqrt{\varphi(x') - \varphi(x)}} \quad (2)$$

with  $A(x) = -\rho_b/\epsilon$ ,  $B(x) = -P(x) (m_i/2e)^{1/2} / \epsilon$ ,  $\rho_b$  = beam density,  $\epsilon$  = permittivity,  $m_i$  = mass of ions,  $e$  = elementary charge.

This is an integro-differential equation of second order; it is nonlinear and singular. The form is fairly general: it is the basic core of all extensions for the problem at hand: moreover it occurs also in other problems, with some modifications.

When  $A$  is constant (homogeneous beam) and  $B$  is constant (homogeneous ion production, which is, for constant pressure, consistent with constant  $A$ ) one finds

$$\varphi = \varphi(0) - k^2 x^2 \quad (3)$$

in which  $\varphi(0)$  and  $k$  are constants.  $\varphi(0)$  is the potential at the origin, here chosen in the middle between the electrodes.  $k$  is determined by the cubic equation

$$k^3 + \frac{A}{2} k + \frac{1}{4} \pi B = 0 \quad (4)$$

Thus  $k$  is a function of  $A$ , representing the density of the ionizing beam, and of  $B$ , representing the mass  $m_1$  and the ion production (which involves the pressure  $p$ ). It turns out that then the ion density is constant in space and time (although the ions move). In a typical experiment (Krebs)  $\rho_b = -2 \times 10^{-6} \text{C/m}^3$  (measured);  $\rho_1 = 10^{-5} \text{C/m}^3$  (calculated)  $d = 0.02 \text{ m}$ ;  $\lambda_D \approx 2d/10$ ;  $p = 10^{-3} \text{ mm Hg}$  and the ion production coefficient (air) is about 800 ions per m and per mm Hg pressure (only 1 ionization for 30 beam electrons crossing the electrode distance).

It was first shown by C.C. Grosjean (see appendix of ref. 1) that the general solution of (2) contains also an infinity of "discrete solutions", obtained explicitly by him, but that (3) and (4) represent the only physical solution.

## 2. Extensions

In ref. 3 more details and further references can be found. When  $A$  and (or)  $B$  are not constant the solution is obtained e.g. by series development after some transformation into a non-singular integro-differential equation. However it can be shown that one obtains a fair approximation by using

averages for A and B. One may also take into account corrections for the (small) contribution due to the electrons created in the ionization and for the initial velocities of the ions. One may add a magnetic field and also a static electric field perpendicular to the electrodes: the latter merely shifts the origin, i.e. the place of maximum potential.

The generalization to three dimensions<sup>4)</sup> leads to

$$\Delta\varphi(\bar{r}) = A(\bar{r}) + \int_G B(\bar{r})J(\bar{r},\bar{r}')F(\bar{r},\bar{r}')[\varphi(\bar{r}') - \varphi(\bar{r})]^{-1/2} d\ell \quad (5)$$

where J is a Jacobian and F an additional factor, at first sight rather unexpected; the line integration is along a generating line G to be determined selfconsistently by the equations of motion and (5). When A and B are constant and when the boundaries are ellipsoids (including elliptic and circular cylinders, the plane-parallel case, etc.) at a constant potential one finds again a solution of the very same type as given by (3) and (4). Again  $\rho_i$  is constant. Moreover the solution is not too much dependent on the form of the boundaries.

### 3. Perturbations. Use of fluid approximation

It is very well possible that the case studied above is sometimes destroyed by instabilities, even before the steady state is reached. However, the study of perturbations through the integro-differential equation is extremely involved and has yielded up to now only a solution in some

trivial cases. In view of this a fluid approximation was worked out. It turned out that, for the steady state, one reobtains the form given by (3) and (4), however with slightly different constants, i.e. a small shift occurs in  $k$ . This means that the fluid approximation is decent (in fact it is based on the conservation laws and thus contains most of the truth), but it is not perfect (in fact it uses an average for the velocity distribution, while the latter is rather peculiar in the case at hand).

Applying then a (much simpler) perturbation analysis to the fluid approximation yielded perturbations<sup>5)</sup> of the type  $x^\alpha \exp i\omega t$ .

#### 4. Cosmic chasmas: double layers

Due to the tremendous charge and associated electric fields chasmas of cosmic dimensions can not occur very easily. However, there is one notable exception e.g. double (or multiple) layers, because here the field at large distances decreases rather rapidly. Hence what is mainly needed is a mechanism to maintain the field in the double layer itself, and observations have shown that those mechanisms do exist<sup>6)</sup>. A different type of such a mechanism will be sketched in the next section.

#### 5. Double layer at the surface of the magnetosphere: a power station

Consider the following simplified model. The solar wind

impinges perpendicularly on a magnetic field like a step function. The ratio of the electron and ion gyration radii is equal to their mass ratio  $r_e/r_i = m_e/m_i$  provided electrons and ions have the same velocity. Thus a charge separation occurs over a distance  $r_i - r_e \approx r_i$  (averaged over circular motions). For  $v = 3 \times 10^5$  m/s and  $B = 10^{-8}$  Tesla there results  $r_i = 3 \times 10^5$  m while  $\lambda_D \approx 10^{-2}$  to 1 m as can be deduced from further calculations with some rough approximations. An  $\bar{E} \times \bar{B}$  drift occurs so that the electrons and ions move parallel to one side. Take the x, y and z axis parallel respectively to  $\bar{E} \times \bar{B}$ ,  $\bar{E}$  and  $\bar{B}$ . Assuming simply that the boundary of the magnetosphere is a flat square of side  $10 R_E$  ( $R_E =$  Earth radius). The origin is taken at the center of one side ( $\parallel \bar{B}$ ) of this square. A huge double layer is formed over this square; its surface charge density is inhomogeneous because of the  $\bar{E} \times \bar{B}$  drift, which makes all the electrons impinging between 0 and x on the line  $y = 0, z = C$  (constant) to pass through the point  $(x, 0, C)$ . One obtains for the number density of either electrons or ions:

$$n_e(x) = \int_0^x \frac{n_{sw} dx'}{v_D} = n_{sw} B \int_0^x \frac{dx'}{E(x')} \quad (6)$$

in which  $n_{sw}$  is the particle flux of either electrons or ions in the solar wind (assumed constant). Now  $E(x) = en_e(x)/\epsilon$  and one obtains the integral equation:

$$n_e(x) = \frac{\epsilon n_{sw} B}{e} \int_0^x \frac{dx'}{n_e(x')} \quad (7)$$

which has the solution

$$n_e(x) = (2\epsilon n_{sw} Bx/e)^{1/2} \quad (8)$$

Then  $E(x) = e n_e(x)/\epsilon$  and the total energy in the double layer would be

$$\begin{aligned} E_{tot} &= 10R_E r_i \int_0^{10R_E} \frac{1}{2} \epsilon E^2(x) dx = 5R_E r_i e^2 \epsilon^{-1} \int_0^{10R_E} n_e^2(x) dx \\ &= 10R_E r_i e n_{sw} B \int_0^{10R_E} x dx = 50R_E^3 r_i e n_{sw} B \quad (9) \end{aligned}$$

It has to be noted that  $r_i e B = mv$  so that the value of  $B$  is irrelevant for  $E_{tot}$  in this model.

Taking  $n_{sw} = 10^{12} \text{ m}^{-2} \text{ s}^{-1}$  (Quiet Sun) there results:

$$n_e(x) \approx 3.5 \times 10^5 \sqrt{x} \text{ m}^{-2}$$

$$E(x) \approx 7 \times 10^{-3} \sqrt{x} \text{ V/m}$$

$$E_{tot} \approx 5 \times 10^{13} \text{ J}$$

However, the total power flux of the solar wind impinging on the magnetosphere is only  $3 \times 10^{11} \text{ W}$  using the above figures and would thus numerically be about two orders of magnitude lower than the energy of the double layer. This is in itself possible but seems unlikely. In fact the results indicate that, although the model is far too crude, the charge separation due to the difference in gyration radii is a powerful

conversion mechanism, capable of converting about all the energy of the impinging solar wind in a double layer surrounding the magnetosphere.

Several improvements can be made. Taking into account that the magnetosphere is not plane will diminish the values obtained above. Some particles spiral towards the poles and the ionosphere and disappear. Most of all the voltage across the double layer (reaching the unacceptable value of  $2000\sqrt{x}$  Volt in the above calculation) diminishes considerably the energy of the impinging particles (500 eV for the ions), decreasing  $E_{tot}$  to a value corresponding approximately to that of the impinging energy of the solar wind. In fact in the above model even the energy needed for the charge separation was neglected. A model taking into account these features yielding a double layer with thickness dependent on  $x$  is under study; it seems very promising but is not yet fully self-consistent.

It is also to be noted that the magnetic field is not a step function nor homogeneous and that one should take into account the energy distribution of the particles in the solar wind; yet these corrections are not expected to be drastic. It has also to be remarked that the drift velocity surpasses the speed of the impinging wind particles, and even exceeds the lightspeed for some values of  $x$ , requiring drastic revision of its formula; in fact, this will rather allow the particles to spend a longer time in the double layer and thus to increase the charge densities, etc.. In addition the current

flowing around the magnetosphere may be subject to various kinds of instabilities, etc..

The double layer described above has its electron and ion layers parallel to the magnetic field, in contradiction to most double layers studied. Moreover there occurs in fact a short circuit along these magnetic field lines and through the ionosphere. As a result double layers with their layers orthogonal to the magnetic field have to occur. Presumably one may identify these with the observed double layers<sup>6)7)</sup> (in series or alone). Moreover the powerful ( $10^9$ W) observed kilometric radiation may very well find also its power station in the double layer discussed here.

The parallel electron and ion currents flowing around the magnetosphere as suggested in this model, flow to one side of the magnetosphere. This asymmetry can be put to test.

A similar mechanism, but in reverse order, may be active in the solar corona and contribute to the acceleration of the solar wind.

### Acknowledgments

It is a pleasure to thank Dr. P. Carlqvist and Dr. M. Raadu, both of the Royal Institute of Technology, Stockholm, Sweden for valuable discussions.

### References

1. Callebaut, D.K. (1965) *Physica* 31, 1177
2. O'Neil, T. (1980) *Phys. of Fluids* 23 (11), 2216
3. Callebaut, D.K. and Knuyt, G.K. (1981) in "Relation between Laboratory and Space Plasmas" (H. Kikuchi, ed.), Reidel Publ. Co, 207
4. Callebaut, D.K. and Knuyt, G.K. (1978) *Plasma Physics*, 20, 511 (I) and 524 (II)
5. Callebaut, D.K. and Verbruggen, M.J. (1982) Proc. 1982 Intern. Conf. on Plasma Phys., Göteborg, Sweden, 240
6. Carlqvist, P. (1982) These proceedings
7. Alfvén, H. (1977) *Rev. Geophys. Space Phys.* 15, 271

Jean-Pierre J. LAFON  
 OBSERVATOIRE de PARIS-MEUDON  
 DEPARTEMENT RECHERCHES SPATIALES  
 92190-MEUDON (France)

A TOPOLOGICAL THEORY FOR SOLVING PLASMA SHEATH PROBLEMS  
 ... AND OTHER PROBLEMS

---

ABSTRACT

In spherical, plane or cylindrical symmetry, the solution of the coupled Vlasov and Poisson equations governing collisionless plasma sheaths in steady state can be reduced to a classification of trajectories of charged particles in electromagnetic fields depending on their space densities in a consistent way. We first give a topological theory concerning the classification of sets of continuous parameters satisfying an infinite number of conditions depending on a continuous parameter. Using this theory, the sheath problem can be solved in a most simplified way at least by numerical iteration. Due to the low sensitivity of the electric potential to variations of the space charge density, the same method can still be used in a large range of cases in which the potential weakly departs from spherical, plane or cylindrical symmetry, though the densities of charged particles are strongly non symmetrical.

I - INTRODUCTION

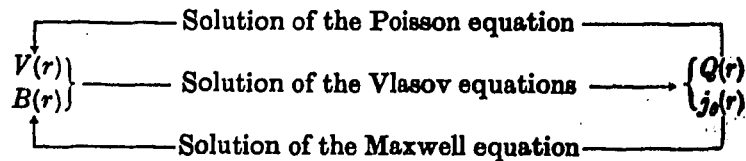
This paper is devoted to the solution of inequalities of the form

$$F(x; \alpha, \beta, \dots) \geq 0 \quad \forall x \in [a, b]$$

and applications to plasma sheaths and double layers.

An important subclass of problems concerning the structure of plasma sheaths is that in which there is a spherical, plane, or cylindrical symmetry, in steady state. All physical parameters, such as distribution functions of charged particles and electromagnetic fields, depend on only one parameter, say  $r$ , the radial distance in spherical symmetry, the distance to the axis of symmetry in cylindrical symmetry, the linear distance to some origin in plane symmetry. Moreover the topology of the trajectories of the charged particles can be characterized by two parameters,  $\xi$ ,  $E$ , the angular momentum with respect to the center of symmetry  $\xi$  and the energy  $E$  in spherical symmetry, .. and so on.

In general, the Vlasov equations express that the distribution functions of the charged particles are constant along the particle trajectories ; in other words, if  $f_s^0$  denotes the distribution function of particles of any given species indexed by  $s$  at some point in space taken as an origin for them, the distribution function of particles of the same species at any other point in space will be equal to  $f_s^0$  for initial velocity components such that the particles can travel from their origin to this point. Finally, if all the distribution functions of the particles are given at points from which these are considered as originating, and if the electromagnetic fields through which they travel are also given, it is, in principle, possible to determine all the distribution functions at any point in space, as soon as one knows for which initial parameters (position and velocity) particles follow trajectories reaching this point. This suggests numerical iteration for solving the coupled Vlasov and Poisson equations governing non collisional systems together with the Maxwell equation for the magnetic field (if any), according to the following scheme (LAFON, 1973)



$Q(r)$  denotes the space charge in the sheath.

Now, in spherical, plane or cylindrical symmetry, at each step of the iteration, one has only to find which trajectories, originating at some distance  $r_0$  for which the distribution functions are known, reach each distance  $r$ , after crossing all equipotential surfaces corresponding to  $\rho$  between  $r$  and  $r_0$ .

For instance, let us discuss the case of the spherical plasma sheath surrounding a metallic body immersed in a non-collisional, non-magnetized isotropic plasma :  $r_0$  is equal to the radius  $p$  of the body for the particles emitted by the body, or to infinity (i.e. some large radius  $R$ ) for particles coming from the unperturbed plasma. Of course

$$p \leq r \leq R < \infty$$

Then, it is natural to express the distribution function  $f_s$  of particles of some species indexed by  $s$  as a function of the radial distance  $r$  and of the two constants of motion characterizing the topology of a trajectory of a particle of species  $s$ ,  $\xi_s, E_s$  ;  $f_s(\xi_s, E_s) = f_s^0(\xi_s, E_s)$  for

particles travelling (and reaching all distances  $\rho$ ) between the distances  $r_0$  and  $\rho$ , whereas  $f_s(\xi_s, E_s) = 0$  for other particles. The two constants of motion  $\xi_s$  and  $E_s$  can be expressed as functions of  $u$  and  $v$ , the radial and orthoradial components of the velocity, as follows :

$$\begin{aligned}\xi_s &= m_s r v_s \\ E_s &= \frac{1}{2} m_s (u^2 + v^2) + q_s V(r)\end{aligned}$$

where  $q_s, m_s$  denote the electric charge carried by the particle and its mass ;  $V(r)$  denotes the electric potential.

The expression can be a little more complicated though of the same form when there is a magnetic field (LAFON, 1973)

Thus a necessary condition for a particle coming from the body to reach the distance  $r$  is

$$u = \frac{2(E_s - q_s V(r))}{m_s} - \frac{\xi_s^2}{m_s^2 r^2} \geq 0$$

and a necessary and sufficient conditions for this particle to effectively reach the distance  $r$  is

$$\frac{2(E_s - q_s V(\rho))}{m_s} - \frac{\xi_s^2}{m_s \rho} \geq 0 \quad \forall \rho \in [p, r]$$

which, for any given function  $V(\rho)$  is an inequality of the form

$$F(r; \xi_s, E_s) \geq 0 \quad \forall \rho \in [p, r] \quad (1)$$

One can show that all problems concerning the determination of distribution functions in the sheath can be reduced to similar inequalities. (LAFON, 1975 a and b, 1973).

Thus it is interesting to have a systematic method independent of the form of the function  $F$  for solving inequalities like (1) in the most general case.

We have given a systematic and general solution scheme of this problem under the form of 3 mathematical theorems (LAFON, 1977) from which numerical algorithms can be easily derived (LAFON 1973, 1975). Two of these theorems are stated in Section II.

## II — TOPOLOGICAL THEOREMS FOR SOLVING SHEATH PROBLEMS..AND OTHER PROBLEMS

The following section is devoted to the solution of inequalities of the form

$$F(x; \alpha, \beta, \dots) \geq 0 \quad \forall x \in [a, b] \quad (2)$$

The problem is the determination of the ranges of  $n$  parameters  $\alpha, \beta, \dots$  ( $n \geq 2$ ) such that a given function of  $n + 1$  variables  $x, \alpha, \beta, \dots$  is positive or equal to zero for all values of  $x$  in the interval  $[a, b]$ . The theorems can be stated as follows (LAFON, 1977)

Assumptions : 1  $F(x; \alpha, \beta, \dots)$  is  $x, \alpha, \beta, \dots$  - continuously differentiable for any  $\alpha, \beta, \dots$  and for  $a \leq x \leq b$  ;

2 All the  $\alpha, \beta, \dots$  derivatives  $F'_{\alpha}$  or  $F'_{\beta, \dots}$  are not simultaneously zero.

3) The interval  $[a, b]$  can be divided into a finite number of subsequent subintervals for any  $x$  in which

-  $F = 0$  and  $F'_x = 0$  for any  $x$ , and for a finite number of sets  $\alpha, \beta, \dots$  depending or not on  $x$ .

or -  $F = 0$  implies  $F'_x \neq 0$  except for a finite number of  $x$  for which  $F'_x = 0$  for all  $\alpha, \beta, \dots$  such that  $F = 0$

4) All the roots of  $F = 0, F'_x = 0$  for  $a \leq x \leq b$  are bounded.

Notations  $P_x$  set of points in the  $\alpha, \beta, \dots$  space for which  $F = 0$

$W_{xx}, W_{xx}^-$  regions of the  $\alpha, \beta, \dots$  space where  $F \geq 0, F \leq 0$  respectively

$$W_{ab}, W_{ab}^- \quad \bigcap_{a \leq x \leq b} W_{xx}, \quad \bigcap_{a \leq x \leq b} W_{xx}^-$$

$$N_{ab} = \bigcup_{\circ} W_{ab} \cup \bigcup_{\circ} W_{ab}^-$$

$\circ A$  region  $A$  of the  $\alpha, \beta, \dots$  -space without its boundary

Theorem 1 :  $\bigcup_{\circ} W_{ab}$  and  $\bigcup_{\circ} W_{ab}^-$  are the regions of the  $\alpha, \beta, \dots$  - space in which respectively  $F > 0$  and  $F < 0$  for any  $x \in [a, b]$ .  $N_{ab}$  contains only the points of the curves  $P_x$  for  $a \leq x \leq b$ .

$$N_{ab} = \left( \bigcup_{a \leq x \leq b} W_{xx} \right) \cap \left( \bigcup_{\circ} W_{ab} \right) = \left( \bigcup_{a \leq x \leq b} W_{xx}^- \right) \cap \left( \bigcup_{\circ} W_{ab}^- \right)$$

$$\bigcup_{\circ} N_{ab} \neq \emptyset$$

Any point of the  $\alpha, \beta, \dots$  - space is in one of the regions  $\bigcup_{\circ} W_{ab}, \bigcup_{\circ} W_{ab}^-, N_{ab}$  but never in two of them.

Theorem 2 : There is some  $x$ , say  $L$ , such that  $a < L \leq b$  and for  $b \geq x \geq L$   $W_{ax} = \emptyset$  whereas, for  $a \leq x < L$ ,  $W_{ab} \neq \emptyset$ . The interval  $[a, L]$  can be divided into a finite number of subintervals  $[x_j, x_{j+1}]$  ( $j = 1, 2, \dots, m$ ;  $x_1 = a$ ;  $x_m = L$ ) for  $x$  in which  $W_{ax} \neq \emptyset$  and can be delimited as follows .

1) If, for  $x_j < x < x_{j+1}$  there is no solution for the system  $F = 0$ ,  $F'_x = 0$ , except for some  $x$ , say  $x^k$  ( $k = 1, 2, \dots$ ) for which  $F'_x = 0$

$$W_{ax} = W_{ax_j} \cap W_{x^1 x^1} \cap W_{x^2 x^2} \cap \dots$$

2) If for  $x_j < x < x_{j+1}$ , the solution of the system  $F = 0$ ,  $F'_x = 0$  is made of some sets of fixed values of  $\alpha$ ,  $\beta$ .., say  $\alpha_k$ ,  $\beta_k$ .. ( $k = 1, 2, \dots$ ) independent of  $r$

$$W_{ax} = W_{ax_j} \cap W_{xx}$$

3) If for  $x_j < x < x_{j+1}$ , the system  $F = 0$ ,  $F'_x = 0$  has solutions  $\alpha_k(x)$ ,  $\beta_k(x)$ .. ( $k = 1, 2, \dots$ ) depending on  $x$ ,  $W_{ax}$  is  $W_{ax_j} \cap W_{xx}$  reduced by the hypersurface  $\alpha_k(t)$ ,  $\beta_k(t)$ .. corresponding to  $a < t < x$

Figs 1 to 3 illustrate these three cases separately in only two dimensions ( $\alpha, \beta$ ). The dashed zones represent  $W_{ab}$ . Fig 4 is another illustration of case 3 in two dimensions also.  $Q$  denotes the envelope of the curves  $P_x$  (solution of  $F = 0$ ,  $F'_x = 0$ )

### III - APPLICATIONS TO SHEATHS AND DOUBLE LAYERS

In practice  $W_{ax}$  is determined progressively, for increasing or decreasing values of  $x$ . One follows its deformation by following the evolution of the ends of the arcs of  $P_x$  included in the boundary of  $W_{ax}$ . For each discrete increment of  $x$  from  $x$  to  $x + dx$ , a simple test concerning the position of these points (for  $x$ ) with respect to  $W_{x+dx, x+dx}$  indicates which case must be considered (LAFON, 1975a, appendix 1). This is an very easy way to obtain the distribution functions at any point.

The method is systematic, independent of the potential profile, whichever it is a physically likely profile or a pure numerical intermediate during iteration.

Now, due to the low sensitivity of the potential solutions of the Poisson equation to perturbations of the space charge density (LAFON, 1975 b, 1976), this theory can still be used to investigate cases in which the space charge density is strongly perturbed whereas the symmetry of the potential is weakly perturbed : the electron density is 12 times greater on the enlightened side than on the dark

side of the body, in the case of a cylinder emitting photoelectrons in a plasma illustrated by Fig. 5 (other examples in LAFON, 1976)

### REFERENCES

- LAFON J.P.J. - Journal of Plasma Physics, 10, 1973, 383-396  
 LAFON J.P.J. - Plasma Physics, 17, 1975a, 731-740 and 1175.  
 LAFON J.P.J. - Plasma Physics, 17, 1975b, 741-756  
 LAFON J.P.J. - Radio Science, 11, 1976, 483-493  
 LAFON J.P.J. - Journal of Mathematical Physics, 18, 1977, 1178-1187.

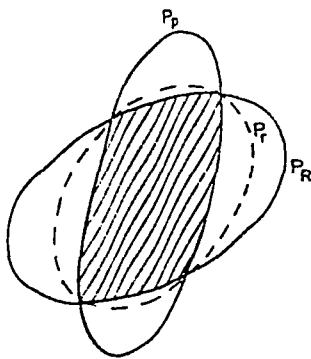


Fig. 1

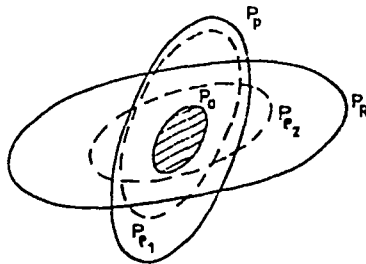


Fig. 2

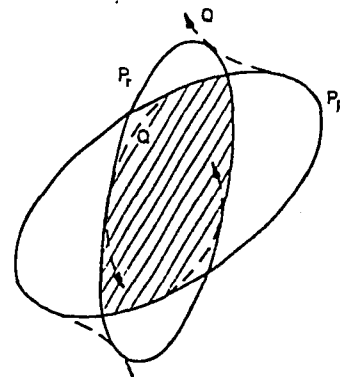


Fig. 3

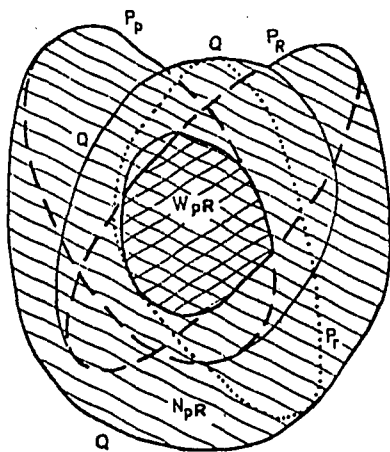


Fig. 4

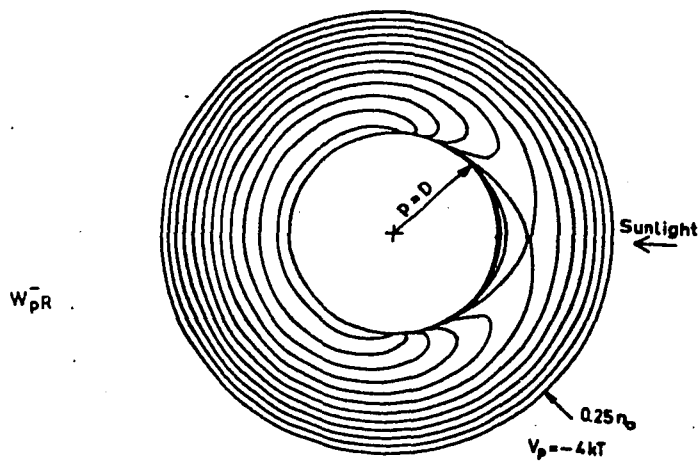


Fig. 5 Iso-density curves for electrons in a sheath around a photoemitting cylindrical conductor.-

Jean-Pierre J. LAFON  
 OBSERVATOIRE de PARIS-MEUDON  
 DEPARTEMENT RECHERCHES SPATIALES  
 92190-MEUDON (France)

ON THE POPULATION OF CLOSED ORBITS IN OPEN AND  
 CLOSED COLLISIONLESS GASES OF CHARGED PARTICLES  
 APPLICATION TO PLASMA SHEATH PROBLEMS

---

Hereafter we discuss the conditions under which collisionless steady state models of plasmas with charge separation and gravitational plasmas are valid.

Consider a dynamical system of charged particles in electromagnetic fields bounded by two surfaces (one inside the volume bounded by the other) as shown on Fig. 1.

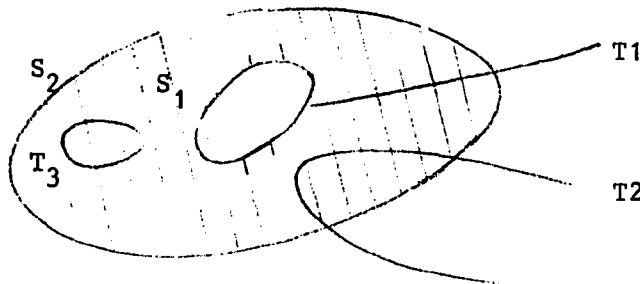


Figure 1

The system is called "open" if the surfaces  $S_1$  and  $S_2$  behave as sources and sinks of charged particles. The electromagnetic field can be such that both "free" trajectories crossing the system like  $T_1$  or  $T_2$ , and closed ("trapped") orbits like  $T_3$  are possible.

Now, assume that the mean characteristic time  $\tau_{\text{cross}}$  for free trajectories, i.e. the mean time spent by particles following free

trajectories inside the system (crossing time) is much lower than the mean time between two successive collision  $\tau_{\text{coll}}$  (the collision frequency to the minus 1) and that we observe phenomena in time scales of the order of  $\tau$  with

$$\tau_{\text{cross}} \ll \tau_{\text{coll}} \ll \tau \quad (1)$$

Collisions are highly probable and frequent on closed orbits, on which in absence collisions particles spend infinite time ; they tend to depopulate these orbits at a high rate. By contrast, they are highly improbable and rare on free orbits, so that closed orbits can be repopulated at a very low rate.

It follows that it is an accurate approximation to assume that closed orbits are unpopulated whereas free orbits are populated. Since sources and sinks for particles on free orbits are on the limiting surfaces, such a situation generates no particular instability.

Now, if the system is closed, in other words if there is no source of particles on  $S_1$  and  $S_2$  ( $S_1$  may even not exist), collisions tend to depopulate closed orbits whereas there is no mechanism for repopulating any trajectory. Thus the system will progressively loose its particles and so be instable.

#### Application to plasma sheaths

The open systems illustrate what occurs in plasma sheaths surrounding biased bodies in plasmas.  $S_1$  is the surface of the body ;  $S_2$  is some electrode or some " sheath edge " i.e. some surface beyond which there are no longer trapped orbits or the dominant physical phenomena are no longer those dominant within the sheath (for instance the mean free path is such that collisions destroy the trajectories). A collisionless model with unpopulated closed trajectories is adequate for such a sheath.

By contrast the closed system can illustrate for instance what occurs in a plasma column in cylindrical symmetry. Such a system is obviously unstable under condition (1) and can be described by a collisionless model only within time intervals  $\tau$  such that

$$\tau \ll \tau_{\text{coll}} \quad (2)$$

In a similar way gravitational plasmas like galactic disks can be described using closed collisionless models with populated closed orbits only, during periods satisfying condition (2).

To summarize, collisionless models with non populated closed orbits can be valid in the limit of large time scales under condition (1) if they are open.

## DOUBLE LAYERS IN LABORATORY PLASMAS

Noriyoshi Sato

Department of Electronic Engineering, Tohoku University  
Sendai 980, Japan

ABSTRACT A review is presented of recent measurements of electric double layers in laboratory plasmas. According to the methods used for double-layer generation, the experiments are classified into four categories and some points of the results in each category are presented. A special topic is concerned with double layers formed in a nondischarge plasma under a strong magnetic field. Some details of discussions deal with a process of double-layer formation and a dynamics of negative potential dip formed on the low-potential tail of double layers. A few remarks are made on double layers under a mirror configuration of magnetic field. Preliminary measurements of potential formation between two different plasmas are also described.

I. INTRODUCTION

Electric double layers (DLs) consist of two thin adjacent regions of opposite charge excess which gives rise to a potential drop across the layer. Although a number of theoretical<sup>1</sup> and experimental investigations have been carried out on the DLs and related problems, there is still an increasing interest in the DLs in plasmas. There are several reasons promoting investigations concerned with the DLs. First of all, the DL is strongly nonlinear phenomenon, belonging to the class of the BGK solutions of the Vlasov equation, and provides a mechanism for anomalous plasma resistivity.<sup>1</sup> These problems are of current interest in plasma physics. Moreover, the DLs are suggested to be responsible for auroral discharges and solar flares.<sup>2</sup> In fact, direct observations confirmed a local potential drop above the Earth's auroral region.<sup>2</sup> On the other hand, the DLs are important to be investigated for development of high-power gas laser<sup>3</sup> and intense beam-production technique.<sup>4</sup> It must be also remarked

that there is a close relation between the DL and the electrostatic potential configuration (tandem potential and thermal barrier) proposed for improving plasma confinement in open-ended fusion devices.<sup>5</sup> In general, when we discuss plasma behaviors in a magnetic field, we must be careful to subtle effects caused by an electric field along the magnetic-field line, which are often missed in the MHD theory. The DL is a typical example of such phenomena.

Since the first research of space charge layers (sheaths and DLs) was done by Langmuir in 1929,<sup>1</sup> it has been well known that the DLs appear under various circumstances. Although the condition for DL formation was given by Bohm,<sup>1</sup> the formation process and properties of the DLs were not so clear until recent progress in theory and experiment which are revealing important features of the DLs.

It is not difficult to show well-known examples of the DLs in laboratory plasmas. When we use a hot cathode for electron emission in a low-pressure discharge tube, there appears the DL in front of the cathode if the emission is sufficient to maintain the discharge current.<sup>6</sup> In a constricted discharge tube,<sup>7</sup> the DL is formed at the place of sudden change of the tube diameter to keep the current continuity through the discharge tube. The stationary striation, which is accompanied by a series of the DLs, is known to appear in a discharge tube under a certain condition.<sup>8</sup> The phenomenon is attributed to a balance between ionization and particle loss to the wall. The simplest method to get the DL is to apply a large positive potential to a Langmuir probe immersed in a weakly-ionized plasma. When this potential (with respect to the plasma potential) is above the ionization potential of the gas used, an additional discharge occurs around the probe. The DL is formed at the boundary between the main plasma and a "new" plasma produced by this discharge. For all these examples, effects of ionization and wall (boundary) are decisive on the DL generation. Although these examples have some essential properties of the DLs, this review is mainly concerned with the DLs in laboratory plasmas where ionization and wall might be neglected for main features of the DLs.

In Sec.II, we try to classify the DLs observed in such a case into four categories, depending on the methods used for the DL generation, and typical results in each category are presented. A main part of Sec.III describes the DLs in a nondischarge plasma. This includes the DLs with potential drop  $1 \leq e\phi_D/T_e \leq 2 \times 10^3$  ( $\phi_D$ : potential drop across the DL,  $T_e$ : electron temperature in eV), a process of the DL formation, a dynamics of negative potential dip on the low-potential tail of the DLs, the DLs under a mirror configuration of magnetic field, an electrostatic ion cyclotron instability caused by three-dimensional structure of the DLs, and also a potential formation between two different plasmas. Section IV contains conclusions.

## II. VARIOUS EXPERIMENTS ON DL

There are various experiments on the DLs, as already described in the previous review papers.<sup>9</sup> Almost all of them were performed on the DLs in discharge plasmas except our works. Typical experiments are presented in this section, although our recent experiments are described in Sec.III.

Before presenting the works, we classify them into four categories, depending on the methods used to generate the DLs.

### Category (1) DLs generated by driving a large discharge current between cathode and anode:

In this case, a plasma is produced by low-pressure discharge between cathode and anode. When the discharge current is kept to be lower than a certain critical value, we have a normal discharge, i.e. the maintaining voltage  $U$  is almost constant against an increase in the discharge current  $I$ . The critical value depends on the gas pressure. At  $I$ =the critical value, however, the discharge becomes abnormal, i.e.  $U$  shows an abrupt increase and  $I$  is limited. Under such a condition, the DL is recognized in the plasma.

### Category (2) DLs generated by applying a large positive potential to an electrode immersed in a plasma:

The DL is also generated by applying a large positive potential to a metal electrode immersed in a discharge plasma, which drives an electron current to the electrode

just as in case of a Langmuir probe. Electrodes with various shapes (needle, plate, sphere, etc.) can be used in the experiments. In this case, however, we often have a situation where the DL is generated by an additional discharge around the electrode, as mentioned in Sec.I. Besides, when the current to the electrode is comparable to the main discharge current, this electrode may work as another anode and then the situation corresponds to the Category (1).

Category (3) DLs generated by beam injection into a plasma:

Both an electron beam and an ion beam are used to generate the DLs in a plasma. In the case of electron-beam injection, above a certain critical beam current, the Pierce instability gives rise to a potential drop near the beam injection, limiting the beam current. This local drop of potential develops to generate the DL. We must be careful to ionization due to the beam in this case. Ion-beam reflection by a metal plate biased positively results in an increase of potential near the plate, which gives rise to the DL generation under a certain condition.

Category (4) DLs generated by applying a potential difference between two plasmas:

When two plasmas are produced by using two independent plasma sources, we can have two plasmas with different potentials if a potential difference is applied between their sources. The DL is found to be generated when these plasmas are in contact with each other. This method is quite simple and is used for measurements described in Sec.III.

Strictly speaking, it is without saying that there are some works which cannot be simply classified. Especially when effects of ionization are not negligible, it is often not so easy to classify the works into the four categories, because there is a close relation among the above categories.

2-1 DL in Category (1)

Torvén and Babić carried out the first clear experiment on the DL generated in an axially uniform positive column with an extremely large discharge current between cathode and anode.<sup>10</sup>

At a critical current in a mercury discharge, they found a visible boundary across the positive column, which was attributed to the DL. Under this condition, the electron drift speed was close to  $(T_e/m)^{1/2}$  ( $m$ : electron mass). Although the layer was stationary, its voltage was strongly fluctuating. Just below the critical value, they observed pulse signals appeared periodically in time, which were confirmed to propagate towards the anode with ion acoustic speed  $(T_e/M)^{1/2}$  ( $M$ : ion mass).

A similar experiment was recently carried out by Levine and Crawford.<sup>11</sup> The work is shown in Fig.1, where an abrupt increase in  $U$  (and a limitation of  $I$ ) yields a clear critical current at a pressure of 0.8 mTorr. They used a Langmuir probe for direct measurement of an axial potential profile. The result gave a potential drop due to the DL, as found in Fig.1. We can find a high-frequency noise caused by an electron beam formed on the high-potential side of the DL.

Lutsenko et al.<sup>12</sup> also observed a current limitation due to the DL in a plasma column with a strong axial magnetic field, although the DL was always moving towards the anode in this case. It is to

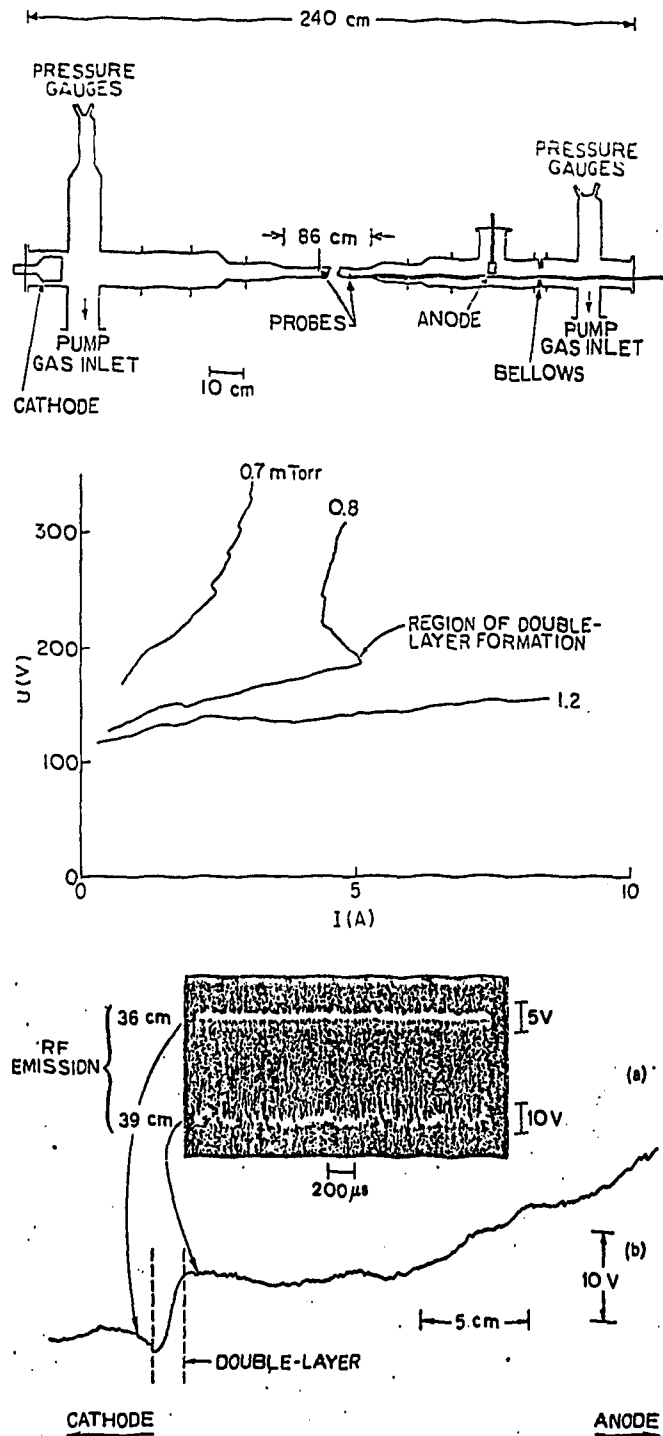


Fig.1. Apparatus and results in Ref.11.

be noted that the DLs and related phenomena were considered to be taken into account in the experiments on turbulent heating of plasmas.

## 2-2 DL in Category (2)

A typical example<sup>13</sup> in this category is shown in Fig.2. An arc discharge between a mercury cathode and  $E_1$  was used to produce a plasma which diffused through  $E_2$  towards the endplate (called "anode" in Ref.13) along a weak magnetic field of 50 - 600 G. When a positive bias  $U_0$  was applied to the endplate through R (resistance), the endplate acted essentially as a Langmuir probe. But, above a certain critical value of the plate potential relative to the plasma, there occurred an ionization in the sheath formed in front of the plate. Then the sheath was converted into the DL (B in Fig.2). The critical value was confirmed to decrease with an increase in the background pressure. A further increase in  $U_0$  resulted in an movement of the DL towards  $E_2$  (C in Fig.2).

We carried out almost the same experiment by using an apparatus shown in Fig.3, where a diffused plasma was produced by an Ar discharge between A (anode) and K (oxide cathode) under a strong magnetic field.<sup>14</sup>

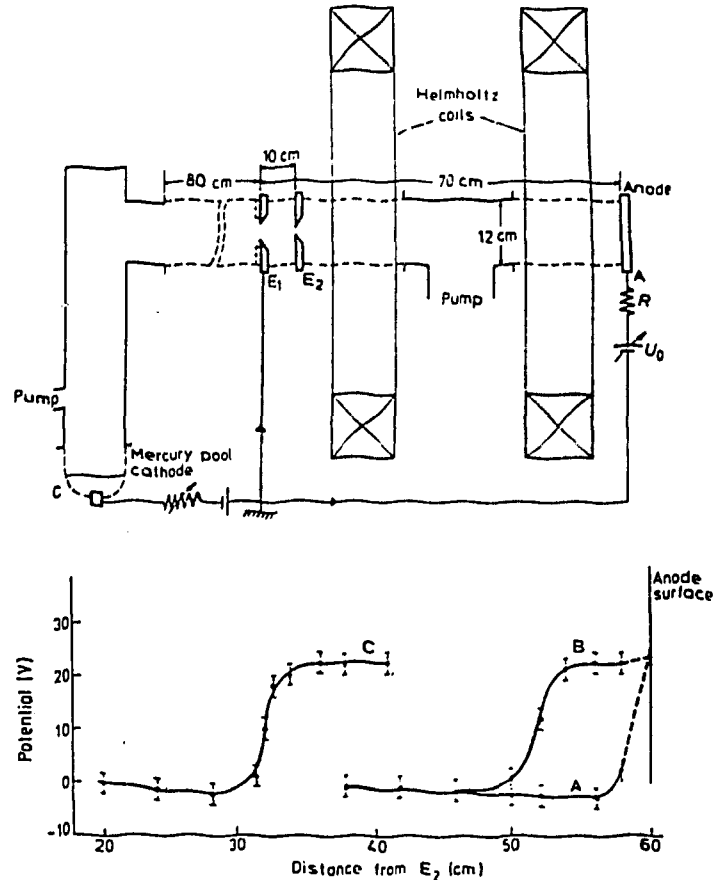


Fig.2. Apparatus and results in Ref.13

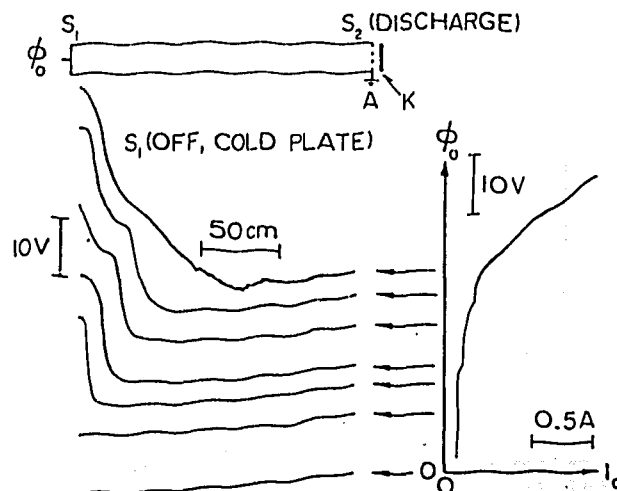


Fig.3. Apparatus and results in Ref.14.

When a potential difference  $\phi_0$  between the endplate and A was increased, it was found that the DL appeared in the plasma at  $\phi_0 \geq U_i$  (ionization potential). The DL with two-stage structure was also generated if  $\phi_0 \geq 2U_i$ .

The experiment of Stenzel et al.<sup>15</sup> was carried out under a somewhat complicated situation (see Fig.4) in order to simulate magnetic substoms and solar flares. A potential was applied to a small plate to drive a current in the center of neutral sheet of magnetic field topology with a discharge plasma. When the current was increased to a critical value, a spontaneous current disruption was observed. The disruption induced a large inductive spike in the plate voltage (due to an effective inductance of the circuit), which was confirmed to drop off in the plasma forming the transient DL. An electron beam and resulted noise were found on the high-potential side of the DL.

As described in Refs.13 and 14, we cannot neglect effects of ionization when we have an electrode with extremely large positive potential in a weakly-ionized plasma. At least a careful check is necessary for the ionization effects in the DL experiments belonging to this category.

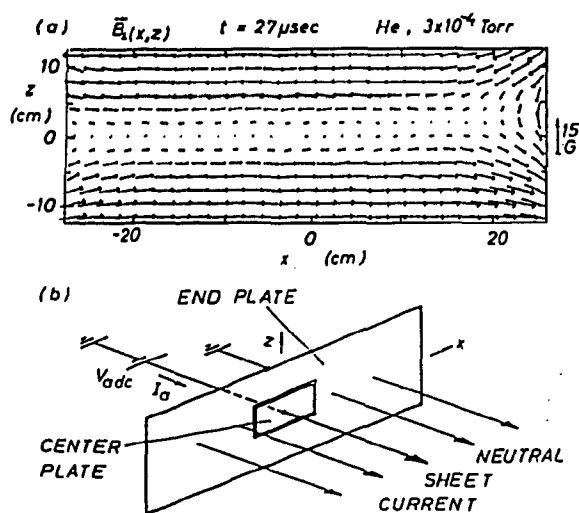
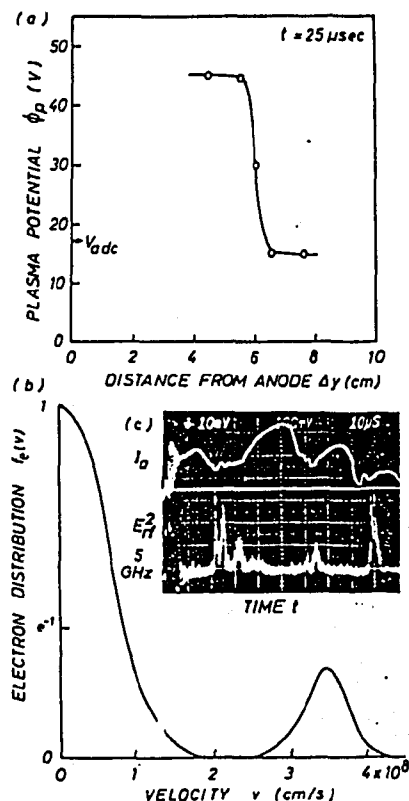


Fig.4. Experimental configuration and results (right) in Ref.15.



## 2-3 DL in Category (3)

The first measurements of the DLs generated by an electron-beam injection into a plasma were made in a modified double-plasma machine.<sup>16</sup> A similar work was carried out by using a triple-plasma machine,<sup>17</sup> as shown in Fig.5. In this case, two plasmas were independently produced in sources I and II. An electron beam was injected from the source II into a region called "target" between the sources, where a plasma was supplied from the source I kept at a potential higher than the source II.

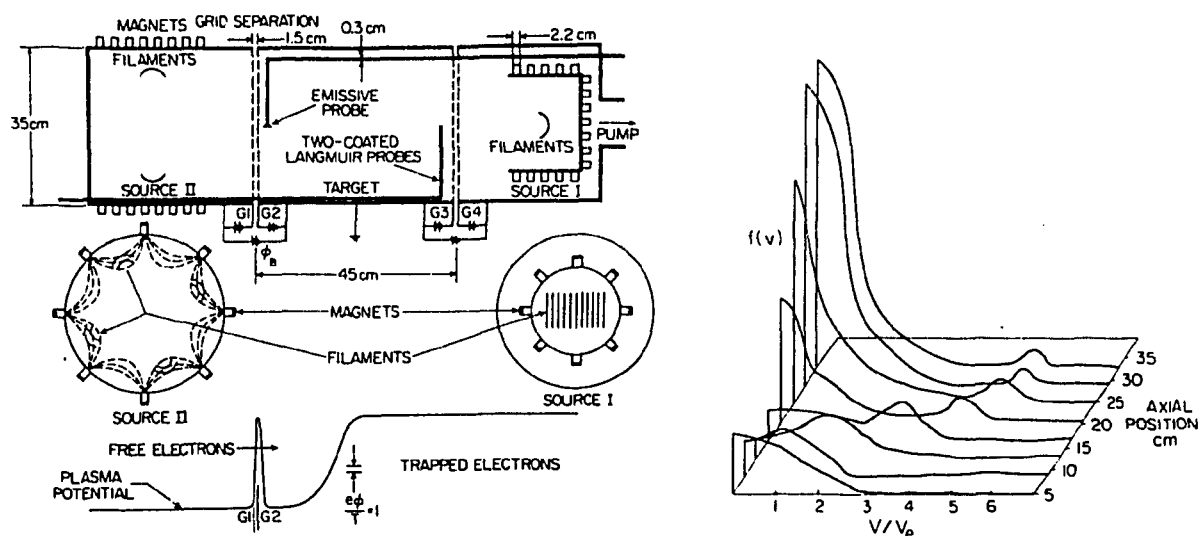


Fig.5. Apparatus and results in Ref.17.

The DL generated had a potential drop up to  $e\phi_D/T_e \approx 14$ . A clear electron-beam generation due to the DL was also reported. In Ref.16, even if there was no plasma source corresponding to the source I in Fig.5, the DL was generated because ionization due to the beam provided a plasma in the target region. But, when an extremely large beam was supplied into the target region, the DL was no more stationary but observed to propagate with a speed close

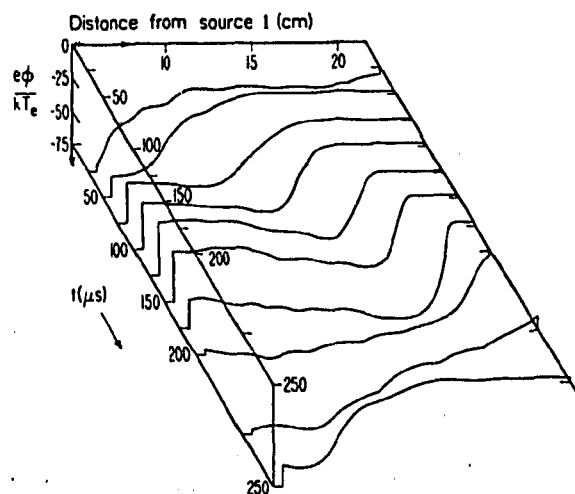


Fig.6. Moving DL in Ref.16.

to ion acoustic speed. Detailed measurements of potential profiles at various times are shown in Fig.6. The DL disappeared when it arrived at the opposite end. But it reappeared at the place near the beam injection and the moving DL was formed again. This repetition corresponded to periodic changes of plasma parameters.

Baker et al.<sup>18</sup> used almost the same experimental geometry as in Ref.17, although a method of plasma production was different. The machine was much bigger with and without a weak magnetic field to magnetize electrons. The DL thickness was, in many cases, greater than a meter. The measurements of two-dimensional configuration gave a similar shape of potential  $\phi$  as expected in space (see Fig.7).

We injected an electron beam into a nondischarge plasma emitted thermionically from a source called "plasma emitter",<sup>19</sup> as shown in Fig.8. The beam density was controlled by changing a grid potential  $V_c$  at a fixed beam energy determined by an acceleration potential  $V_b$ . At a critical value of the beam density, we observed the Buneman instability [(B) in Fig.8], as predicted theoretically. A further increase in the beam

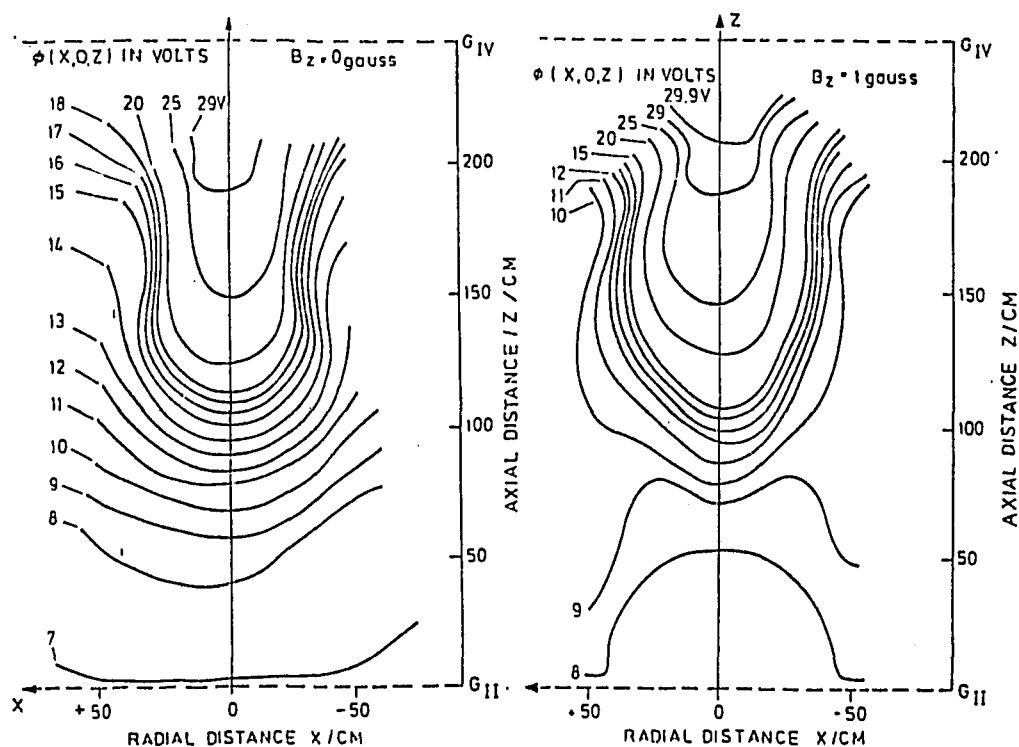


Fig.7. Two-dimensional configuration of DL potential in Ref.18.

density resulted in the Pierce instability [(D)] after a transient region [(C)], which produced a negative potential well in the plasma, limiting the beam current. A quick beam injection, however, being accompanied by ion trapping in the potential well, was observed to lead to the DL formation, as shown in Fig.8. In the region (C), there appeared a periodic change of formation and disruption of the DL, producing an oscillating potential comparable to the injected beam energy. This oscillation of potential gives rise to high-energy ions on the high-potential side of the DL. The phenomenon is attributed to detrapping of ions trapped in the potential well.

The electron-beam injection was also used to

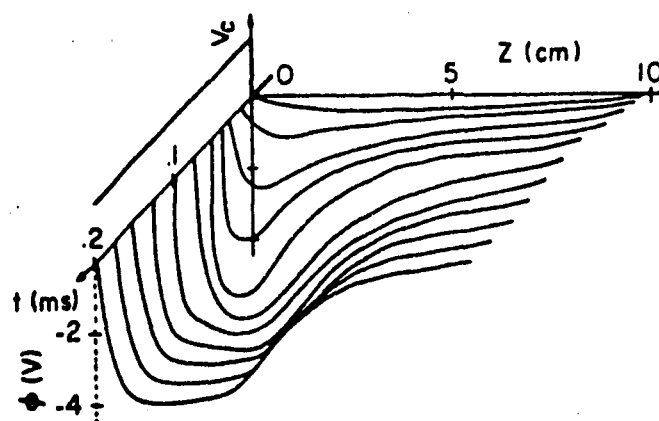
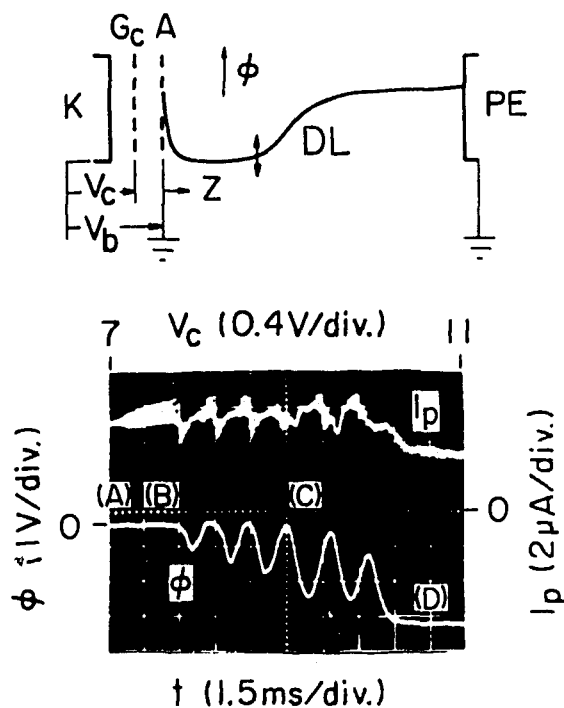


Fig.8. Experimental configuration and results in Ref.19.

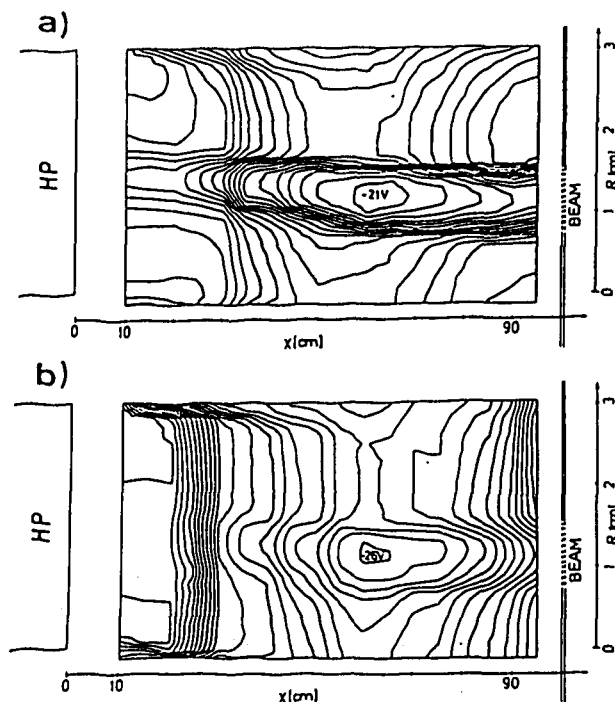


Fig.9. DL potential configuration under a strong magnetic field in Ref.20.

generate the DL in a Q machine, where a plasma was produced at a hot plate (HP) by surface ionization of Cs vapor.<sup>20</sup> The measurements demonstrated a two-dimensional configuration of potential (see Fig.9) under a strong magnetic field.

It was found that the characteristic width perpendicular to the magnetic field was determined by the ion Larmor radius.

On the other hand, the DL was generated when an ion beam was injected into a plasma under a situation in Fig.10.<sup>21</sup> The ion beam was injected along a converging magnetic field towards a positively biased

plate in front of the N-pole of a permanent magnet. The DL was observed to be formed in the plasma when the plate potential was sufficiently large to reflect the ion beam. The potential drop of the DL was slightly smaller than the beam voltage. The measured potential configuration showed a V(or U)-shaped profile of the DL (see Fig.11). In a further investigation,<sup>22</sup> the DL was shown to be generated by the ion beam reflection due to the mirror effect of magnetic field even if the plate was biased negatively or kept to be floating.

#### 2-4 DL in Category (4)

In this case of the DL generation, a potential difference is given between two independently produced plasmas. In Fig.12, two plasmas were produced by Ar discharge at a pressure of  $4 \times 10^{-4}$  Torr.<sup>23</sup> The potential difference was provided by applying a potential

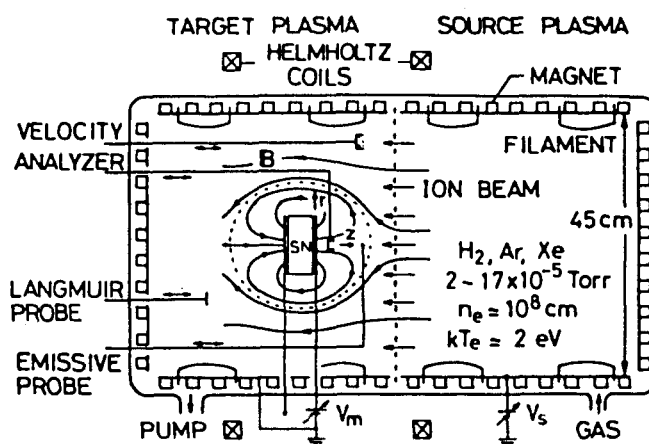


Fig.10. Apparatus in Ref.21.

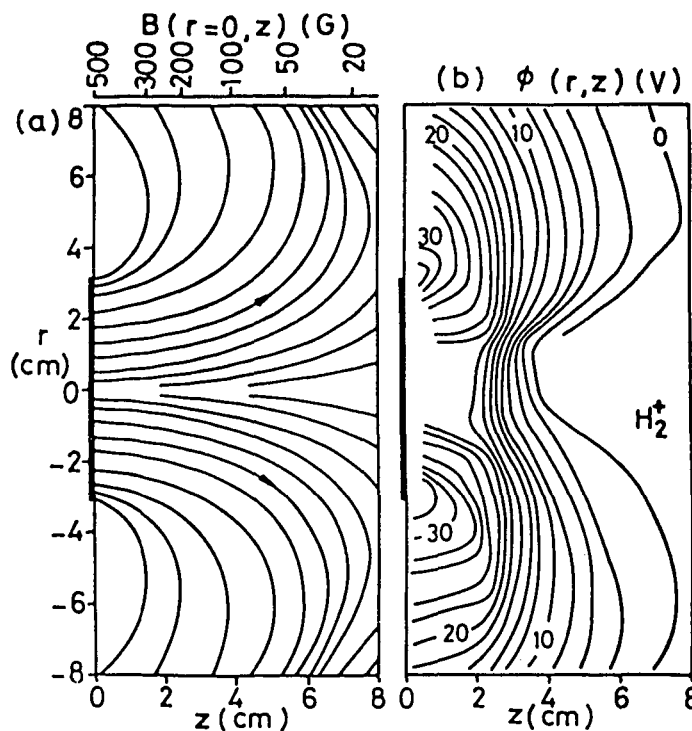


Fig.11. Configurations of magnetic field  $B$  and DL potential  $\phi$  in Ref.21

$V_g$  between two mesh anodes. Since the electron drift speed was smaller than the electron thermal speed in this case, ion acoustic instability was considered to give rise to the DL generation, being consistent with theory.<sup>1</sup> But, the DL obtained is quite similar to the result in Fig.3, where the ionization was important in the DL generation.

This method was also used in the recent work of Torvén and Liting.<sup>24</sup> They succeeded to obtain the DL with potential drop  $\phi_D$  up to 1000 V in a weakly magnetized plasma column. This

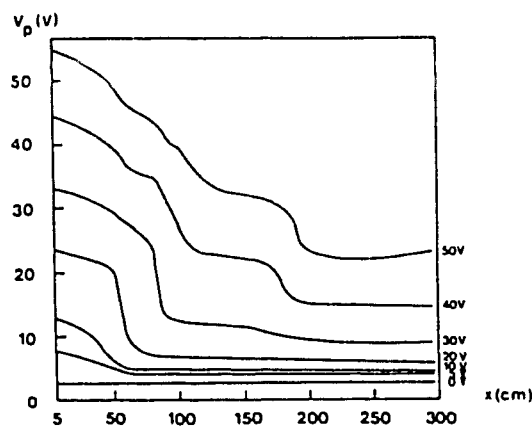
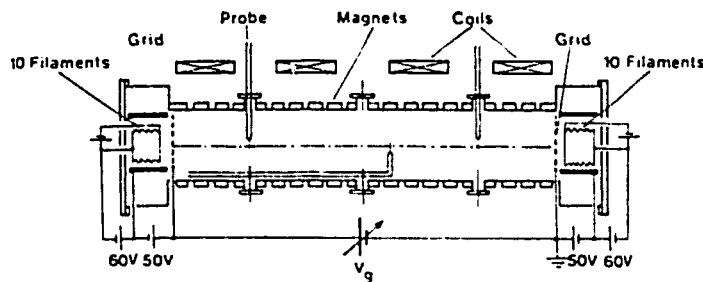
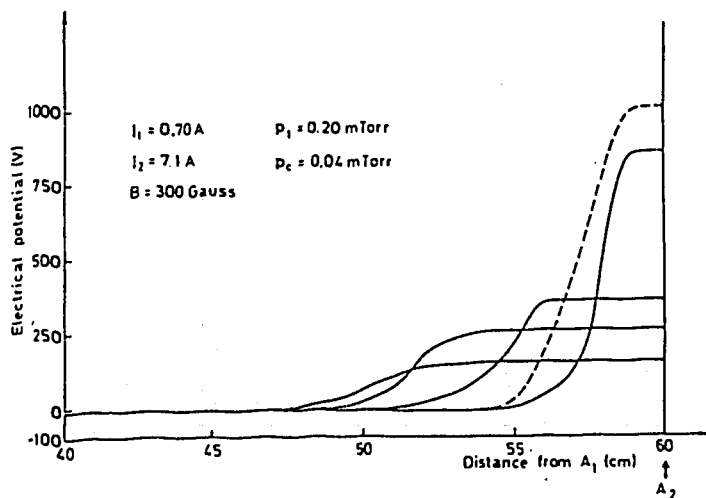
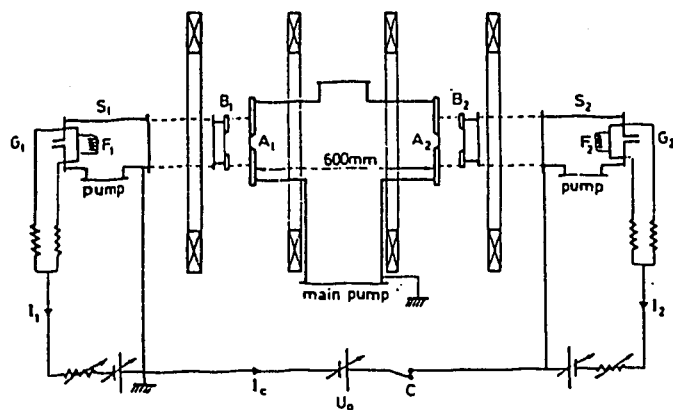


Fig.12. Apparatus and results in Ref.23.



value of  $\phi_D$  is the highest potential drop of the stationary DLs ever reported. The DL was stable for a wide range of plasma parameters, but instabilities leading to large-amplitude fluctuations could be introduced for certain parameter combinations.

Main results presented in Sec.III are concerned with the DLs belonging to this category.

Fig.13. Apparatus and results in Ref.24.

### III. OUR RECENT RESULTS ON DL

Our recent measurements on the DLs were mainly performed in a Q machine. A plasma is produced by surface ionization of K vapor at two hot plates [sources 1 ( $S_1$ ) and 2 ( $S_2$ ) with separation of 227 cm] under a strong magnetic field B of 2-4 kG, as shown in Fig.14. In 3-3, however,  $S_1$  is not heated and is used as a cold plate.  $S_2$  is replaced by a discharge plasma source in 3-6.

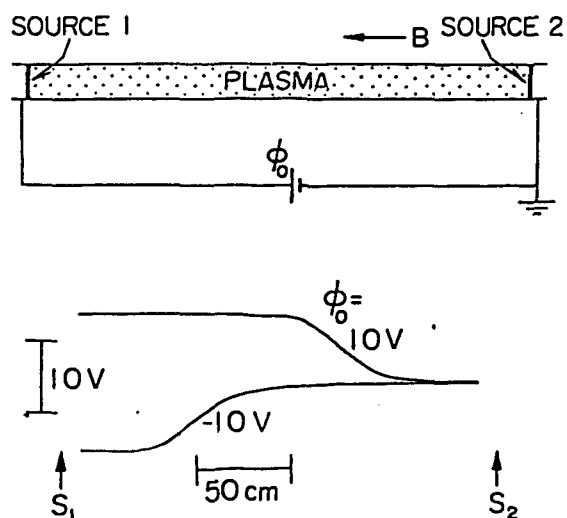


Fig.14. Experimental configuration and DLs at  $\phi_0 = \pm 10$  V.

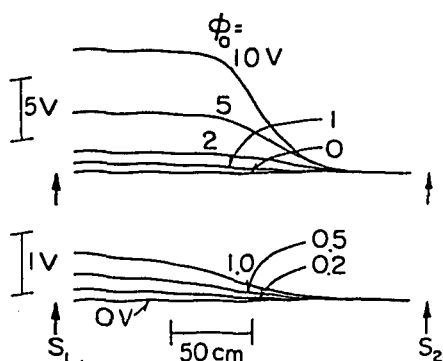


Fig.15. DLs at  $\phi_0 \leq 10$  V. localization due to the one-dimensional

#### 3-1 Stationary DL

In this case,<sup>25</sup> a plasma is produced at  $S_1$  and  $S_2$  of 3.5 cm in diameter under a uniform magnetic field. A potential difference  $\phi_0$  is applied between  $S_1$  and  $S_2$ . The plasma is a mixture of two plasmas (supplied from  $S_1$  and  $S_2$ ) with different potentials. Emissive probe

measurements yield an electric field DL along the plasma column, as shown at  $\phi_0 = \pm 10$  V in Fig.14. The potential drop  $\phi_D$  is close to  $\phi_0$ . The results at  $\phi_0 \leq 10$  V are demonstrated in Fig.15. Even if  $\phi_0$  is so small that  $e\phi_0$  is comparable to  $T_e$  ( $\approx 0.2$  eV), a localized structure of electric field is recognized. We must be careful to this structure in experiments on current-driven instabilities when the current

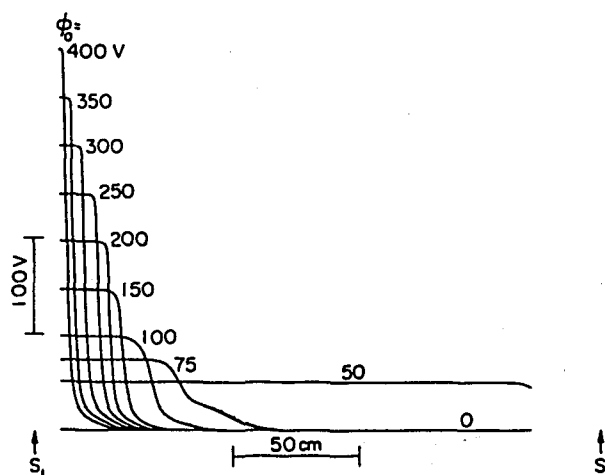


Fig.16. Very strong DLs.

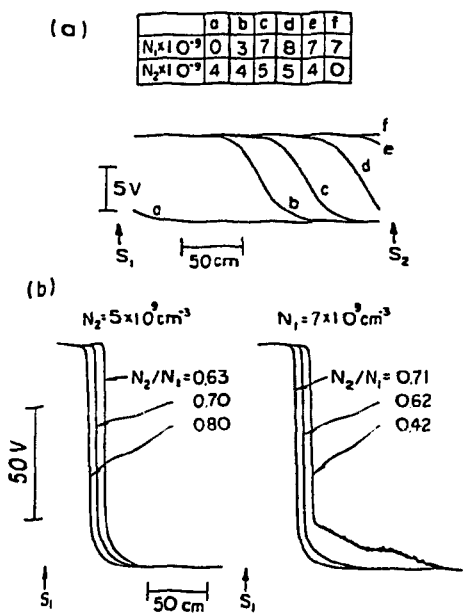


Fig.17. Control of DL position

is driven under this situation. On the other hand, we can also generate the DLs at much larger values of  $\phi_0$ , as shown in Fig.16, where the ratio  $N_1/N_2$  of plasma densities supplied from  $S_1$  and  $S_2$  is larger than those in Figs.14 and 15. When  $\phi_0 \geq 100$  V, the DLs have a sharp potential drop, yielding  $e\phi_D/T_e$  up to  $2 \times 10^3$  which is by one to three orders of magnitude larger than the values in other experiments. The DL width is well consistent with theoretical prediction.

The DL position shifts towards  $S_1$  with an increase in  $\phi_0$ . At a fixed value of  $\phi_0$ , the DL position can be controlled by changing  $N_1$  and/or  $N_2$ . As  $N_2/N_1$  is increased, the DL approaches  $S_1$ , as demonstrated at  $\phi_0 = 10, 100$  V in Fig.17. In this way, we generate the DL at an expected position.

Figure 18 shows a relation between the DL generation and an electric current passing through the plasma column ( $I_0$ : dc

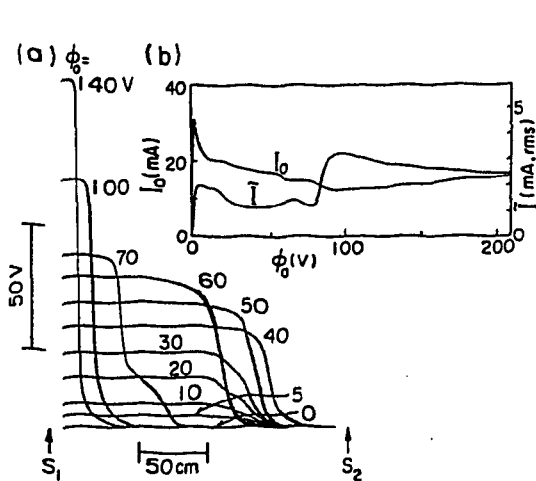


Fig.18. Relation between DL generation and current passing through plasma column

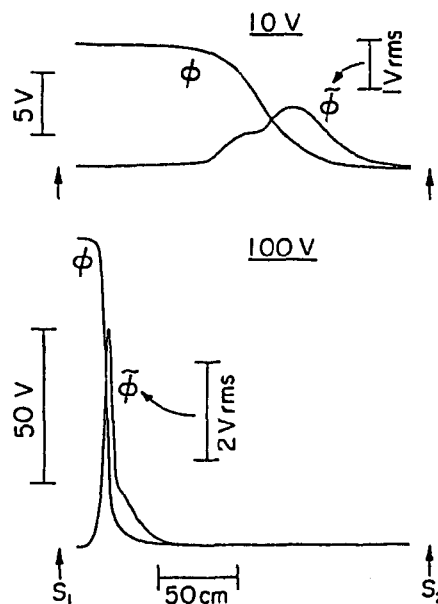


Fig.19. Spatial profiles of DL and low-frequency fluctuation

current,  $\tilde{I}$ : low-frequency fluctuation). The DL generation corresponds to a current limit and an appearance of fluctuation. According to the measurements of potential fluctuation  $\tilde{\phi}$  along the plasma column, there are potential spikes of frequency 1-10 kHz in the DL region, being accompanied by positive spikes in the electron current. At large values of  $\phi_0$ ,  $\tilde{\phi}/\phi_0$  is negligibly small and the DL can be compared with an ideal theory. As  $\phi_0$  is decreased, however,  $\tilde{\phi}/\phi_0$  increases up to a few tens of percent, yielding an apparent broad width of the DL.

Spatial profiles of electron and ion densities,  $n_e$  and  $n_i$ , are shown in Fig.20. The densities decrease in the directions towards the DL even at the place where the potential profile is flat in our scale. An electron beam produced by the DL becomes broad gradually on the high-potential side of the DL. This broadening is ascribed to generation of electron plasma waves (Trivelpiece-Gould mode) propagating towards  $S_1$ . Their dispersion relation is plotted in Fig.21. An ion beam is also confirmed to be produced on the low-potential side of the DL.

### 3-2 A Process of DL Formation

A process of the DL formation is investigated by applying a step potential  $\phi_0$  to  $S_1$  with respect to  $S_2$ . A sampling method is used to measure spatial profiles

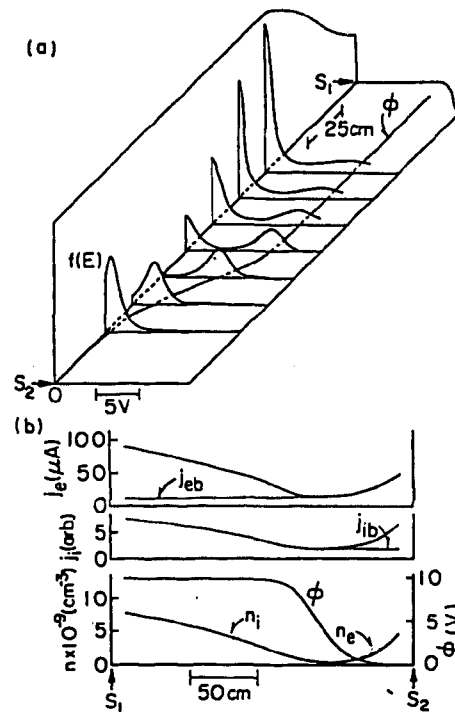


Fig.20. Spatial changes of electron energy distribution  $f$  and densities.

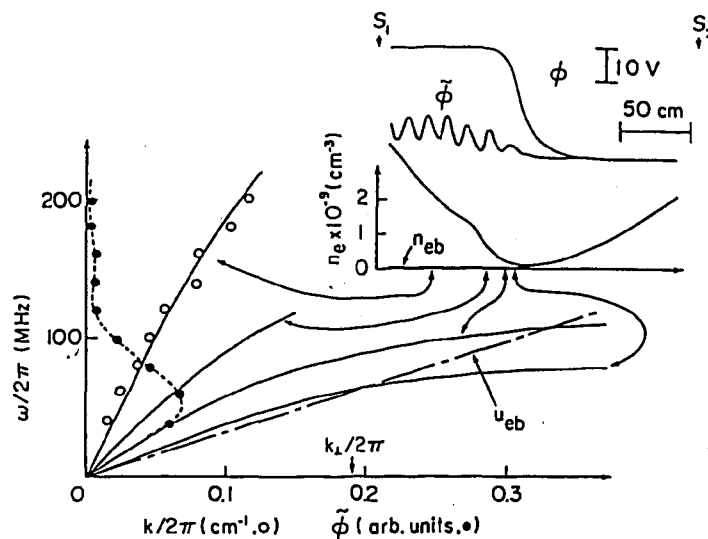


Fig.21. Generation of electron plasma waves and their dispersion relation.

of potential  $\phi$  and electron current  $j_e$  to the probe.<sup>25</sup>

A typical result is shown in Fig.22. Just after the application of  $\phi_0$  at time  $t=0$ ,  $\phi$  increases up to  $\phi_0$  on the whole region. This is accompanied by an increase in  $I_0$  ( $j_e$  is almost uniform spatially) and a generation of fluctuations. The potential is localized in the sheath in front of

$S_2$ . This penetration of  $\phi$  is due to quick response of electrons in the background of immobile ions. At  $t \geq 0.1$  ms, however, we can find a gradual drop of  $\phi$  near  $S_2$  and a decrease in  $I_0$ . On this time scale, ions are accelerated by the potential drop in front of  $S_2$  to be absorbed by  $S_2$ , being responsible for the decrease in  $\phi$  near  $S_2$ . The localized potential drop moves towards  $S_1$ . This movement is followed by a flow of the plasma from  $S_2$ , as found in the  $j_e$  profiles. In the  $\phi$  profile, we can find a special position (shown by an arrow) where  $\phi$  shows a small jump accompanied by fluctuation. In a region between this position and  $S_2$ , no fluctuation is recognized. A small negative potential barrier limiting  $I_0$  is supposed to exist around this position.

In fact, the negative dip of potential is observed as shown by the lower figure in Fig.23,<sup>26</sup> where a detailed structure on the low-potential tail is demonstrated. The negative dip is formed during a decrease of the current  $I_{S1}$  passing through the plasma column (I in Ref.25). But, this dip disappears

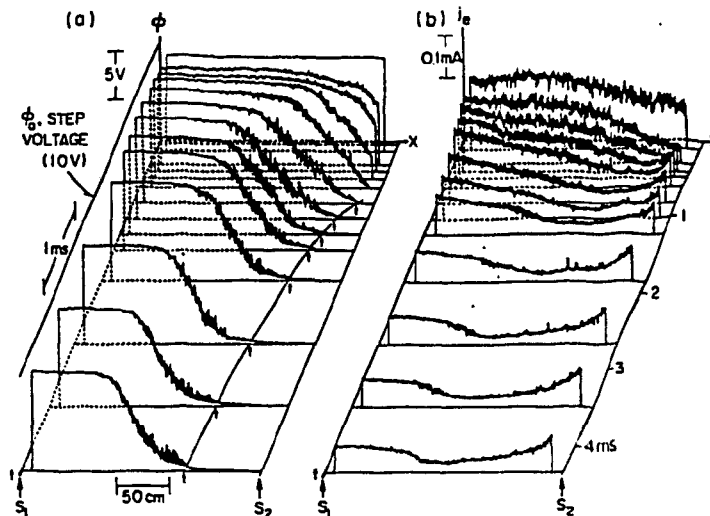


Fig.22. Process of DL formation

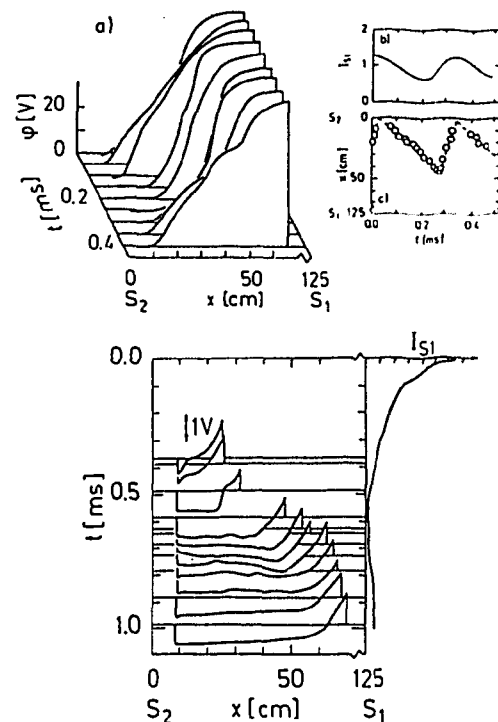


Fig.23. Detailed structure on the low-potential tail of DL

in the following phase of small increase of  $I_{S1}$ . The repetition of formation and disruption of this dip results in a "back and forth" motion of the tail, being responsible for  $\tilde{\phi}$  of the DL. Under a certain condition, there appears a large periodic change in  $I_{S1}$  in the steady experiment. In such a case, a clear feature of this motion is observed, as shown by the upper figure in Fig.23.

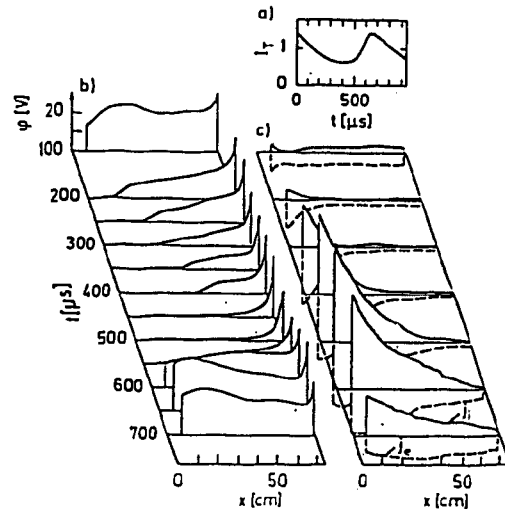


Fig.24. Moving DL.

3-3 Moving DL

In this experiment,  $S_1$  (not heated) is used as a cold target to which a potential  $\phi_0$  is applied with respect to the hot plate  $S_2$ . In this case, the system is not stable and always has large oscillations in plasma parameters.<sup>27</sup> Measurements at various phases of the oscillation in  $I_T$  (target current) are made on axial profiles of  $\phi$ , electron and ion current,  $j_e$  and  $j_i$ .<sup>28</sup> The result shows a close relation between the oscillation and a dynamics of

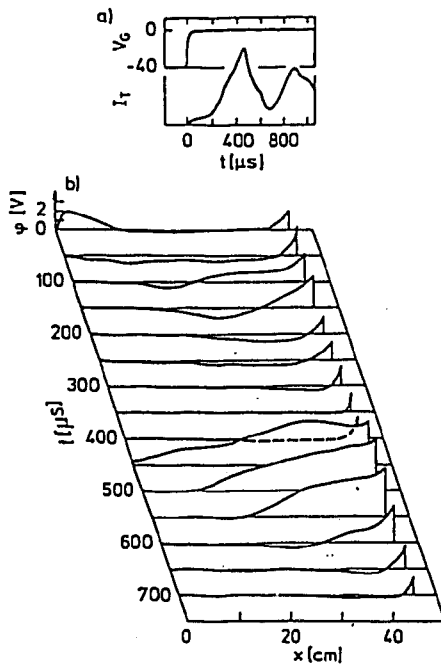


Fig.25. Dynamics of negative potential dip in moving DL.

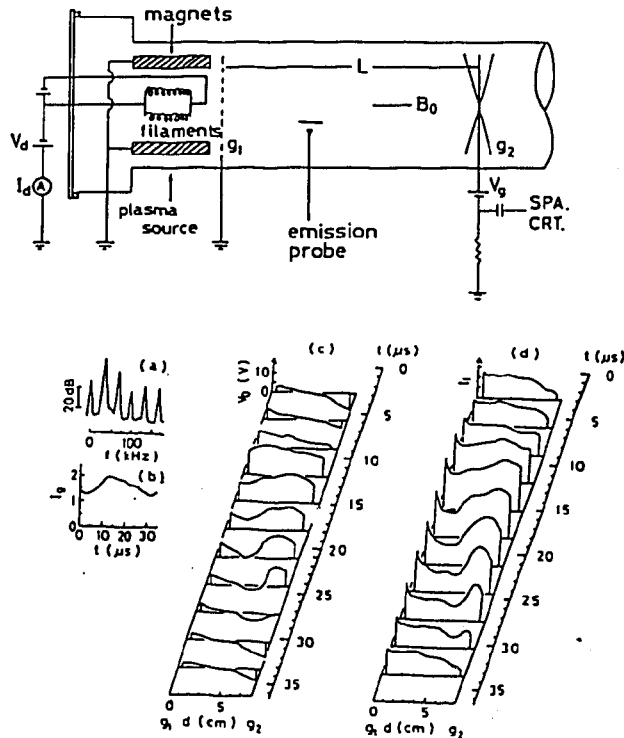


Fig.26. Moving DL in a discharge plasma.

moving DL. The moving DL formed in front of  $S_2$  ( $x=0$  cm) moves towards  $S_1$ , being followed by a flow of the plasma from  $S_2$  during the decrease in  $I_T$ . When the DL arrives at  $S_1$ ,  $I_T$  increases and  $\phi$  increases along the whole plasma column. Then the DL reforms at  $S_2$ . The repetition of the phenomenon gives rise to the oscillation in  $I_T$ . A detailed structure of the DL tail can be found in Fig.25. A negative potential dip is formed during the DL movement and disappears at  $S_2$ , resulting in the increase in  $I_T$ . This dynamics of the negative potential dip is the same as in the fluctuation of the stationary DL in 3-2.

The same moving DL is also observed in a discharge plasma. A potential difference is applied between a mesh grid  $g_1$  and an asterisk grid  $g_2$  immersed in a diffused plasma supplied from the source through  $g_1$ , as shown in Fig.26.<sup>29</sup> In this case, a much bigger dip of negative potential is generated because  $T_e$  ( $\approx$  a few eV) is higher than that in a Q machine. It is to be noted that this experimental configuration is almost the same as in the previous works on current-driven ion acoustic instability.<sup>30</sup> Their results may have some relation to the moving DL described above, because the DL moves with speed close to ion acoustic speed. A similar behavior of the moving DL can be found in Fig.6, where the DL is generated by electron-beam injection.

#### 3-4 Effects of Magnetic Mirror on DL

It is quite important to know properties of the DLs in plasmas under nonuniform magnetic fields. Here effects of a magnetic mirror on the stationary DLs are described.<sup>31</sup> The DLs are generated in the same way as in 3-1. A mirror configuration is provided near the center of a Q machine, as shown in Fig.27. The mirror ratio  $R_m$  is varied in the range 1-1.8. Under the uniform magnetic field ( $R_m=1$ ), the

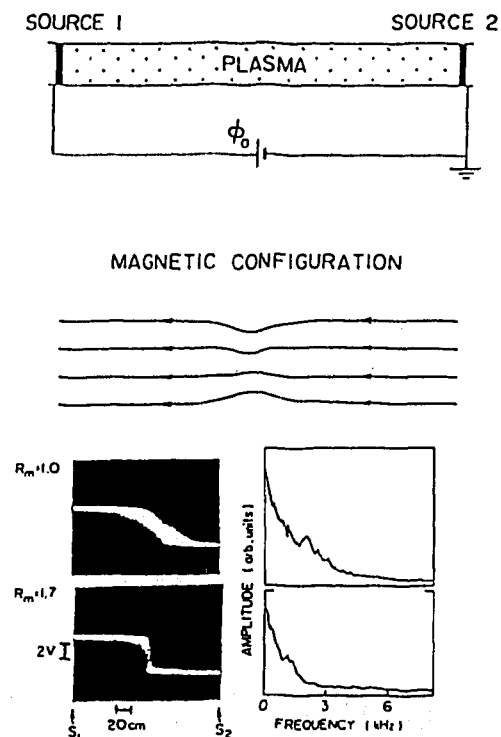


Fig.27. Experimental configuration and results on mirror effects on DL.

DL position is set by controlling the plasma densities supplied from  $S_1$  and  $S_2$ . When the DL position is around the mirror, the DL is very sensitive to the mirror. The effects are clear even at  $R_m=1.3$ . With an increase in  $R_m$ , the DL width becomes small. This is because the fluctuation of the DL tail is decreased in the presence of the mirror (see Fig.28). Besides, the DL position is fixed at the mirror position. As the mirror is moved, the DL is observed to move together with the mirror, as shown in Fig.29 where  $R_m=1.8$ .

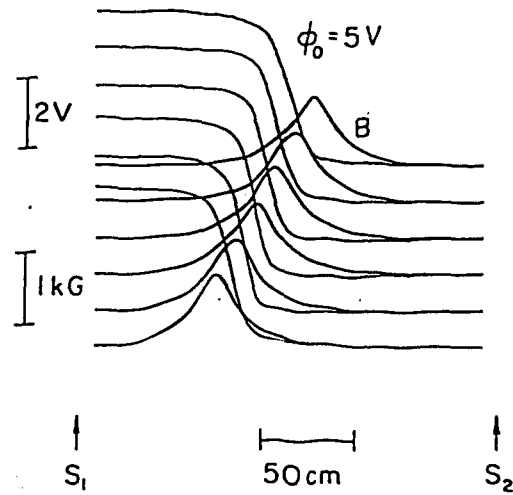


Fig.29. Control of DL position by magnetic mirror

When the DL position at  $R_m=1$  is far from the mirror, we cannot observe such strong effects of the mirror.

### 3-5 DL with Three-Dimensional Configuration

Here the diameter of  $S_2$ , 8 mm, is much smaller than that of  $S_1$ . Even in this case, the stationary DL is generated by applying a potential difference between  $S_1$  and  $S_2$  under a strong

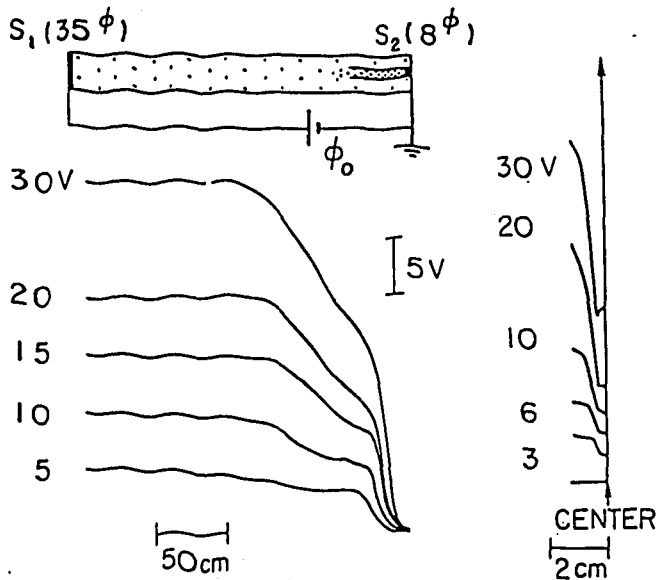


Fig.30. Experimental Configuration and results on three-dimensional DL.

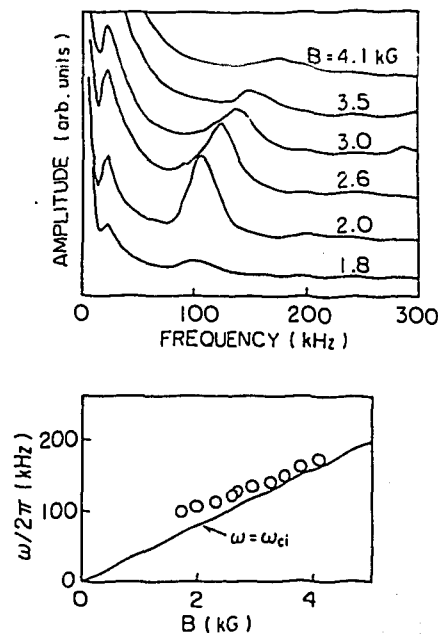


Fig.31. Electrostatic ion cyclotron instability.

uniform magnetic field,<sup>32</sup> as shown in Fig.30. The DL, however, has a two-stage structure in the axial direction. Measurements of radial profiles of  $\phi$  yields a three-dimensional configuration of the DL (sometimes called "two-dimensional" because of its axisymmetric structure). In the presence of the DL with this structure, we can find a generation of oscillation (see Fig.31) which was not observed in the case of the one-dimensional DL in 3-1. The oscillation, the frequency of which is plotted against the magnetic field  $B$  in Fig.31, is confirmed to be due to an electrostatic ion cyclotron instability. The instability is caused by the radial structure of  $\phi$ . This fact is consistent with the measurements of this instability in a single-ended Q machine,<sup>33</sup> where the instability was generated by applying a positive potential to a cold plate whose diameter is smaller than the cross section of the plasma column.

### 3-6 Potential Formation between Two Different Plasmas

Phenomena concerned with potential formation in plasmas are of current interest in plasma physics and technology. The DL is one of the examples in such a general problem. Finally, an experiment on potential formation between two different plasmas is presented as a different example of investigations.

In this case,<sup>34</sup>  $S_2$  is replaced by a source (anode A and oxide cathode K) for a discharge plasma. An Ar gas is fed into the machine. Now we have a Q-machine plasma produced at  $S_1$  and an Ar discharge plasma supplied from  $S_2$ .  $T_e$  of the discharge plasma, a few eV, is higher by an order of magnitude than that of the Q-machine

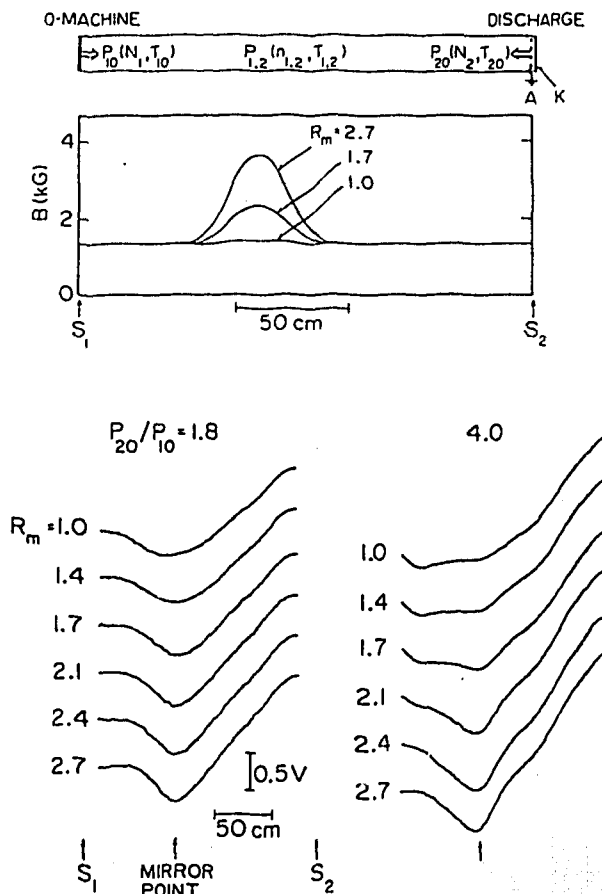


Fig.32. Experimental configuration and results on potential formation between two different plasmas

plasma. There is no appreciable difference between ion temperatures of the both plasmas. A is grounded electrically so that the potential of the discharge plasma is fixed. But,  $S_1$  is kept to be floating. We have no external potential supply between the two plasmas which flow along a strong magnetic field in the opposite directions. There is no net electric current passing through the plasma column. A bump of magnetic field (mirror) with mirror ratio  $R_m \leq 2.7$  can be provided near the center of the machine, as shown in Fig.32.

When we have only the discharge plasma ( $S_1$  is not heated), measurements of axial potential profile show a monotonous decrease of  $\phi$  towards  $S_1$ , as expected from ambipolar diffusion along the magnetic field. When  $S_1$  is heated hot enough for plasma production, however, we can recognize a potential increase near  $S_1$ . With a gradual density increase of the plasma from  $S_1$ , a spatial region of this potential increase spreads towards  $S_2$  and there appears a stable potential minimum along the plasma column at a position where the plasma pressures of the two plasmas ( $P_{1,2}$ ) are balanced. The magnetic bump added to the uniform field around this position is observed to enhance and further localize the potential dip, as shown in Fig.32. The dip is surrounded by two regions with higher potential of an order of corresponding electron temperature.

This potential dip is a kind of thermal barrier<sup>5</sup> and isolates two groups of electrons (from  $S_1$  and  $S_2$ ) from each other except for extremely high energy electrons. In general, a plasma flow has a potential decreasing towards its front. In our case, we have two different plasmas flowing in the opposite directions. It is reasonable to expect such a potential minimum at a position of their contact as observed in our work. The physical meaning is the same as in the case of the negative potential dip formed on the tail of the DL in 3-2 and 3-3.

#### IV. CONCLUSIONS

In this review, the DLs observed in the various experiments are classified into four categories, although the categories are closely related to each other. Our recent results, which belongs to the Category (4) in Sec.II, are presented in some detail.

Most of our works are performed in a nondischarge plasma

under a strong magnetic field. The results clarify many new features of collisionless double layers. Our DLs, however, are confirmed to be always fluctuating. The DLs observed in discharge plasmas seem to be more stable than the DLs in a non-discharge plasma. If there is a small amount of volume ionization in plasmas, the ionization may be effective to stabilize the DLs in such plasmas. It is without saying that the DLs are destroyed by a large amount of ionization under a certain condition.<sup>35</sup>

The experiment on formation of the potential minimum between two different plasmas suggests a possibility to produce a thermal barrier in open-ended fusion devices.

#### ACKNOWLEDGEMENTS

The author is indebted to his many collaborators in the works referred in Sec.III. He also thank financial supports for the works by the Grant-in-Aid for Scientific Research from the Ministry of Education, Japan.

## REFERENCES

1. H. Schamel, Symposium on Plasma Double Layers, Risø, 1982 (see this volume).
2. P. Carlqvist, Symposium on Plasma Double Layers, Risø, 1982 (see this volume).
3. W. B. Bridges, A. N. Chesler, A. S. Halsted, and J. V. Parker, Proc. IEEE 59, 724(1971).
4. A. Mohri, K. Narihara, Y. Tomita, T. Tsuzuki, Z. Kabeya, K. Akaishi, and A. Miyahara, Jap. J. Appl. Phys. 19, L174(1980).
5. G. I. Dimov, V. Z. Zakaidakov, and M. E. Kishirevskii, Fiz. Plazmy 2, 597(1976) [Sov. J. Plasma Phys. 2, 326(1976)]; T. K. Fowler and B. G. Logan, Comments Plasma Phys. Cont. Fusion 2, 167(1977); D. E. Baldwin and B. G. Logan, Phys. Rev. Lett. 43, 1318(1979).
6. F. W. Crawford and A. B. Cannara, J. Appl. Phys. 36, 3135(1965).
7. M. J. Schönhuber, Z. angew. Phys. 15, 454(1963); F. W. Crawford and I. L. Freeston, Proc. of Sixth International Conference on Phenomena in Ionized Gases, Paris, 1963 (ed. P. Hubert and E. Crémieu-Alcan, EURATOM-CEA) I, p.461.
8. S. W. Rayment and N. D. Twiddy, J. Phys. D2, 1747(1969).
9. S. Torvén, Wave Instabilities in Space Plasmas (ed. P. J. Palmadesso and K. Papadopoulos, Reidel, 1979), p.109; F. W. Crawford, J. S. Levine, and D. B. Ilić, ibid., p.129.
10. S. Torvén and M. Babić, Proc. of Twelfth International Conference on Phenomena in Ionized Gases, Eindhoven, 1975 (ed. J. G. A. Hölscher and D. C. Schram, American Elsevier Pub. Com., New York, 1975), p.124.
11. J. S. Levine and F. W. Crawford, J. Plasma Phys. 24, 359(1980).
12. E. I. Lutsenko, N. D. Sereda, and L. M. Kontsvoi, Zh. Tekh. Fiz. 45, 789(1975) [Sov. Phys.-Tech. Phys. 20, 498(1976)].
13. S. Torvén and D. Anderson, J. Phys. D: Appl. Phys. 12, 717 (1979); S. Torvén and L. Lindberg, J. Phys. D: Appl. Phys. 13, 2285(1980).
14. R. Hatakeyama, S. Iizuka, T. Mieno, J. Juul Rasmussen,

- K. Saeki, and N. Sato, Proc. of 1980 Autumn Meeting of Physical Society of Japan, Fukui, p.62.
15. R. L. Stenzel, W. Gekelman, and N. Wild, Proc. of 1982 International Conference on Plasma Physics, Göteborg (ed. H. Wilhelmsson and J. Weiland, Chalmers University of Technology), p.27.
  16. B. H. Quan and A. Y. Wong, Phys. Rev. Lett. 37, 1393(1976); P. Leung, A. Y. Wong, and B. H. Quan, Phys. Fluids 23, 992 (1980).
  17. P. Coakley and N. Hershkowitz, Phys. Rev. Lett. 40, 230(1978), Phys. Fluids 22, 1171(1979); P. Coakley, L. Johnson, and N. Hershkowitz, Phys. Lett. 70A, 425(1979).
  18. K. D. Baker, L. P. Block, R. Kist, W. Kampa, N. Singh, and H. Thiemann, J. Plasma Phys. 26, 1(1981).
  19. S. Iizuka, K. Saeki, N. Sato, and Y. Hatta, Phys. Rev. Lett. 43, 1404(1979); K. Saeki, S. Iizuka, and N. Sato, Phys. Rev. Lett. 45, 1853(1980).
  20. D. Jovanović, J. P. Lynov, P. Michelsen, H. L. Pécseli, J. Juul Rasmussen, and K. Thomsen, Proc. of 1982 International Conference on Plasma Physics, Göteborg (ed. H. Wilhelmsson and J. Weiland, Chalmers University of Technology), p.136.
  21. R. L. Stenzel, M. Ooyama, and Y. Nakamura, Phys. Rev. Lett. 45, 498(1980), Phys. Fluids 24, 708(1981).
  22. Y. Nakamura and R. L. Stenzel, Symposium on Plasma Double Layers, Risø, 1982 (see this volume).
  23. Ch. Hollenstein, M. Guyot, and E. S. Weibel, Phys. Rev. Lett. 45, 2110(1980).
  24. S. Torvén and S. Liting, Proc. of 1982 International Conference on Plasma Physics, Göteborg (ed. H. Wilhelmsson and J. Weiland, Chalmers University of Technology), p.26.
  25. N. Sato, R. Hatakeyama, S. Iizuka, T. Mieno, K. Saeki, J. Juul Rasmussen, and P. Michelsen, Phys. Rev. Lett. 46, 1330 (1981), Plasma Research Report THUP-1, Tohoku Univ.(1981)
  26. S. Iizuka, P. Michelsen, J. Juul Rasmussen, R. Schrittwieser, R. Hatakeyama, K. Saeki, and N. Sato, Proc. of 1982 Inter-

- national Conference on Plasma Physics, Göteborg (ed. H. Wilhelmsson and J. Weiland, Chalmers University of Technology), p.134.
27. N. Sato, G. Popa, E. Märk, E. Mravlag, and R. Schrittwieser, *Phys. Fluids* 19, 70(1976).
  28. S. Iizuka, P. Michelsen, J. Juul Rasmussen, R. Schrittwieser, R. Hatakeyama, K. Saeki, and N. Sato, *Phys. Rev. Lett.* 48, 145(1982).
  29. H. Fujita, S. Yagura, E. Yamada, Y. Kawai, and N. Sato, *Symposium on Plasma Double Layers, Risø*, 1982 (see this volume).
  30. H. Tanaca, M. Koganei, and A. Hirose, *Phys. Rev.* 161, 94(1967); S. Watanabe, *J. Phys. Soc. Jpn* 35, 600(1973); Y. Kawai, Ch. Hollenstein, and M. Guyot, *Phys. Fluids* 21, 970(1978).
  31. N. Sato, T. Kanazawa, R. Hatakeyama, and K. Saeki, *Proc. of 1981 Spring Meeting of Physical Society of Japan, Hiroshima*, P.118; R. Schrittwieser, R. Hatakeyama, T. Kanazawa, and N. Sato, *Proc. of 1982 International Conference on Plasma Physics, Göteborg* (ed. H. Wilhelmsson and J. Weiland, Chalmers University of Technology), p.135.
  32. T. Kanazawa, R. Hatakeyama, and N. Sato, *Proc. of 1981 Autumn Meeting of Physical Society of Japan, Niigata*, p.93.
  33. R. Hatakeyama, N. Sato, H. Sugai, and Y. Hatta, *Phys. Lett.* 63A, 17(1977); N. Sato, *Proc. of 1980 International Conference on Plasma Physics, Nagoya* (Fusion Research Association of Japan), II, p.138.
  34. R. Hatakeyama, Y. Suzuki, and N. Sato, *Symposium on Plasma Double Layers, Risø*, 1982 (see this volume).
  35. S. Iizuka, P. Michelsen, J. Juul Rasmussen, R. Hatakeyama, K. Saeki, and N. Sato, *Proc. of Fifteenth International Conference on Phenomena in Ionized Gases, Minsk, 1981*.

STRONG STATIONARY SPACE CHARGE DOUBLE LAYERS IN A  
MAGNETIC MIRROR

R. Schrittwieser\*, R. Hatakeyama, T. Kanazawa, and N. Sato

Department of Electronic Engineering  
Tohoku University, Sendai - 980, Japan

Abstract: A strong stationary double layer in a double-ended Q-machine is, for decreasing the magnetic field strength locally, subject to a series of modifications: at first it is split up into two double layers, separated by a thin plasma layer. Thereafter ions and eventually also electrons are lost at the plasma chamber walls and the double layer becomes narrower and is locked to the position of lowest magnetic field strength.

### I. Introduction

It is meanwhile a well established fact that ultrastrong stationary double layers (DL) can easily be formed by applying a potential difference between the hot plates of a double-ended Q-machine.<sup>1,2</sup> DL's have hitherto mainly been investigated in discharge plasmas<sup>3-6</sup> and are possible candidates for the acceleration of electrons precipitating into the ionosphere.<sup>9-12</sup> Several authors have pointed out that DL's are affected by longitudinal density and/or temperature gradients,<sup>4,6,7,12</sup> as present in the ionosphere due to a longitudinally varying magnetic field<sup>6,9,11</sup> or in a discharge tube due to a varying cross-section.<sup>4,7,8</sup>

### II. Experimental Set-up

The experiments were carried out in the Tohoku University  $Q_T$ -machine with  $K^+$ -plasma created on two hot Ta-plates of a diameter of 3 cm each

(HP1 and HP2) and 3.2 m apart. Magnetic field strength, temperature and plasma density are respectively:  $B = 1 - 4$  kG,  $T_e \approx T_i \approx 0.2$  eV,  $n \approx 5 \times 10^8 - 10^{10}$  cm<sup>-3</sup>. The radius of the plasma chamber is  $r_{ch} = 7.8$  cm. The plasma potential is measured by an axially movable electron emissive probe under the assumption that its floating potential is a sufficiently accurate measure for  $\Phi_{pl}$ .<sup>13</sup> To create a DL a voltage  $\Phi_{HP1} \approx 5 - 20$  V is applied to HP1 whereas HP2 is grounded. The potential drop of the DL is always  $\Phi_{DL} \approx \Phi_{HP1}$ . The current drawn through the plasma column is several mA.<sup>1</sup>

To produce a magnetic mirror field configuration one of the 33 magnetic field coils (carrying the current  $I_{B1}$ ) near the center of the Q-machine carries a lower or even reversed current  $I_{B2}$ .  $R_{max} = B_{min}/B_0$  is the mirror ratio in the "mirror point"; i.e., the center of the coil which carries  $I_{B2}$ . A simple consideration shows that the cross-section of the plasma column  $A_{pl}(z)$ , assuming fully magnetized particles, is  $A_{pl}(z) \sim 1/B(z)$  and the apparent radius  $r_{pl}(z) = r_0 \sqrt{B_0/B(z)}$ , where  $r_0$  and  $B_0$  are the radius of the plasma column and the magnetic field strength in the homogeneous field region respectively. For  $I_{B1} = 100$  A and  $I_{B2} \leq -255$  A the B-field in the mirror point is reversed and a double cusp field is formed. For  $I_{B2} \approx -240$  A in the mirror point  $r_{pl} = r_{ch}$ ; i.e., the edge of the (fully magnetized) plasma column touches the wall of the plasma chamber. In this case the magnetic field strength in the mirror point is 50 G and  $R_{max} \approx 0.04$ .

### III. Experimental Results

Fig. 1 shows the typical development of a DL in a homogeneous magnetic field (uppermost figure) for decreasing  $R_{max}$ . The solid lines show the axial profile of the plasma potential, the dashed lines are the ion saturation current ( $I_{is}$ ) profiles and the dotted lines the B-field

strength profiles. For  $1 \geq R_{\max} \geq 0.72$  nearly no change of the DL shape is found. For  $0.58 \geq R_{\max} \geq 0.30$  the potential profile shows a plateau slightly right from the mirror point. This indicates a splitting of the DL into two, separated by a thin layer of field free plasma. For  $R_{\max} = 0.16$  the DL changes its shape strongly, becoming much steeper and shifting about 50 cm towards the low potential side. Finally, the  $R_{\max} = 0.02$  the DL shifts back to the mirror point without changing its steepness.

#### IV. Discussion

As long as both electrons and ions can be assumed to be magnetized, the only effect of the mirror field is to locally reduce the current density since the cross section of the plasma column is given by the magnetic field lines. This should lead to a broadening of the DL,<sup>3,12</sup> which we do, however, not observe. (In the contrary case, i.e., a local constriction of the magnetic field, a decrease of the DL width has indeed been found.<sup>2</sup>)

The thin plasma layer which appears for  $R_{\max} \leq 0.6$  is, we believe, due to the following effect: Those particle species which possess a longitudinal drift, be it through the DL (the free particle species) or due to the presumably electron rich sheaths in front of the HP's, will mainly be inside the loss cone and pass more or less unaffected through the mirror. Particles outside the loss cone (mainly the trapped particles species of the DL) will be accelerated towards the lower B-field region; i.e., towards the mirror point. Despite the reflection of electrons on the high potential and of ions on the low potential side of the DL, eventually enough particles of both species gather near the mirror point, forming a layer of quasineutral plasma. This process is supported by the mirror effect which might trap a number of particles that have entered the low B-field region. Due to the larger thermal speed of the electrons the plateau is shifted towards the low potential side.

The total change of shape and the shift of the DL for  $R_{\max} = 0.16$  is due to the large Larmor radius of the ions whereas the electrons can still be considered magnetized. A rough estimate, based on the B-field strength on the axis, yields an ion Larmor radius  $r_i \approx 1.4$  cm and  $r_{pl} \approx 3.8$  cm for  $r_0 = 1.5$  cm. Although  $r_i + r_{pl} < r_{ch}$  a part of the ions from the plasma column edge are lost at the walls since we have to take into account not only that the B-field strength in this configuration decreases towards the edge of the plasma chamber but also that the actual radius of the plasma column, also in the homogeneous field region, is larger than the radius of the HP's. Hence, while ions are lost, electrons are still accelerated towards the mirror point pushing the positive space charge layer towards the low potential side and thus steepening the DL.

Finally, for  $R_{\max} = 0.02$  the plasma column bulge touches the chamber walls and also electrons from the column edge get lost at the walls. Similarly, as in the case of a magnetic field constriction,<sup>2</sup> the mirror now acts as a barrier, separating a considerable part of the two trapped particle species from each other and thereby locking the DL to the mirror point.

Acknowledgements: One of the authors (R.S.) expresses his deep gratitude to Prof. N. Sato and his collaborators for their extraordinary hospitality. He acknowledges the support by the Japan Society for the Promotion of Science and the Austrian Ministry for Science and Research. He thanks Prof. F. Cap for his encouragement.

\*Permanent address: Institute for Theoretical Physics, University of Innsbruck, A-6020 Innsbruck, Austria.

References:

1. N. Sato, R. Hatakeyama, S. Iizuka, T. Mieno, K. Saeki, J.J. Rasmussen and P. Michelsen, *Phys. Rev. Lett.* 46, 1330 (1981); S. Iizuka, P. Michelsen, J.J. Rasmussen, R. Schrittwieser, R. Hatakeyama, K. Saeki, and N. Sato, in Proceedings of the 1982 International Conference on Plasma Physics, Göteborg, Sweden, in print.
2. R. Schrittwieser, R. Hatakeyama, T. Kanazawa, and N. Sato, in Proceedings of the 1982 International Conference on Plasma Physics, Göteborg, Sweden, in print.
3. I. Langmuir, *Phys. Rev.* 33, 954 (1929).
4. M.J. Schönhuber, *Zeitschr. Angew. Phys.* 15, 454 (1963).
5. P. Coackly, N. Hershkowitz, R. Hubbard, and G. Joyce, *Phys. Rev. Lett.* 40, 230 (1978); P. Coackly and N. Hershkowitz, *Phys. Fluids* 22, 1171 (1979); J.S. Levine, F.W. Crawford, and D.B. Ilić, *Phys. Lett.* 65A, 27 (1978); S. Torven and D. Anderson, *J. Phys. D; Appl. Phys.* 12, 717 (1979); S. Torven, in Wave Instabilities in Space Plasmas (ed. P. J. Palmadesso and K. Papadopoulos), D. Reidel, 1979, p. 109; P. Leung, A.Y. Wong, and B.H. Quon, *Phys. Fluids* 23, 992 (1980); J.S. Levine and F.W. Crawford, Institute for Plasma Research, Stanford University, SU-IPR Report No. 807. March 1980.
6. R.L. Stenzel, M. Ooyama, and Y. Nakamura, *Phys. Rev. Lett.* 45, 1498 (1980); *Phys. Fluids* 24, 708 (1981).
7. F.W. Crawford and I.L. Freeston, in Proceedings Vith International Conference on Phenomena in Ionized Gases, Paris 1963, Vol. I, p. 461.
8. D. Anderson, M. Babic, S. Sandahl, and S. Torven, in Proceedings IXth International Conference on Phenomena in Ionized Gases, Bucharest 1969, p. 142.
9. F.S. Mozer, C.W. Carlson, M.K. Hudson, R.B. Torbert, B. Parady, J. Yatteau, and M.C. Kelley, *Phys. Rev. Lett.* 38, 292 (1977).
10. L.P. Block, *Astrophys. and Space Sci.* 55, 59 (1978).
11. S.D. Shawan, C.G. Falthammer, and L.P. Block, *J. Geophys. Res.* 83, 1049 (1978).
12. P. Carlquist, *Cosmic Electrodyn.* 3, 377 (1972); in Wave Instabilities in Space Plasmas, (ed. P.J. Palmadesso and K. Papadopoulos), D. Reidel, 1979, p. 83; F.W. Crawford, S. Levine, and D.B. Ilić, *ibid*, p. 129.
13. S. Iizuka, P. Michelsen, J.J. Rasmussen, R. Schrittwieser, R. Hatakeyama, K. Saeki, and N. Sato, *J. Phys. E.; Sci. Instrum.* 14, 1291 (1981); *Phys. Rev. Lett.* 48, 145 (1982).

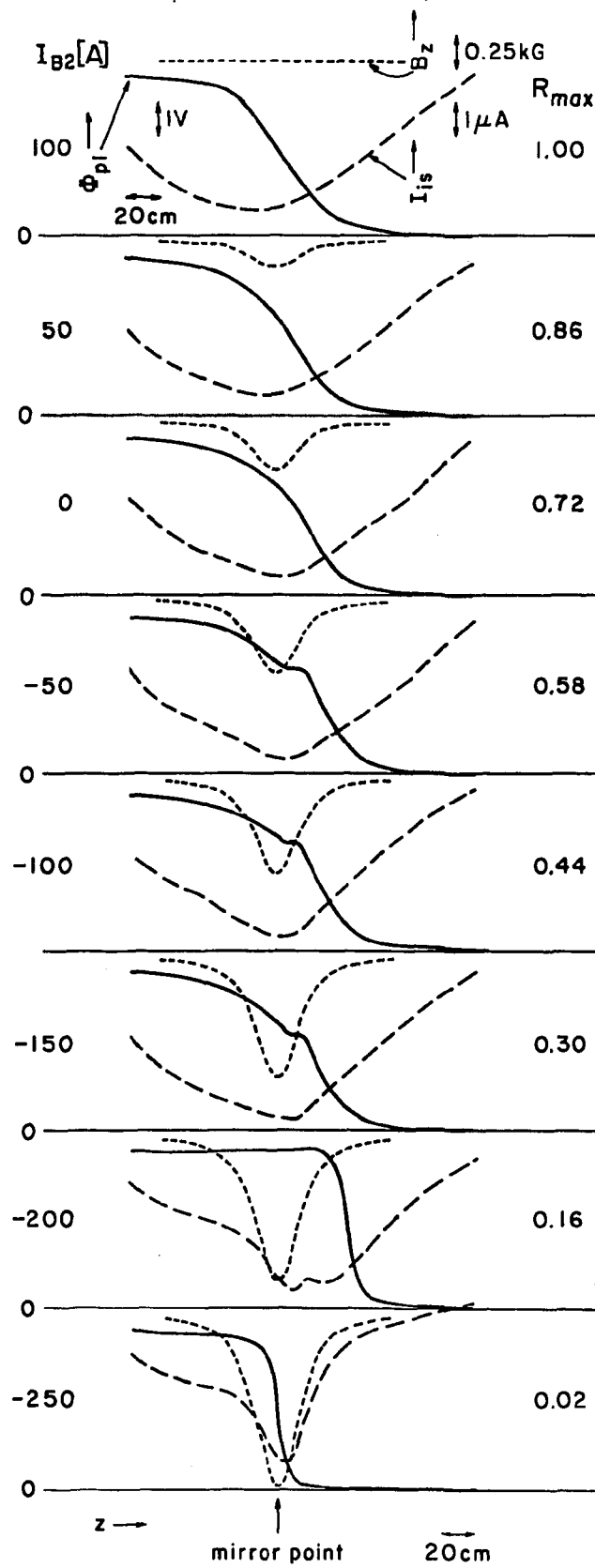


Fig. 1. Axial profiles of the plasma potential  $\Phi_{p1}$  (solid lines), the ion saturation current  $I_{is}$  (dashed lines) and the magnetic field strength on the axis  $B_z$  (dotted lines) with the mirror ratio  $R_{max}$  as parameter.

### Three dimensional double layers in magnetized plasmas

D. Jovanović<sup>+</sup>, J.P. Lynov, P. Michelsen, H.L. Pēcseli,  
J. Juul Rasmussen, K. Thomsen

Assoc. Euratom-Risø National Laboratory, Physics Dept., Risø,  
P.O. Box 49, DK-4000 Roskilde, Denmark

<sup>+</sup>Permanent address: Inst. of Physics, P.O. Box 57, 11001 Beograd,  
Yugoslavia.

**Abstract:** Experimental results are presented which demonstrate the formation of fully three dimensional double layers in a magnetized plasma.

Most of the previous double-layer experiments are essentially concerned with one dimensional structures in unmagnetized plasmas (see e.g. Coakley and Hershkowitz (1979), Leung et al. (1980) and references therein), or very strongly magnetized plasmas (e.g. Sato et al. 1981). For instance Bloch (1981), Stenzel et al. (1981), Baker et al. (1981) and Anderson (1981) report three dimensional features. These observations are, however, restricted to weak magnetic fields i.e. the ions can essentially be considered as unmagnetized although the electron Larmor radius is smaller than the scale length for the potential variation perpendicular to the applied field,  $B$ . In the present experiment we investigate the effect of a finite ion Larmor radius,  $\rho_i$ , and demonstrate the existence of stationary double layers also in the limit of very small  $\rho_i$ .

The experiment is performed in a double ended Q-machine operated in electronrich condition (Motley, 1975). A cesium plasma of density  $\sim 10^7$  cm<sup>-3</sup> and temperature  $\sim 0.2$  eV is produced by surface ionization on two hot ( $\sim 2000^\circ$ ) tantalum surfaces denoted HP1 and HP2, see Fig. 1a. The plasma is confined radially by a magnetic field, variable in the range 0.10-0.35 T. The plasma column thus produced has a radius  $R = 1.5$  cm and a length  $L = 1.25$  m. The column is separated by two fine meshed tantalum grids orientated  $\perp B$  with a limiting aperture of radius  $R_b = 0.4$  cm centered at the axis. By biasing the source end of the device (i.e. HP1) negatively with respect to the other end, i.e. HP2, which is grounded, we may inject an electron beam along  $B$  into the main plasma. (This mode of operation somewhat resembles a standard double-plasma operation, Leung et al. (1980)). By varying the bias of the grid G1 facing HP1 (see Fig. 1a) we can adjust the current density in the electron beam (Iizuka et al. 1979). The grid G2 facing HP2 is grounded and thus constitutes an absorbing surface for the electrons and fast ions produced at HP2. Variations of plasma potential, axially and radially, were detected by a movable, emissive Langmuir probe. We emphasize that the mean free path for collisions is much larger than  $L$  in our case i.e. the plasma is collisionless to a very good approximation, in contrast to the experiments of e.g. Coakley and Hershkowitz (1979), Leung et al. (1980) or Anderson (1981). The neutral background pressure is less than  $10^{-5}$  torr in our device, so we are not limited to a maximum voltage drop across the double layer determined by the ionization energy of the neutral background.

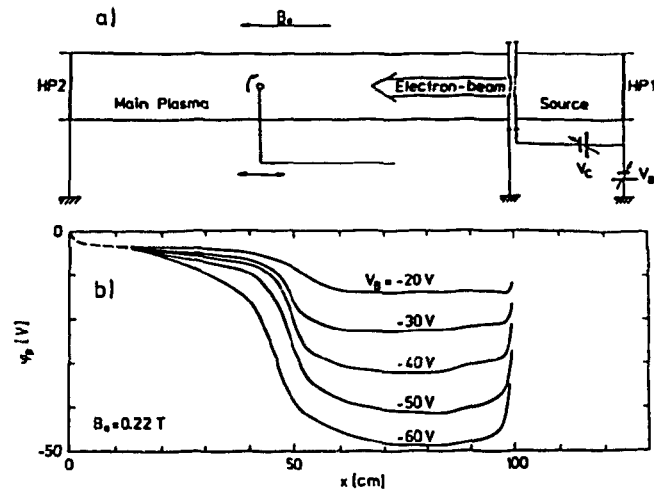


Fig. 1. a) Experimental set up, schematically.  
b) Axial measurements of double-layers.

The main features of the experiment may be summarized as follows. The hot plate HP2 supplies the main plasma with ions and electrons. An electron beam is injected, from the source plasma, into the central core of the main plasma. The surplus of electrons in this region lowers the local potential causing a deceleration of the incoming electrons. Electrons that manage to overcome this decelerating potential will subsequently be accelerated along  $B$  towards HP2. Ions originating from HP2 will be accelerated towards the region with negative potential to compensate the surplus of electrons there. For stationary conditions, however, the continuity of the ion flow implies that the contribution to the local charge density of the accelerated ions decreases. These essentially one-dimensional arguments thus indicate that a self consistent low potential region may form in front of the grids. In a strongly magnetized plasma, i.e.  $\rho_i \ll R_b$  we expect a one dimensional argument to be acceptable and our measurements of the potential variation indeed confirm the existence of a stationary potential variation along the axis, see Fig. 1b.

Radial measurements are performed for each 5 cm along the axis and continuously across the plasma column. These data are then digitized and interpolated numerically to produce figures like Figs. 2 and 3. The spatial resolution of the probe is better than 0.5 mm radially and better than 2 mm axially. (The construction of this particular emissive probe is described by Iizuka et al. (1981)). The potential jump observed as moving from HP2 towards HP1 possesses all the desired properties of a Double-Layer (DL) and will be denoted as such in the following. The scale length  $d$  of the DL along the axis is much larger than the Debye length,  $\lambda_D$ , if it is calculated using the  $\sim 0.2$  eV thermal energy of the main plasma. If, however, we calculate  $\lambda_D$  using the energy of the incoming electron beam we find that  $d$  and  $\lambda_D$  are comparable. Measurements for varying beam energies show, however, that there is not a simple proportionality, see Fig. 1b. Obviously the potential depletion induced by the electron beam is significant only

in the central core of the plasma. Outside this core the potential is of course determined by the plasma potential,  $\phi_p$ , of the main plasma. (Note that  $\phi_p < 0$ , due to the voltage drop at the sheath of the hot plate, HP2, see e.g. Motley (1975)). Actually, we note that the negative core has a slight influence on the unperturbed plasma, see Fig. 2a. This is not entirely unexpected since  $\rho_i \sim 0.2$  cm (calculated from  $T_i \sim 0.2$  eV) is not truly infinitesimal. We note that a small fraction of the residual plasma of the source plasma leaks outside the limiting aperture and slightly deforms the equipotential surfaces at the outer radius of the main plasma. This minor effect is unavoidable in our present construction but does not affect our interpretation of the results.

We repeated the measurements described previously in a reduced magnetic field, so  $\rho_i > R_b$ , see Fig. 2b. The double-layer is now detected across the full plasma column. Because of their large Larmor radii, ions are now accelerated also radially, and the previous one-dimensional arguments are insufficient. An ion transported radially into the central core will be trapped there, by the slightest energy loss (e.g. collisions or radiation of low frequency wave types). By moving along the axis it will subsequently be lost either by recombination at G1 and G2, or to the negatively biased source plasma. The resulting deficit of ions outside the core will leave a surplus of electrons which lowers the potential, see Fig. 2b. Intuitively we expect that the characteristic B-transverse scale-length of the double-layer is roughly given by the ion Larmor radius. By varying B we confirmed this scaling. In Fig. 3a we show an example where  $\rho_i \sim R_b$ . Notice that here the double layer is not fully radially developed.

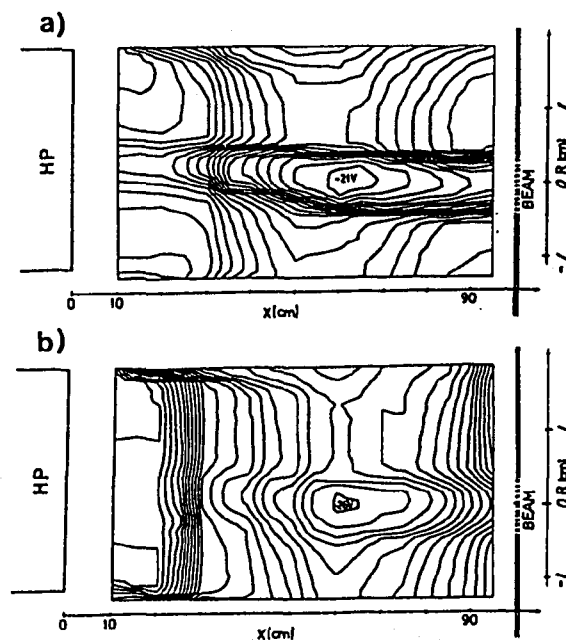


Fig. 2. Equipotential contours for two different magnetic fields: a)  $B = 0.34$  T, b)  $B = 0.10$  T.

According to the previous qualitative arguments, the formation of a double layer across the full plasma column is accompanied by a significant reduction in plasma density outside the core. This feature was also confirmed by determining the electron velocity distribution by using the Langmuir probe in non-emissive condition and differentiating the probe characteristic.

On Figs. 3b-c we show results corresponding to Fig. 3a. Measurements along the column (slightly off center), Fig. 3b, clearly show the incoming electron beam being decelerated as it creates the potential depletion and subsequently being accelerated towards HP2. Notice the large electron component of the main plasma in the vicinity of HP2. Radial measurements of the electron distribution, see Fig. 3c, demonstrate that most of the plasma is concentrated in the central core in agreement with our previous discussion. The evolution of the electron energy distribution as experienced by the radially moving probe has many features in common with an "inverted V event", e.g. Frank and Ackerson (1971).

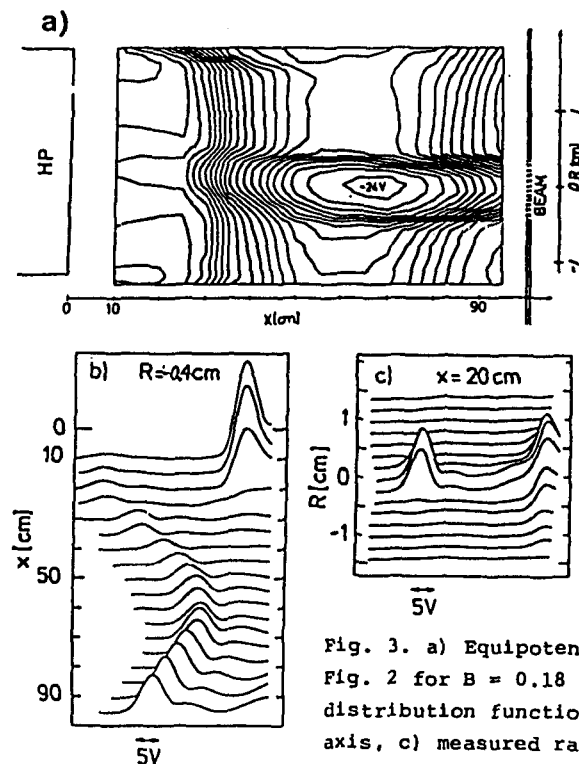


Fig. 3. a) Equipotential contours like Fig. 2 for  $B = 0.18$  T, b) Electron energy distribution functions measured along the axis, c) measured radially for an axial position  $x = 20$  cm.

We have also investigated spectral distribution of the noise associated with the double layer. In Fig. 4 we show samples of low frequency noise spectra. The figures are obtained by a standard spectrum analyzer, and show a frequency versus radius diagram. The shaded areas correspond to regions where the noise levels exceeded a certain reference level. We find that the noise above frequencies  $\sim 5$  kHz is concentrated to the current channel. The exact nature of the instability responsible for the enhanced noise level is yet uncertain. There are two candidates: i) the current along B and ii) the azimuthally  $E \times B$  rotating electrons at the edge of the current channel. Actually a closer inspection reveals that the noise intensity is slightly enhanced at this edge. We notice the absence of a peak in the spectrum at the ion

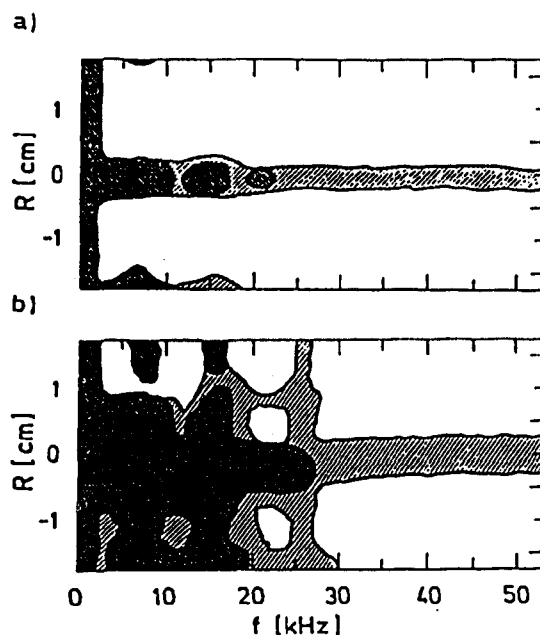


Fig. 4. Radial noise spectra for two positions along the axis: a)  $x = 60$  cm, b)  $x = 25$  cm.

cyclotron frequency, although waves with an approximate dispersion relation  $\omega^2 \sim \Omega_{ci}^2 + k_{\perp}^2 C_S^2$  can be driven unstable by an electron beam (Motley and D'Angelo, 1963). However, the parallel phase velocity  $\sim \Omega_{ci}/k_{\parallel}$  for these waves correspond to the electron beam velocity ( $\sim 3 \cdot 10^6$  m/s for 30 eV electrons), and the resulting parallel wavelength  $2\pi/k_{\parallel}$  is much larger than the length of the device so these waves cannot be excited at all. The stability of the double layer does not seem to be significantly affected by the enhanced noise level.

The results summarized in Figs. 1-3 represent time averaged values. Thus the instantaneous width of the double-layer is somewhat overestimated from Fig. 1b (see also Sato et al., 1981). However, the boundaries of the current channel are very sharp in for instance Fig. 2a and 3a, indicating a very stable configuration. Note also that the peak noise level is confined to the central core in all cases.

Various aspects of potential double layers are of current interest for the understanding of a variety of ionospheric phenomena, see e.g. the recent monograph edited by Akasofu and Kan (1981). Our experimental conditions cannot be scaled directly to the conditions prevailing in the ionosphere but they have many features in common with for instance the conditions assumed by e.g. Wagner et al. (1980). In our case the hot plate producing the main plasma may thus represent their conducting boundary modelling the effect of the ionosphere. The electron beam represents their current sheet. Note however that in our case ions are injected from one end only.

The results of this work represent our initial efforts of understanding the formation of stationary three dimensional double layers. More detailed investigations of the high frequency noise, the effect of magnetic field inhomogeneities and the temporal evolution are in progress. As far as the formation of the double layer is concerned, we interpret the dynamic process in terms of the Pierce instability (Pierce, 1944, Iizuka et al., 1979), modified by the finite radial geometry. Theoretical results (Jovanović, 1981) indicate that the instability is confined to the beam region and that the finite geometry has a negligible effect on the stability criterion and the linear growth rate. Preliminary results, including nonlinearities, show a decrease in the wavelength of the most unstable mode, while the potential decreases close to the beam inlet.

The expert technical assistance of M. Nielsen and B. Reher and valuable discussions with N. Sato and S. Iizuka are gratefully acknowledged.

#### References:

- Akasofu, S.-I. and Kan, J.R., Physics of Auroral Arc Formation, American Geophys. Union, Geophys. Monogr. 25, 1-465, 1981.
- Andersson, D., J. Phys. D: Appl. Phys., 14, 1403-1418, 1981.
- Baker, K.D., Singh, N., Block, L.P., Kist, R., Kampa, W., and Thiemann, H., J. Plasma Physics, 26, 1-27, 1981.
- Block, L.P., Geophys. Monogr. 25, Amer. Geophys. Union 218-225, 1981.
- Coakley, P., and Hershkowitz, N., Phys. Fluids, 22, 1171-1181, 1979.
- Frank, L.A., and Ackerson, K.L., J. Geophys. Res., 26, 3612-3643, 1979.
- Iizuka, S., Michelsen, P., Juul Rasmussen, J., Schrittwieser, R., Hatakeyama, R., Saeki, K., and Sato, N., J. Phys. E: Sci. Instr., 14, 1291-1295, 1981.
- Iizuka, S., Saeki, K., Sato, N., and Hatta, Y., Phys. Rev. Lett., 43, 1404-1407, 1979.
- Jovanović, D., Risø-M-2312, 1982.
- Leung, P., Wong, A.Y., and Quon, B.H., Phys. Fluids, 23, 992-1004, 1980.
- Motley, R.W., Q-Machines, Academic Press, New York, 1-190, 1975.
- Motley, R.W., and D'angelo, N., Phys. Fluids, 6, 296-299, 1963.
- Pierce, J.R., J. Appl. Phys., 15, 721-726, 1944.
- Sato, N., Hatakeyama, R., Iizuka, S., Mieno, T., Saeki, K., Juul Rasmussen, J., and Michelsen, P., Phys. Rev. Lett., 46, 1330-1333, 1981.
- Stenzel, R.L., Ooyama, M., and Nakamura, Y., Phys. Rev. Lett., 45, 1498-1501, 1980.
- Wagner, J.S., Tajima, T., Kan, J.R., Leboeuf, J.N., Akasofu, S.-I., and Dawson, J.M., Phys. Rev. Lett., 45, 803-806, 1980.

Potential Double Layers Formed by Ion Beam  
Injection into a Cusped Magnetic Field

Y. Nakamura and R. L. Stenzel<sup>\*)</sup>

The Institute of Space and Astronautical Science  
Komaba, Meguro-ku, Tokyo 153, JAPAN

Abstract

Experimental observation of a potential double layer in a collisionless magnetoplasma is presented. The double layer is formed when an ion beam is injected along converging field lines produced by a permanent magnet. The height of the double layer is nearly equal to the smaller of the beam energy and the bias voltage of the magnet. The double layer is formed even when the magnet is floating, i.e., no current is drawn to the boundary. Two-dimensional potential profiles are measured.

I. INTRODUCTION

Potential double layers which are thought to accelerate field aligned electrons have been one of main topics in space plasma physics.<sup>1</sup> A recent direct observation by an artificial satellite seems to confirm the existence of double layers in the auroral plasma.<sup>2</sup> Laboratory experiments<sup>3</sup> and computer simulations<sup>4</sup> show that an electron current drawn through a plasma, which satisfies the Bohm and Langmuir conditions, can create a double layer.

In a previous experiment<sup>5</sup> we observed that a two-dimensional double layer was formed when an ion beam was injected along converging magnetic field lines and reflected at a boundary drawing electron saturation current and that the height  $V_d$  of the double layer was somewhat smaller than that of the incident beam  $V_b$ . The beam ions were assumed to be hot ions<sup>6</sup> which are injected from the plasma sheet into the auroral plasma. The Larmor radius of beam ions was comparable to the dimension of the dipole magnet. As a result of this, beam ions were considered to be weakly magnetized. In the present work the intensity of the magnetic field is four times larger than in the previous experiment.

## II. EXPERIMENTAL SETUP

The experiment was performed in a double plasma device with surface dipole magnets as sketched in Fig.1.<sup>5</sup> The setup is similar to the one which measured the loss of beam ions to localized cusps.<sup>7,8</sup> Typical plasma parameters were; for the density  $n_e \approx 10^8 \text{ cm}^{-3}$ , temperature  $\kappa T_e \approx 2 \text{ eV}$ ,  $\kappa T_i \approx 0.2 \text{ eV}$ , gases  $\text{H}_2, \text{Ne}, \text{Ar}$ , and  $\text{Xe}$  at pressures  $2 \times 10^{-5} < p < 2 \times 10^{-4} \text{ Torr}$  with a base pressure of  $10^{-6} \text{ Torr}$ . When the source plasma anode was biased positively ( $\phi_b > 0$ ), an ion beam of energy  $eV_b (\approx 0.85e\phi_b)$  was injected into the target plasma whose anode was grounded. In the center of the target plasma (45cm diam), a permanent magnet (6cm diam, 3cm length,  $B=2\text{kG}$  at the pole face) was suspended with a dipole moment parallel to the chamber axis. A thin stainless steel disc which was insulated from the magnet and whose bias voltage  $\phi_m$  was applied externally was placed on the magnet. Plasma density and temperature were determined from a plane Langmuir probe (2mm diam) in regions of weak magnetic field. Electron temperatures were independently confirmed from sound speed measurements. The plasma potential  $\phi$  was obtained with an emissive probe (0.1mm diam, 2mm long) heated by 50Hz ac current, and its floating potential was measured by time sampling with a boxcar integrator at the zero heating voltage. Ion and electron velocity distributions were measured with retarding analyzers.

## III. EXPERIMENTAL RESULTS

To reproduce the double layer observed in the previous paper, the disc was placed at 3cm from the surface of the magnet, where the field strength ( $B=500\text{G}$ , see Fig.5a) is equal to that at the

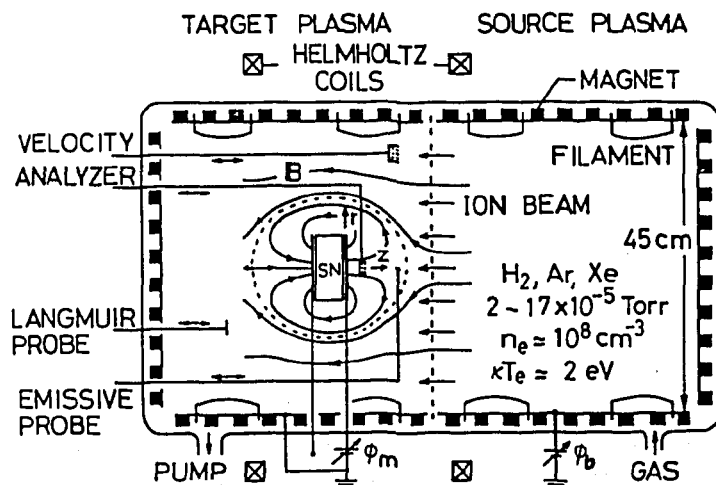


Fig. 1. Schematic view of the experimental setup.

pole face of the previous magnet. Measured axial potential profiles for different  $\phi_m$  at a fixed beam energy is shown in Fig.2a. When  $\phi_m < \phi_b$ , a sheath is observed, when  $\phi_m > \phi_b$ , a double layer is formed, which agree with the previous results.<sup>5</sup> A weak axial magnetic field ( $B_0$ ) generated by

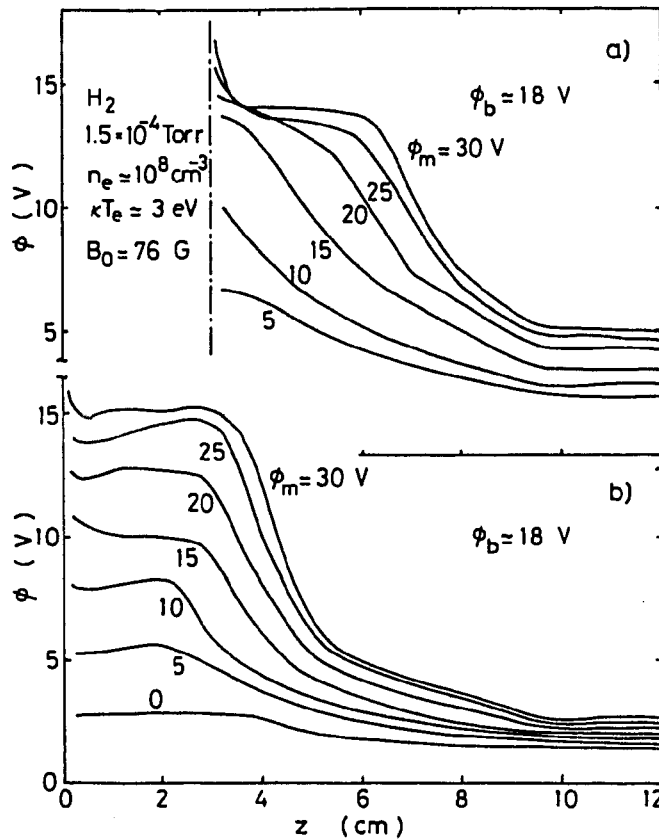


Fig. 2. Axial potential profiles at  $r=0$  for different disc voltages  $\phi_m$  at a fixed beam voltage  $\phi_b$ . (a) The disc was placed at 3cm from the magnet. (b) The disc was on the magnet.

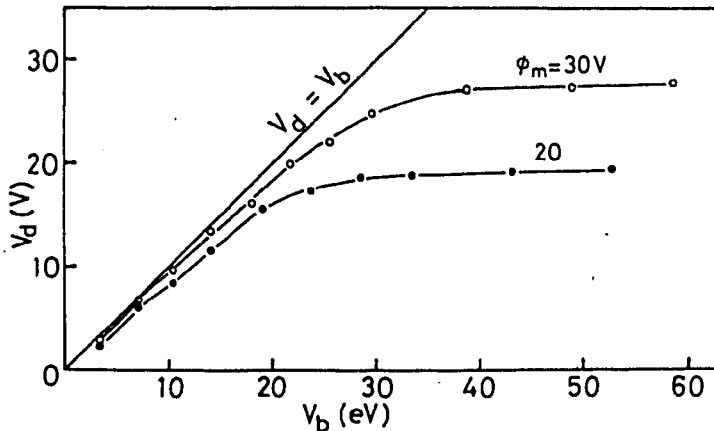


Fig. 3. Dependence of the height  $V_d$  of double layers on the beam energy  $V_b$  for different  $\phi_m$ .

Helmholtz coils was applied in the direction opposite to the dipole moment. Under the same plasma condition, the disc was placed on the magnet and potential profiles were measured again (Fig. 2b). In this case double layers were formed even when  $\phi_m < \phi_b$ . The measured height  $V_d$  of double layers as a function of beam energy  $V_b$  and the disc potential  $\phi_m$  are shown in Figs. 3 and 4, respectively. When  $V_b < \phi_m$  for a constant  $\phi_m$ , the height of the double layer is somewhat smaller than  $V_b$  and is proportional to  $V_b$  as has been observed previously. When  $V_b$  is increased further,  $V_d$  saturates at about  $\phi_m$  (Fig. 3). When  $\phi_m < V_b$  for a constant  $V_b$ ,  $V_d$  is nearly proportional to  $\phi_m$ . When  $\phi_m$  is increased further,  $V_d$  saturates at about  $V_b$  or  $\phi_b$ .

An example of measured two-dimensional potential distribution is shown in Fig. 5b together with the magnetic field topology. The V-shaped structure is similar to but further away from the magnet than the one observed previously.

<sup>5</sup> In this case no external magnetic field was applied ( $B_0=0$ ), which needed less plasma density in the target region to form a double layer. The width ( $\approx 4$ cm) of the double layer is compara-

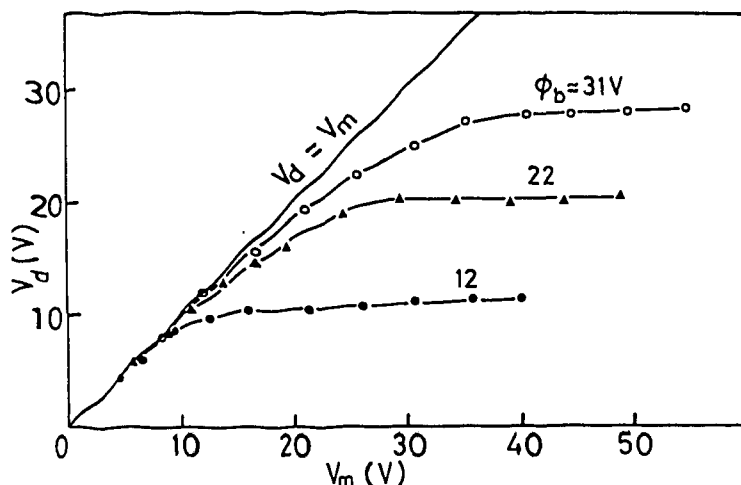


Fig. 4. Dependence of  $V_d$  on the bias voltage  $V_m (= \phi_m)$  of the disc for different  $\phi_b$ , i.e.,  $V_b$ .

ble to the  $H_2^+$  Larmor radius ( $\approx 2cm$ ,  $B=300G$ ,  $V_b = 15eV$ ). The axial distance for beam ions to move in a Larmor period is  $(2eV_b/M)^{1/2}/f_{ci} \approx 15cm$  which is much larger than the double layer dimension.

Axial potential profiles when  $B_0=0$  for a fixed  $\phi_b$  and for different  $\phi_m$  are shown in Fig.

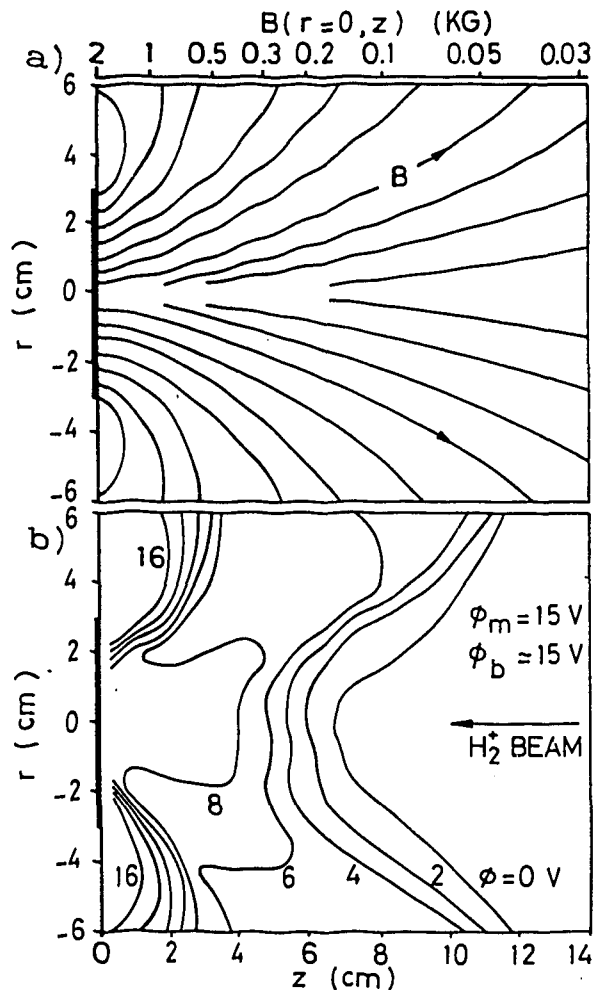


Fig. 5. Two-dimensional display of magnetic field lines and equipotential contours. (a) Magnetic field lines (arbitrary spaced). Top scale gives field strength on axis. (b) Contours of constant plasma potential ( $\Delta\phi = 2V$  between contours).

6. When no beam was injected, an electron-rich sheath with a thickness of several Debye lengths (the dotted curve) was formed in front of the disc (see Fig. 7). The voltage-current characteristics of the disc indicate that it acts like a Langmuir probe. A gentle increase of the electron current is due to the increase of the effective area of the disc.<sup>9</sup> Figure 6 shows that double layers are formed at any value of  $\phi_m$  as long as the ion beam is injected. Two-dimensional scans of ion saturation current to the cold emissive probe biased at  $-50V$  reveal that the ion density decreases toward the surface of the magnet when no beam is injected. When a double layer exists, the ion density is peaked at the high potential side of the double layer, which indicates that

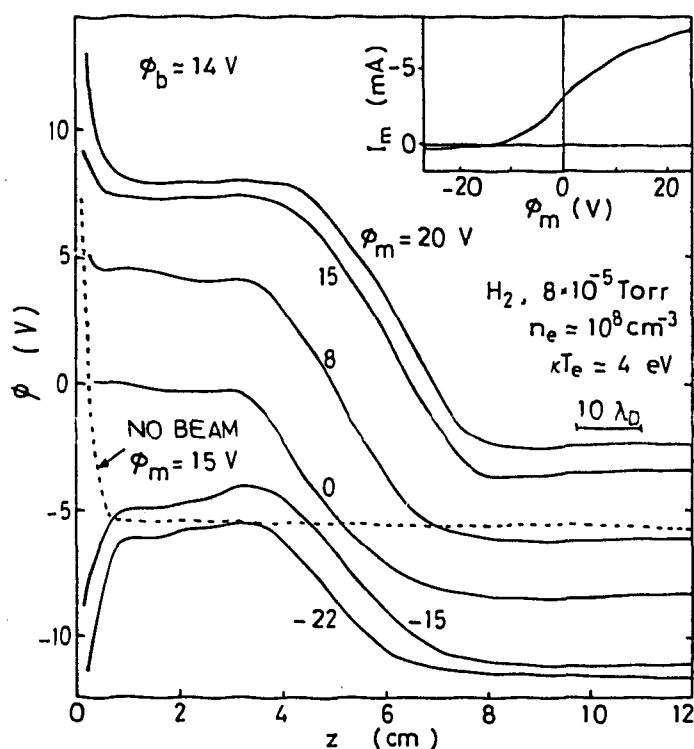


Fig. 6. Axial potential profiles for different disc bias voltages. The figure inside is the voltage-current characteristics of the disc.

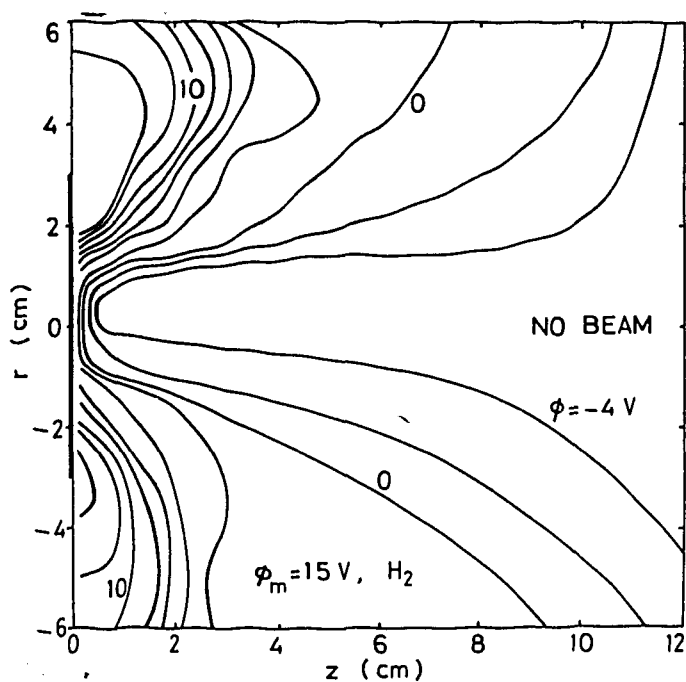


Fig. 7. Two-dimensional equipotential contours when no beam is present.  $\phi_m = 15V$ .

beam ions focus due to converging magnetic field. In the previous experiment,<sup>5</sup> magnetic field was not strong enough to cause the focusing effect so that the reflection of the beam was needed to make the high density region. In the present case, the effect is strong enough for the double layer to form even when the disc attracts ions ( $\phi_m < 0$ ). Once the double layer forms, it promotes the effect by decelerating beam ions. Electrons follow magnetic field lines to neutralize the enhanced density of beam ions. When  $\phi_m$  is lower than the plasma potential at the low potential side of the double layer, the electrons are reflected back with the ion-rich sheath formed in front of the disc. Therefore, the incident ion beam makes the potential barrier which confines plasma ions and electrons together with the negatively biased disc. Since Ar and Xe ions are weakly magnetized even in the present case, reflection ( $\phi_m > \phi_b$ ) of those beams is necessary to form a double layer.

Figure 7 is a typical example of two-dimensional equipotential contours without an ion beam when  $\phi_m = 15V$ . The contours are similar to the magnetic field lines except the electron-rich sheath in front of the disc and also similar to those measured near cusps.<sup>8</sup>

### References

- \*) Permanent address: Department of Physics, University of California, Los Angeles, California 90024.
1. Physics of Auroral Arc Formation, edited by S.I.Akasofu and J.R.Kan, Geophys.Monograph Series, Vol.25(American Geophys. Union,1982); Y.Nakamura,Bull.Jap.Phys.Soc.Japan, 36,No.6, 469(1981)(in Japanese).
  2. M.Temerin, K.Cerny, W.Lotko and F.S.Mozer, Phys.Rev.Lett., 48,1175(1982).
  3. See, for example, P.Michelsen,J.J.Rasmussen, R.Schritt-wieser R. Hatakeyama, K.Saeki and N.Sato, Phys. Rev. Lett., 48, 145(1982).
  4. See, for example, N.Singh and R.W.Schunk,Geophys. Res. Lett. 9, 446(1982).
  5. R.L.Stenzel, M.Ooyama and Y.Nakamura,Phys. Rev. Lett.,45, 1498(1980); Phys. Fluids, 24, 708(1981).
  6. D.W.Swift, Space Sci. Rev.,22, 35(1978).
  7. Y.Nakamura, B.H.Quon, and A.Y.Wong, Phys. Lett.,53A, 85 (1975).
  8. N.Hershkowitz, J.R.Dekock, and C.Chan, Nuclear Fusion, 20, 695(1980).
  9. Y.Nakamura, Y.Nomura and R.L.Stenzel, J. Appl. Phys.,52, 1197(1981).

DOUBLE SHEATHS FORMED BY ION-BEAM REFLECTION IN  
FRONT OF A LANGMUIR PROBE IN AN UNMAGNETIZED  
PLASMA.

Å. Skøelv, R.J. Armstrong and J. Trulsen,  
University of Tromsø, P.O. Box 953, N-9001 Tromsø,  
Norway.

1. Introduction.

An ion beam incident on a plane Langmuir probe gives rise to an extra knee in the electron saturation part of the current-voltage characteristic [1]. For probe bias sufficient to reflect the beam, the beam ions contribute effectively to the charge density around the probe. A positive space charge layer is formed at the stagnation point inside the electron-rich sheath. This has been confirmed experimentally [2]. We will here present results from an experimental and a numerical study of this double sheath formation.

2. Experiment.

The measurements were performed in a double-plasma device with parameters: pressure  $p \sim 0.12$  mTorr, density  $n_e \sim 4 \cdot 10^{14} \text{ m}^{-3}$ , plasma and beam temperature  $T_e \sim 2$  eV,  $T_i \sim 0.3$  eV and  $T_b \sim 0.04$  eV, beam energy  $V_b \sim 5-20$  eV and beam density  $n_b/n_e \sim 0.1$ . The plasma was unmagnetized. A circular plane probe of 2 cm diameter was used. The equipotential surfaces around the probe

were measured with a movable small emissive probe using the floating-probe technique [3].

In figure 1 an example of potential profiles in front of the centre of the probe for different probe biases  $V_{pr}$  is given. The sheath expansion effect due to the ion beam is clearly seen [2].

### 3. Numerical simulation.

To compute the current to, the equipotential surfaces and space charge density around the probe, an iterative static particle simulation code was developed [4]. The trajectories of a large number of simulation particles, typically 50 000, under the influence of the electric fields in the plasma are calculated, one at a time. Each particle contributes to the charge density along its trajectory with amounts inversely proportional to its local velocity. The Poisson equation is then solved to update the potential surfaces for the next iteration. Simulations were performed with parameters:  $n_e = 10^{14} \text{ m}^{-3}$ ,  $T_e = 1 \text{ eV}$ ,  $T_i = 0.1 \text{ eV}$ ,  $T_b = 0.03 \text{ eV}$ ,  $V_b = 10 \text{ eV}$ ,  $n_b/n_e = 0.4$  and probe diameter 1 cm.

Computed potential profiles in front of the centre of the probe for a probe bias below the beam energy are given in figure 2(A). Corresponding equipotential surfaces are given in figure 2(B). Figure 3 shows the results for a probe bias above the beam energy. Axial charge density profiles with and without an ion beam, for a bias sufficient to reflect the beam, are given in figure 4. The formation of a positive space charge layer inside the probe sheath is clearly seen.

References:

- [1] W.J. Weber, R.J. Armstrong, J. Trulsen: J. Appl. Phys. 50, 4545 (1979).
- [2] Y. Nakamura, Y. Nomura, R.L. Stenzel: J. Appl. Phys. 52, 1197 (1981).
- [3] R.F. Kemp, J.M. Sellen: Rev. Sci. Instr. 37, 455 (1966).
- [4] L.W. Parker: NASA cr-401 (1966).  
ESSA Tech. rept. ERL 100-AL 2 (1968).  
Å. Skøelv, R.J. Armstrong, J. Trulsen: to appear (1982).

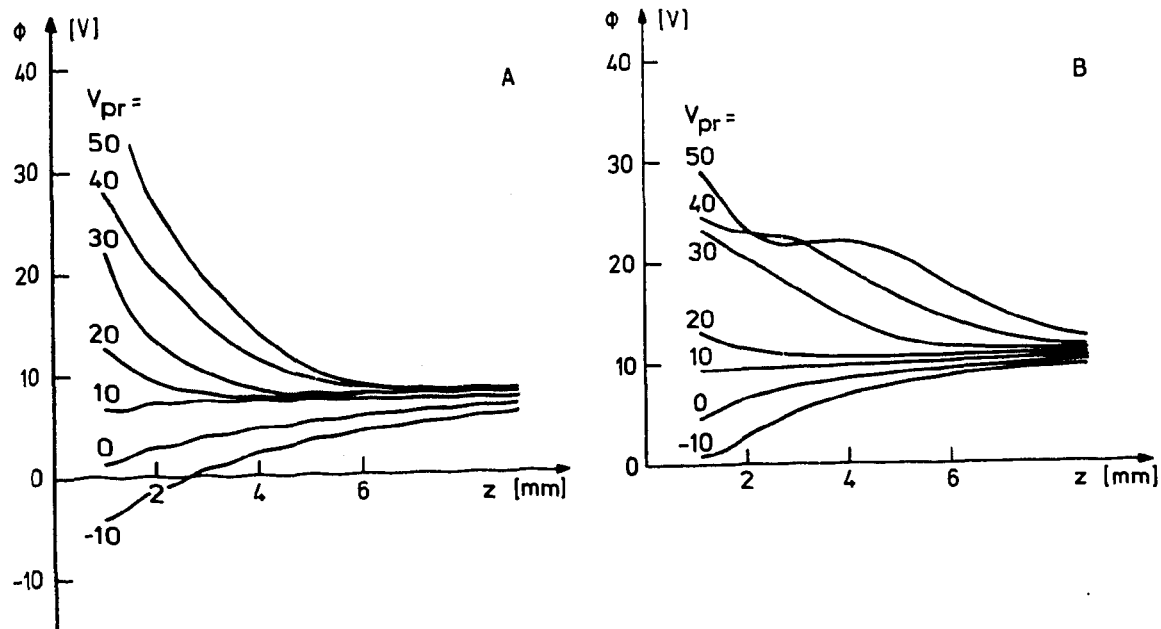


Figure 1. Measured axial potential profiles for different probe biases.  
A. No beam. B. Ion beam.

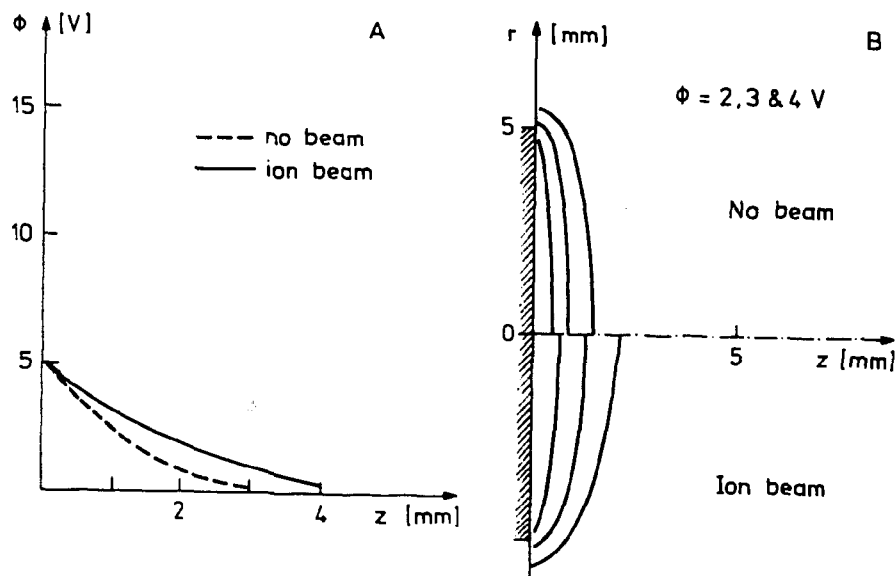


Figure 2.. Computed axial potential profiles (A) and equipotential surfaces in front of the probe (B) with and without the ion beam. Probe bias  $V_{pr} = 15$  V and beam energy  $V_b = 10$  V.

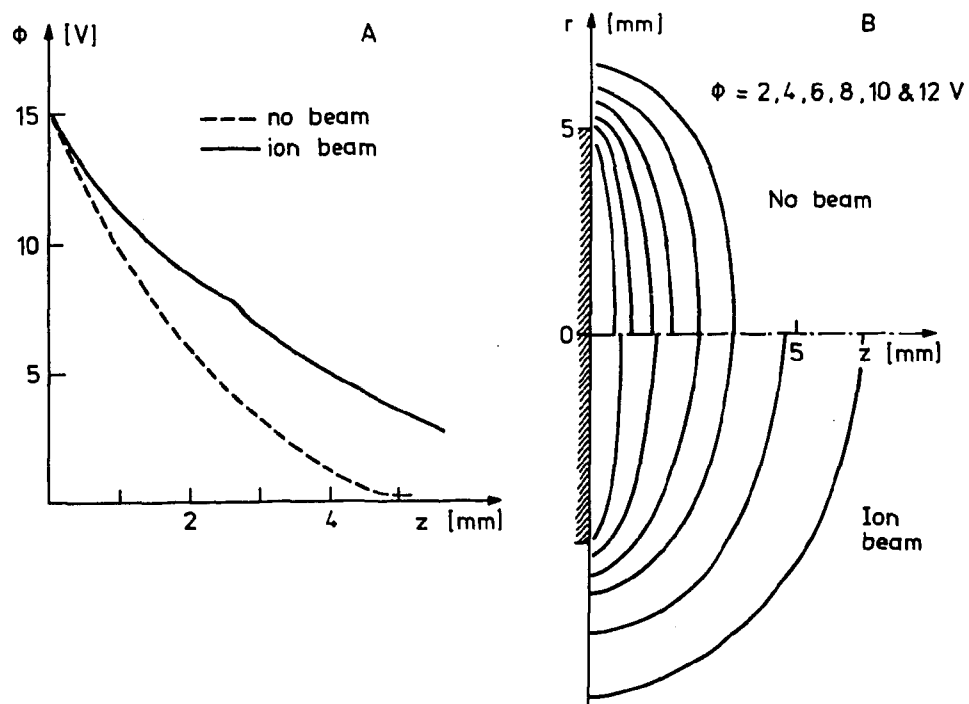


Figure 3. computed axial potential profiles (A) and equipotential surfaces in front of the probe (B) with and without the ion beam. Probe bias  $V_{pr} = 15$  V and beam energy  $V_b = 10$  V.

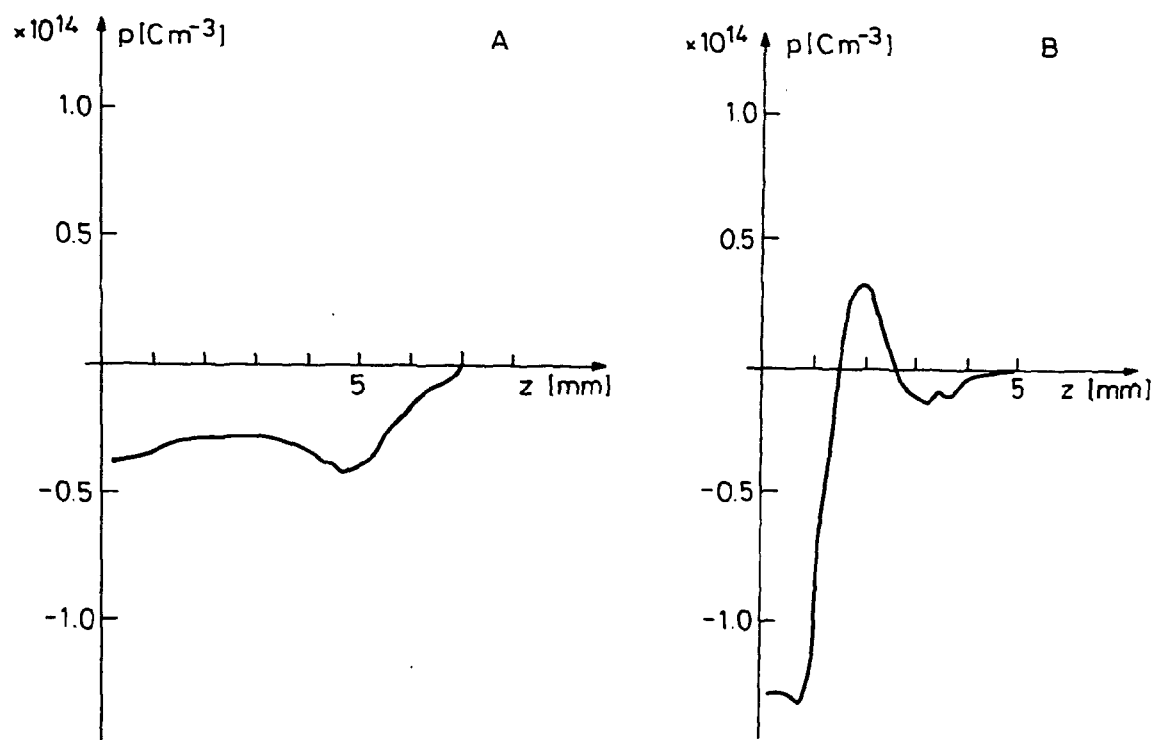


Figure 4. Computed axial charge density profiles.  
Probe bias  $V_{pr} = 15$  V.  
A. No beam. B. Ion beam.

Experimental Studies of Electron Scattering Due to Beam-Plasma Interaction  
near a Double Layer

L. Lindberg

Department of Plasma Physics, Royal Institute of Technology  
S-100 44 Stockholm, Sweden

Abstract A stationary, fluctuating double layer ( $V_{DL} \approx 25$  V) in a current-carrying magnetized plasma column is investigated by means of a retarding field electron energy analyser, Langmuir- and Faraday-cup probes and hf-probes. Most of the electrons accelerated in the double layer are, in a single transit, scattered by the hf-field produced by beam-plasma interaction. The energy spectrum is broadened and a considerable fraction of the beam electrons becomes temporarily trapped, forming an energetic, 8 eV non-isotropic population with enhanced density of low energy electrons. The trapped population, and possibly also the beam, expands across the magnetic field, also as a consequence of the hf-field, which has perpendicular components of the same magnitude as the axial.

### 1. Introduction

When a double layer (DL) is formed in a current carrying magnetized plasma column, beam-plasma interaction leads to generation of a hf-field and rearrangement of the electron velocity distribution<sup>1,2</sup>. An interesting feature associated with the DL is an apparently rapid radial expansion of the plasma across the magnetic field, taking place in the "anode" plasma, Fig.1. An important question is whether the expansion takes place only in that electron population which is trapped between the DL and the fluctuating potential minimum that exists in front of the anode<sup>2</sup>, or whether non-trapped beam electrons in a single transit could become scattered as much as several gyro radii. This would require a very intense hf-field.

### 2. Retarding field energy analysis

The energy of the electrons hitting the anode is studied by an analyser built into the anode, Fig.2(a). The first grid is part of the anode and covers a central hole ( $\phi 3$ mm). Entering plasma is separated into ions and electrons by the second grid (+35 V). The analyser measures only the axial component of the kinetic energy and cannot analyse the trapped electrons in the anode plasma.

It would be desirable to use an analyser movable along the axis, and radially, but that would disturb the plasma seriously. Instead we place the

DL at various positions relative to the anode by suitable choice of the anode current,  $I_a^{1,2}$ . Fig.2(a) shows the collector current  $I(V)$  (time average) and (b) its derivative  $I'(V)$  ( $= dI(V)/dV$ ) as functions of the grid potential.  $I(V)$  measures the integrated flux of electrons with axial velocity exceeding a certain value,  $v_z = (2 W_z/m)^{1/2}$ , hence  $I'(V) \sim W_z^{1/2} f(W_z)$  where  $f(W_z)$  is an energy distribution function. The two energy scales in Fig.2(b) are related to the cases  $I_a = 600$  and  $25$  mA. At  $25$  mA, when no DL exists, a single peak, representing the distribution in the cathode plasma is seen. Already at  $50$  mA a population with low  $v_z$ -energies begins to appear, and at  $I_a \geq 100$  mA, when a DL is clearly formed, the flux of low  $v_z$ -electrons increases rapidly to a remarkably high level. The distribution of high energies broadens - also to energies exceeding those of the original beam, in good agreement with earlier probe measurements<sup>2</sup>.

### 3. Radial expansion of the anode plasma

Judging from the emission of visible light the anode plasma expands suddenly across the magnetic field close to the DL, Fig.1(a). Further downstream the diameter increases only slowly towards the anode. An expansion, to approximately the same diameter, is also seen at low anode current when the DL is formed close to the anode. The apparent expansion is relatively independent of the strength of the magnetic field in the range  $2.5 - 10$  mT. An expansion can also be seen in the cathode plasma column, but this is less striking - the boundaries become diffuse when the DL is moved out from the anode.

An approximate measure of the expansion is obtained from Langmuir probe measurements: Fig.4 shows normalised profiles of probe saturation currents at various sections in front of and behind the DL ( $I_a = 700$  mA). Compared with the initial plasma beam diameter, limited by the aperture of the plasma source ( $15$  mm), we see a considerable widening already in the cathode plasma, followed by a very marked widening in the anode plasma just close to the DL and thereafter only a slight increase in the width, all consistent with the visual observations.

### 4. Langmuir probe measurements

A pair of short cylindrical Langmuir probes, one perpendicular to the beam, the other parallel, was previously used to distinguish between beam and thermal electrons<sup>2</sup>. Close to the DL the beam was clearly distinguished as causing a difference between the perpendicular and the parallel probe characteristics.

The trapped electron population can be studied by means of the parallel probe: Everywhere in the anode plasma the  $I_{||}(V)$ -characteristic, Fig.5, as

well as its derivative,  $I'_n(V)$  have shapes similar to exponential functions. However, if we evaluate the temperature anywhere between  $V_{p1} - 30$  to  $V_{p1} - 10$  V we find approximately 8 eV but near  $V_{p1}$  only 3 eV. We can describe the trapped population as a non-isotropic, ~8 eV distribution with enhanced density of low-energy electrons. Among the energetic electrons only those with low  $v_z$ -energies can be trapped, while the low-energy part may be isotropic. The lack of thermal equilibrium could be maintained because of rapid replacement of the energetic part of the distribution. Extrapolation of the 8 eV part of the probe characteristic to  $V_{p1}$  indicates that at  $V_{p1}$  roughly 1/3 of the probe current is due to 3 eV electrons and 2/3 to 8 eV, which means that the two populations have approximately equal densities,  $3 \cdot 10^{15} \text{m}^{-3}$ . (In reality there is a gradual transition between 8 and 3 eV.)

##### 5. Faraday cup measurements in the anode plasma

A small double-sided Faraday-cup probe (O.D: 1.5 mm), Fig.6(a) has been used to investigate the electron velocity distribution in the anode plasma. The outer shield is operated at a constant potential equal to the average local plasma potential. The characteristics of the inner electrodes, and their derivatives  $I'_1(V)$  and  $I'_2(V)$  are recorded. Like the retarding field analyser it measures approximately only the axial component of the kinetic energy,  $W_z$  and  $W_{-z}$ , and the collector currents represent flux densities. Unfortunately the probe disturbs the plasma because the shield takes saturation current, and there is a shadow effect; When tested in the cathode plasma at low beam current (without DL) it indicated 3 - 5 times lower current in the backflow direction, but the energy distributions were alike. In the anode plasma we may expect less shadow effects because of the rapid radial diffusion, and there the probe should be useful as energy analyser.

Fig.6(a) and (b) show  $I'_1(V)$  and  $I'_2(V)$  measured 70 mm behind the DL at various radii ( $I_a = 700$  mA). Obviously the flux of energetic electrons is much higher and extends to higher energies in the forward direction - a confirmation of our earlier statement<sup>2</sup> that most beam electrons are not trapped. On basis of the current collected at  $V_{p1}$  we estimate the density of the beam electrons near the axis to  $5 \cdot 10^{14} \text{m}^{-3}$ . Near the axis,  $r = 0$  and 7.5 mm, there is a backflow of quite energetic electrons, which either have been scattered between the probe and the anode, or reflected at the potential minimum in front of the anode at instants when it is very low. At greater distance from the axis,  $r = 15$  and 22 mm, i.e. far outside the original beam radius (7.5 mm), there is a considerable flow of energetic electrons towards the anode, but almost no backflow. This indicates a flux of non-trapped beam electrons also at large radii. At present we cannot decide whether these have been

scattered on a single transit or were scattered already in the cathode plasma before acceleration in the DL, cf. Fig.4.

As concerns the backwards moving electrons both the  $I_2(V)$  and  $I_2'(V)$ -curves are almost exponential, indicating a nearly Maxwellian distribution, corresponding to the trapped 8 eV population indicated by probes.

#### 6. High frequency observations

Since the hf-field is found to scatter the beam electrons in energy very much<sup>2</sup> it might also cause the radial scattering, provided it has also components perpendicular to the magnetic field. Measurements of perpendicular components using twin coaxial probes<sup>1,5</sup> have now shown average levels of the same order as the axial components.

Some preliminary real time recordings of the axial component are shown in Fig.7 (BW 50 - 350 MHz), recorded at random, with slow sweep (1  $\mu$ s/div) to show the hf amplitude variations. Even if the actual hf waveform is not seen, unsymmetries in the records indicate a high content of harmonics.

#### 7. Scattering processes

Electrons can become scattered by elastic and inelastic collisions with neutrals, and by the localized hf-field<sup>1,2</sup>. Trapped electrons can be repeatedly scattered and easily diffuse across the magnetic field. The interesting question is to what extent the non-trapped electrons, in a single transit through the plasma, become scattered. Because of the low neutral density,  $\sim 2 \cdot 10^{18} \text{ m}^{-3}$  (Hg-vapor in contact with  $-10^\circ\text{C}$  wall) only  $\sim 6\%$  of the beam electrons could be scattered by collisions<sup>3,4</sup> - the majority should pass directly to the anode unscattered. A very small fraction<sup>3</sup> could however be scattered  $\sim 90^\circ$  and build up the 8 eV trapped population, provided the potential minimum in front of the anode were constantly deep. This is however contradicted by the energy analyser measurements, Fig.2(b). The gradual fall-off of the collector current at low-energies, compared with earlier probe measurements<sup>2</sup>, which show a high peak at low energies, indicates that the potential minimum fluctuates and at certain instants is not very deep, letting electrons through. We conclude that collisional scattering of beam electrons is of minor importance and cannot explain the formation of the trapped energetic electron population.

#### 8. Scattering of beam electrons

The retarding field analyser measurements, Fig.2(b),  $I_a = 600 \text{ mA}$ , indicate a remarkably high flux of electrons with low  $v_z$ -energies - more than 40% of the electrons reaching the anode have  $v_z$ -energies below half the average beam energy (25 eV). Disregarding for a moment the contribution of low energy

electrons due to ionization processes in the anode plasma (which can be estimated to  $\sim 10\%$ ), the same curves show the rate at which electrons with low  $v_z$ -energies are produced by scattering of beam electrons on their first passage. We conclude that the hf-field scatters most beam electrons on a single passage, producing a distribution with wide energy spectrum<sup>2</sup>, and that a considerable fraction lose a great deal of their z-directed momentum. These may be temporarily trapped, forming the  $\sim 8$  eV population.

#### 9. Scattering of trapped electrons

The light emission, Fig.1(a) indicates only the presence of electrons energetic enough to excite the background neutral gas, and does not indicate where the radial scattering really takes place. If the light were due to excitation by beam electrons, making a single transit, it would show the expansion to take place at the region of strong hf-field, which begins 50 - 100 Debyelengths downstream from the DL, i.e. not so close to the DL as the light indicates. We conclude that the light emission is mainly due to trapped, energetic electrons and indicates the shape of the equipotential surfaces around the anode plasma. This is consistent with equipotential lines, Fig.1(b), sketched on basis of radial profiles of sampled hot probe floating potential measurements at various sections of the plasma column, Fig.3.

We find scattering by the hf-field to dominate over collisional scattering for the beam electrons. The same should hold for the trapped electrons. Scattering due to the hf-field can only occur in the local region of intense hf-field near the DL<sup>1,2</sup>, which is bounded both in axial and radial direction (radial because of the limited diameter of the exciting electron beam, Fig.4). This could explain the observation, §3, that the anode plasma expands radially to a certain diameter, which depends very little on the length of the plasma column or on the magnetic field.

Acknowledgement The author is very grateful to Dr S. Torvén for stimulating discussions, and to Mr B. Johansson, E. Lagerström, S. Rydman and J. Wistedt for valuable technical assistance.

#### References

1. Torvén, S. and Lindberg, L., 1980, J.Phys.D.Appl.Phys. 13, 2285.
2. Lindberg, L., 1982, Experimental Observation of Local Beam-Plasma Interaction Near a Double Layer, Proc. 1982 Int.Conf. on Plasma Physics, Gothenburg, Sweden.
3. v.Engel, A., 1955, Ionized Gases, Clarendon Press, Oxford.
4. Brown, S.C., 1959, Basic Data of Plasma Physics, MIT Press, J.Wiley, N.Y.
5. Lindberg, L., 1981, High Frequency Probe Circuits for Plasma Diagnostics, TRITA-EPP-81-08, Dept of Plasma Physics, Royal Inst. of Technology, S-100 44 Stockholm, Sweden.

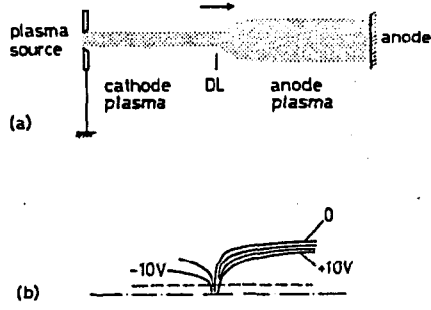


Fig. 1

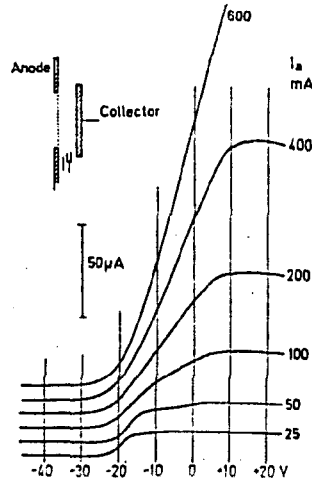
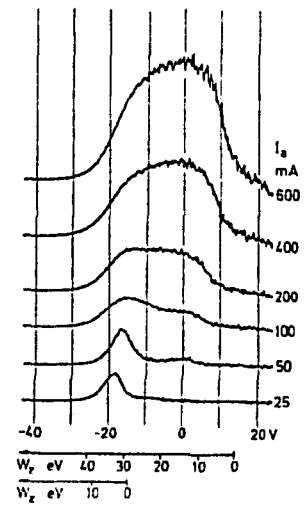


Fig. 2(a)



(b)

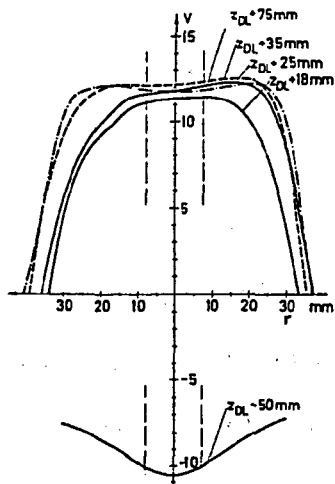


Fig. 3

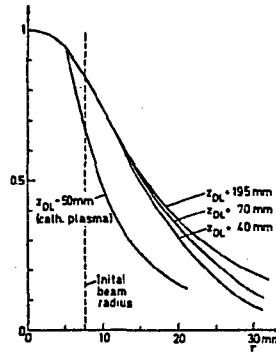


Fig. 4

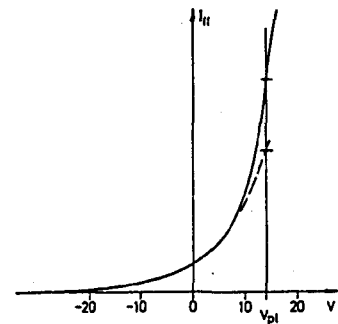


Fig. 5

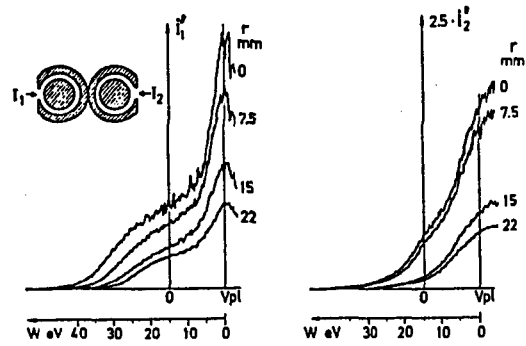


Fig. 6(a)

(b)

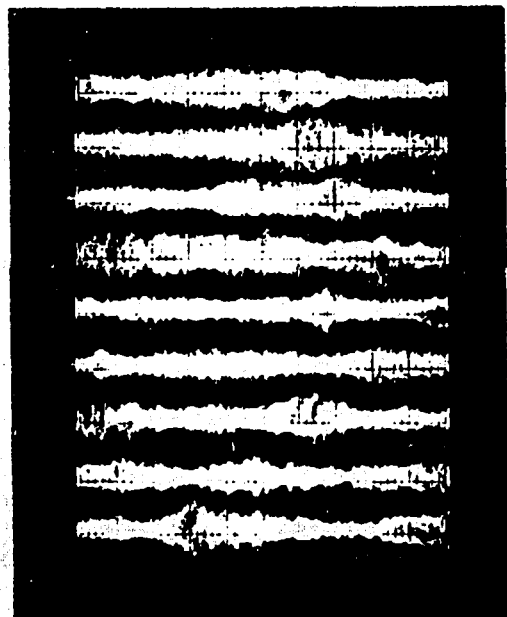


Fig. 7

## ELECTRON TEMPERATURE DIFFERENCES ACROSS DOUBLE LAYERS

Chung Chan, Noah Hershkowitz  
Nuclear Engineering Department  
University of Wisconsin-Madison  
Madison, Wisconsin 53706

Karl E. Lonngren  
Electrical and Computer Engineering Department  
University of Iowa  
Iowa City, Iowa 52240

Abstract

The difference in electron temperature on two sides of a double layer is studied experimentally in a triple plasma device. It is shown that the temperature differences can be varied and are not a result of beam plasma interactions.

Although double layers have been studied in laboratories for many decades,<sup>(1)</sup> many recent experiments<sup>(2)</sup> have been motivated by their association with the auroral electric field formation in the magnetosphere. Double layers are regions of charge separation which separate two neighboring plasmas with different potentials. For the case of magnetospheric double layers, the two neighboring plasmas are the hot rarefied magnetospheric plasma and the cold dense ionospheric plasma, i.e. are two plasmas at different temperatures. This particular aspect of magnetospheric double layers has not been emphasized in previous laboratory investigations. In order to relate the laboratory results to the studies of magnetospheric double layers, the interaction between the hot magnetospheric and the cold ionospheric plasmas cannot be neglected. Moreover, Hultqvist<sup>(3)</sup> has suggested that auroral electric fields can also be produced via thermoelectric effects associated with such hot and cold plasmas with the presence of turbulence induced scattering.

There have been some experimental indications that electrons have different thermal energies at the two sides of laboratory double layers. For example, Baker et al.<sup>(4)</sup> observed hotter electrons (5 eV) on the high potential side than on the low potential side (3 eV) while Hollenstien et al.<sup>(5)</sup> reported colder electron temperatures (1.5 eV) on the high potential side compared to the low potential side (3 eV). So far, these observations of electron temperature differences have not been studied or explained in any detail. This is in part due to the difficulties previous experiments had in varying the high potential side trapped electron distribution function because of the configurations of the experimental devices. In most cases, some trapped electrons were provided via

thermalization of the low potential side free electrons, via ionization, etc. so the trapped electron distribution could not be decoupled from the free electrons. As a result, it is not clear whether the observed electron temperature differences across double layers were due to thermalization of the trapped or free electron distributions, wave-particle interactions (e.g. heating) or inhibition of thermal energy transport by the presence of the double layer.

In this paper, we consider the basic issue of electron temperature differences across double layers. Our experimental results indicate that the temperature of the high potential side trapped electrons can be varied without affecting the low potential side free electrons or the double layer itself. The observed electron temperature difference is not a result of thermalization of the free or trapped electron distribution functions.

The experiments were performed in a triple plasma device DOLI which has been described elsewhere.<sup>(6)</sup> Argon plasma was produced by filament discharges in two source chambers, each separated from the target chamber by two grids (A and B on the low potential side, and C and D on the high potential side). By adjusting the thermal energies of the two source plasmas ("neighboring plasmas"), the differences of electron temperature across the double layer can be studied in a more controlled manner. Measurements of plasma potential were made with emissive probes. The electron velocity distribution functions were determined with collecting Langmuir probe arrays. At a typical target plasma density of  $10^7 \rightarrow 10^8 \text{ cm}^{-3}$ , electron temperature  $T_e \approx 2 \text{ eV}$  and an axial magnetic field of 20 G, the electrons can be considered magnetized. With operating

neutral Argon pressure  $10^{-5} \rightarrow 10^{-4}$  Torr, the electron-electron mean free path  $\lambda_{ee} \gtrsim 10^5$  cm, the electron-ion mean free path  $\lambda_{ei} \sim 10^5$  cm and the electron-neutral mean free path  $\lambda_{en} \gtrsim 10^3$  cm were much longer than the device.

The distributions of particles entering the double layer are determined by the boundary conditions which depend on the potentials applied on the grids and anodes as well as the self-consistent plasma potentials and densities in the two sources. We have also demonstrated in an earlier paper<sup>(6)</sup> that these experimental double layers were indeed well described by a one-dimensional BGK model using boundary conditions very similar to the experiments. In these experiments, low potential free electrons drift in with high velocity. At the high potential side, these free electrons generate streaming instabilities (ion acoustic wave, Langmuir wave, etc.) and it is not clear whether the thermalization of these beam electrons affect the temperature of the trapped electrons. Figure 1a shows a double layer with a confining potential  $e\phi/T_{ep} \sim 3$  and low potential side free electrons which do not drift in with noticeable energies. High potential source electrons leak through grids C and D due to the very small Debye length ( $\lambda_D < .3$  mm) in the high potential source. As the density in the target chamber is typically two orders of magnitude lower than the source, this species of electrons is then electrostatically trapped between the double layer potential step and the potential barrier of grid C. The thermal energy of these trapped electrons is determined by the temperature of the high potential source electrons and energy exchange with the passing electrons. Plasma electrons at the low potential side of the double layer are in much better thermal contact with the high density low potential

source electrons (since no potential barrier is present) and the double layer potential accelerates them into the high potential side.

The electron temperature profile across the double layer is shown in Fig. 1b (solid circle). As the temperature of the high potential trapped electrons and the low potential side free electrons were not too different, the double layer electric field can not be due to thermoelectric effects but rather is a result of charge separation due to particle distributions (BGK description). We also notice an increase in the energy spread of the free electrons entering the high potential side of the double layer (solid line in Fig. 1b). The free electrons apparently thermalize with the trapped electrons via beam plasma instabilities because all relevant collision mean free paths are much longer than the device.

A convenient way to address the issue of electron thermal conduction is to heat up the high potential side electrons and study the effects on the low potential side electrons. Because of the low energy and density of our plasma, a "Maxwell Demon"<sup>(7)</sup> was employed to heat electrons in the high potential source by absorbing cold electrons. The potential and electron temperature profiles with and without high potential side electron heating are shown in Figures 1a,b. The temperature of the high potential side trapped electrons has been increased from 1.7 eV to 3.0 eV while the low potential side plasma electrons remain unchanged at  $T_e \sim 1.3$  eV. The energy spread of the free electrons after being accelerated by the double layer also has the same profile regardless of the heating (compare the solid line and the dashed line in Figure 1b). Note that the double layer potential structure is not significantly changed by the heating but the high potential source plasma potential becomes slightly

more positive. From Figure 1b, it is apparent that the heating of the high potential side electrons does not affect the low potential side electrons. Therefore, the observed large electron temperature differences across the double layer are not caused by thermalization of the accelerated free electrons nor by wave heating of the high potential side trapped electrons but rather, the double layer actually separates the high potential side hotter electrons from the low potential side colder electrons. From the electron velocity distribution function  $f(v)$  for  $v < 0$  shown in Figure 2, a large fraction of the high potential side cold electrons are found to be missing as a result of the "Maxwell Demon". Consequently, the density of the high potential side electron has also decreased significantly by the "Maxwell Demon". However, the "Maxwell Demon" does not alter the tail of distribution of the high potential side electrons which have enough energies to overcome the double layer confining potential. The bulk of the high potential side electrons are trapped by the double layer potential step so they cannot reach the low potential side. Therefore, at the low potential side only the high potential side tail electrons can interact with the low potential free electrons. On the other hand, the characteristic of the trapped electron will be important for determining the double layer potential. The fact that a similar potential jump can be sustained by an increase in the trapped electron temperature together with a decrease in the trapped electron density implies that the potential step  $\phi$  can be related to the trapped electron density  $n_p$  and temperature  $T_{ep}$ . For example, a Boltzmann relation will exhibit the above dependence

$$e\phi = T_{ep} \ln \frac{n_p}{n_t} \quad (1)$$

where  $n_t$  could be the density of the tail of the trapped electrons at the foot of the double layer.

With electron heating in the high potential source, the experimental conditions in Figures 1 and 2, resemble the situation where a hotter and less dense plasma is separated from a colder and denser plasma by means of a double layer. At the foot of the double layer, the tail of the high potential side hotter electrons interacts with the low potential side colder electrons (see Figure 2 (C-D)) but the electric fields are essentially zero there. According to Fälthammar,<sup>(8)</sup> only if the product of the electron density  $n_e$  and temperature  $T_e$  varies in a special way (such that  $n_e T_e^{1+\alpha/2}$  is constant) does the thermoelectric field vanish. The constant  $\alpha$  is the thermal diffusion coefficient and has the value of 1.4 for a collisional plasma. For a collisionless plasma, turbulence induced scattering can play a role similar to the Coulomb collision processes and the above argument should still be applicable because the diffusion process does not depend on the detailed scattering mechanism. For double layers shown in Figure 1, the condition that  $n_e T_e^{1+\alpha/2}$  stays constant implies:

$$n_t T_{et}^{1+\alpha/2} = n_c T_{ec}^{1+\alpha/2} \quad (2)$$

where  $T_{et}$  is the temperature of the tail electrons and  $n_c, T_{ec}$  are the density and temperature of the low potential side electrons at the foot of the double layers. In our experiments,  $\alpha$  was found to be approximately equal to unity and equation (2) is also consistent with a heat flux balance at the foot of the double layer.

In conclusion, our experimental results indicate that double layers can separate plasmas with different thermal energies and densities. The

observed temperature differences across the double layer are not a result of beam plasma interactions (e.g. thermalization of electron beam). We also demonstrate that the trapped electron distribution is not unique for a given potential profile in agreement with the BGK prediction.

### Acknowledgements

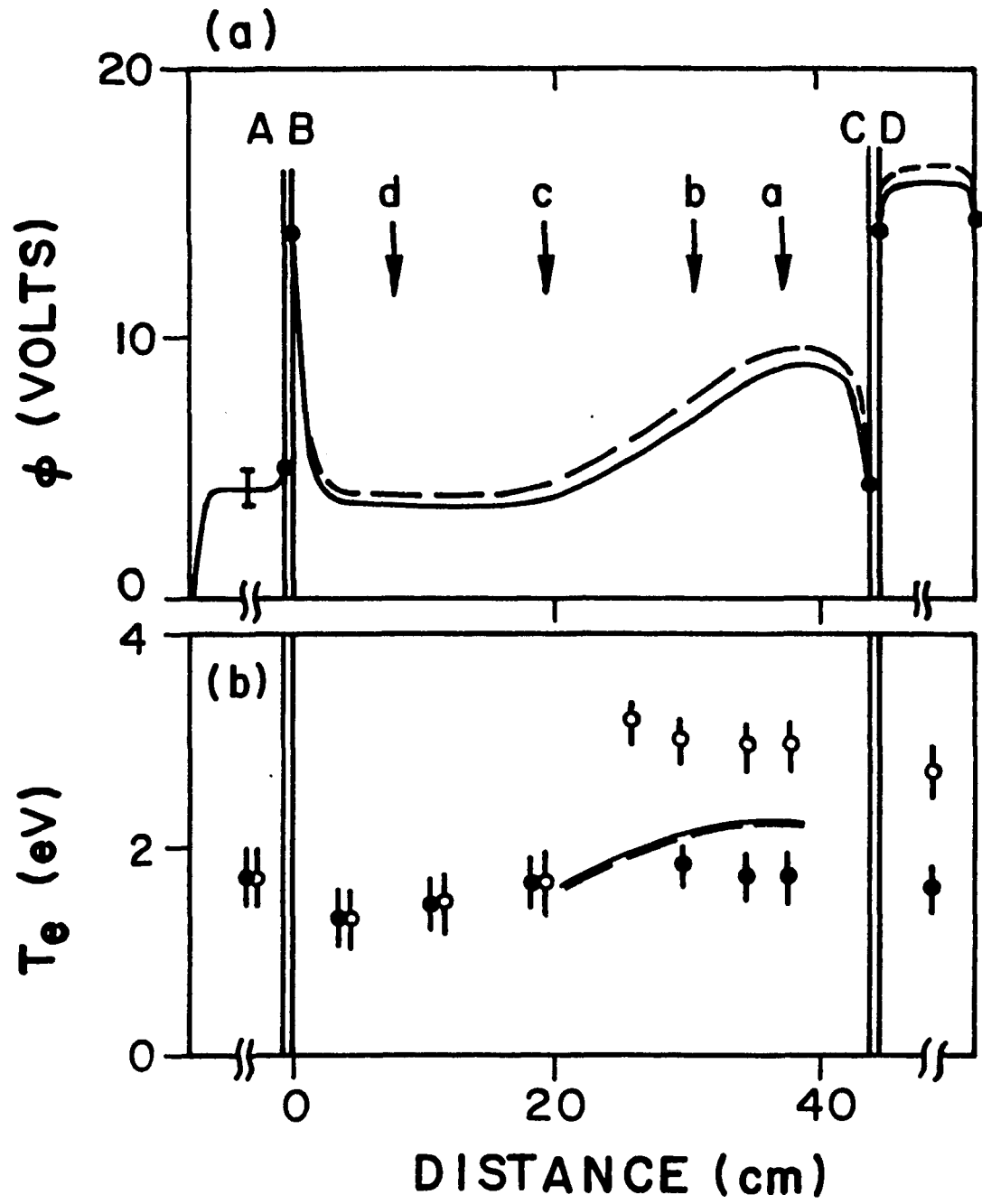
Research was supported by grants from NASA and NSF.

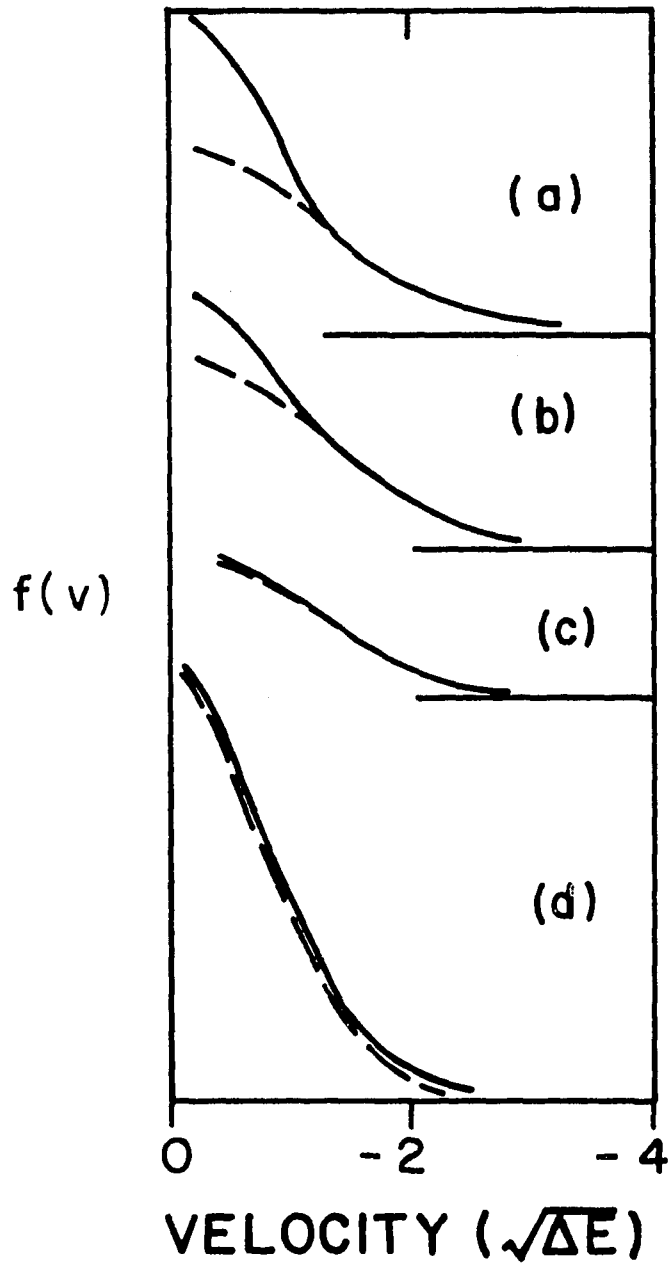
### References

1. I. Langmuir, Phys. Rev., 33, 954 (1929).
2. L.P. Block, Geophys. Spa. Sci. 55, 59 (1978); J.S. Levine and F.W. Crawford, J. Plasma Phys. 24, 359 (1980).
3. B. Hultqvist, Planet Spa. Sci. 19, 749 (1971).
4. Baker et al., J. Plasma Phys. 26, 1 (1981).
5. Ch. Hollenstein, M. Guyot and E.S. Weibel, Phys. Rev. Lett. 26, 2110 (1981).
6. N. Hershkowitz, G.L. Payne, C. Chan and J.R. DeKock, Plasma Phys. 23, 903 (1981).
7. K.R. MacKenzie et al., Appl. Phys. Lett. 18, 529 (1971).
8. C-G. Fälthammar, Rev. Geophys. Spa. Sci. 15, 457 (1977).

Figure Captions

- Figure 1a Axial potential profile and the boundary conditions for the double layer. Dashed (--) and solid lines (—) represent data with and without heating.
- Figure 1b The electron temperature profile corresponding to Figure 1a. Open circles and closed circles denote plasma electron temperature with and without heating. Dashed and solid lines denote the energy spread of the passing electrons while accelerated into the high potential side, with and without heating, respectively.
- Figure 2 The corresponding electron velocity distribution functions  $f(v)$  for  $v < 0$  at locations which are indicated in Figure 1a. Dashed and solid lines denote data with and without heating.





Double Layer Formation During Current Sheet  
Disruptions in a Magnetic Reconnection Experiment

R. L. Stenzel, W. Gekelman and N. Wild

Department of Physics, University of California, Los Angeles, CA 90024 USA

ABSTRACT

When the current density in the center of a neutral sheet is increased to a critical value spontaneous current disruptions are observed. The release of stored magnetic field energy results in a large inductive voltage pulse which drops off inside the plasma forming a potential double layer. Particles are energized, microinstabilities are generated, the plasma is thinned, and the current flow is redirected. These laboratory observations support qualitatively recent models of magnetic substorms and solar flares.

Introduction

The stability of a current sheet in plasmas plays an important role in the physics of magnetic substorms and solar flares [Alfvén, 1977; Akasofu, 1977]. In the case of the substorm, for example, it is assumed that the magnetospheric crosstail current is partially disrupted by some kind of plasma instability. The current flow is then diverted along the magnetic field lines into the polar regions where the deposition of excess magnetic field energy occurs. Auroral potential structures [Kan and Lee, 1981] are generated and play an important role in the process of particle energization. Due to observational difficulties in space some processes such as magnetic field line reconnection can be investigated more easily in laboratory plasmas [Stenzel et al., 1982a]. Here, we describe observations of the disruption of the current sheet leading to the formation of a potential double layer at which stored electromagnetic energy is converted into particle kinetic energy [Stenzel et al., 1982b].

Experimental Configuration

A large (1 m x 2 m) dense ( $n_e \approx 10^{12} \text{ cm}^{-3}$ ) argon discharge plasma is generated with a specially developed oxide cathode of 1 m diameter. Parallel to the axially magnetized ( $B_y \approx 15 \text{ G}$ ) plasma column are two metallic conductors carrying pulsed currents ( $\sim 30 \text{ kA}$ , 200  $\mu\text{sec}$ ) and inducing an axially flowing plasma current ( $\sim 1000 \text{ A}$ ). Using magnetic probes in conjunction with a digital data acquisition system the transverse magnetic field topology is mapped point by point by repeating the experiment

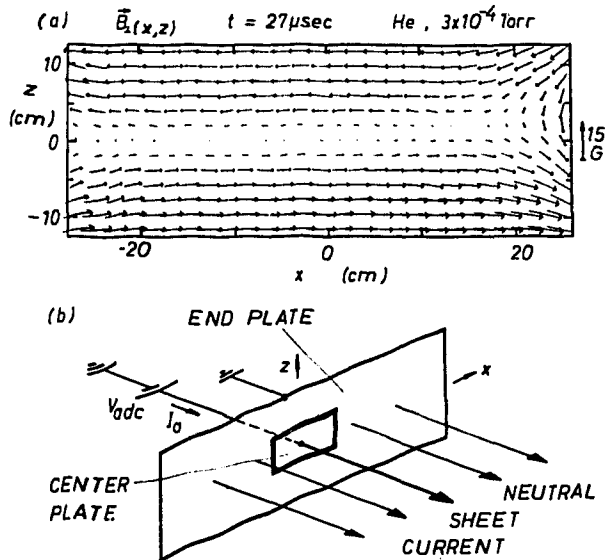


Fig. 1. Experimental arrangement. (a) Measured transverse magnetic field topology showing the existence of a neutral sheet. (b) End plate arrangement for producing an enhanced current in the center of the current sheet.

( $t_{\text{rep}} \approx 2$  sec). Figure 1a shows that during the current rise ( $t \leq 80 \mu\text{sec}$ ) the self-consistent reconnection of magnetic field lines in a plasma [Dungey, 1958] establishes a neutral line ( $B_\perp \approx 0$  for  $-25 \leq x \leq 20$  cm,  $z \approx 0$ ). The plasma current  $\vec{J}_y = \nabla \times \vec{A}_\perp$  flows in the form of a current sheet.

We are interested in the stability of the current sheet when the current density in the central region is raised above its normal value. This is accomplished as shown in Fig. 1b. The neutral sheet current is terminated on a grounded metallic end plate (32 cm x 75 cm) whose central region (6 cm x 13 cm) is separated and connected to an external dc supply. When the supply voltage is increased ( $V_{\text{adc}} > 0$ ) the current to the center plate  $I_a$  rises until a critical value is reached at which it disrupts spontaneously. The associated processes inside of the plasma are studied in-situ with probes.

### Experimental Results

Figure 2a shows the induced center plate current  $I_a(t)$  at different applied potentials  $V_{\text{adc}}$ . At low currents a smooth sinusoidal waveform is observed but when the current is raised to  $I_a \geq 200$  A spontaneous sharp current drops develop which, for  $V_{\text{adc}} \geq 15$  V, can lead to complete current loss. The disrupted center plate current is diverted to the surrounding grounded end plate. Thus, the disruption is an instability of the current sheet. If we start with a different topology, e.g., a magnetic island produced by taking up the total plasma current at the small end plate no disruptions are observed.

The current path through plasma and conductors can be represented by an electrical circuit with inductance  $L$ . Due to the current disruptions an

inductive voltage  $L \, dI/dt$  arises which drops off at the location of the current disruption. Figure 2b shows the instantaneous plate voltage to ground,  $V_a(t)$ , and the plate current,  $I_a(t)$ . At every current disruption an inductive voltage spike far in excess of the dc potential builds up ( $V_{adc} = 10 \text{ V}$ ).

With Langmuir probes the local instantaneous plasma potential has been measured in order to determine whether the inductive voltage drops off at the sheath or inside the plasma. As shown in Fig. 3b the high positive plasma potential near the anode decreases abruptly inside the plasma rather than at a sheath. A potential double layer [Block, 1978] has been formed ( $\Delta\phi \approx L \, dI/dt \approx 35 \text{ V}$ ;  $d \approx 5 \text{ mm} \gtrsim 100 \lambda_D$ ). Its transverse ( $x, z$ ) dimensions are approximately those of the small plate. It exists only during current disruptions. On the high potential side ( $\Delta y < 6 \text{ cm}$ ) the electron density is greatly ( $\sim 50\%$ ) reduced. The electron distribution function [Fig. 4a]

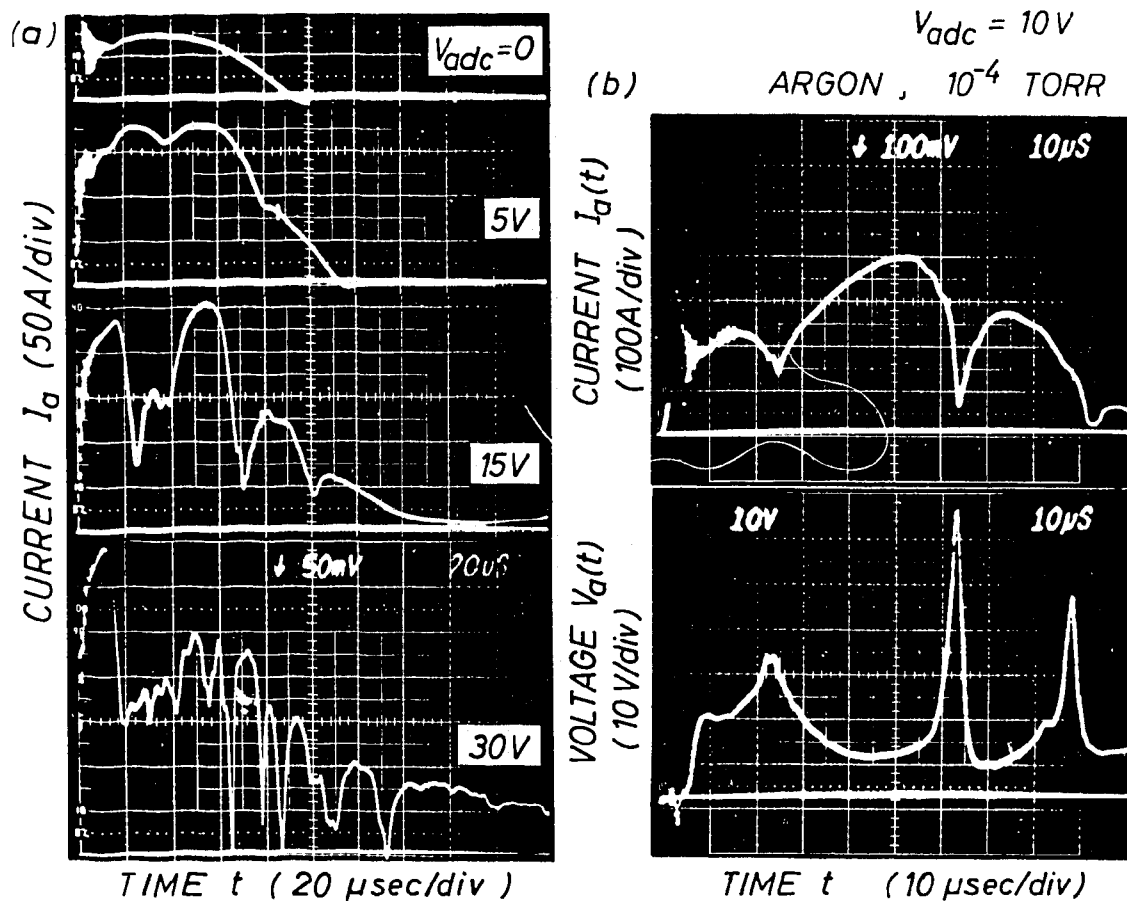


Fig. 2(a). Current  $I_a$  to the center plate for different dc plate voltages  $V_{adc}$  showing the evolution of current disruptions with increasing currents. (b) Center plate current and voltage vs. time. During current disruptions the plate voltage exhibits large inductive voltage spikes ( $L \, dI_a/dt \gg V_{adc}$ ).

measured with a directional velocity analyzer [Stenzel et al., 1982c] exhibits a beam of free electrons accelerated at the double layer. Beam-plasma instabilities generate bursts of electron plasma waves with  $\omega \geq \omega_{pe} \approx 2\pi \times 6$  GHz [Fig. 4b]. On the low potential side, facing the double layer, ion energy analyzers detect energetic ( $\sim 40$  eV) ions. Low-frequency electrostatic and magnetic turbulence is generated in the surrounding plasma.

### Discussion

The disruptive instability is believed to arise from a density loss in the center of the current sheet, possibly triggered by local plasma heating. The local current decrease causes an inductive emf which raises the plasma potential near the end plate and expels ions from the current channel. The feedback between rising potential and decreasing charged particle density leads to the rapid current drop. Counterstreaming ions and electrons enable the formation of the potential double layer. The double layer plays an important role in the energy transfer mechanism. Stored magnetic field energy is converted at the double layer into particle kinetic energy.

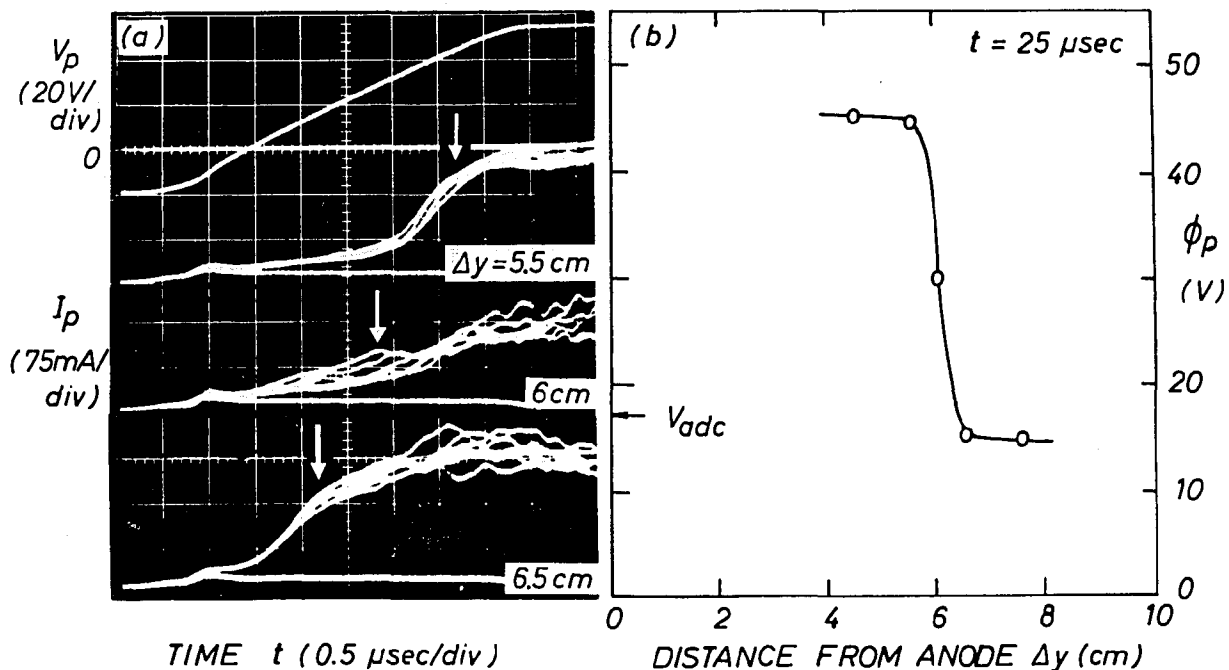


Fig. 3(a). Langmuir probe I-V traces swept rapidly during the first current disruption. Plasma potential indicated by arrows drops rapidly with distance  $\Delta y$  from end anode. (b) Axial plasma potential profile  $\phi_p(\Delta y)$  showing a potential double layer at  $\Delta y \approx 6$  cm.

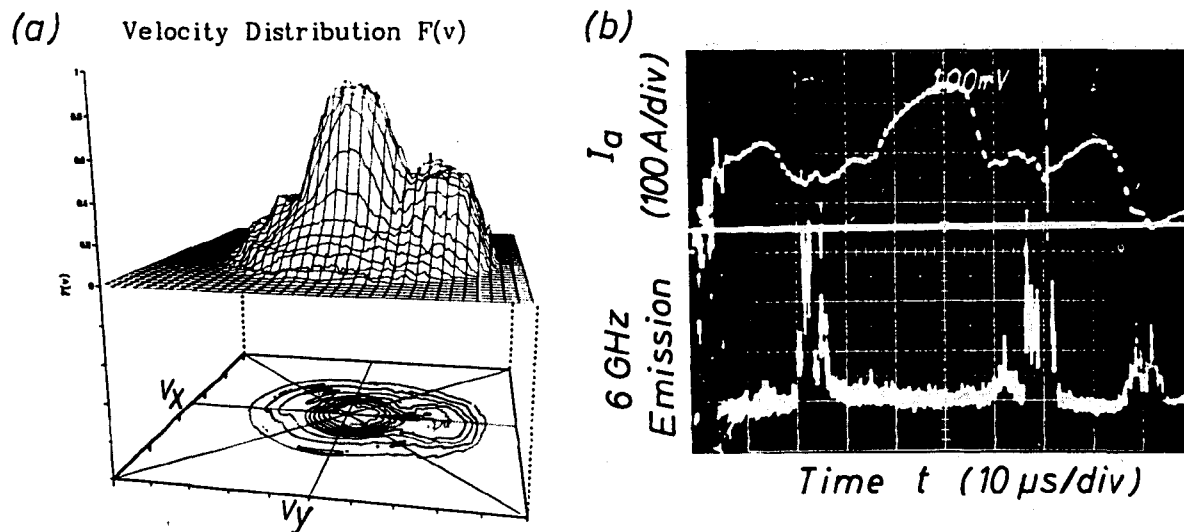


Fig. 4(a) Electron distribution function  $f_e(v_x, v_y)$  on the high potential side of the double layer showing a beam of free electrons accelerated by the double layer. (b) Plasma wave emission (bottom trace) due to beam-plasma instabilities at multiple disruptions of the plate current (top trace).

Microinstabilities lead to the thermalization of the particle beams, to heating and electromagnetic radiation [Whelan and Stenzel, 1981]. Many of these phenomena have been discussed in models of magnetic substorms and solar flares [Akasofu, 1979; McPherron, 1979].

#### Acknowledgments

The authors gratefully acknowledge assistance from Mr. M. Urrutia-Paez and D. Whelan.

This research was supported in part by the National Science Foundation under grants NSF ATM81-19717, NSF PHY79-23187, and by the National Aeronautics and Space Administration under grant NAGW-180.

#### References

- Akasofu, S.-I., Physics of Magnetospheric Substorms, D. Reidel Publ. Co., Dordrecht, Holland, 1977.
- Akasofu, S.-I., Magnetospheric substorms and solar flares, Solar Phys. **64**, 333-348, 1979.
- Alfvén, H., Electric currents in cosmic plasmas, Rev. Geophys. Space Phys. **15** (3), 271-284, 1977.
- Block, L. P., A double layer review, Astrophys. Space Sci. **55**, 59-83, 1978.

- Dungey, J. W., Cosmic Electrodynamics, Cambridge University Press, London, 1958.
- Kan, J. R., and L. C. Lee, Formation of auroral arcs and inverted V-precipitations: An overview, in Physics of Auroral Arc Formation, S.-I. Akasofu and J. R. Kan, eds., p. 206, American Geophys. Union, Washington, DC, 1981.
- McPherron, R. L., Magnetospheric substorms, Rev. Geophys. Space Phys. 17. (4), 657-681, 1979.
- Stenzel, R. L., W. Gekelman and N. Wild, Magnetic field line reconnection experiments, Part 4. Resistivity, heating and energy flows, J. Geophys. Res. 87 (A1), 111-117, 1982a.
- Stenzel, R. L., W. Gekelman and N. Wild, Double layer formation during current sheet disruptions in a reconnection experiment, Geophys. Res. Lett., June 1982b.
- Stenzel, R. L., R. Williams, R. Agüero, K. Kitazaki, A. Ling, T. McDonald and J. Spitzer, A novel directional ion energy analyzer, Rev. Sci. Instrum. 53, 59-63, 1982c.
- Whelan, D., and R. L. Stenzel, Electromagnetic wave excitation in a large laboratory beam-plasma system, Phys. Rev. Lett. 47(2), 95-98, 1981.

EXPERIMENTS ON TURBULENT POTENTIAL JUMPS  
IN A LONG CURRENT-CARRYING PLASMA

Ch. Hollenstein

Centre de Recherches en Physique des Plasmas  
Association Euratom - Confédération Suisse  
Ecole Polytechnique Fédérale de Lausanne  
CH-1007 Lausanne / Switzerland

In the last few years, many different kind of experiments on Double Layers were reported. In most of these investigations, the Double Layers are found to be laminar. Up to now, little is known about turbulent layers. To our knowledge, only in two experiments turbulent layers were observed [1,2]. Turbulent potential structures are obtained in low density current carrying plasmas with  $v_{de} < v_{te}$ . The most important observed feature of turbulent potential jumps is the high amplitude ion turbulence within the structure. Furthermore, on the high potential side, strong local electron heating due to the relaxing electron beam is found. In this paper, we would like to summarize our investigations on stationary turbulent potential jumps and recent measurements on the formation of this potential jumps.

The experiments were carried out using a long triple plasma device. Detailed description of the device and of the experimental condition is given in previous papers [1,3,4]. Plasma parameters were such as, electron density  $n_e \approx 2 \cdot 10^9 \text{ cm}^{-3}$ , electron temperature  $T_e \approx 1 \text{ eV}$  and the ion temperature  $T_i = 0.1 \text{ eV}$ . Argon gas at a pressure of  $4 \cdot 10^{-4} \text{ Torr}$  was used. The plasma was emmersed in a magnetic field of 25 Gauss.

Within this experimental arrangement one or more stationary turbulent potential jumps were observed. Typical jump width of about  $500 \lambda_{De}$  and jump amplitudes  $e\phi/kT_e \approx 10$  were observed. It is found that each of this stationary turbulent potential jump is accompagned by a local depression of the electron density, high amplitude low frequency turbulence ( $\omega < \omega_{pi}$ ) on the low potential side and strong localized electron heating on the high potential side [3]. Detailed investigations on the turbulence attributed with the potential structures were performed. Two main types of turbulences can be distinguished: on the low potential side the high amplitude, low frequency ( $\omega < \omega_{pi}$ ) and high frequency turbulence

( $\omega \approx \omega_{pe}$ ) on the high potential side. The electron beam detected on the high potential side is found to excite the well-known beam plasma instability around  $\omega_{pe}$ . The unstable waves propagate in direction of the beam and obey the dispersion relation  $\omega \approx kv_{beam}$ . The relaxation of the beam within about 20 cm correlates with the measured localized electron heating on the low potential side intense ion beam and low frequency fluctuations are observed. Typically, the frequency spectra of this turbulence is found to be as low as  $\omega_{pi}/2$ , and values of  $W/nT_e \approx (\delta n/n)^2 \approx 10^{-1}$  are reached near the jump. Correlation measurements demonstrated that this unstable waves obey the dispersion relation  $\omega \approx k c_s$ . The turbulence is dominated by low frequency waves ( $\omega < \omega_{pi}/4$ ) having a propagation angle with respect to the electron drift of  $90^\circ$ . Propagation angles of about  $45^\circ$  were observed for waves higher in frequency ( $\omega_{pi}/4 < \omega < \omega_{pi}$ ) [4].

For the understanding of the physics of turbulent layers there is great interest in studying the formation of such structures. For this purpose the voltage applied to the biasing grid was pulsed. The pulse rise time was in the order of a few  $\mu s$  and variable pulse lengths were possible (Fig. 1a). Using box-car techniques time-resolved measurements from different Langmuir probes, electrostatic ion energy analyser, hot probes and capacitive probes could be performed.

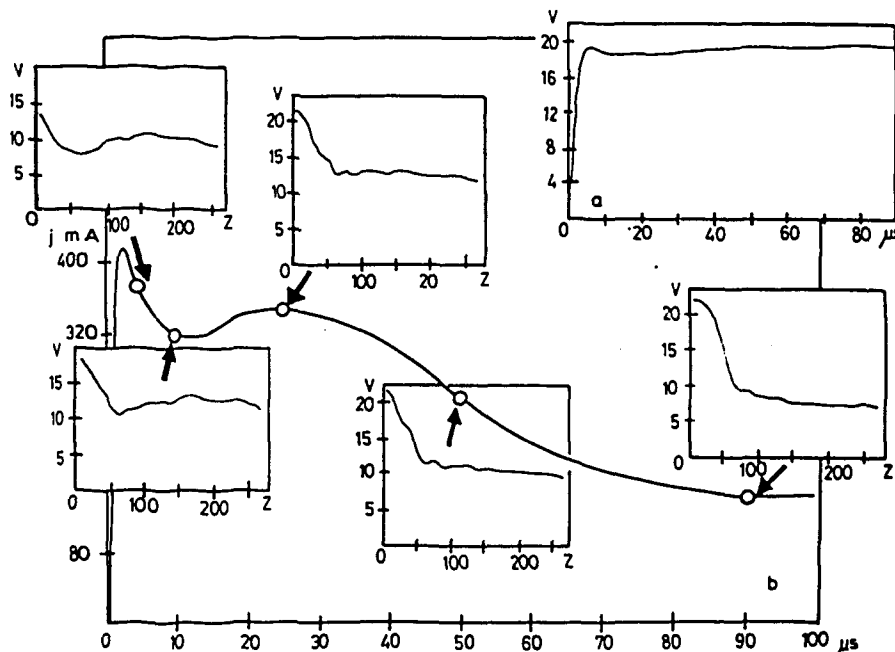


**Fig. 1:** a) Grid voltage  $V_g$   
 b) Time evolution of the plasma current and the plasma potential

The evolution in time of the plasma current is shown in Fig. 1b. The current shows two maxima and reaches its steady state value after about 100  $\mu$ s. The plasma potential near the first current peak jumped up to about 10 V, showing a typical potential through at the later jump position. The potential jump is developed nearly at the same time as the plasma current gets constant. Minor changes at later times are remarked on the low potential side. The electron saturation currents of a cylindrical Langmuir probe show that already in the early phase of the formation remarkable density depressions have been built up (Fig. 2a). The measured electron temperature grows up in time to reach its maximum at about 100  $\mu$ s (Fig. 2b). The steady state temperature profile is obtained after 150  $\mu$ s.

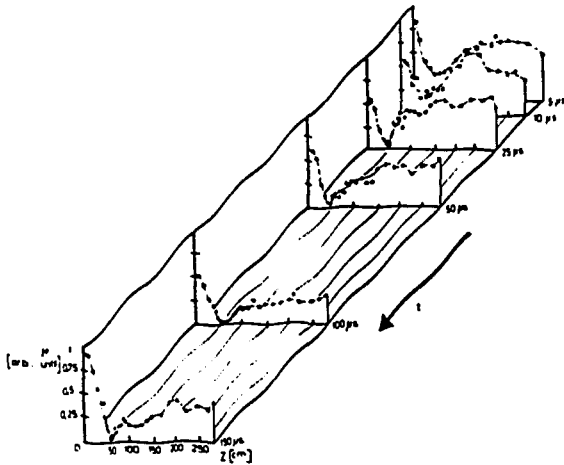


Fig. 2a: Spatial profiles of the electron saturation current  $j_e$

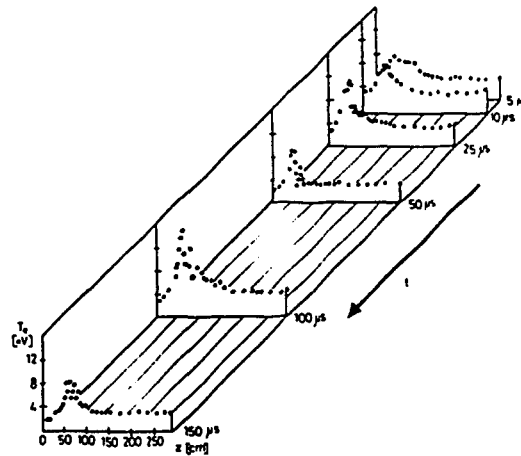
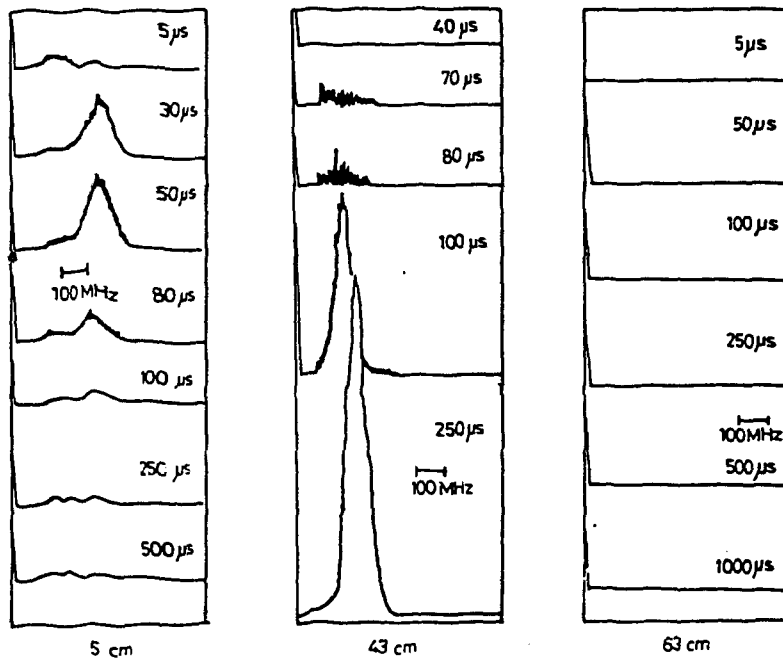
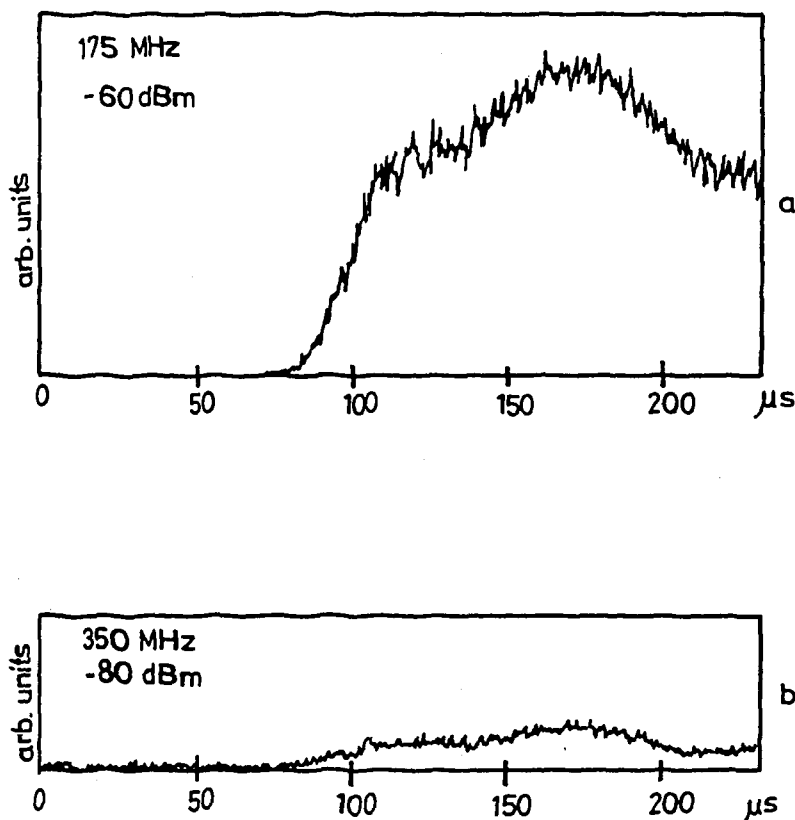


Fig. 2b: Spatial profiles of the electron temperature  $T_e$

Time-resolved measurements of the frequency spectra of the high frequency turbulence for different probe positions are presented in Fig. 3a. Near to the biased grid, the measurements show the appearance of high frequency fluctuation within the first 5  $\mu$ s. However, it decreases after reaching a maximum intensity at 50  $\mu$ s towards small levels. Near the potential jump region, the appearance of the fluctuations is delayed by about 70  $\mu$ s. Fluctuations around 200 MHz rapidly rise in time and saturate. However, on the low potential side high frequency turbulence was never observed. Figure 3b shows the time development of the turbulence on the high potential at a frequency of 175 MHz. The same type of behaviour is found at the double frequency (350 MHz). A difference of about 20 dBm is observed between the intensity at these frequencies.



**Fig. 3a:** Time evolution of the high frequency spectra at different positions



**Fig. 3b:** Time evolution of the high frequency noise at 175 MHz and its harmonics

The knowledge of the distribution functions of the different species is of crucial importance for the understanding of the potential jumps and Double Layers. Time resolved measurements of the evolution of the electron distribution were performed by means of a probe consisting of two oppositely-faced plane Langmuir probes. By careful design and probe cleaning, identical Langmuir traces and derivations were achieved in the currentless case. The measured time evolution on axis of the device for different times is presented in Fig. 4. At 5  $\mu$ s, strong anisotropic distributions are noticed all along the device. Maxwellian-shaped velocity distributions are found in the directions of the electron drift while in the opposite direction much less particles are noticed. The current

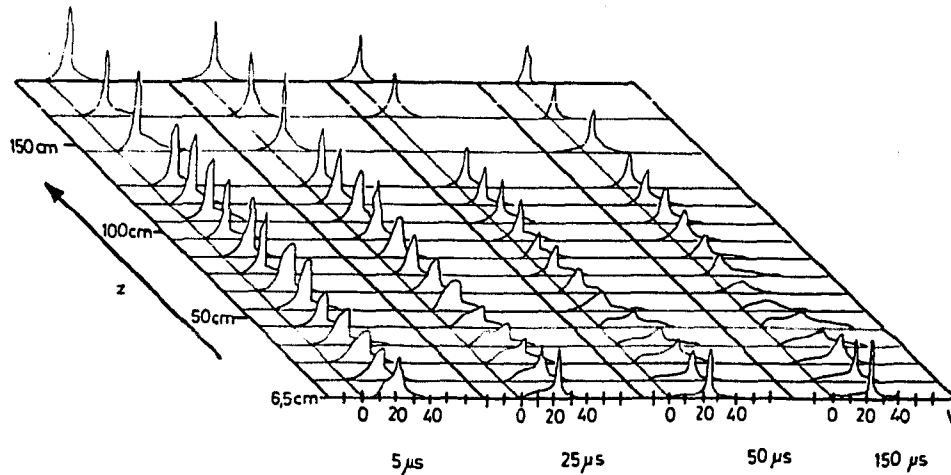


Fig. 4: Spatial evolution of the electron distribution  $f_e(E)$  at different times

within the plasma is mainly due to this anisotropic distribution. The plasma current calculated from the measured difference of the two saturation currents agrees with the measurements presented in Fig. 1. Later in the time evolution anisotropic distributions are mainly observed on the low potential side and on the high potential side isotropic distributions and strong electron beams are detected.

The ion distribution was measured using a single grid electrostatic energy analyser with typical resolution of 0.1 eV. Time-resolved measurements of the ion distribution is presented in Fig. 5. As well as for the electrons, the ions show anisotropic distributions. Complicated ion beam systems appear at the very beginning and disappear very quickly. At about 100  $\mu$ s a strong ion beam indicates the establishment of the potential jump.

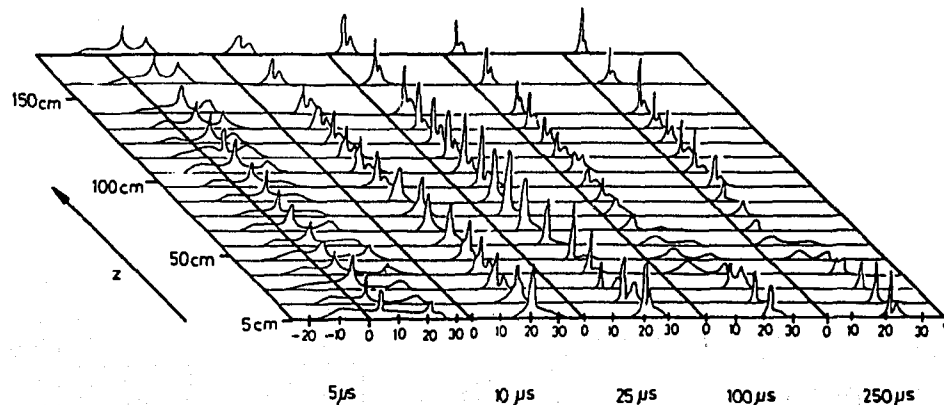


Fig. 5: Spatial evolution of the ion distribution  $f_i(E)$  at different times

Anisotropies of the distributions may trigger low frequency instabilities which may play an important role in the evolution and physics of turbulent potential jumps and Double Layers. Anisotropic electron distributions with small drifts with respect to the ions may lead to a Buneman-like instability, which leads to strong turbulence. Therefore, even in low drift plasmas strong turbulence can be developed, which may be important in the physics of turbulent layers.

I would like to thank Dr. J. Vaclavik and Dr. M. Guyot for many helpful suggestions. This work was supported by the Swiss National Science Foundation, the Ecole Polytechnique de Lausanne and by Euratom.

#### References

- [1] Ch. Hollenstein, M. Guyot and E.S. Weibel, Phys. Rev. Lett. 45, 2110 (1980).
- [2] E.W. Ng and J.S. DeGroot, Bull. Am. Phys. Soc. 26, 1011 (1981).
- [3] M. Guyot and Ch. Hollenstein (to be published).
- [4] Ch. Hollenstein and M. Guyot (to be published).

A Potential Double Layer Formed by a Shock  
Wave in a Plasma

S.Yagura, H.Fujita and E.Yamada  
*Electrical Engineering, Saga University,*  
*Honjo-machi I, Saga 840, JAPAN*

A potential double layer (DL) is formed by a shock wave in a triple plasma device which can control an initial velocity of an injected ion beam. The density compression produced by the ion beam injection is found to form a potential step giving a DL profile. The potential step is about equal to or higher than an electron temperature. We observed an electron trapping caused by a potential step at the both sides on the shock wave and a reflection of ions at the shock front.

### 1. Introduction

There exist only few studies[1,2] on a relation between a potential double layer (DL)[3] and a shock wave[4], in spite of that both phenomena should be apparently similar in the profiles of potential and density step. The DL and the shock wave have been discussed by measuring fluctuations of a potential and a density, respectively. A time evolution of propagating DL or electrostatic shocks has been described by a modified Korteweg-de Vries equation with a cubic nonlinearity [2]. We describe a laminar shock wave experimentally on the view point of DL and the ion or electron trapping by the potential step.

### 2. Experiments

The experiments were performed in a triple plasma device (35 cm in diameter and 80 cm in length), as shown in Fig.1. The target plasma between two source plasmas was produced by ionizing collisions between an argon gas and primary electrons penetrated through the grids so that the target plasma density ( $\approx (2\sim 4) \times 10^8 \text{ cm}^{-3}$ ) is lower than the source one. A plasma potential was measured by an emissive probe with a noble technique which gives a high time resolution and gets



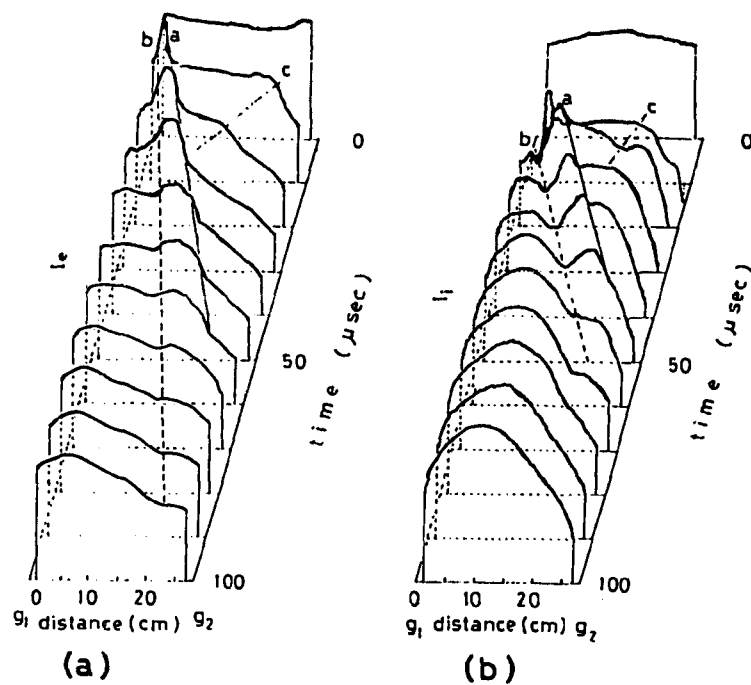


Fig.2 (a) Spatial profiles of the electron density estimated by an electron saturation current collected by a needle probe at various times. (b) Spatial profiles of the ion density estimated by an ion saturation current collected by a needle probe at various times.

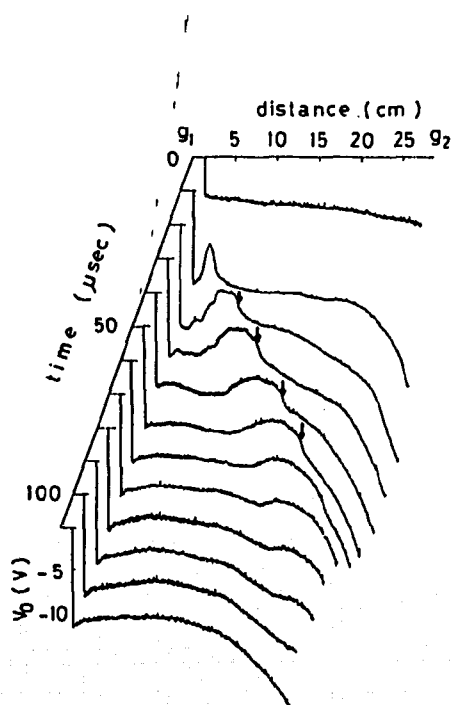


Fig.3 Spatial profiles of the plasma potential  $V_0$  measured by an emissive probe at various times.

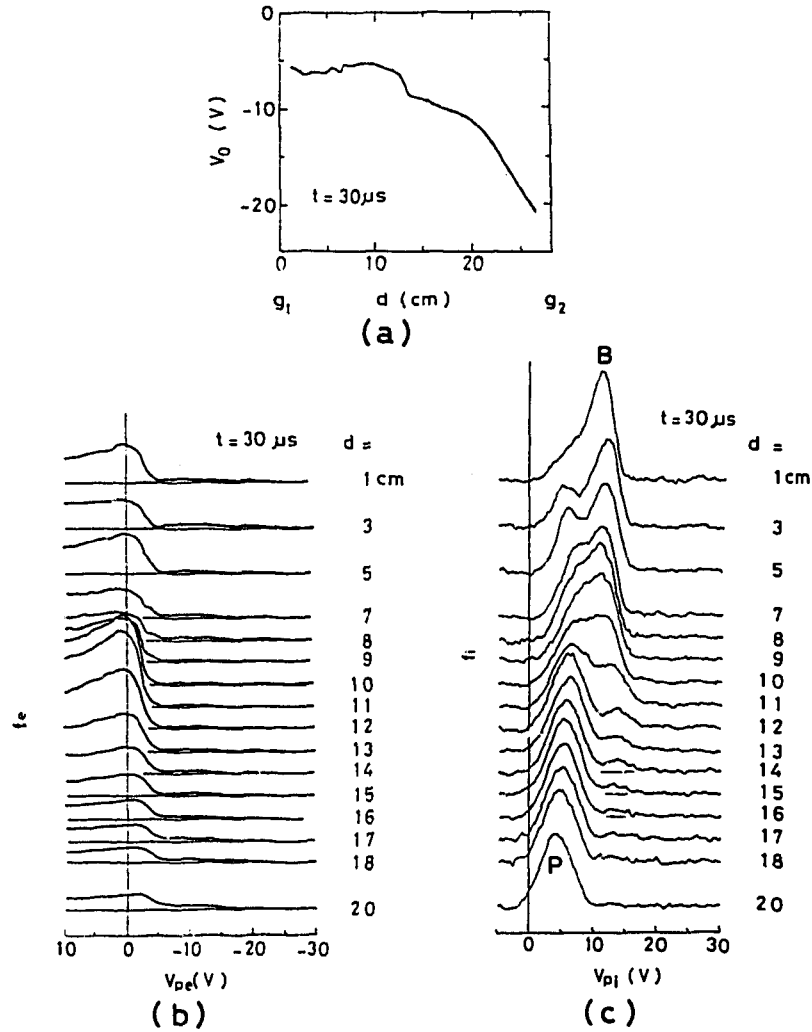


Fig.4 (a) A spatial profile of the plasma potential at  $t = 30 \mu\text{s}$ .

- (b) Electron energy distributions measured by a needle probe at various positions at  $t = 30 \mu\text{s}$ . The distributions are estimated by  $dI_{pe}/dV_{pe}$ , where  $I_{pe}$  is a probe current and  $V_{pe}$  is a probe potential
- (c) Ion energy distributions measured by an electrostatic energy analyzer facing towards  $g_1$  at various positions at  $t = 30 \mu\text{s}$ .

indicated by "a" as shown in Fig.2(b). In this paper, we wish to describe a potential profile in the presence of such a shock wave, as shown in Fig.3. Note in this figure that a DL like form is established in front of the shock wave as shown by arrows and the potential step is about  $(1\sim 1.4)kT_e/e$  corresponding to a weak DL[5]. Considering a potential profile in Fig.3, it can be anticipated that electrons are trapped at the region of potential step and ions are reflected at the shock front. We clarify electron trapping by the potential step at a fixed time ( $t=30\ \mu\text{s}$ ) in Fig.4(a) from measurements of an electron energy distribution function measured by a needle probe, as shown in Fig.4(b). The probe potential  $V_{pe}$  at which a height of the distribution becomes maximum is shifted towards a positive side at the region of the positive potential step, and  $V_{pe}$  at which the height becomes zero is constant even in the region of the potential step. Thus, it can be considered that the electrons with the low energy are trapped at the potential step. Moreover, we describe an ion reflection by the potential step at a fixed time ( $t=30\ \mu\text{s}$ ) measured by an electrostatic analyzer facing to  $g_1$ . As shown in Fig.4(c), reflected ions whose potential  $V_{pi}$  is about 13 V are observed at the region ( $d\approx 12\sim 14\ \text{cm}$ ) in front of the potential step ( $d\approx 7\sim 11\ \text{cm}$ ) where the bulk ions marked "P" are accelerated towards  $g_2$  due to a push of the positive potential step caused by a positive shift of the plasma potential. Beam ions marked "B" are retarded due to a reaction of accelerated bulk ions.

### 3. Conclusion

It is experimentally shown that a DL with a potential step of about  $\Delta\phi \leq (1\sim 1.4)T_e/e$  is formed in front of the laminar shock wave with the large fluctuation of density ( $\delta n/n_0 \approx 15\sim 40\%$ ). An electron trapping caused by a potential step at the both sides on the shock wave and a reflection of ions in front of the potential step are observed.

### References

- [1] P.G.Coakley and N.Hershkowitz: Phys. Lett. 83A(1981)131
- [2] S.Torvén: Phys. Rev. Lett. 12(1981)1053
- [3] S.Torvén and D.Andersson J.Phys. D 12 (1979)717

- [4] H.Ikezi, T.Kamimura, M.Kato and K.E.Lonngren: Phys. Fluids  
16(1973)2167
- [5] N.Hershkowitz, G.L.Payne, C.C.Chan and J.R.DeKock:  
Plasma Phys. 23(1981)903

## DYNAMICAL DOUBLE LAYERS

S. Iizuka<sup>1,2</sup>, P. Michelsen<sup>1</sup>, J. Juul Rasmussen<sup>1</sup>, R. Schrittwieser<sup>1,3</sup>, R. Hatakeyama<sup>2</sup>, K. Saeki<sup>2</sup>, and N. Sato<sup>2</sup>.

1) Assoc. EURATOM-Risø Nat. Lab., DK-4000 Roskilde, Denmark

2) Dept. Elec.Eng., Tohoku Univ., Sendai, Japan

3) Inst. Theor. Phys., Innsbruck Univ., A-6020 Innsbruck, Austria

Abstract: Experimental investigations of the evolution of oscillating double layers are presented. The oscillations are associated with the formation and destruction of a negative potential barrier on the low potential side of the double layer.

Introduction: Many experiments in various types of laboratory plasmas have clearly revealed the existence of double layers (DL) (see e.g. Sato<sup>1</sup> and references therein). Most of the experiments have focussed on stationary DL and comparatively few investigations have been reported on the dynamical features. Investigations of such features are of importance in connection with moving DL and with the formation and stability of stationary DL.

We have investigated experimentally the dynamical double layer evolution by performing time resolved measurements of the DL-profile<sup>2</sup>. The investigations are related to recent experiments<sup>3</sup> where strong DL were generated in a Q-machine plasma by applying potential differences between two plasma sources. The results of these experiments showed the initial formation, the subsequent movement, and the final stationary state of DL. It was also found that the stationary DL were accompanied by low frequency potential oscillations localized on the low potential tail of the DL. These fluctuations were responsible for an apparent broadening of the DL-profile as obtained from time averaged measurements and were especially pronounced for lower DL-potentials ( $\lesssim 80$  V). Similar fluctuations in the DL-profile were also reported in in other experiments (e.g. Ref. 4).

Experimental results: The experiments were performed in the Risø Q-machine using a set up similar to that of Ref. 1. For some of the measurements the machine was operated double-ended, and the plasma was produced by surface ionization of cesium on two 3 cm -

diameter hot tantalum plates (source 1 ( $S_1$ ) and source 2 ( $S_2$ ) with separation  $d = 125$  cm). In other cases the machine was operated single-ended with a cold collector plate C replacing  $S_1$  terminating the plasma column. Then the length  $d$  of the column could be varied from 10 cm to 120 cm. The plasma was confined radially by a homogeneous magnetic field  $B \approx 0.4$  T. The plasma densities were  $(0.5-10) \times 10^8$   $\text{cm}^{-3}$ , temperatures  $T_i \sim T_e \approx 0.2$  eV. The neutral background pressure was  $10^{-6}$  Torr and collisions were entirely unimportant. The diagnostics consisted of an axially movable probe which may function as a usual Langmuir probe or as an electron emissive probe, when heated by either a direct or a pulsed current<sup>2</sup>.

In double-ended operation stationary DL were easily generated, when a potential  $\phi_0$  was applied to  $S_1$  with respect to  $S_2$ <sup>3</sup>. However, in the single-ended operation stationary DL could not be formed. A positive potential applied to the collector resulted in strong oscillations in the plasma potential and density, which were found to be related to the dynamics of a moving DL<sup>5</sup>.

First we consider the formation of stationary DL in double-ended operation. This process is investigated by applying a positive step voltage  $\phi_0$  to  $S_1$  and the characteristics of the formation which are independent of  $\phi_0$  evolve as follows<sup>1,3</sup>: Just after applying  $\phi_0$  the plasma potential  $\phi$ , increases up to  $\phi_0$  almost simultaneously in the whole column accompanied with an increase in  $I_{S1}$  (the current through the system (see Fig. 1)). The potential drop is then localized to the sheath in front of  $S_2$ . This initial increase of  $\phi$  is caused by an electron adjustment and takes place in a time too short for the ions to react. Since, this time scale is also shorter than the response time of our measuring circuit ( $> 5$   $\mu\text{s}$ )<sup>2</sup> we were not able to follow this fast evolution in detail. After a time of the order of the ion plasma period the ions start reacting and ultimately the potential profile relaxes: the potential drop detaches from  $S_2$  and a DL starts moving from  $S_2$  to  $S_1$  accompanied by a decrease in  $I_{S1}$  as seen in Fig. 1 where the potential evolution around the low potential tail of this DL is shown on an expanded scale. This current decrease is caused by a small negative potential barrier formed on the low potential tail of

the DL (see Fig. 1). The potential dip is of the order of 0.4 V which is sufficient for limiting the current carried by the electrons of temperature 0.2 eV. During the moving phase the DL propagates with a velocity around  $1.5 \times 10^5$  cm/s ( $\approx 3c_s$ ,  $c_s$  is the ion acoustic speed) and the moving DL is followed by an expanding plasma from  $S_2$ <sup>3</sup>. When the DL stops, the potential barrier dissolves, the current increases and a stationary DL is obtained. This is, however, subject to a "back and forth" oscillation of the low potential tail as will be described in the following.

The low frequency potential oscillations observed on the low potential tail of the stationary DL were found to be correlated with oscillations in the plasma current  $I_{S1}$ . Thus time resolved measurements of the potential oscillations could be performed by using  $I_{S1}$  as a triggering signal. Figure 2 shows an example of the evolution of the DL-profile within one period of the current oscillation. The DL steepens during a current decrease, i.e. the low potential foot point (defined as the point where the plasma potential is zero) moves towards  $S_1$  (see Fig. 2c), while the high potential edge is almost fixed. The maximum potential slope is reached at the current minimum and at that instant the DL width is  $L \approx 100 \lambda_D$ , comparable with theoretical expectations. Then the current increases within a relatively short time and the potential profile becomes broad again. This cycle repeats. The velocity of the foot point in the steepening phase is  $v \approx 1.7 \cdot 10^5$  cm/s ( $\approx 3 c_s$ ) (Fig. 2c), which is around the ion flow speed in the device<sup>5</sup>. The broadening, on the other hand, takes place on a much faster time scale i.e.  $v > 10^6$  cm/s. The period of the oscillations is almost determined by the transit time of the foot point in the steepening phase, and accordingly we find that the period is proportional to the distance between  $S_2$  and the upper fixed edge of the DL.

The evolution of the potential as seen in Fig. 2 is very similar to the oscillations observed, when a current is drawn to a cold non-emitting collector C in the Q-machine in single-ended operation<sup>5</sup>. Figure 3 shows a typical evolution of the plasma potential and saturation currents when a positive potential  $V_C$  is applied to C. The strong oscillation in the plasma current

$I_C$  (Fig. 3a) is seen to be related to a moving potential profile of a DL-like form. During the phase of current decrease this DL moves from  $S_2$  to C with the velocity  $\sim 3 c_s$  (Fig. 1b) followed by a flow of plasma from  $S_2$ . When the DL reaches C,  $I_C$  increases to a maximum in a short time ( $< 100 \mu s$ ) and the potential increases along the whole plasma column. Then the DL reappears near  $S_2$  and  $I_C$  starts decreasing. The repetition of this cycle results in the oscillations in  $I_C$ . A detailed study<sup>5</sup> of the tail of the moving DL showed the existence of a negative potential barrier following the DL. This barrier reflects electrons and is thus responsible for the decreased electron density on the high potential side and the limitation of  $I_C$  during this phase. Note that the potential barrier has a depth of the order of  $T_e/e \approx 0.2 \text{ V}$  and is hardly visible in Fig. 3, but it may be observed on an expanded potential scale as seen in Fig. 1 (see also Fig. 25 of Ref. 1). When the DL reaches C it stops and the ions may "fill" the potential dip. Thus the barrier dissolves and a normal sheath forms in front of the C accompanied by a rapid increase in  $I_C$  and in the potential in the whole plasma.

If we imagine the high potential edge of the stationary DL in the double-ended operation as a virtual collector since this edge is fixed, we can explain the DL oscillation in Fig. 2 in a way very similar to the oscillations in the single-ended case just described. We should note that the oscillations in Fig. 2 is especially pronounced for relative small values of  $\phi_0 (< 80 \text{ V})^3$  and they may to some extent be suppressed by adjusting the ratio of densities supplied from the two sources<sup>3</sup>. In the case of Fig. 2 we have chosen the parameters to maximize the fluctuation amplitude to facilitate the measurements.

Discussion: The experimental set-up in the single-ended case has some similarities with the thermionic converter or the plasma diode (see e.g. Ref. 6), but in this device the plasma column is considerably shorter ( $\sim 100$  Debye lengths) than in our case. However, the mechanism of the unstable current oscillations in such a diode, as clarified by the numerical simulation by Burger<sup>7</sup> is indeed very similar to our results with respect to the evolution of the potential distribution. Silevitch<sup>8</sup> applied the model of the current oscillations in the plasma diode to describe a periodic disruption of the auroral

DL similar to the behaviour of the DL observed in our experiment in the case of double-ended operation. The instability of the DL leading to the disruption was explained in terms of a negative dynamical resistance and the fluctuating DL was proposed as a candidate for flickering auroras<sup>8</sup>.

Recently it has been suggested that the existence of a negative potential dip in the form of a solitary structure in a current carrying plasma leads to current limitations and subsequently to the formation of a weak double layer<sup>9,10,11</sup> often denoted ion acoustic double layer with  $\Delta\phi \lesssim T_e/e$ . The negative potential dip observed in the present experiment accompanying strong DL,  $\Delta\phi \gg T_e/e$ , acts in a similar way as the above-mentioned solitary structure with respect to current limitations, but we believe it to be of somewhat different origin. In our case the potential dip is formed on the low potential tail of the moving DL in front of an expanding plasma<sup>5</sup>. It can be seen that this dip cannot exist selfconsistently in a stationary frame, because the accompanying DL-potential jump  $\Delta\phi \gg T_e/e$ , and will thus be cancelled by inflowing ions when it stops. The potential dip preceding the ion acoustic DL is believed to be created by the ion acoustic turbulence in the current carrying plasma<sup>11</sup> and can exist in a stationary frame where ion trapping results in the formation of an ion hole. The scenario of the formation of acoustic DL preceded by a negative potential dip evolving into an ion hole is clearly revealed in numerical simulations,<sup>11,12</sup>

### References

- 1) N. Sato, Invited lecture, these proceedings p. 116
- 2) S. Iizuka et al. J. Phys. E: Sci. Instrum. 14, 1291 (1981)
- 3) N. Sato et al. Phys. Rev. Lett. 46, 1330 (1981)  
Plasma Res. Rep., Tohoku University THUP-1 (1981)
- 4) S. Torvén and D. Andersen, J. Phys. D: Appl. Phys. 12, 717 (1979); S. Torvén and L. Lindberg *ibid* 13, 2285 (1980)
- 5) S. Iizuka et al. Phys. Rev. Lett. 18, 145 (1982)
- 6) C.K. Birdsall. These proceedings p. 84,
- 7) P. Burger J. Appl. Phys. 36, 1938 (1965)
- 8) M.B. Silevitch J. Geophys. Res. 86, 3573 (1981)
- 9) A. Hasegawa and T. Sato Phys. Fluids 25, 632 (1982)
- 10) H. Schamel, Invited lecture, these proceedings p. 13
- 11) K. Nishihara et al. These proceedings p. 41
- 12) T. Sato and H. Okuda J. Geophys. Res. 86, 3357 (1981).

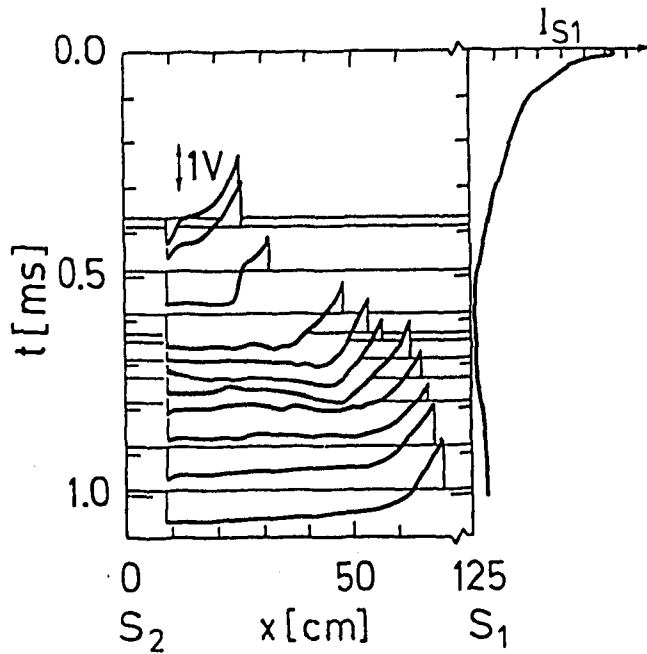


Fig. 1. Temporal evolution of the low potential tail of the DL and the corresponding current  $I_{S1}$ , when a step voltage is applied to  $S_1$ ,  $\phi_0 = 35 V_0$  (double-ended operation).

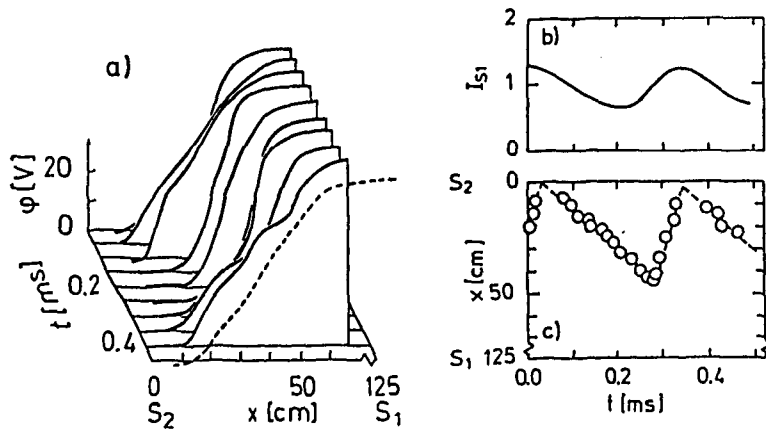


Fig. 2. a) Temporal evolution of the DL profile with a constant bias applied to  $S_1$ ,  $\phi_0 = 61 V$  (broken curve shows the time averaged profile), b) Plasma current, c) Trajectory of the DL foot point (double-ended operation).

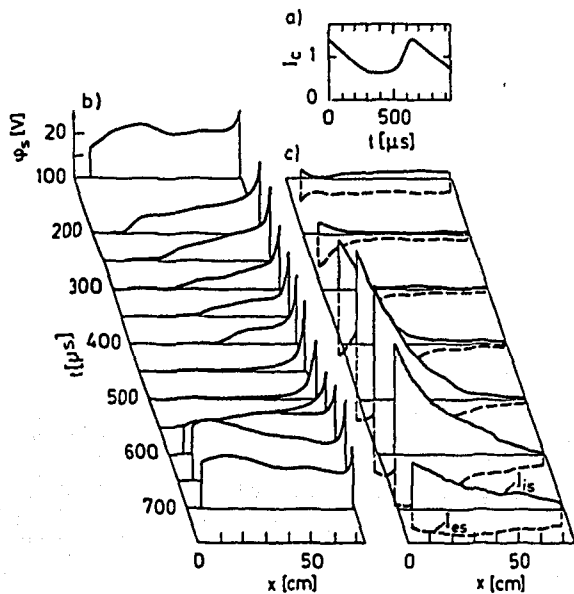


Fig. 3. Temporal evolution of a) collector current  $I_C$ , b) plasma potential  $\phi$ , and c) ion saturation current  $I_{is}$  and electron saturation current  $I_{es}$ .  $V_C = 72 V$ . Single-ended operation:  $S_2$  at  $x = 0$  cm and collector at  $x = 75$  cm.

ON THE RELATION BETWEEN ION OSCILLATIONS AND TRAVELLING  
DOUBLE LAYERS IN A POSITIVELY BIASED SINGLE-ENDED Q-MACHINE

G.Popa, M.Sanduloviciu

Faculty of Physics, "Al.I.Cuza"University, R-6600, IASI ,  
ROMANIA

E.Mravlag

Inst.f.Theoretical Physics, University of Innsbruck, Innsbruck  
AUSTRIA

As is known low-frequency oscillations can be excited in a low-density single-ended Q-machine between the hot plate (HP) and an "exciting" electrode (E) biased positively with respect to HP /1/. For large positive bias ( $>2V$ ) the oscillations of the ion component have been shown to exhibit for fundamental frequency the character of a standing wave with half a wavelength corresponding to the distance between HP and E (SATO et al./2/, SCHRITTWIESER /3/, MICHELSEN et al./4/). On the other hand, more detailed measurements of this phenomenon have recently revealed potential double layers travelling from HP to E (IIZUKA et al./5/) which are associated with sudden overall changes of the space potential upon their arrival at E. Therefore this phenomenon, which was previously termed "ion acoustic instability"/3,4/ or "so-called ion acoustic instability"/6/ is now also being referred to as "potential relaxation instability"/1/.

In this paper we present an experimental result which shows the presence of a small travelling phenomenon which is superimposed on a dominant standing wave behaviour of the ions. This travelling phenomenon may be associated with the above mentioned moving double layers which was previously stand out as a jump of the axial potential which propagates from HP to E /5/.

The experiments were performed with the Innsbruck single-ended Q-machine. The plasma parameters were the

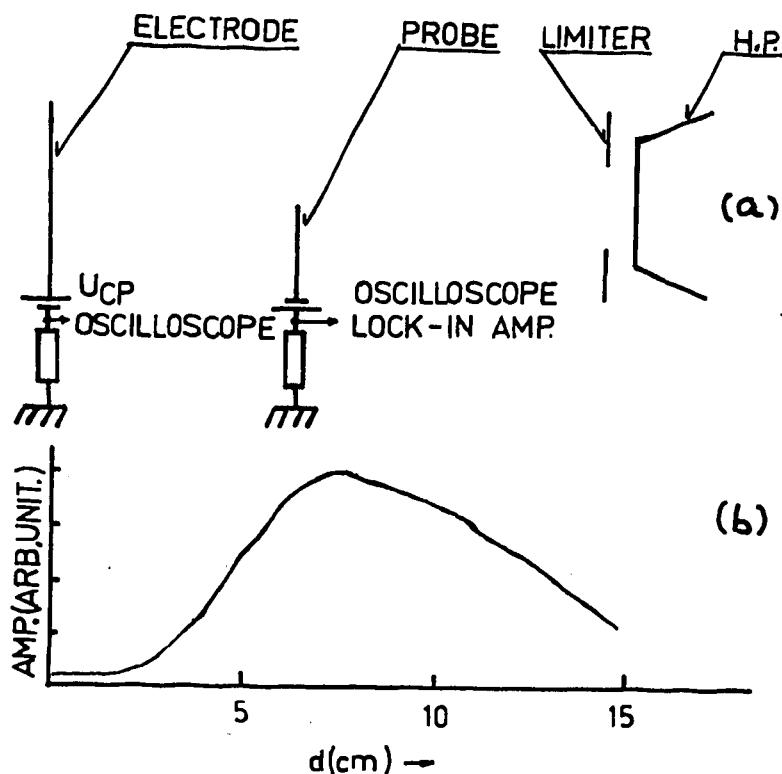


Fig. 1

- 1a : Experimental setup. The distance between the hot plate and the exciting electrode was 19 cm .
- 1b : Axial amplitude profile of the oscillations between the hot plate and the exciting electrode.

following : plasma density (measured with negatively biased E)  $n_p = 5 \cdot 10^7 \text{ cm}^{-3}$  ; background pressure  $< 2 \cdot 10^{-5}$  torr ; magnetic field  $B = 1500 \text{ G}$  ; hot plate temperature approximately 2000 K. The experimental setup is shown in fig. 1a .

We observed the oscillation processes with a Langmuir probe (S) biased such that it draws ion saturation current ( $V_p = -9 \text{ V}$ ). Fig.2 shows oscilloscope pictures obtained for different axial position of the probe between HP and E. In this figure the a.c. component of the probe current is compared to a.c. component of the current flowing through E (trace E). We can observe two superimposed phenomena. First we see an oscillation with a large amplitude (marked with ↓ in Fig.2) which does not show any phase change over the whole distance HP-E and whose axial amplitude

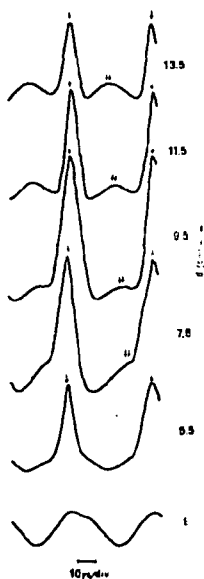


Fig.2

Oscilloscope traces at different axial positions of the probe with respect to the exciting electrode. The trace E represents the current flowing through the exciting electrode.

necessary to explain the driven mechanism of the ion standing waves.

The velocity of this phenomenon, which is approximately  $6 \cdot 10^5$  cm/sec, is about 2 times the ion acoustic velocity of the plasma. The "amplitude" of the perturbation is usually very small compared to the amplitude of the standing wave (Fig.2) so that it may explain why this instability was believed to have purely standing wave character.

#### Acknowledgements

The authors would like to thank Professors F.Cap and M.Pahl for their encouragements. This work was supported in part by the Fonds zur Förderung der wissenschaftlichen Forschung under project no. S-18/02, and also by the

profile is shown in Fig. 1b .

Secondly we observed a probe current variation (marked with  $\downarrow\downarrow$  in Fig.2) which corresponds to a local density change whose position varies with the distance between HP and S. The spatial position of this density perturbation is time depend and moves from HP to E.

Owning that the ion standing wave picture is valid, a fact additionally confirmed by a higher harmonic structure of the a.c. signal, we interpret this traveling density perturbation which appears simultaneously with the standing ion wave ,as a moving D.L. The presence of this moving D.L. starting, probably, from space-charge sheath in front of H.P., after our opinion is

Research Office of the U.S. Governement through the loan of electronic devices.

References

- /1/ R.SCHRITTWIESER, J.J.RASMUSSEN- Phys. Fluids., 25 ,  
48 (1982)
- /2/ N.SATO, G.POPA, E.MARK, E.MRAVLAG, R.SCHRITTWIESER -  
Phys.Fluids, 19, 70 (1976),
- /3/ R.SCHRITTWIESER- Phys.Lett., 65A, 235 (1978)
- /4/ P.MICHELSEN, H.L. PECSELI, J.J.RASMUSSEN, R.SCHRITTWIESER  
Plasma Physics, 21 , 61 (1979)
- /5/ S.IIZUKA, P.MICHELSEN, J.J.RASMUSSEN, R.SCHRITTWIESER -  
R.HATAKEYAMA, K.SAEKI, N.SATO - to be published
- /6/ G.POPA, M.SANDULOVICIU, S.KUHN, M.OERTL, R.SCHRITTWIESER  
Phys. Lett., 87A , 175 (1982).

Fine Structures of Potential Formation in a  
Bounded Plasma with Current

H.Fujita, S.Yagura, E.Yamada, Y.Kawai<sup>(a)</sup> and N.Sato<sup>(b)</sup>

*Department of Electrical Engineering, Saga University,  
Honjo-machi I, Saga 840, Japan*

(a) *Research Institute for Applied Mechanics, Kyushu University,  
Higashi-ku, Fukuoka 812, Japan*

(b) *Department of Electronic Engineering, Tohoku University,  
Sendai 980, Japan*

Abstract

Structures of the instability exciting a coherent wave are studied by measuring the spatial profiles of the potential and density at various temporal phases of the electron current to a biased grid which bounds a plasma. The density fluctuations with a large amplitude up to 50 % are observed to grow spatially. The discrete spectrum which satisfies the boundary condition  $f_n \cdot L/n = C_s$  is found to be caused not by the usual current-driven instability but by the plasma expansion from the source with the speed  $=C_s$  resulting in a formation of a moving double-layer. Here,  $f_n$  is nth frequency of the wave,  $L$  is the distance between two grids and  $C_s = \sqrt{T_e/M}$ .

1. Introduction

It is well known that an electron current through a plasma causes a number of low frequency instabilities[1-5]. In a collisionless plasma bounded by two grids with applying a dc potential, the so-called ion acoustic instability has been generated[2-4], where a discrete spectrum which satisfies the boundary condition  $f_n \cdot L/n = C_s$  was observed. Here,  $f_n$  is the nth frequency of the spectrum,  $L$  is the distance between the two grids and  $C_s = \sqrt{T_e/M}$ . In this case, the observed spectrum may be classified into two cases: one is a discrete spectrum superposed on a broad spectrum[3,4] where the frequency with the maximum amplitude agrees with theoretical prediction(case A), and the other is only a discrete spectrum[2,3] where the maximum amplitude is observed at the fundamental frequency(case B). However, structures of the instability, which may be

understood by measuring spatial and temporal behaviors of the potential formations, are still unclear. Recently, dynamics of the instability caused between the plasma source and a cold plate of the variable potential in a Q-machine was studied by observing the potential formation[6]. It is very interesting to study such dynamics also in a discharge plasma with  $T_e \gg T_i$  where the Landau damping of the ion acoustic wave is small.

In this paper, we describe an experimental investigation of structures of the instability in a discharge plasma bounded by two grids with applying a dc potential. The observed spectrum corresponds to the case B. The instability is found to be caused not by the current-driven ion acoustic instability but by the plasma expansion with the speed  $\approx C_s$ , from the measurements of spatial profiles of the potential and the density at various temporal phases of the grid current.

## 2. Review of the Instability Caused in a Bounded Plasma

We summarize the instability caused in a discharge plasma bounded by two grids of a variable potential. Tanaka *et al.* observed the spectrum corresponding to the case B (see Fig.5 in ref.[2]) by an electron current flowed to an anode which also served to bound a plasma with a grid kept at a floating potential. In this case, the plasma was produced in the measured region. The spectrum in both cases A and B were observed between two asterisk grids placed in a diffused plasma (see Figs.3 and 5 in ref.[3]). The spectrum in the case A was caused at a low grid potential and that in the case B was at a high grid potential. Kawai *et al.* predicted the spectrum corresponding to the case A (see Fig.3 in ref.[4]) in a plasma box. The measured region was surrounded by a plasma source so that the plasma diffused from many directions. Recently, Iizuka *et al.* measured temporal evolutions of a cold plate current, plasma potential and the plasma density in a single-ended Q-machine plasma bounded by the plate[6]. A potential profile with double layer (DL) like form existed during the phase of the current decrease and move from the plasma source to the collector with the speed  $\approx (2-3)C_s$ . Thus, this phenomena was explained not by the usual current-driven instability but by the ambipolar diffusion of the plasma from the source.

### 3. Results in the Present Experiment.

Figure 1 shows a discharge tube used in this experiment. An argon plasma was produced in the end section with coaxial typed electrodes. Axial magnetic fields ( $\leq 15$  G) were applied to obtain a uniform plasma ( $n_e \approx (0.6-5) \times 10^8 \text{ cm}^{-3}$ ,  $T_e \approx (2-5) \text{ eV}$ ,  $P \approx (1.5-2.5) \times 10^{-4} \text{ Torr.}$ ). The plasma was bounded between the mesh grid  $g_1$  and an asterisk grid  $g_2$  of a variable potential  $V_g$ . The grid  $g_2$  which satisfied the boundary condition  $f_n \cdot L/n = C_s$  was sometimes replaced by a mesh grid which changed the condition such as  $f_n \cdot L/n < C_s$ . With increasing  $V_g$ , the fluctuations of the grid current  $\delta I_g / I_{g0}$  enhanced strongly up to 50 % at a certain value of  $V_g$  above which a coherent wave was observed, as shown in Fig.2(a). The spectrum reveals higher harmonic waves which provide no dispersive property even at high frequencies unlike the ion acoustic wave. As shown in Fig.2(c), a potential profile with DL like form is observed during the phase of the current increase in  $I_g$  and moves from  $g_1$  to  $g_2$  with the speed  $\approx C_s$ . A negative gradient of the potential profile is obtained during the phase of the current decrease and the resultant inhomogeneous plasma with a similar profile of the potential is observed, as shown in Fig. 2(d). Thus, the moving DL limits the grid current leading to a discrete spectrum. Considering that the transit time  $\tau$  of DL from  $g_1$  to  $g_2$  can be expressed as  $\tau = L/C_s$  and the boundary condition  $1/f_1 = L/C_s$ , just after the arrival of DL at  $g_2$ , a "new" DL should start at  $g_1$  and arrive at  $g_2$ . Thus, fine structures of the potential formation are explained by this iteration. A two-stream distribution of electrons was observed by a needle probe during the phase of the current increase so that a stream with the higher energy would give rise to the current. The energy difference between the two streams were

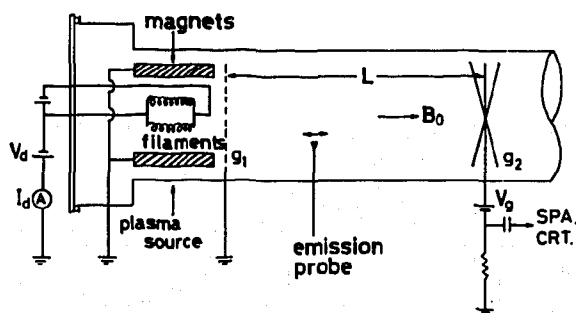


Fig.1 Experimental apparatus.  
SPA.; spectrum analyzer,  
CRT.; oscilloscope.

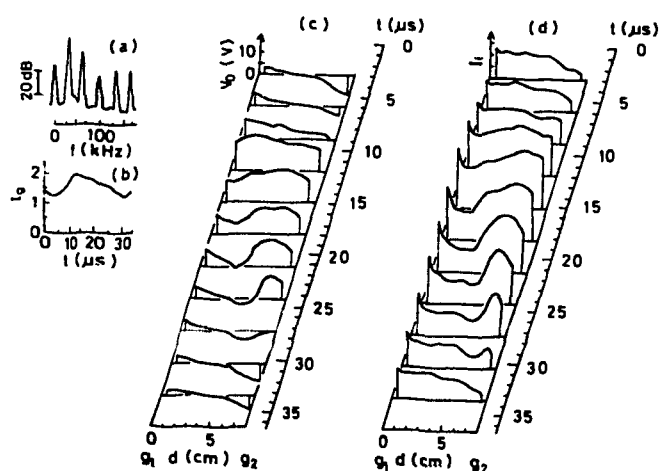


Fig.2 (a) A wave spectrum observed by the asterisk grid  $g_2$ . (b) A wave-form of  $I_g$ . Spatial profiles of the potential(c) and the density(d) at various times in (b).

equal to the potential between the source plasma (grounded) and the plasma at a maximum grid current ( $t \approx 12 \mu s$  in Fig.2(c)).

#### 4. Conclusion

Structures of the instability exciting a coherent wave are clarified in a bounded plasma under the condition that a maximum amplitude is observed at the fundamental frequency. The instability is found to be caused not by the current-driven instability but by the plasma expansion. Our results obtained in a discharge plasma with  $T_e \gg T_i$  seem to be similar to those in a Q-machine plasma with  $T_e \approx T_i$  [6], although there still exist some differences in such points as the speed of the moving DL and spatial growth of density fluctuations. More developed experimental studies will be required under such conditions that a discrete spectrum satisfying the boundary condition is superposed on a broad spectrum based on linear theory, and the measured region exists in the produced plasma or in a higher density plasma.

#### References

- [1] D.B.Frenneman *et al.*, Phys. Fluids 16,871(1973)
- [2] H.Tanaka *et al.*, Phys. Rev. 161,94(1967)
- [3] S.Watanabe, J. Phys. Soc. Jpn. 35,600(1973)
- [4] Y.Kawai *et al.*, Phys. Fluids 21,970(1978)
- [5] M.Yamada and H.W.Hendel, Phys. Fluids 21,1555(1978)
- [6] S.Iizuka *et al.*, Phys. Rev. Lett. 48,145(1982)

LOW-FREQUENCY OSCILLATIONS ASSOCIATED WITH THE  
DOUBLE-LAYER IN A D.P.-MACHINE PLASMA

G.Popa - Faculty of Physics, "A.I.Cuza" University,  
R-6600 Iași, Romania

1. Introduction

The D.P.-machine /1,2/ originally used for experiments as beam plasma interaction, ion wave and solitons, was recently transformed in a triple plasma device in order to produce double layers (D.L.) /3,4/.

In this paper a simple method is established for the D.L. generation in a single chamber of a D.P. machine at low neutral pressure and plasma density. For some experimental conditions the D.L. formation might be associated with set on of some low frequency oscillations.

2. Experimental setup

The experiments were performed in the D.P.-machine at University of Iași /5/. The vacuum chamber consists of a stainless steel cylinder of dimensions 80 cm long and 30 cm diameter ended by massive discs through which the experimental equipment for producing and delineating the plasma is attached (Fig.1).

The system is pumped on by a  $500 \text{ ls}^{-1}$  oil diffusion pump to a base pressure of  $1 \times 10^{-6}$  Torr. The gas (argon) is introduced continuously through a needle valve which allowed the system to be operated at neutral pressures ranging from  $10^{-5}$  to  $5 \times 10^{-4}$  Torr.

The two equal plasmas called source and target plasma are separated by a fine stainless steel grid ( $G_1$ ) 8x8 lines per mm and 47% transmission. The filaments for electron emission are made from 0.1 mm diameter tantalum wire and are axially placed on pairs of stainless steel rings ( $F_1$  and  $F_2$ , Fig.1) near the wall of the vacuum chamber.

The vacuum chamber acts as main anode (A Fig.1) for both plasmas and it is at ground potential. The plasma potential is controlled with respect to ground potential by an internal mesh anode ( $A_2$  Fig.1) made of 0.5 mm diameter stainless steel wires spaced 2 mm apart. The mesh anode is as a cylinder which covers all length of a chamber (24 cm diameter) so that it separates plasma volume (inside) from filaments (outside). There are no filaments on the end discs and other grids ( $G_2$ ) separate these discs and plasma.

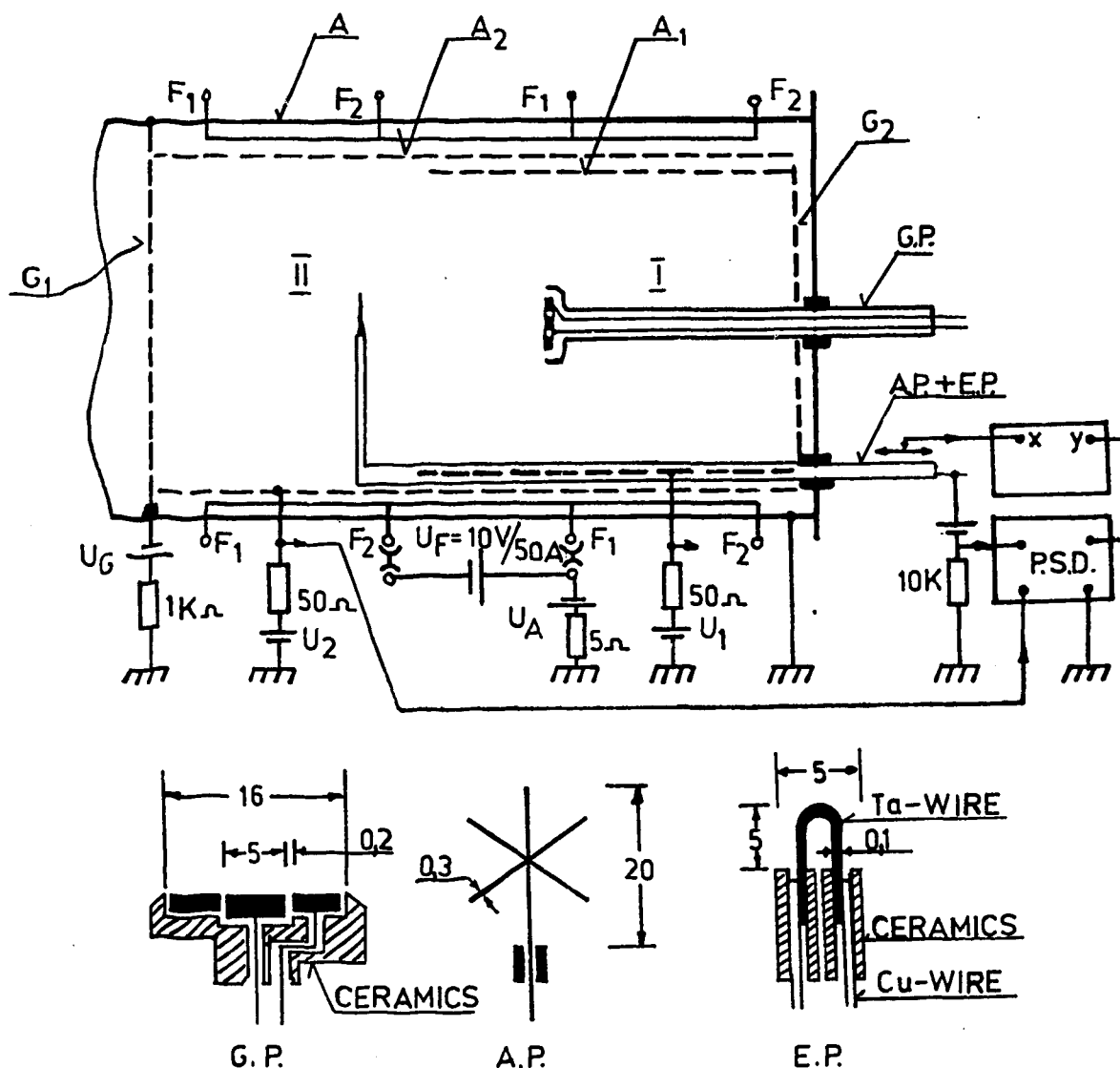


Fig.1. Schematic diagram of the experimental setup. All size in mm.

The plasma diagnostics was made in the target chamber by a guard ring plane probe (G.P) and an emissive probe (E.P). G.P consists of a stainless steel collector and guard ring (Fig.1) mounted at the end of an insulated shaft which is moved axially by hand and it was used to determine electron temperatures, densities and plasma potentials (where possible). The typical parameters are as follows :  $n_e = 5 \cdot 10^6 - 10^8 \text{ cm}^{-3}$ ,  $T_e = 1 - 8 \text{ eV}$  and ionization degree less than 0.1%.

The emissive probe (Fig.1) was used exclusively for measuring the plasma potential. It was measured as the floating potential of E.P. using an electronic voltmeter with 100 MΩ input resistance [6]. E.P. is mounted on an insulated shaft which is axially motor driven. On the same shaft an asterisk shape electrode (A.P) [7] was mounted in order to measure both phase - and

amplitude - variations of the oscillations along the plasma column.

The oscillation was observed as fluctuation of both the total discharge current (I) and the A.P. electron saturation current using a storage oscilloscope and an interferometer system (P.S.D).

The experiments were performed in argon in the target chamber using a secondary mesh anode ( $A_1$  Fig.1) made of 0.5 mm diameter stainless steel wires spaced 2 mm apart which covers half length of the chamber and it is independently biased (ranging from 0 to 80 V) with respect to the ground. This anode collects less than 16 % of the total current and divides the plasma into two regions: region I surrounded by both mesh anodes  $A_1$  and  $A_2$  and region II surrounded by  $A_2$  only.

### 3. Results

In previous experiments /1/ it was shown that both the plasma potential and the electron temperature are controlled by a small secondary anode. In this work it is shown that secondary anode  $A_1$  (biased positively e.g.  $U_1 = 50$  V with respect to the ground) keeps the plasma potential close to  $U_1$  value all over the chamber only for a neutral pressure larger than about  $7 \cdot 10^{-5}$  Torr. The

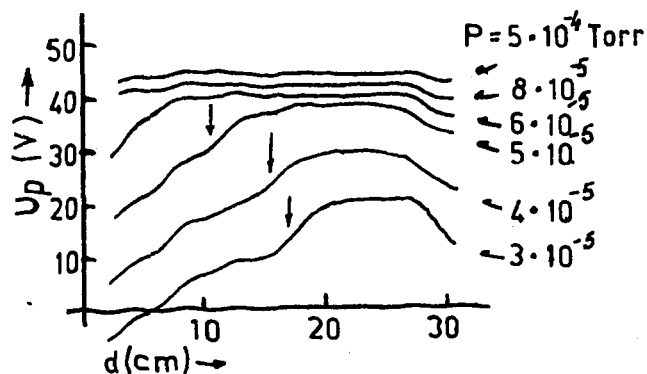


Fig.2. Plasma potential versus axial position between grids  $G_1$  and  $G_2$  for various neutral pressure ( $U_1 = 50$  V,  $U_2 = 0$  V,  $U_{G_1} = U_{G_2} = 0$  V)

axial profiles of the plasma potential are presented in Fig.2 for various neutral pressure. When the neutral pressure becomes lower than the above limit the plasma potential decreases from  $U_1$  value in the region I towards  $U_2 (= 0$  V) value in the region II and a steady state D.L. appears (marked) by arrows in Fig.2.

There are two important features to these double layers. One is that the D.L. is weak.

Thus for experimental conditions corresponding to  $p = 4 \cdot 10^{-5}$  Torr in Fig.2, the probe characteristics give one group of electrons with  $n_e = 6.5 \cdot 10^7 \text{ cm}^{-3}$  and  $T_e = 3.1 \text{ eV}$  so that  $e\phi/kT_e \approx 3$  and  $L/\lambda_D \approx 10$  (where  $\phi$  is the potential jump and  $L$  is the D.L. length).

Another feature is that for some experimental conditions the coherent low frequency oscillations appear which might be associated with D.L. formation. These oscillations can be observed as fluctuations of both the discharge current ( $\tilde{I}$ ) and the A.P. electron saturation current. The ratio of the a.c. amplitude to the d.c. discharge current (fig.a) and frequency oscillations (fig.b) are

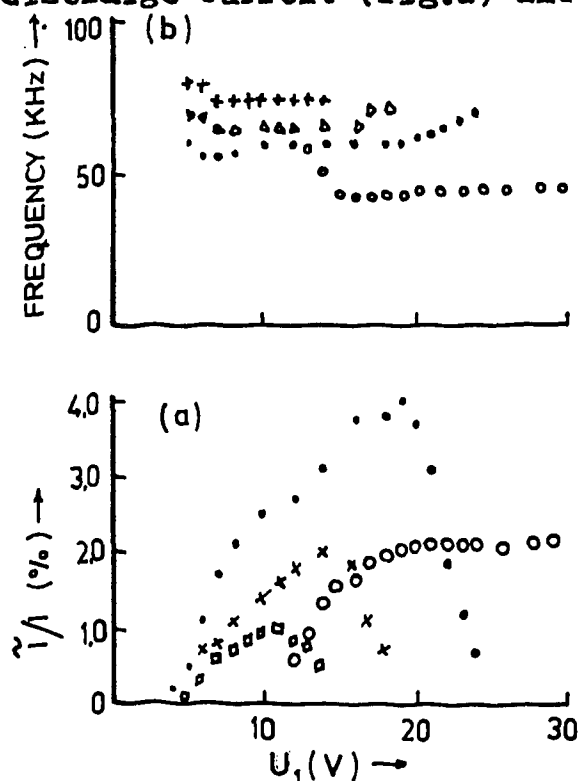


Fig.3. a) Relative amplitude of the a.c. discharge current and b) frequency of the oscillations versus the d.c. anode bias  $U_1$  for a total discharge current ( $I=100$  mA) and different neutral pressure ( $\square 5.0 \cdot 10^{-5}$  Torr,  $\times 4.5 \cdot 10^{-5}$  Torr,  $\bullet 4.0 \cdot 10^{-5}$  Torr,  $\circ 3.0 \cdot 10^{-5}$  Torr)  $U_{G_1} = -50$  V,  $U_{G_2} = U_2 = 0$  V.

pictures (1-10) of the oscillations measured as fluctuations of the A.P. electron saturation current at different position along the axis comparing with oscillations ( $\tilde{I}$ ) of the discharge current. Using  $\tilde{I}$  as reference signals the interferometer system (P.S.D.) recovers the A.P. oscillations and the wave patterns in fig.4.(b) is measured. The A.P. positions which correspond to

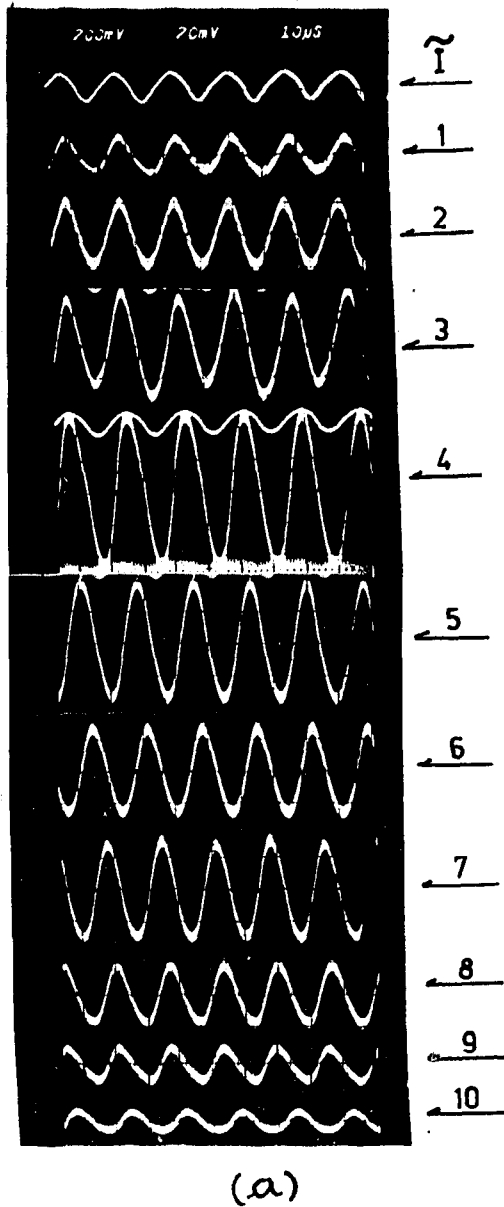
presented versus the d.c. bias of the anode  $A_1$  for a total discharge current of 100 mA and different neutral pressure (Fig.3).

These oscillations appear for a neutral pressure less than about  $5.5 \cdot 10^{-5}$  Torr and their amplitude increase with decreasing of the neutral pressure or this corresponds to the experimental conditions for D.L. formation.

The frequency of the oscillations is slightly increasing with decreasing of the neutral pressure and its value is always well below to the ion plasma frequency which was higher than 150 KHz for above experimental conditions.

In order to indentify the instability both phase - and amplitude - variations of the oscillations are measured with an axially movable electrode (asterisk) in both regions I and II. Fig.4.(a) presents the

the pictures (1-10) are marked by arrows on the interferometer patterns. The oscillations have no phase shift in region II (1-4



pictures) and they might be considered as a potential relaxation/8/ between grid  $G_1$  and the place of the transition from region II and region I respectively, where a steady state D.L. was measured for some experimental conditions (Fig.2).

These oscillations excite ion waves which propagate into region I. Their wavelength ( $\lambda = 9.5$  cm) is a little higher than that corresponding to the electron temperature ( $T_e = 7.8$  eV) measured in region I in a steady state regime ( $U_1 = 0$  V). This could be explained by the fact that the oscillations onset and the ion wave propagation take place for a positive bias ( $U_1 = 10$  V) of  $A_1$  which produces an increasing of the electron temperature.

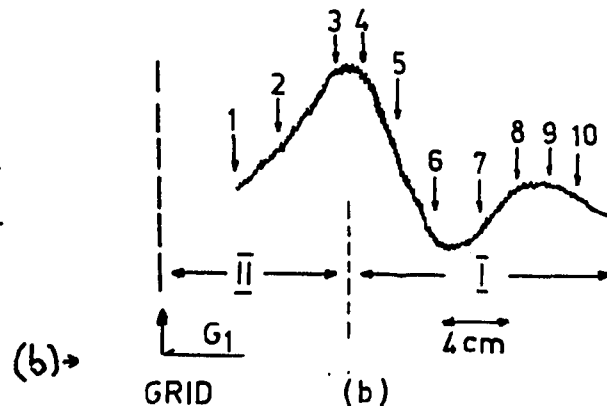


Fig.4.(a) Oscillations of the electron saturation current (1-10) comparing with discharge current oscillation (I); (b) Interferometer patterns along the plasma column axis. ( $p = 4.5 \cdot 10^{-5}$  Torr,  $U_{G_1} = -60$  V,  $U_{G_2} = U_2 = 0$  V,  $U_1 = 10$  V).

#### References

1. R.J.Taylor, K.R.Mackenzie, H.Ikezi - Rev.Sci.Instrum., 43 (1972) 1675.

2. R.J.Armstrong, J.Trulsen - Description and performane of an UHV double plasma machine, Report ISSN 0373-4854, Univ.Tromsø (1978).
3. P.Coakley, N.Hershkowitz - Phys.Fluids, 22 (1979) 1171.
4. P.Leung, A.Y.Wong, B.H.Quon - Phys.Fluids, 23 (1980) 992.
5. G.Popa - Proc.of the IV National Conference on Plasma Physics, Bucharest, iune 1980.
6. S.Iizuka, R.Michelsen, J.J.Rasmussen, R.Schrittwieser, R.Hatakeyama, K.Saeki, N.Sato - J.Phys.E : Sci.Instrum. 14 (1981) 1291
7. N.Sato, G.Popa, E.Märk, E.Mravlag, R.Schrittwieser - Phys. Fluids, 19 (1976) 70.
8. S.Iizuka, R.Michelsen, J.J.Rasmussen, R.Schrittwieser, R.Hatakeyama, K.Saeki, N.Sato - to be published

## Potential Formation between Two Kinds of Plasmas

R. Hatakeyama, Y. Suzuki, and N. Sato

Department of Electronic Engineering, Tohoku University,  
980 Sendai, Japan

**Abstract:** A potential depression is observed between two magnetized plasmas with different electron temperatures in the absence of net electric current passing through them. The potential dip is large enough to reflect both groups of electrons supplied from the two plasmas. When a local magnetic bump is added to a uniform magnetic field, the shape of the potential dip becomes sharp and its position is locked around the mirror point.

### 1. Introduction

There has been an increasing interest in electrostatic potential formation in plasmas, since potential structures have strong influences on many important properties of plasmas and also on plasma confinements. Recent researches of electric double layers have been carried out under such circumstances.<sup>1-3)</sup> It is now clear that local potential drops can be formed in plasmas in the presence of external energy (voltage and/or current) sources. Here we present an observation of potential depression formed between two plasmas with different electron temperatures even when there is no externally supplied potential and current between the plasmas. The phenomenon is closely related to a thermal barrier in the tandem-mirror concept<sup>4)</sup> and double layers without current.<sup>5)</sup>

### 2. Experimental apparatus

Two different kinds of plasmas are produced, respectively, at two ends of a linear device, as shown in Fig.1. A Q-machine plasma with density  $N_1$  ( $10^8 - 10^{10} \text{ cm}^{-3}$ ), electron and ion temperatures,  $T_{e10}, T_{i10}$  ( $\leq T_{e10} \approx 0.2 \text{ eV}$ ) is produced by contact ionization of potassium atoms at hot Ta-plate [source 1 ( $S_1$ )].<sup>3)</sup> The other plasma with density  $N_2$  ( $10^8 - 10^{10} \text{ cm}^{-3}$ ) is produced by an Ar-gas discharge between anode A and cathod K [source 2 ( $S_2$ )], and the electron temperature  $T_{e20}$  ( $\approx 1.8 \text{ eV}$ ) is much higher

than  $T_{e10}$  but the ion temperature  $T_{i20}$  is nearly equal to  $T_{i10}$ . The separation between  $S_1$  and  $S_2$  is 200 cm. The two plasmas of about 3.5 cm in diameter diffuse along a magnetic field  $B$  in opposite directions. The pressures of these plasmas near the sources are defined by  $P_{1,20} = N_{1,2}T_{1,20}$  ( $T_{1,20} = T_{e1,20} + T_{i1,20}$ ) respectively while their local pressures are defined by  $P_{1,2} = n_{1,2}T_{1,2}$  ( $T_{1,2} = T_{e1,2} + T_{i1,2}$ ). In this experiment,  $A$  is ground and  $S_1$  is kept at floating potential (there is no potential difference applied externally between them). Thus, net electric current does not exist in the system. The magnetic-field configuration is also given in Fig.1. A local bump with mirror ratio  $R_m < 3.0$  can be produced between  $S_1$  and  $S_2$ . Floating potentials of emissive probes (resolution  $\approx 1$  mm) are used to determine the plasma potentials.

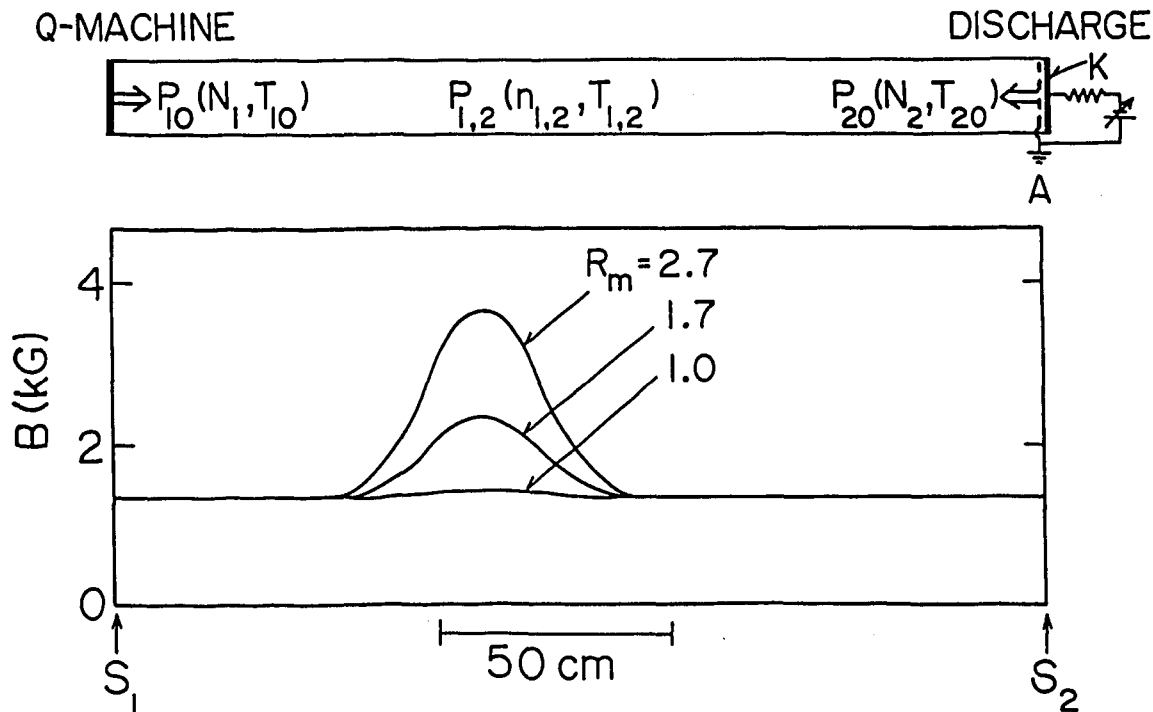


Fig.1. Experimental device with two different plasma sources ( $S_1$ ,  $S_2$ ) and magnetic configurations  $B$ .

### 3. Experimental results

First of all potential distributions are measured along the uniform magnetic field ( $R_m = 1$ ). It is found that a potential minimum appears between  $S_1$  and  $S_2$  under appropriate conditions.

The axial position of this potential dip can be controlled by changing the ratio  $P_{20}/P_{10}$ , as presented in Fig.2. The dip shifts towards  $S_1$  when  $N_2$  is increased with  $N_1$  kept constant. When  $P_{20}/P_{10} \geq 6$ , the potential minimum does not appear in the experimental region. This result is also confirmed when  $N_1$  is decreased with  $N_2$  fixed constant. The measurement implies that there may exist a plasma-pressure balance between two plasmas at the position where the negative dip is formed. The local plasma-pressure ratio  $P_2/P_1$  at the potential minimum and the depression depth  $\Delta\phi$  are plotted as a function of  $P_{20}/P_{10}$  in Fig.3, where  $\Delta\phi$  is defined by a potential difference from the relatively uniform potential in the region of the low electron temperature. In this figure, open and closed circles are values measured for the constant  $N_1$  and  $N_2$  in Fig.2, respectively, and  $P_1$  (or  $P_2$ ) is measured at the position, where the potential minimum could be

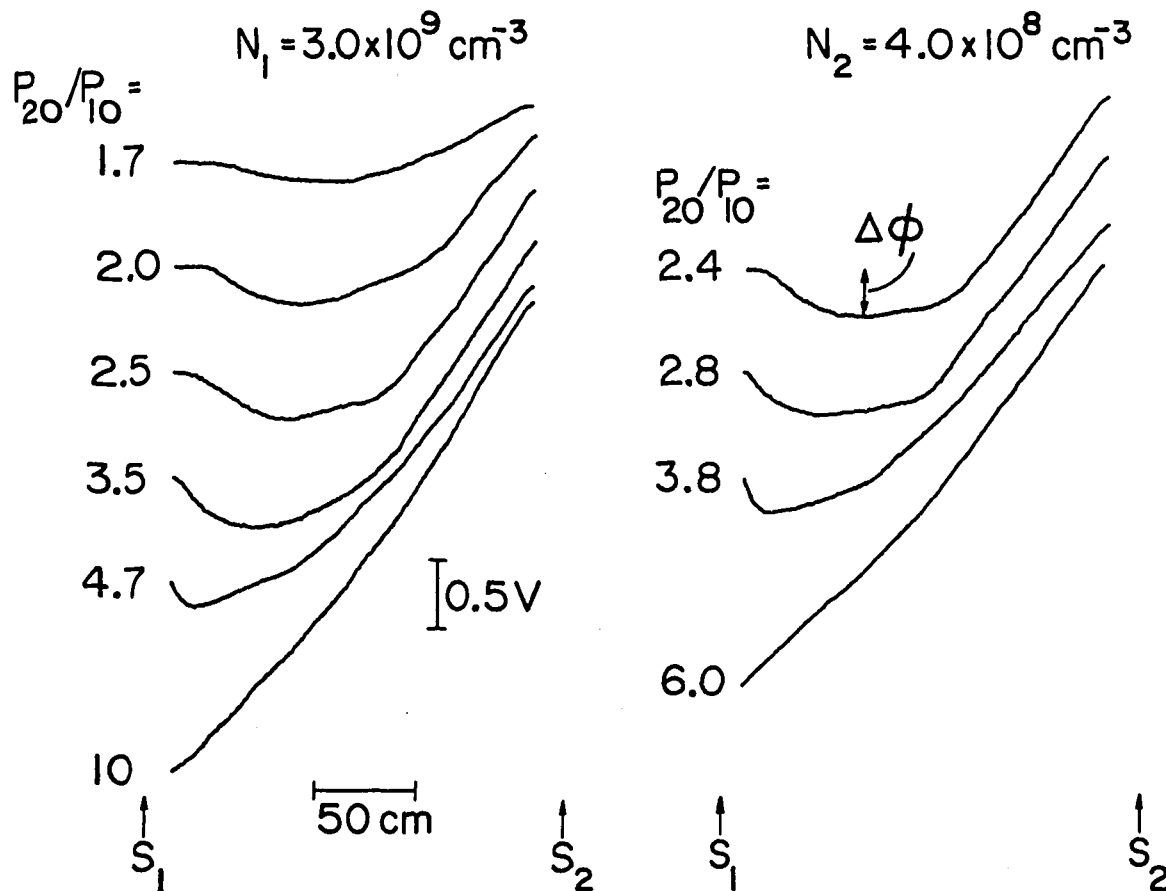


Fig.2. Axial potential distributions for various ratios of the plasma pressures at the sources with  $N_1$  or  $N_2$  kept constant in the uniform magnetic field.

observed under the operation of  $S_1$  and  $S_2$ , when we operate only  $S_1$  (or  $S_2$ ). The local pressure ratio is approximately unity and the depression depth is an order of  $T_{e1}/e$  under various conditions. Thus, the potential depression, which is large enough to reflect electrons with low temperature, is found to be formed around the position where the pressures of low- and high-temperature plasmas are balanced with each other.

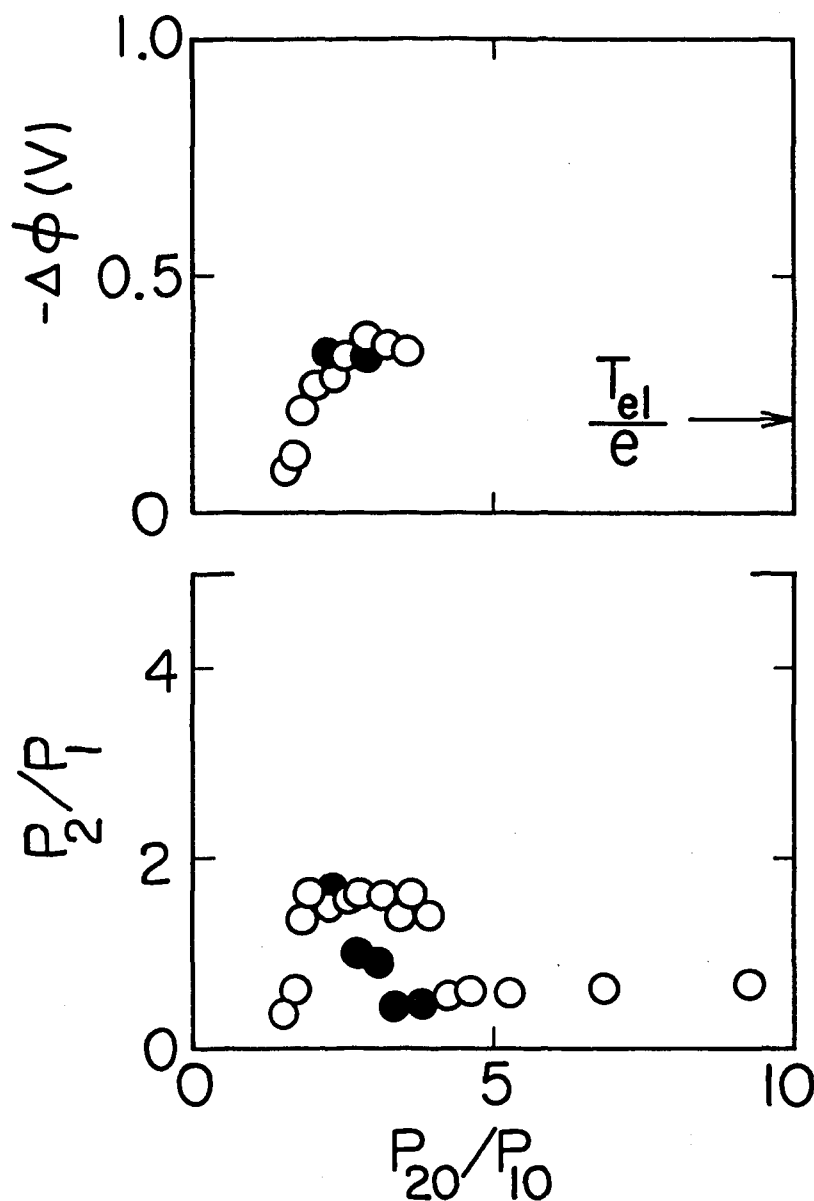


Fig.3. Depth of negative potential dip  $\Delta\phi$  and local pressure ratio  $P_2/P_1$  around the potential minimum versus pressure ratio at the sources. Open and closed circles correspond to values at constant  $N_1$  and  $N_2$ , respectively.

Let us investigate magnetic mirror effects on the phenomenon described above. When a local magnetic bump is added to the uniform field, a local change of the potential distribution is observed near the mirror point even in the case of a monotonous potential variation in the uniform magnetic field (for instance, the profile for  $P_{20}/P_{10} = 6$  in Fig.2). This tendency becomes appreciable under the conditions where gentle negative dips are already produced in the uniform magnetic field, as demonstrated in Fig.4. The potential dip becomes sharp and shifts towards the mirror point with a gradual increase in  $R_m$ . The depression depth increases slightly with an increase in  $R_m$  in the case where the potential minimum is already present at  $R_m = 1$ . The maximum depth, however, is  $(1 - 3)T_{e1}/e$  at  $R_m < 3.0$  even if  $P_{20}/P_{10}$  is varied. It is to be noted that electrons with high temperature can also be reflected by the potential slope from  $S_2$  towards the potential dip, which provides the potential difference of an

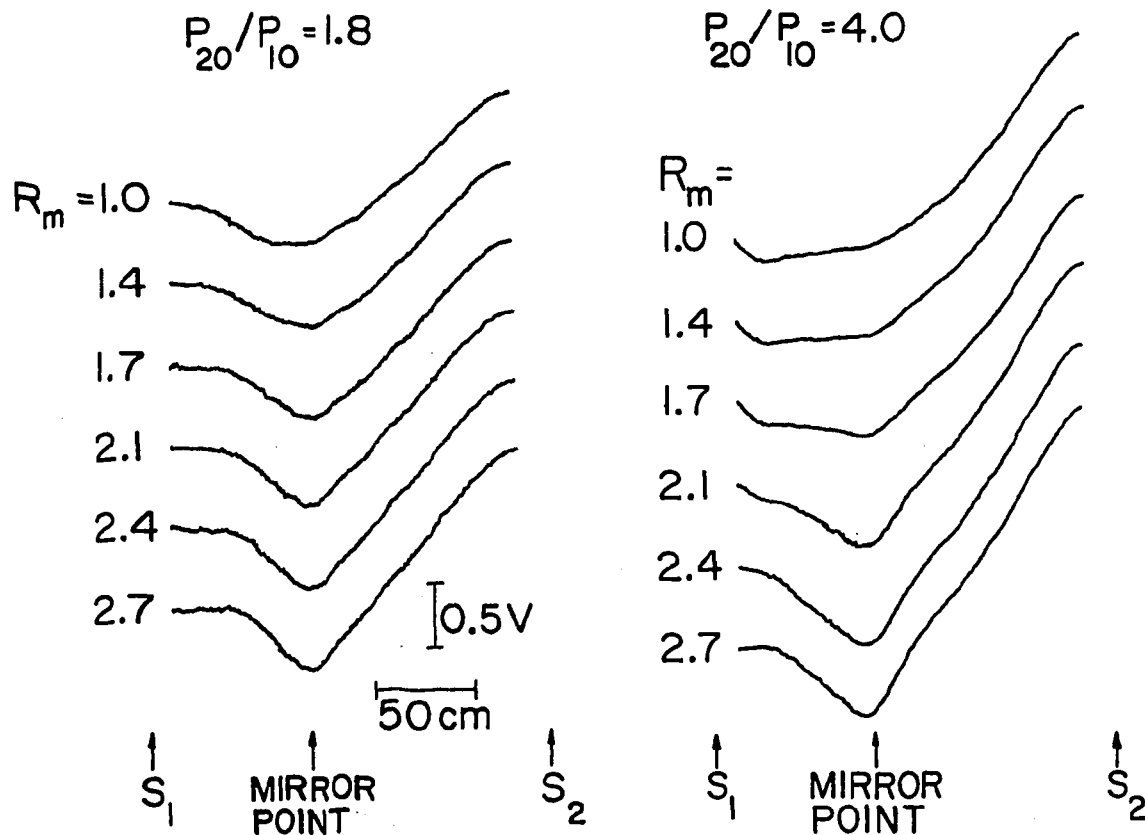


Fig.4. Axial potential distribution in the magnetic field having a bump with mirror ratio  $R_m$  as a parameter at typical plasma pressure ratios  $P_{20}/P_{10} = 1.8$  and  $4.0$ .

order of  $T_{e20}/e$ , as found in Fig.4.

Axial profiles of density and electron temperature are measured together with the potential profile. The density minimum appears near the same position as the potential. The electron temperature increases towards  $S_2$ , but a rather rapid change is observed around the mirror point. The measured density profile is consistent with the expected one calculated from the Boltzman relation using the measured potential and electron temperature profiles.

#### 4. Conclusions

The potential depression is formed between two kinds of magnetized plasmas with low and high electron temperatures even in the absence of net electric current passing through them. At the position of the potential dip, the pressures of the two plasmas are balanced in the uniform magnetic field. The dip is surrounded by two spatial regions with higher potential of an order of corresponding electron temperature. The local magnetic-field bump added to the uniform field enhances and localizes the potential depression which further tends to isolate the two groups of electrons from each other, implying the property of a thermal barrier in the tandem-mirror research.<sup>4)</sup>

We acknowledge discussions with Dr. K. Saeki and experimental supports of T. Mieno, T. Kanazawa and T. Haiji.

#### References

- 1) E. M. Wescott et al., J. Geophys. Res. 81, 4495 (1976); F. S. Mozer et al., Phys. Rev. Lett. 38, 292 (1977); S. D. Shawhan et al., J. Geophys. Res. 83, 1049 (1978).
- 2) P. Coakley and N. Hershkowitz, Phys. Fluids 22, 1171 (1979); S. Iizuka et al., Phys. Rev. Lett. 43, 1404 (1979); P. Leung et al., Phys. Fluids 23, 992 (1980).
- 3) N. Sato et al., Phys. Rev. Lett. 46, 1330 (1981).
- 4) D. E. Baldwin and B. G. Logan, Phys. Rev. Lett. 43, 1318 (1979); J. Kesner et al., Nucl. Fusion 21, 1265 (1981).
- 5) F. W. Perkins and Y. C. Sun, Phys. Rev. Lett. 46, 115 (1981).

Observations of Large Amplitude Solitary Pulses  
in the Current-Limiting Phase of High-Voltage  
Straight Discharge

Y. Takeda and K. Yamagiwa\*

Department of Physics, College of Science and Tech.  
Nihon University, Tokyo 101, Japan

\* Department of Physics, Faculty of Science, Shizuoka  
University, Shizuoka 422, Japan

Abstract

An optically-isolated transmission system used in conjunction with a floating double electric probe was developed to measure directly fluctuating large amplitude electric fields and to isolate the measuring system from high common-mode voltages generated in the high-voltage straight discharge in a longitudinal magnetic field.

A train of repetitive pulses of the axial electric field, frequently with the negative polarity where the electric field is directed axially from the cathode-side toward the anode-side, and with amplitude 10 kV/cm (although considerably underestimated value) was observed in close correlation with the enhanced current limitation.

Moreover an intense E-field pulse, identified as a moving double layer, with amplitude typically 15 kV/cm and 30 nsec in half width was observed at the instant of abrupt current limitation.

1. Introduction

Recently the formation of shock-like jumps in potentials, called potential double layers, has attracted increasingly wide interests as an example of highly nonlinear phenomena in laboratory and cosmic plasmas, because the double layer accelerates charged particles and provides a mechanism for enhanced resistivity.

Lutsenko et al.<sup>1)</sup> produced a double layer which moved a large fraction of the length of their device. They produced a large potential drop, typically 10 kV at the cathode end of the device. The potential structure propagated toward the anode side moving from the low-potential side toward the high-potential side. However, they could only infer the actual potential distribution of their moving double layer since they

monitored the plasma characteristics with only a few ring-shaped capacitive probes placed externally to the plasma.

The existence of propagating double layers in the current-limiting or disrupting phase of HV straight discharge has also been indicated recently by one of the present authors (Y.T.)<sup>2)</sup> with electrostatic (capacitive) measurements of the axial potential distributions and potential fluctuations.

The enhanced increase of apparent resistivity in the presence of potential double layers has been predicted by computer simulation performed by J.S. Degroot et al.<sup>3)</sup> and recently by T. Sato et al.<sup>4)</sup>

In this paper we present the most remarkable results of direct observation of large amplitude E-field with an optically-isolated transmission system<sup>5)</sup> (called "optoisolator" henceforth) used in conjunction with a floating double electric probe in the enhanced current-limiting phase of high voltage straight discharge in the longitudinal magnetic field.

## 2. Experimental arrangements

The apparatus and its parameters of the present experiment have been described in the preceding paper.<sup>6)</sup> The experimental apparatus and diagnostic tools are shown in Fig. 1. We have carried out HV straight discharge in a magnetic mirror with mirror ratio  $R_m=1.25$ . The intensity of the magnetic field at the mirror point is typically 1.5 KG. An initial plasma is created by a hydrogen or deuterium-loaded titanium washer gun and injected into a highly evacuated discharge vessel of Pyrex glass having an inner diameter of 10cm and a length of about 1.7m. A muzzle of the gun acts as the anode and the cathode is a copper disk, 5cm in dia.. The distance between the electrodes is 60cm. The electric power of discharge is supplied from a low-inductance capacitor of 2.2  $\mu$ F with a charging voltage up to 30 kV. The electron density and temperature of the initial plasma are measured with a 4 mm microwave interferometer and a double electric probe and their values in the center of the apparatus are typically  $8 \times 10^{12} \text{ cm}^{-3}$  and 10 eV, respectively.

The block diagram of the optoisolator used in conjunction with the floating double electric probe is shown in Fig. 2. In the optoisolator electric signals picked up by the probe are relayed as modulation of a laser diode and via an optical

fibre to a PIN photodiode and amplifier combination which converts a.m. light signals into electric signals.

The electrodes separation of the double probe is 1.2mm (approximately  $100\lambda_D$ , where  $\lambda_D$  is the Debye length). The probe tips are tungsten wires 0.15mm in dia. and 1.4mm in exposed length. The double probe was inserted into the discharge vessel at the center of the device and the electrodes are usually arranged parallel to the magnetic field. Because of extremely high level of fluctuations detected by the double probe, two channel coaxial attenuators (60 dB each) were inserted between the probe and the optical transmitter (E/O converter). The optoisolator and coax. attenuator system has good frequency characteristics up to 80 MHz (3 dB point) and the rise time 5 nsec for pulse response. The measured CMRR of the system is better than 40 dB up to 80 MHz. The video signals of the optical receiver were recorded on a high-speed transient recorder (Iwatsu Electric Co., TS-8121) and its D/A converted data were displayed on a X-Y recorder.

The direction of the measured electric field was inferred by monitoring electrostatic potential fluctuations simultaneously picked up by two capacitive probes<sup>6)</sup> placed on the outer surface of the discharge vessel at the symmetric axial positions against the midplane which are intrinsically sensitive to fluctuating electric fields perpendicular to the magnetic field.

The voltage in the central part of the plasma column was measured by differentiating local potentials detected by two capacitive probes<sup>1)</sup> consisting of a 4.0cm wide metal strip wound on one-turn around the discharge tube and placed at the symmetric axial positions 11 cm apart against the midplane. The strip voltages were measured on an oscilloscope by a frequency independent voltage divider (Tektronix P6015), one part of the divider being the oscilloscope (Tektronix 556, DC-50MHz).

### 3. Observations of large amplitude E-field pulses in the current-limiting phase of the discharge

Typical video signals of the optical receiver recorded on the transient recorder are shown in Fig. 3 and 4, where the electrodes of the double probe were arranged parallel to and almost perpendicular to the magnetic field, respectively.

By comparing two records of the fluctuating electric field in the first phase of current limitation ( $0 < t < 3.0 \mu\text{sec}$ ), it is found that the fluctuating large-amplitude electric field in the direction perpendicular to the magnetic field almost disappears in the early phase of current limitation.

On the contrary fluctuations in the electric field perpendicular to the magnetic field were greatly enhanced in the second current-limiting phase ( $3.5 < t < 5.0 \mu\text{sec}$ ). In this phase fluctuations in the electric field parallel to the magnetic field were considerably decreased, although an intense negative solitary pulse typically appeared at  $t = 3.75 \mu\text{sec}$ , with amplitude 10 kV/cm and 15 nsec in pulse width. It should be noted that the discharge current was remarkably limited just at the instant of the appearance of the large amplitude, negative E-field pulse.

Moreover comparing Fig. 4(b) with that of (c), it is noted that the fluctuating electric field perpendicular to the magnetic field has close correlation with UHF electrostatic potential fluctuations picked up by the capacitive probes.

Fig. 5 shows an elongated current-limiting phase of the discharge and the electric field measured by the double probe in which a train of repetitive E-field pulses with the negative polarity appeared in the first current-limiting phase. The direction of the electric field is inferred to be parallel to the magnetic field, because as seen in Fig. 5(b) eminent electrostatic potential fluctuations do not appear in the corresponding period of the discharge.

As seen in Fig. 6, a sharp, intense positive E-field pulse with amplitude 15 kV/cm, and 30 nsec in pulse width was observed accompanying a series of precursory solitary pulses at the instant of the abrupt current limitation ( $t = 2.75 \mu\text{sec}$ ). The differential wire strip voltage, as seen in Fig. 6(a), shows a corresponding pulsive increase just at the instant. Hence the large amplitude E-field pulse at  $t = 2.75 \mu\text{sec}$  is clearly identified as a moving double layer.

In summary we present the first direct observations of large amplitude electric-field pulses in the enhanced current-limiting phase of HV straight discharge in the longitudinal magnetic field which have frequently the negative polarity.

In association with the simultaneous measurement of the voltage with ring-shaped capacitive probes the axial E-field pulse was dramatically identified as a strong double layer.

### References

- 1) E.I. Lutsenko, N.D. Sereda and L.M. Kontsevoi, *Sov. Phys. Tech. Phys.* **20**, 498 (1976)
- 2) Y. Takeda, *Proc. 1980 Int. Conf. on Plasma Physics (Nagoya)*, Vol. 1 (1980) 416
- 3) J.S. DeGroot, C. Barnes, A.E. Walstead, and O. Buneman, *Phys. Rev. Lett.*, **38**, 1283 (1977)
- 4) T. Sato and H. Okuda, PPPL-1681 (1980), Plasma Phys. Lab. Princeton Univ.
- 5) H. Chuaqui, *J. Phys. E: Sci. Instrum.*, **14**, 291 (1981)
- 6) Y. Takeda and M. Yokota, *Phys. Lett.* **87A** 291 (1982)

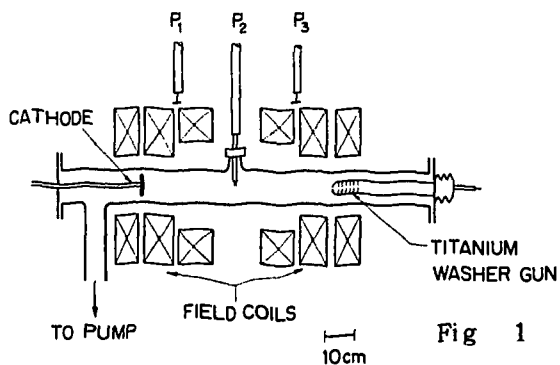


Fig.1 Experimental apparatus and the axial arrangement of the double electric and capacitive probes.

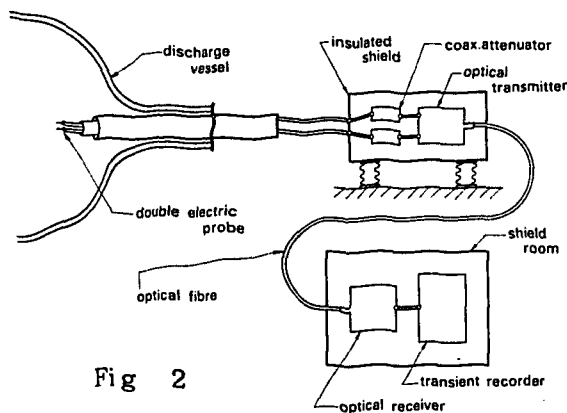


Fig 2

Fig.2 Schematic diagram of the optoisolator in conjunction with the double probe.

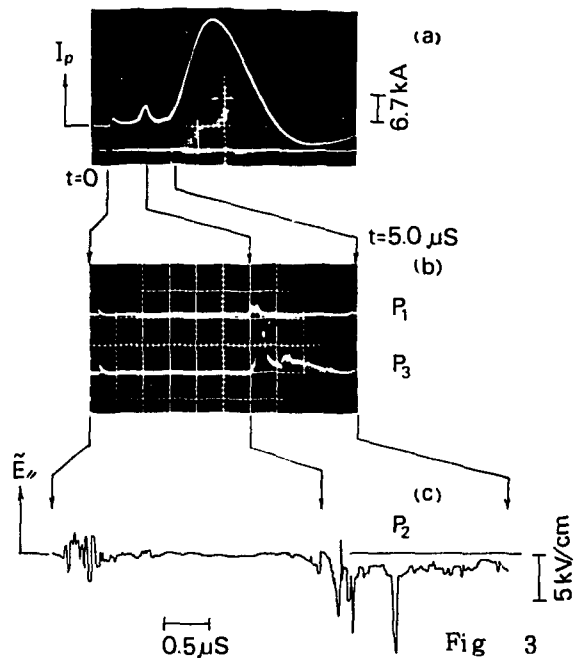


Fig.3 Time traces of (a) discharge current, (b) detected signals of capacitive probes  $P_1$  and  $P_3$ , where the pass-bands of BPF are identical and 250-350 MHz.

(c) D/A converted data record of the optical receiver in conjunction with the double probe  $P_2$ . The direction of the measured E-field is parallel to the magnetic field.

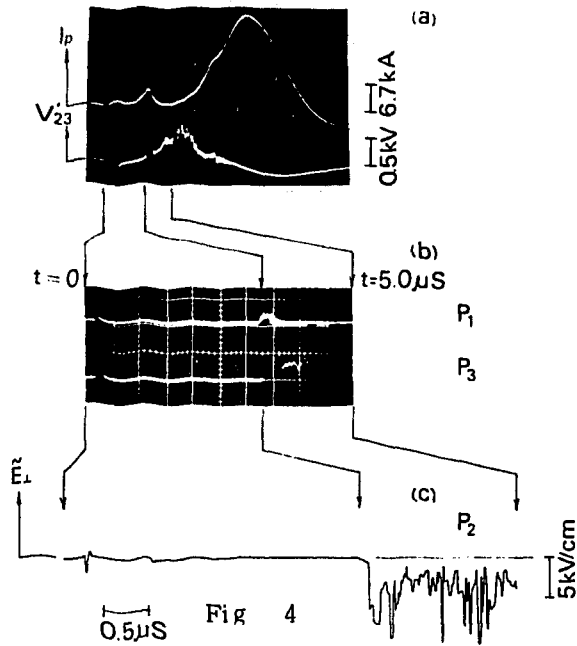


Fig. 4 Similar to Fig. 3 but the lower trace of (a) shows the voltage\* measured with ring-shaped capacitive probes and the direction of the measured E-field is perpendicular to the magnetic field.

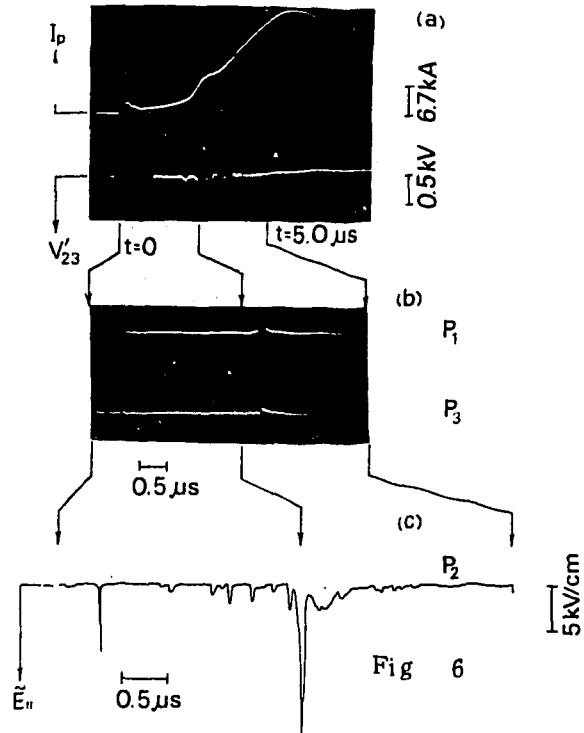


Fig. 6 Similar to Fig. 4 but the direction of the measured E-field is parallel to the magnetic field.

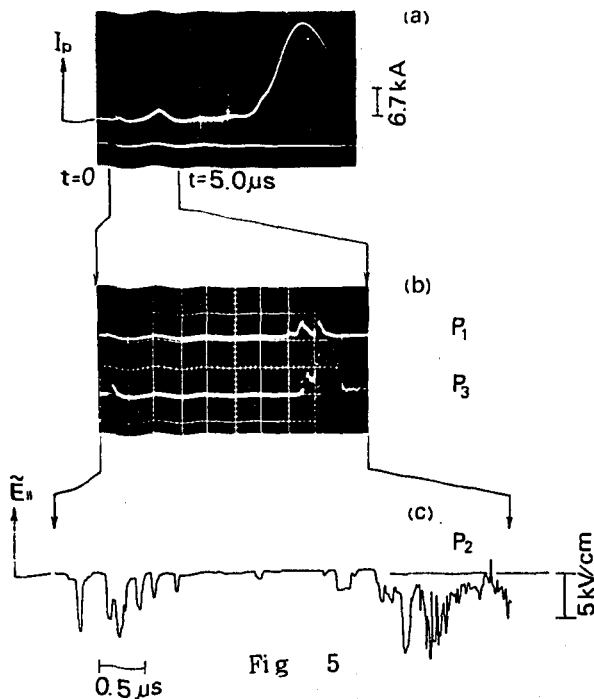


Fig. 5 Similar to Fig. 3 but in an elongated current-limiting phase of the discharge.

$$* V_{23}' = \frac{C_s}{C_s + C_d} V_{23}$$

where  $V_{23}$  is the voltage between the wire-strip probes placed at the symmetric axial positions 11 cm apart against the midplane.  $C_s$  and  $C_d$  denote the capacitance of the ring-shaped capacitive probe to the part of the plasma column and the capacitance (2000 PF) of a ceramic disk capacitor for capacitively dividing the probe voltage.

## ANODIC INSTABILITIES AND ITS CONNECTION WITH DOUBLE LAYERS

M. Sanduloviciu

Faculty of Physics, "Al.I.Cuza" University, R-6600, IASI,  
ROMANIA

It is known that the glow discharge without positive column behaves, under certain conditions, like a generator of electrical oscillations. The frequency and the amplitude of these oscillations depend on the nature of the gas in which the discharge occur, the parameters of the discharge (the gas pressure, the d.c. discharge current etc) and on the geometric form and dimensions of the electrodes and those of the discharge space. These self-sustained oscillations are usually called anodic instabilities, because they are accompanied by strong variations of the anodic potential drop and by periodical variations of the light emission in the anodic glow region. In order to explain this phenomenon, most of the authors try to make a connection between the phenomenon's periodicity and the instable processes located in the anodic glow and in its very proximity.

We shall further show that, in order to understand the apparition of the mentioned self-sustained oscillations in the glow discharge without positive column, it is necessary to take into account the fact that the oscillant circuit, whose reactive elements determine the frequency of the oscillations and the energy source which feeds them, are not located in the same region of the discharge. As we have already proved in (1-4), the discharge oscillatory circuit contains in itself, as reactive elements, a capacitor whose plates are represented by the internal surfaces of the discharge tube wall and the environment (the ground) and an inductance located in the anodic glow region (Fig.1). The internal surface of the discharge tube wall may acts as a plate of a capacitor due to the fact that its charging is performed by means of a process of secondary electronic emission caused by fast electrons, originated in the cathode and accelerated

in the cathode fall. The secondary electrons produced of the wall form a negative space charge, in its proximity, which plays (as we shall demonstrate hereinafter), a special role in the self-sustaining oscillation mechanism. In this mechanism, the anodic glow plays two different roles: as inductance of a oscillatory circuit proper to the discharge and as source of energy for the maintenance of the oscillations.

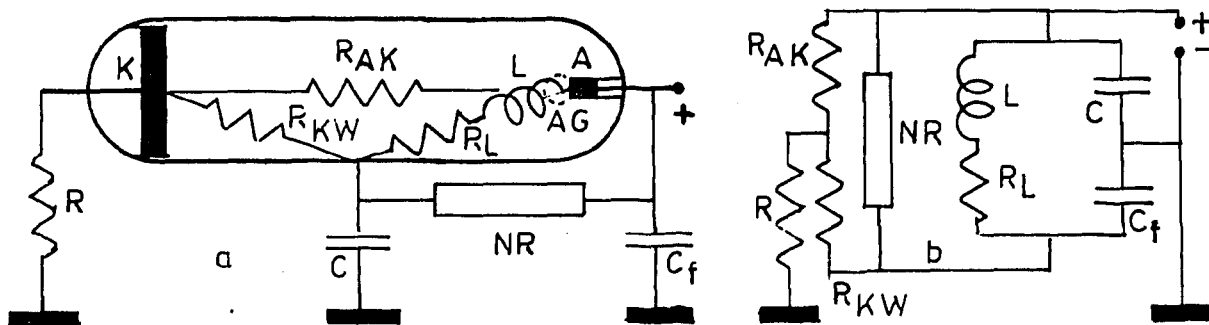


Fig.1. a) The localisation of the ohmic and reactive elements in a d.c. glow discharge; b) Equivalent circuit of a glow discharge A-anod, K-catode, NG-negative glow, W-wall's inner surface,  $R$ -current limiting resistor,  $R_L$ -ohmic resistance of inductance,  $R_{KW}$ -ohmic resistance of the ionized gases between K and W,  $R_{AK}$ -ohmic resistance of the ionized gases between A-K, AG-anodic glow,  $L$ -inductance of glow discharge,  $C$ -capacitance of W with respect to the surrounding,  $C_f$ -filter capacitor,  $R_N$ -negative resistance.

The frontal structure of the anodic glow commonly corresponds to a double layer resulting from an agglomeration of a large number of electrons in front of the anode (or of the anodic spot). Thus appears a potential drop in which the electrons are accelerate. Consequently, in this region ionization processes are produced and positive charges, feeding the discharge, are created. Depending on the nature of the atoms and of the quantum processes that may occur, different stationary states

of the anodic glow, are made possible. The transition from one state to another is achieved when the potential drop of the double layer reaches certain values, so that the conditions for the apparition of a new quantum process are being created. If the quantum process is accompanied by the creation of new charged particles a collapse of the anodic drop occur and conditions for the double layer formed process to re-occur are being created. (it is also possible that a increase of double layer potential drop is accompanied with a disappearance of certain quantum processes so that a jump diminution of charged-particles' number occur). The connection between the anodic fall collapse and the modification of the quantum processes can be demonstrated using the spectral emission of the anod glow (5). The above described mechanism is however not sufficient to explain the periodicity of the self-sustained oscillations. It is also necessary that the apparition of the mentioned new quantum process (which determined the collapse of anodic fall drop) to be triggered, through a mechanism of reaction, by the (damped) oscillations appearing at each jump of the anodic glow in the proper oscillatory circuit of the discharge.

The jumping of the anodic glow from one stationary state to another can be proved experimentally by using a discharge tube with a metal wall. On these conditions, the controlled modification of the wall potential is made possible. Thus we see that a variation of the wall potential (around the floating potential) is followed by the jumping pass of the anodic glow from one state to another. If the internal surface of the discharge tube wall is connected by means of a resistor and a measure instrument with the anode and if the electric current is plotted versus the wall potential, a characteristic corresponding to a negative differential resistance is obtained. Fig.2 shows the result of such an experiment. Thus proves that, between the anode and the internal wall surface, the discharge behaves like an energy generator which can sustain (under certain conditions) oscillations.

lations in the oscillatory circuit of the discharge located between the discharge tube internal surface and the anode.

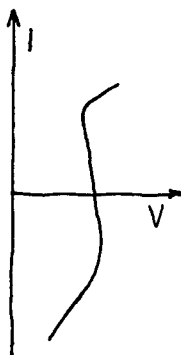


Fig.2. Negative resistance of a glow discharge

The behaviour as a negative resistance can be explained if one takes account of the fact that the supplementary electrical charges, spontaneously created during the new quantum process suddenly increase the electrical conductivity of this DL. As a result, the more the current increases the more the voltage-fall on the DL drops. As we have already mentioned, for appearing of the self-sustained oscillations the pass of the anodic glow between the two states is to be triggered by the oscillations from the oscillatory circuit.

This becomes possible owing to the fact that the internal surface of the discharge tube wall represents one of the plates of the discharge oscillatory circuit capacitor, whose potential varies, consequently, with the periodicity of the oscillatory circuit to which it belongs. These variations of the wall potential with respect to the anode are accompanied by periodical variations of the number of electrons collected by the anode, electrons which are extracted from the space charge formed in the very proximity of the inner surface wall. Thus, groups of electrons periodically arriving in the anodic region modifying the anodic potential drop which starts the pass of the anodic glow from one state to another. This process is accompanied by a jump variation of the potential differences between the discharge tube internal surface and the anode, which makes possible a energy transfer to the discharge oscillatory circuit connected between them. In fig.3 a schematic representation of the self sustained oscillation mechanism in a d.c. glow discharge is showed.

The phenomena described above, occurring in the anodic glow of a d.c. discharge with no positive column, may

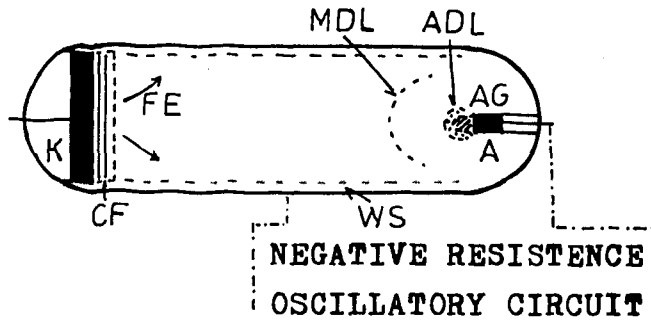


Fig.3. Localisation of the different discharge regions and of the double layers in a d.c. glow discharge. FE-fast electrons, CF-cathode fall, WS-electron space charge near W, MDL-moving double layer, ADL-double layer in front of the anode glow.

probably appear in any plasma device where double layers are formed. These double layers are often unstable, because a small variation of the potential produced by a moving space charge (double layer) determines the appearance (or disappearance) of a certain quantum process, which leads to a modification and redistribution of the electric charges in the layer. This is accompanied by a jump variation of the potential drop in the layer. If the double layer belongs to an electric circuit containing a resonator (a system able to oscillate with a resonance frequency), as for example the glow discharge oscillatory circuit or a limited plasma column, then there can appear self-sustained oscillations that take their energy from the double layer when this passing from one state to another. The mechanism of reaction through which the resonant system oscillation triggered the pass of the double layer from one state to another is made into the plasma itself by means of moving space charge (double layer) which periodically modifies the potential drop corresponding to the double layer. Consequently, the oscillation appeared in the oscillatory circuit of the discharge is not damped, but it becomes sustained.

We should also mention the fact that during the jumping from one state to another, when the potential drop

varies sharply, positive charge carriers, which are being displaced through discharge to the cathode as moving double layers, are being released from the double layers localized to the region of the anodic glow. If there is a positive column, these periodical double layers may excite periodical phenomena in the positive column (6).

1. Sanduloviciu M. - Z. Angew. Phys., 1969, 26, 319-323
2. Sanduloviciu M. - Z. Phys., 1969, 225, 248-269
3. Sanduloviciu M. - Arbeits. Physik und Technik des Plasmas, K. Marx-Stadt, 1974, 453-456
4. Sanduloviciu M., Popa G. - J. de Physique, 1971, 32, 157-159
5. Sanduloviciu M., Luca D., Sanduloviciu R. to be published
6. Sanduloviciu M. - Phys. Lett., 1968, 27A, 313-315.

ON THE CONNECTION BETWEEN DOUBLE LAYERS AND SOME PERIODICAL  
PHENOMENA IN THE POSITIVE COLUMN OF A GLOW DISCHARGE IN  
 $H_2+N_2$  MIXTURE

D.Alexandroaie, M.Sanduloviciu

Faculty of Physics, "Al.I.Cuza"University, R-6600,IASI,  
ROMANIA

1. Introduction

It is known that under certain conditions of gas pressure and discharge current (I) the positive column (PC) in molecular gases presents standing striations (SS). If this stationary state is perturbed (for instance by pulse modulation of I) a propagating phenomenon appears in PC. That means that at the cathode end of PC a moving towards-anode perturbation arises at the moment of the perturbing pulse applying. This moving perturbation modifies close by close the SS positions /1,2/.

This behaviour can be explained considering that the perturbation process gives rise to the appearance of an electric double layer (DL) which moves towards the anode. The modification of the local potential which is produced by this moving DL influences the SS positions. In this paper we present some experimental results which shows the interaction between a moving DL and the space-periodical structure of PC.

2. Experimental procedure

The discharge was performed in a hollow-cathode regime (gas pressure 0.3-2 Torr, glas tube -3 cm inner diameter). The tungsten cathode had the possibility to move inside the discharge tube (DT) so that both the PC length and the number of SS were possible to be changed. The I intensity was varried up to 30 mA. The hydrogen gas was purified and introduced in DT using an osmo-regulator. In order to obtain more outdistanced striations the hydrogen was impurified, in a controllable manner, with nitrogen which was produced by thermal decomposition of the  $NaN_3$ . The nitrogen

was introduced in DT using a needle valve.

The transient state (the appearance and the propagation of the moving DL) was performed by I modulating through a regulator penthode P with short pulses (1-10  $\mu$ s width and  $10^3$  Hz frequency) provided by a function generator with variable phase unit (GVP)(fig.1).

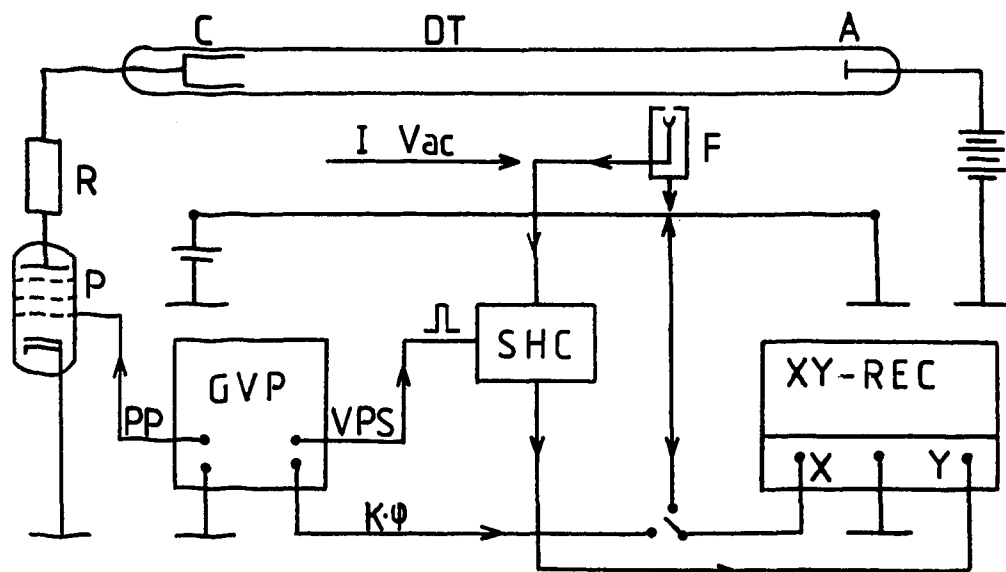


Fig. 1

The local light variations along PC are observed using a photomultiplier F. The corresponding electric signal, which is a periodic-repeatable one, with the perturbing pulse (PP) frequency is applied to the input of a sample-and-hold circuit (SHC). The gate of SHC is driven using the variable phase signal (VPS) from GVP(1-2  $\mu$ s time sample). If the photomultiplier is motionless and the VPS phase is constant the recorder writes only a point. If a signal proportional with distance from the moving F to the anode, is applied to X-input of the recorder then the pattern of the propagating phenomenon as obtained at a moment  $t=360^{-1} \cdot f^{-1} \cdot \varphi$  after its start ( $f$  is the PP frequency and  $\varphi$  is the VPS phase in degrees. When the photomultiplier is fixed, the phase of VPS is varried and a proportional phase signal ( $K \cdot \varphi$ ) is applied to X-input, the time evolution of

the local light intensity it is possible to plot during  $f^{-1}s$ . This procedure was used for recording the anode-cathode potential drop ( $V_{ac}$ ) during the transient process.

With this simple experimental system it is possible to obtain stroboscopic in time or in space successive images of a transient phenomenon from PC.

### 3. Experimental results and discussions

In fig.2 it is plotted the space-time evolution of the propagating phenomenon arrived in PC of a glow discharge in impurified hydrogen ( $p_{N_2}=0.03$  Torr,  $p_{H_2}=0.5$  Torr and 8 mA I intensity).

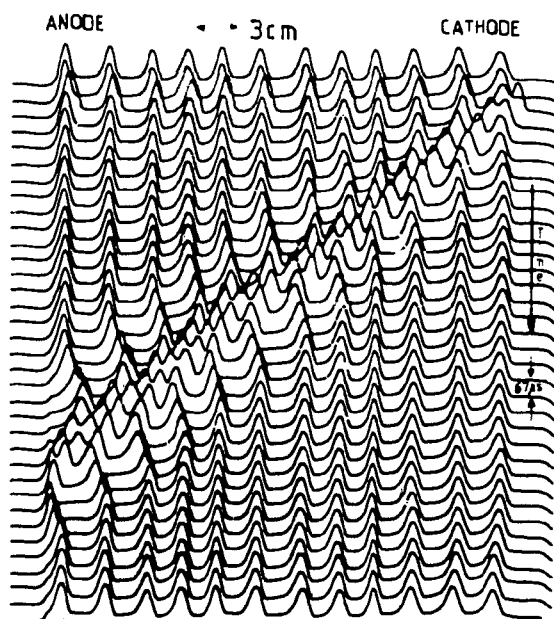


Fig. 2

towards the anode of the propagating phenomenon. A new striation moving towards anode arrives in front of the cathode end of PC immediately after PP releasing. This fact represents the start of propagating phenomenon in PC. When the perturbation in PC approaches a SS the latter starts to move first towards the cathode and after that it starts to move towards the anode. Finally the striation becomes again a standing one taking the place of an other one (towards the anode) so that PC seems to be unchanged. The time evolution of I and

The figure is drawn up of many successive stroboscopic images of PC which are taken at every  $67 \mu s$  starting from perturbing pulse release. The PP period was 6 ms ( $10 \mu s$  width) and time sample was  $1 \mu s$ .

By examining of the picture it is possible to see the standing striations and the evolution

the potential drop  $V_{ac}$  on the discharge tube are shown in fig. 3 a and 3 b respectively. The jump of the potential drop (marked by arrow in fig.3) occurs when the perturbation arrives to the anode.

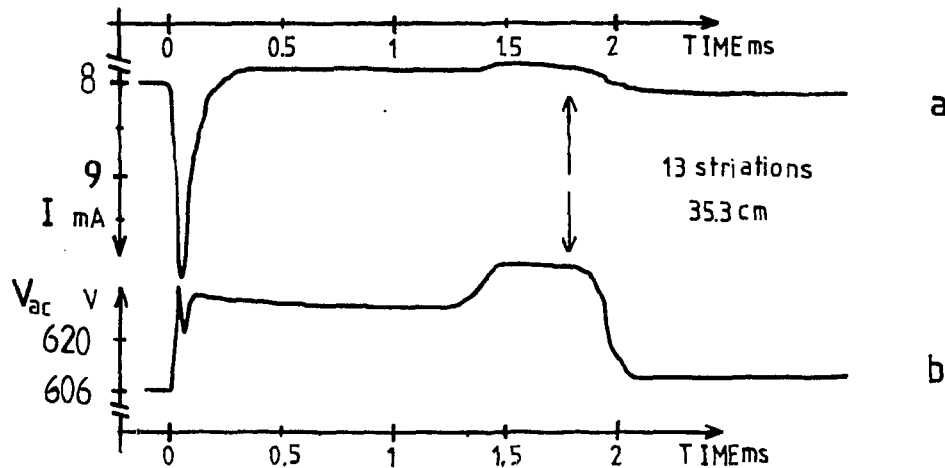


Fig. 3

Without discussing the physical mechanism of the appearance of this striation behaviour let's consider the phenomenological scheme of the SS shaping after /3,4/. One admit that at a moment the local potential distribution from the proximity of a SS changes so that the electrons gain the necessary energy for excitations along a distance which decreases more and more. As a result the striation moves towards the cathode. After the "maximum" of the potential perturbation overcomes the initial SS place the potential restores and during this time the striation moves towards the anode. This behaviour can be explained considering that a DL potential-type perturbation propagates through PC. The DL arises in front of the cathode end of PC after the short pulse was applied. The time evolution of the anode-cathode potential drop  $V_{ac}$  (like in fig.3 b) for different lengths of PC (and a different number of striations) confirms this fact (fig.4). This picture is equivalent to the space-time evolution of the DL potential jump in PC because, when the perturbation arrives at the anode, the va-

value of the jump in the potential drop is equal with the value of the DL potential versus the local one for those PC lengths corresponding to the chosen number of SS /5/.

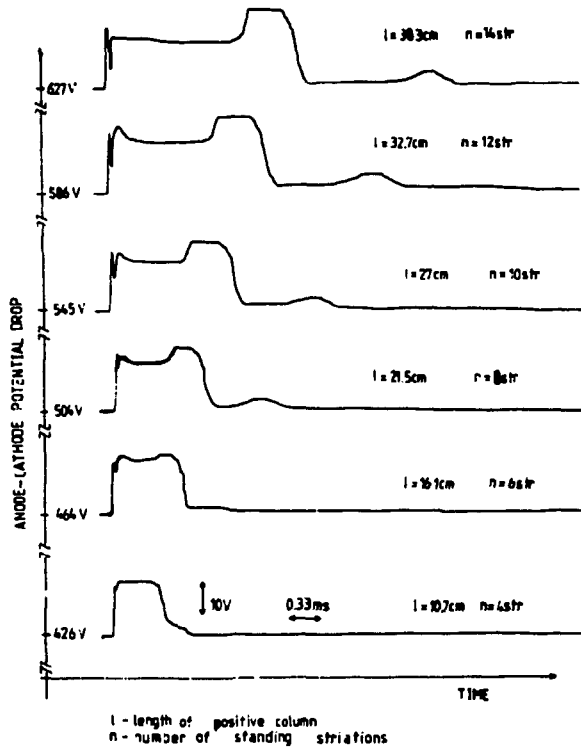


Fig. 4

bution  $V_p$  from PC obtained making smooth the step line potential distribution ( a step is the potential drop for a

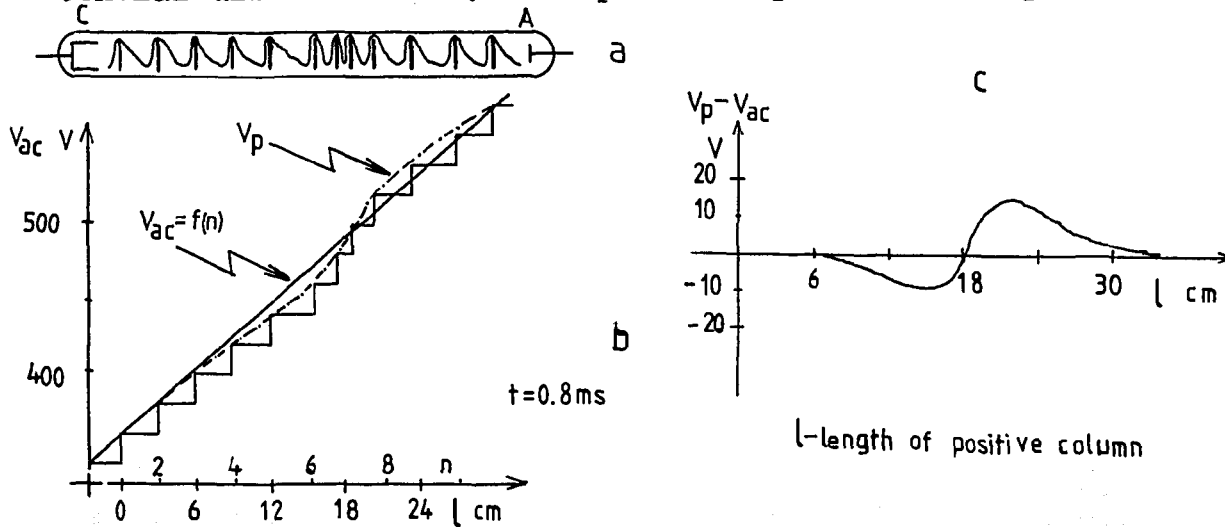


Fig. 5

The graphic scheme in fig.5 proves the previous statement. The potential jump for a SS is found by direct measurements from the slope of the function  $V_{ac}=f(n)$  (n-the number of SS) which within a good approximation is a straight line for a constant discharge current ( 8mA ). In fig. 5 a the light pattern of PC at 0.8 ms after the PP release is shown. In fig. 5 b the dotted line gives the mean-potential distri-

striation). The  $V_p - V_{ac}$  distribution of DL potential is shown in fig. 5 c. Within the limits of the experimental errors a good agreement was observed between this result and that referring to time potential drop variation corresponding to the same number of SS (fig. 4).

#### 4. Conclusions

The presented experimental results shows that when a short pulse modulates the discharge current an electric double layer arises at the cathode end of the positive column and propagates to the anode.

During the electric double layer propagates towards anode, the local potential distribution is modified, causing a changing of the standing striations' positions.

At the same time it has been observed (fig.2,4) that the influence of the moving double layer on the standing striations becomes stronger towards the anode in a convective mode /6/.

#### References

1. S.Phau and A.Rutscher, Ann.Physik,6,244(1960)(in germ.)
2. D.Alexandroaie and M.Sanduloviciu, Rev.Roum.Phys.,24, 415(1979)( in germ.)
3. I.Langmuir, Phys.Rev.,33(1929),958.
4. N.A.Kaptsov, Electrical phenomena in gases and vacuum, Gostehizdat,Moscow,1950(in russian).
5. E.Bădărău, I.Popescu, Gaz ionisés , Dunod,Meridiane, Bucarest,1968.
6. R.J.Briggs, Electron-Stream Interaction with Plasmas, MIT-Press, Cambridge,MIT,1964.

ROLE OF THE DOUBLE LAYERS IN THE APPEARANCE OF SELF-SUSTAINED OSCILLATIONS IN AN ELECTRIC CIRCUIT INCLUDING A MAGNETIZED PLASMA

S. Talagman, M. Sanduloviciu

Faculty of Physics, "Al.I.Cuza" University, R-6600, IASI, ROMANIA

In the following paper we present an experiment by the help of which we have investigated the role of double layers in the apparition of certain self-sustained oscillations in a magnetized diffusing plasma. This experiment was performed by using a device shown in figure 1.

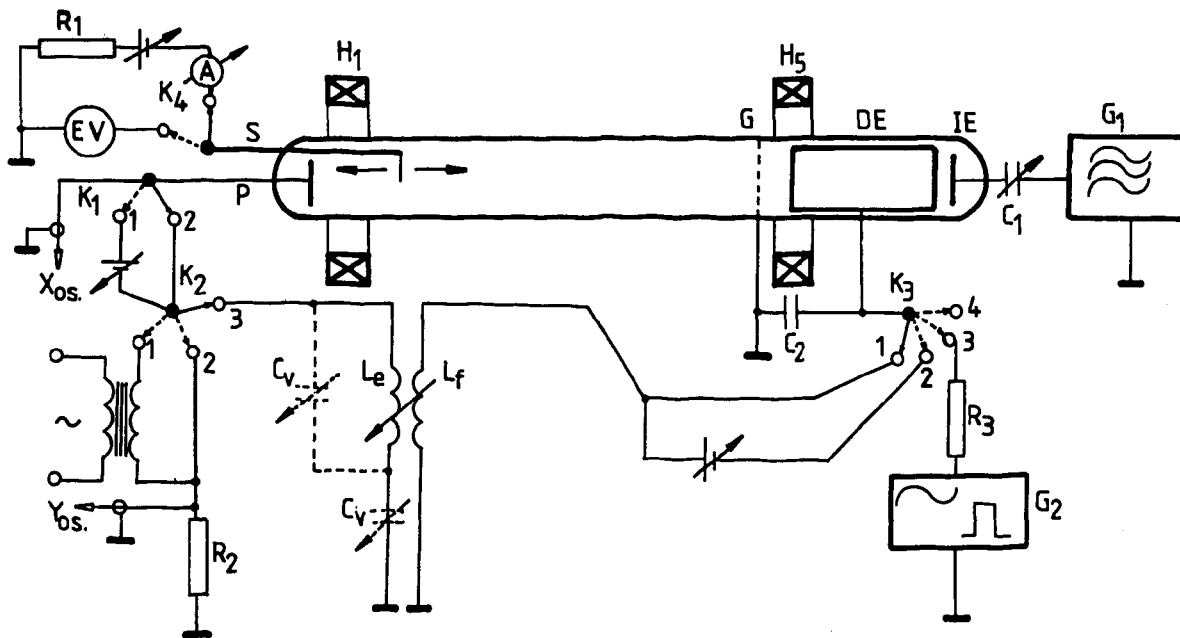


Fig. 1

We have used a r.f. glow discharge as plasma source. The so-obtained plasma has diffused through a grid in a magnetic field, forming a plasma column with a visible diameter varying between 1-2 cm. As working gas we have used air and hydrogen at a pressure of  $6 \cdot 10^{-3}$  Torr. As one can see in fig.1, the r.f. signal is applied between an ignition electrode (I.E.) and the grid G on one hand and

the drive electrode (D.E.) on the other hand. The grid G is directly connected with the ground and the D.E. has a ground connection only for the r.f. component of the current.  $G_1$  is a r.f. generator able to yield a maximum power of 70 W at a frequency of 30 MHz.  $G_2$  represents a generator which can provide a sinusoidal or rectangular signal, with adjustable frequency. The plasma is obtained in the region between the grid G and the I.E. The grid is made of stainless steel and it has a 45% transparence factor. The D.E. is a cylinder and the I.E. is a plate both made of stainless steel. In the region between the plate P and G, the diffusing plasma forms, due to the magnetic field, a controlled diameter (depending on the magnetic field intensity) column with an adjustable length (between 45 cm and 60 cm). Beginning with the front of P, a tantalum cylindric probe ( $\varnothing=0,2\text{mm}$ ) may be displaced along a 20 cm distance. The configuration of the external circuit and the type of experiment can be chosen by the help of the changing switches  $K_1, K_2, K_3, K_4$ . Thus the following driving modes are possible :

- without the external excitation of the column, and this way  $K_3$  is switched to the 4 position ;
- with the external excitation applied at the extremity of the column and in this case  $K_3$  is switched to the 3 position and the generator  $G_2$  is used. This way, different positions for  $K_1$  and  $K_2$  may be obtained;
- with self-excitation, when  $K_3$  is switched to the 1 or 2 positions,  $K_2$  is switched to the 3 position and  $K_1$  to one of the 1 or 2 positions.

In the latter driving mode we have obtained self-sustained oscillations, whose frequency depends on the coupling between  $L_e$  and  $L_f$ . The frequency could also vary by the help of an external capacitor  $C_v$ , connected either in parallel or in series with the inductance  $L_e$ . A modification of the oscillations amplitude is observed when P and (or) D.E. are biased with respect to G. In fig. 2, the dependence of  $1/\omega^2$  on  $L_e$  and  $C_v$  is plotted. The experimental data can be

explained by using an equivalent circuit, presented in fig.3.  $Z_1$  and  $Z_{11}$  represent the plasma columns' impedances between I.E. and G on one hand and between G and P on the other hand. The  $C_{de}$  capacitor corresponds to the proper capacitance of the sheet of the plasma-D.E.system.

The capacitor  $C_p$  includes the capacitance of the double layer formed in front of P and the capacitance of space charge formed close to the grid G from which double layers can detach. The results shown in fig. 2 permit to determine the equivalent capacitance  $C_p$ , which is found to be about 50 pF. The amplitude of the self-sustained oscillations was 1,5 V and it dropped when the grid G was replaced by a less fine one.

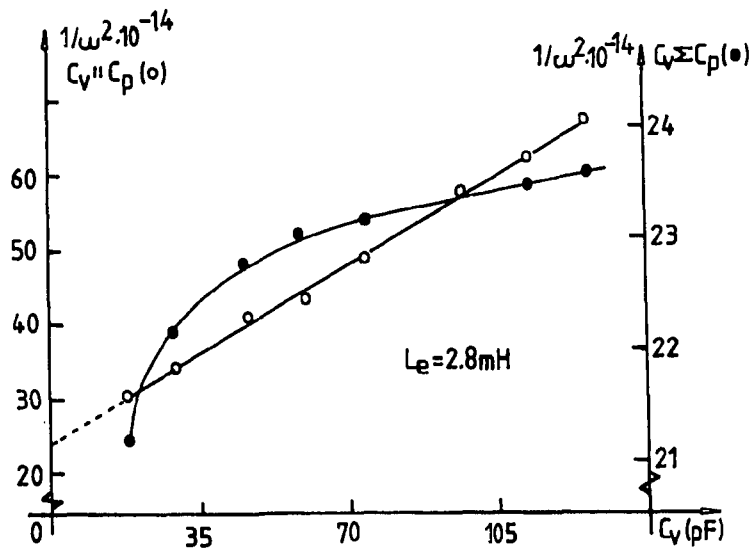


Fig.2

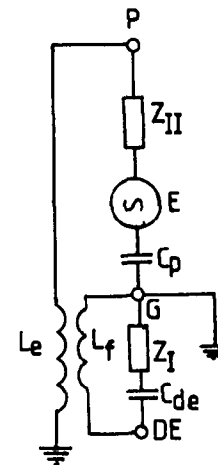


Fig.3

As the experiment shows, the magnetized plasma column between P and G behaves like an energy source (E), which sustains constant amplitude oscillations in a circuit as the one in fig. 3. The fact that these oscillations can appear even if there are no external sources of electric energy in the circuit leads to the idea that between P and G, plasma column behaves as an energy source. This is equivalent to considering that there is a region in the plasma column

which behaves like a negative resistance. In order to render evident this, a current-voltage dynamic characteristic (I.V.) has been drawn by using the circuit resulting from the positioning of  $K_1$  switch in the 1 or 2 position and  $K_2$  in the 1 position and from the appliance of the signals from P and  $R_2$  on the x and y inputs of an oscilloscope. We have observed that, as long as the column is not excited, the current-voltage characteristic is the one in fig.4,a. We can draw the conclusion that there is no behaviour of negative resistance. On exciting the column by the help of  $G_2$  through the D.E. electrode, the current-voltage characteristic becomes the one in fig.4,b. We notice here the apparition of a behaviour of negative resistance.

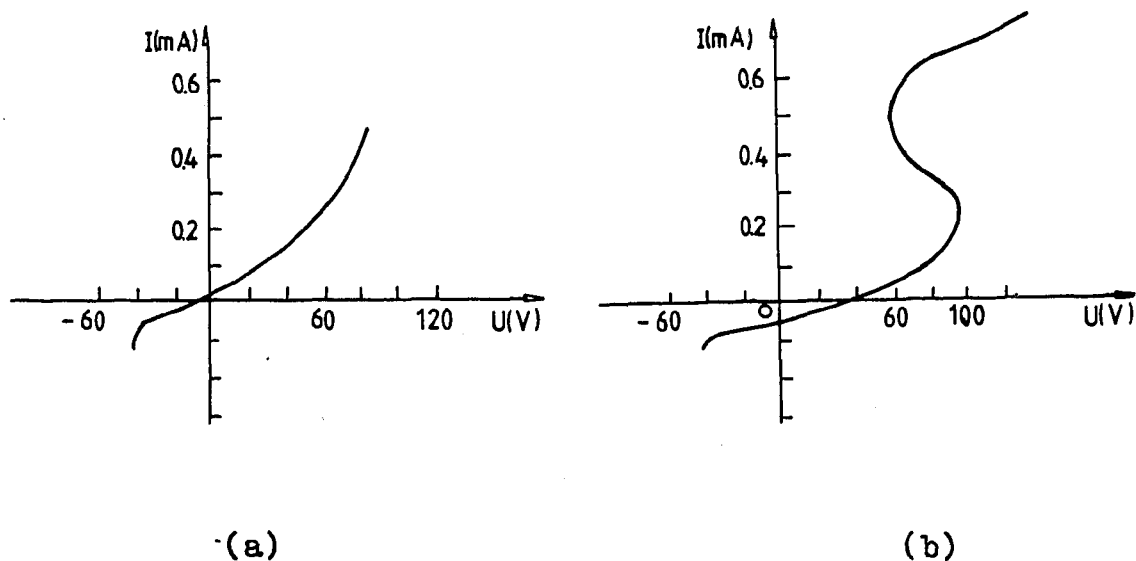


Fig. 4

This result may be explained as follows : the region from the vicinity of grid G behaves like a potential hole, in which there is a certain number of electric charges, The shape of the potential hole may be modified through the type of grid that has been used and the depth of the potential hole, relative to the rest of the plasma, may be modified by excitation performed either by the help of  $G_2$  or by the help of  $L_f$ . In both cases we have an external excitation.

When the depth diminishes, groups of electric charges are injected in the plasma column and from the vicinity of grid G an electrical double layer is released and spread into column towards the plate P, where it interacts with the sheet laid in front of it. This way, a variation of the potential through the sheet in front of P takes place in the moment that the double layer penetrates in the sheet. This potential variation favours the appearance of new quantum processes (therefore new charge bearers) which leads to a collapse of the potential fall on the sheet in front of P. Because the releasing of double layer formed in front of grid G is triggered by the external circuit, the double layers' coming period to the plate depends on the external reactive elements. This can be observed using a photo-multiplier facing this region of the column through a light pipe.

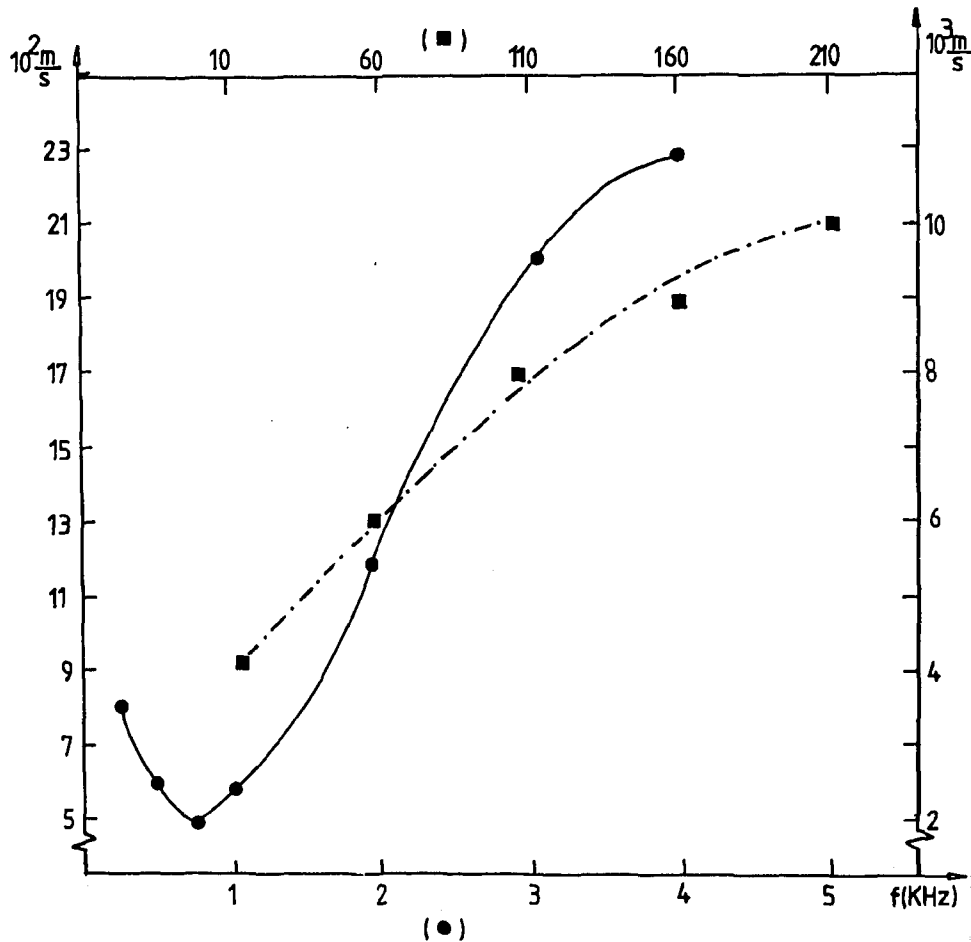


Fig. 5

The same is observed from the region in the vicinity of the grid. In the rest of the column the periodical glow phenomena are weak, depending on the intensity of the magnetic field and on the pressure. By the help of a moving electrical probe S, we have made an evaluation of the double layers' propagation velocity through the column. We have found out that this velocity is of about 900 m/s for frequencies of about 1,5 KHz. The velocity increases, as well as the frequency (fig.5).

## THE SIMULATION OF PLASMA DOUBLE-LAYER STRUCTURES

Joseph E. Borovsky  
Los Alamos National Laboratory  
Los Alamos, NM 87545 USA

and

Glenn Joyce  
Naval Research Laboratory  
Washington, D.C. 20375 USA

Electrostatic plasma double layers are numerically simulated by means of a magnetized 2 1/2-dimensional particle-in-cell method. The investigation of planar double layers indicates that these one-dimensional potential structures are susceptible to periodic disruption by instabilities in the low-potential plasmas. Only a slight increase in the double-layer thickness with an increase in its obliqueness to the magnetic field is observed. Weak magnetization results in the double-layer electric-field alignment of accelerated particles and strong magnetization results in their magnetic-field alignment. The numerical simulations of spatially periodic two-dimensional double layers also exhibit cyclical instability. A morphological invariance in two-dimensional double layers with respect to the degree of magnetization implies that the potential structures scale with Debye lengths rather than with gyroradii. Electron-beam excited electrostatic electron-cyclotron waves and (ion-beam driven) solitary waves are present in the plasmas adjacent to the double layers.

Uniformly magnetized plasma double layers are simulated on a two-dimensional grid, periodic in one direction and bounded by reservoirs of Maxwellian plasma in the other, an extension of previous numerics (Joyce and Hubbard, 1978). Poisson's equation is solved by means of a Fourier transform in the periodic coordinate and a cubic spline in the other. Fixing the electrostatic potential on the boundary-reservoirs in various configurations allows the simulation of either planar or two-dimensional structures.

The structures of planar double layers oblique to externally generated magnetic fields are found to be nearly identical with the structures of field-aligned or unmagnetized double layers, an oblique double layer being slightly thicker than a corresponding unmagnetized double layer. The thicknesses of the simulated oblique double layers are not related to any particle gyroradii. This is corroborated with solutions to Poisson's equation for variously magnetized plasmas (Borovsky, 1982) which yield oblique double-layer scale sizes in terms of Debye lengths.

In certain instances planar double layers are observed to be susceptible to periodic disruption by an instability in the adjacent low-potential plasmas. As viewed in Figure 1, the disruption of an oblique ( $\theta=60^\circ$ ) double layer is preceded by the appearance of large amplitude two-dimensional solitary pulses, the pulses always propagating in the direction of the electron drift, against the ion beam. These pulses form, and the double layers are disrupted, only if the low-potential plasmas are of sufficient spatial extent. (Prior to disruption, the low-potential plasma may be crowded with large amplitude solitary pulses, a point measurement of the potential appearing to be an observation of low-frequency electrostatic turbulence.) This same disruption phenomenon also effects two-dimensional double layers, as will be discussed. In the high-potential plasmas adjacent to the oblique double layers electron-beam driven electrostatic electron cyclotron waves with amplitudes of 3-5  $k_B T/e$  are observed.

When strongly magnetized particles are accelerated through an oblique double layer they obtain large velocity vectors parallel to the magnetic field and become field-aligned beams. On the other hand, if the particles are weakly magnetized, upon acceleration they obtain large velocity vectors nearly parallel to the internal electric field of the double layer to become double-layer-aligned beams. Thus there exists the possibility of producing beams of magnetic-field-aligned electrons and beams of non-magnetic-field-aligned ions emanating from opposite sides of an oblique double layer. This may have implications on the satellite detection of particles in the auroral magnetosphere (Borovsky and Joyce, 1982a).

The equipotential contours of a magnetized and an unmagnetized two-dimensional double layer may be viewed in Figure 2. Two-dimensional double layers are found to be U-shaped structures, the shapes being nearly independent of the strength of the external magnetic field, and the thicknesses of the segments oblique to the magnetic field being approximately equal to the thicknesses of segments which are field-aligned, both being approximately equal to the thicknesses of planar double layers of the same potential jump. These facts again indicate Debye-length scaling for magnetized structures. This may be anticipated since planar double layers were found to scale in terms of Debye lengths. Although two-dimensional structures with the high-potential plasma on the concave side (positive structure) appear to be much the same as structures with the low-potential plasma on the concave side (negative structure), they behave quite differently when two structures are brought close together--the adjacent positive structures will merge while the negative structures will not (Borovsky and Joyce, 1982b).

As was stated above, two-dimensional double layers are subject to periodic disruption as are planar double layers, the instability again being preceded by the appearance of large amplitude solitary pulses in the low-potential plasmas adjacent to the structures. This disruption leads to a sudden increase in the flux of accelerated electrons emanating from the double layer; such an enhancement should be detectable in the auroral zone (Borovsky and Joyce, 1982a). Langmuir waves are observed in the high-potential plasmas adjacent to the structures, for high-potential

plasmas of small spatial extent, the waves being confined to the region containing the electron sheet beam.

As in the case of planar double layers, if particles are strongly magnetized they are accelerated to become field aligned and if they are weakly magnetized they are accelerated to obtain pitch angles nearly equal to the obliqueness of the part of the two-dimensional double layer which they traverse. In the auroral zone this may mean field-aligned sheet beams of down-going electrons and non-field-aligned beams of up-going ions, the latitudinal extents of these ion beams being too narrow for proper resolution by present satellites (Borovsky and Joyce, 1982a).

The authors wish to acknowledge conversations with R. T. Carpenter, C. Chan, P. G. Coakley, C. K. Goertz, R. F. Hubbard, G. L. Payne, D. R. Nicholson, S. D. Shawhan, and D. P. Stern, and wish to thank the Planetary Magnetospheres Branch of the NASA/Goddard Space Flight Center. This work was supported by NASA grant NSG-7632 and by NSF grant ATM78-22487.

#### REFERENCES

Borovsky, Joseph E., The Scaling of Oblique Plasma Double Layers, submitted to Phys. Rev., 1982.

Borovsky, Joseph E., and Glenn Joyce, Numerically Simulated Two-Dimensional Auroral Double Layers, submitted to J. Geophys. Res., 1982a.

Borovsky, Joseph E., and Glenn Joyce, The Simulation of Plasma Double-Layer Structures in Two Dimensions, submitted to J. Plasma Phys., 1982b.

Joyce, Glenn, and Richard F. Hubbard, Numerical Simulation of Plasma Double Layers, J. Plasma Phys., 20, 391, 1978.

## FIGURES

FIGURE 1. The electrostatic potential along a cut through a planar oblique double layer prior to disruption, the cut intersecting a solitary pulse in the low-potential plasma. (Mass ratio=16)

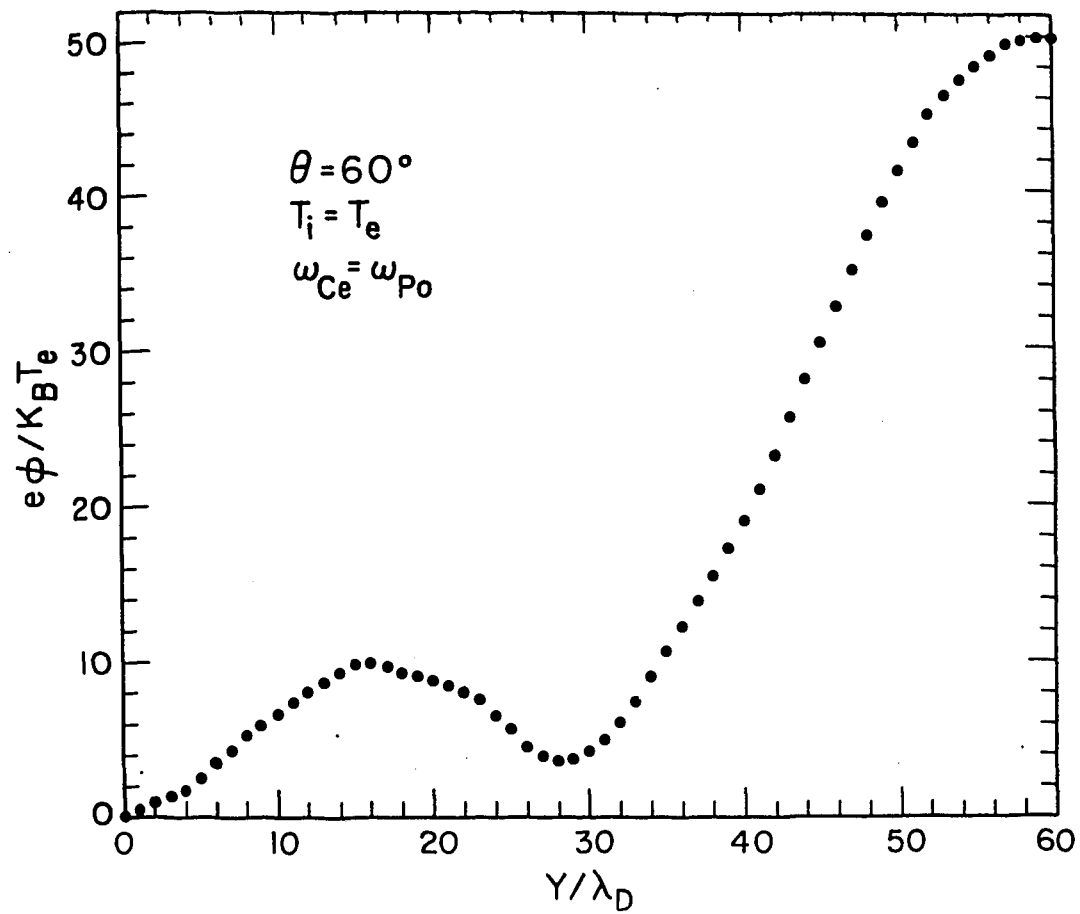
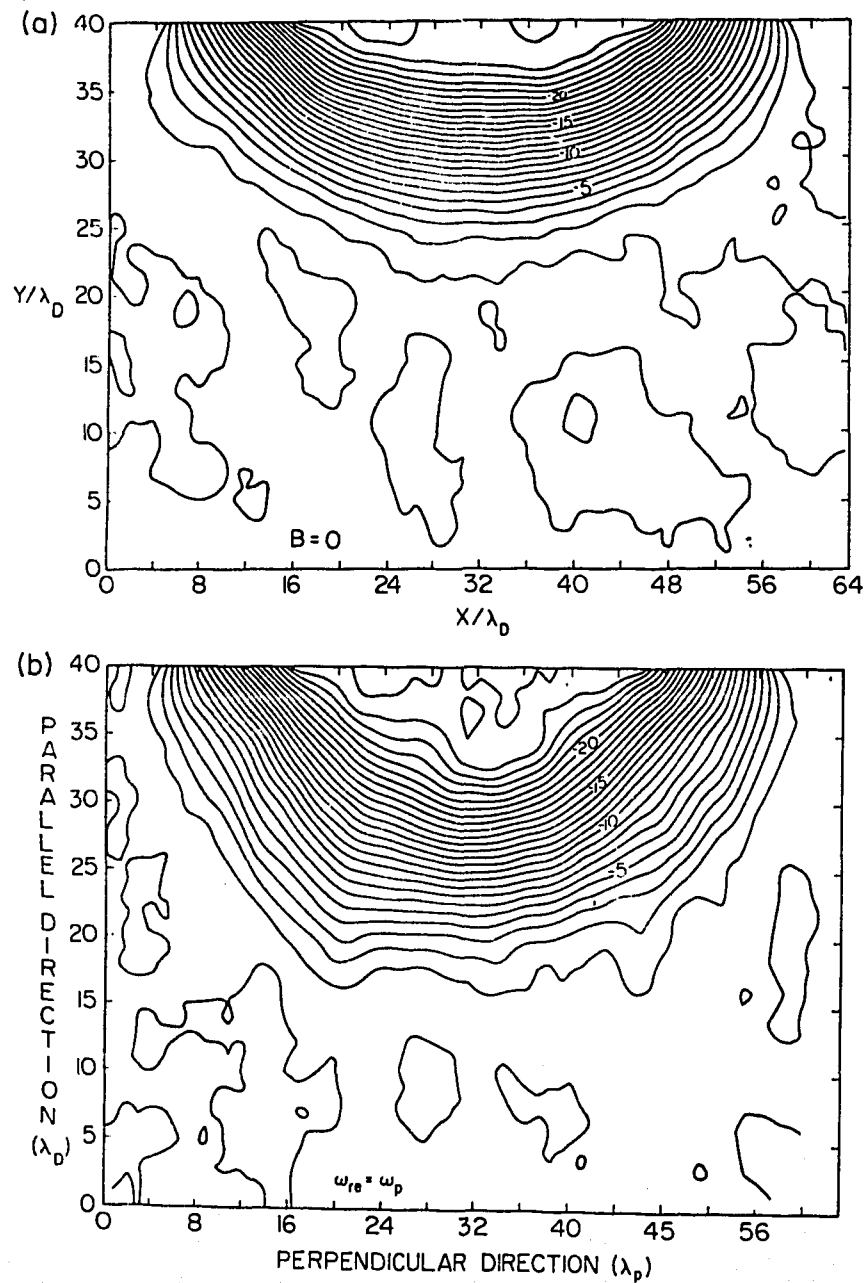


FIGURE 2. The equipotential contours of an unmagnetized (a) and a magnetized (b) two-dimensional double layer simulation, the only parameter differing being the magnetic field strength. In Figure (b) parallel and perpendicular are relative to the magnetic-field direction, which is vertical. (Mass ratio=16)



## DOUBLE LAYERS IN SPACE

P. Carlqvist

Royal Institute of Technology, Department of Plasma Physics,  
S-100 44 Stockholm, Sweden

Abstract

For more than a decade it has been realised that electrostatic double layers are likely to occur in space. We briefly discuss the theoretical background of such double layers. Most of the paper is devoted to an account of the observational evidence for double layers in the ionosphere and magnetosphere of the Earth. Several different experiments are reviewed including rocket and satellite measurements and ground based observations. It is concluded that the observational evidence for double layers in space is very strong. The experimental results indicate that double layers with widely different properties may exist in space.

1. Introduction

The electrostatic double layer may now be considered a well-established phenomenon in laboratory plasmas. During the last two decades a great number of experiments have been performed showing that double layers of various types can arise under widely different plasma conditions (including both magnetized and non-magnetized plasmas) (see Torvén (1979), Torvén and Lindberg (1980), and Sato (1982) and references therein). In some plasma experiments refined equipment and technique have been required to study the double layers. In other plasma experiments again (not primarily aimed for the investigation of double layers) it has even been difficult to avoid the occurrence of double layers.

From the study of cosmic plasmas it has been increasingly clear that such plasmas do not usually differ in any fundamental way from the plasmas produced in the laboratory. It is therefore reasonable to suppose that just as double layers occur in laboratory plasmas they should also occur in cosmic plasmas. In accordance with this view it has been suggested that double layers may exist in many cosmic sites such as in the solar atmosphere (Alfvén and Carlqvist, 1967; Carlqvist, 1969, 1979), in the ionosphere and magnetosphere of the Earth (see references further on in this paper), in the magnetosphere of Jupiter (Shawhan et al., 1975; Shawhan, 1976; Smith and Goertz, 1976), and in double radio sources (radio galaxies; Alfvén, 1978). In the present paper we shall restrict ourselves to discussing the possible occurrence of double layers in the ionosphere and magnetosphere of the Earth. The emphasis will be on

the observational evidence of such double layers as obtained from the ground, from rockets, and from satellites. First, however, we shall briefly consider some theoretical aspects of double layers in space.

## 2. Theoretical background

The cosmic plasma that is most easily accessible to direct study is the plasma in the ionosphere and magnetosphere of the Earth. It is also in this plasma we at present find the strongest indications of the existence of cosmic double layers. Already at the end of the fifties Alfvén (1958) suggested that structures similar to double layers might occur in the upper ionosphere. The structures considered by Alfvén are of the same type as the double layers studied experimentally by Schönhuber (1958) and Crawford and Freeston (1963) separating two plasmas of different temperatures and densities.

In more recent time the possibility of ionospheric and magnetospheric double layers has attracted an increasing interest, especially in connection with the question of how auroral particles are accelerated. Measurements show that auroral electrons often precipitate along the magnetic field lines with their energies peaked in the interval  $\approx 1-10$  keV. The energies of the electrons usually reach a maximum in the middle of the precipitating region, typically having a width of  $\approx 50$  km, thus giving rise to what is known as an "inverted V-structure" (Frank and Ackerson, 1971; Gurnett, 1972).

Several mechanisms, most of which being founded on parallel electric fields, have been proposed to explain how auroral particles are accelerated (see e.g. Fälthammar, 1977, 1978; Meng, 1978). One of the most interesting of these mechanisms is constituted by the double layer (Block, 1969, 1972a, 1975, 1978; Akasofu, 1969; Kan et al., 1979, Goertz, 1979). The auroral particles may be accelerated either in one step by a single double layer or in several steps by many double layers in series. An example of an ionospheric-magnetospheric current system containing a double layer is illustrated in Figure 1 (Alfvén, 1977). Here electrons are accelerated downwards producing auroras at lower levels while ions are accelerated upwards. A two-dimensional model of an ionospheric double layer has been studied by Wagner et al. (1980) using computer simulation methods.

To be able to satisfactorily describe the formation of a double layer in a plasma it is necessary to take into account the whole electric circuit containing the double layer (see Alfvén, 1977, 1981). The reason for this is that the external circuit determines the electric boundary conditions of the double layer. An example of a simple equivalent circuit including a voltage source, an inductance, a resistance, and a double layer is shown in Figure 2 (cf. Figure 1). In such a circuit the double layer may be considered a load which has

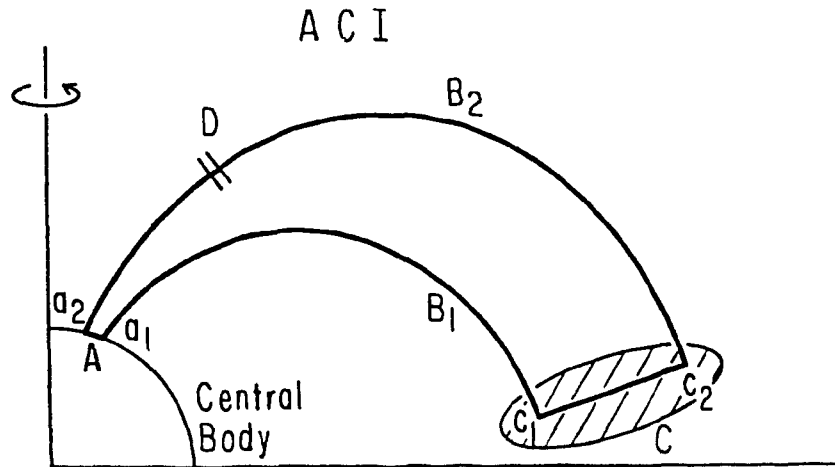


Fig.1. Example of a current loop passing through the ionosphere and magnetosphere of the Earth. The current, which is driven by an electromotive force, mainly produced by plasma motions at C, may give rise to one or more double layers, D (Alfvén, 1977).

to be supplied with energy by a generator. (The generator may consist of a voltage source, an inductance, or both.) Among other things this implies that the potential drop in the double layer cannot be an isolated phenomenon but must exist also in the plasma outside the layer. Hence it is clear that the equipotential surfaces inside the double layer must continue in the surrounding plasma as well. A set of possible equipotential configurations in and around an ionospheric double layer is shown in Figure 3 (Block, 1969). It should be noticed, however, that if there is an inductive generator present in the circuit the equipotential surfaces cannot penetrate into the generator region since the concept of potential does not apply there.

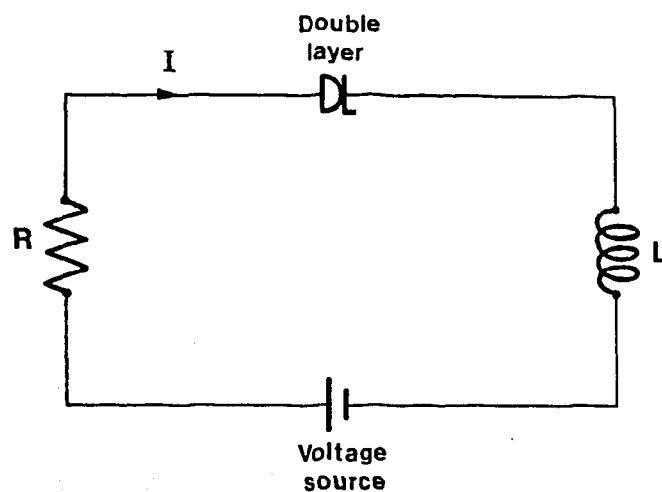


Fig.2. Example of a simple electric circuit containing a double layer in series with a voltage source, an inductance, L, and a resistance, R. A current, I, flows in the circuit.

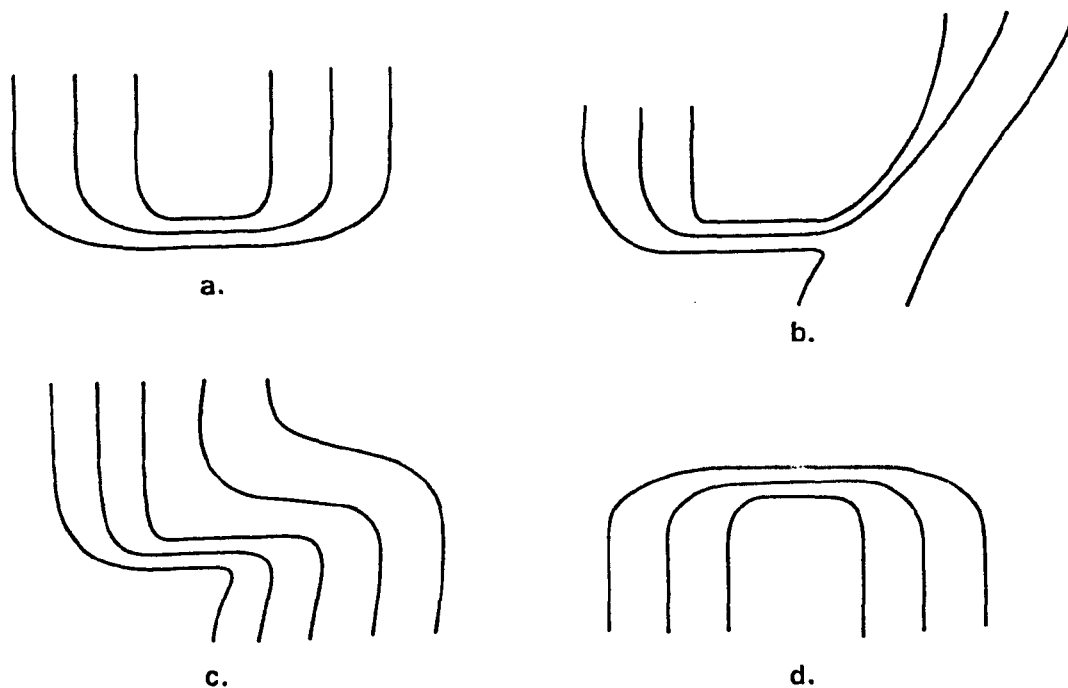


Fig.3. Four possible configurations of equipotential surfaces in and around ionospheric double layers (Block, 1969).

An interesting by-product of the double layer is the drift motion of the plasma surrounding the layer. The electric field,  $\underline{E}$ , which exists in the plasma outside a double layer will together with the magnetic field,  $\underline{B}$ , give rise to drift motions of the plasma,  $\underline{v}_d = \underline{E} \times \underline{B}/B^2$ . Both rotary motions and shearing motions are conceivable (Carlqvist, 1969, 1979; Carlqvist and Boström, 1970). As we shall see later on (Section 3) this drift motion may help to reveal the presence of double layers in the ionosphere and magnetosphere.

An important point to explain is under what conditions double layers can be formed in the ionosphere and magnetosphere. Laboratory experiments together with theoretical investigations and computer simulations indicate that there are at least two main mechanisms which can lead to double layers.

First, double layers may be formed as the result of some current dependent instability, e.g. the two-stream instability, or the ion-acoustic instability (Alfvén and Carlqvist, 1967; Babič and Torvén, 1974; Torvén and Babič, 1975, 1976; Goertz and Joyce, 1975; DeGroot et al., 1977; Sato and Okuda, 1980, 1981; Belova et al., 1980; Raadu and Carlqvist, 1981). Strong magnetic-field-aligned currents ( $i//B$ ) with current densities of more than  $10^{-5} \text{ Am}^{-2}$  have been observed in the plasma above the auroral region (Zmuda et al., 1966, 1967; Vondrak et al., 1969; Cloutier et al., 1970; Armstrong and Zmuda, 1970). The field-aligned currents, which often seem to be concentrated to thin sheets situated inside the inverted V-regions, might be sufficiently strong to initiate instabilities with accompanying double layers in the plasma.

Secondly, double layers may be formed to adapt two current-carrying plasmas of different properties to one another. Such double layers have, as mentioned above, been considered theoretically by Alfvén (1958) and experimentally by Schönhuber (1958) and Crawford and Freeston (1963). More recently Lennartsson (1978a,b) has in some detail investigated how double layers of a similar type may be formed in the magnetosphere. He considers a current loop connecting the hot magnetospheric plasma with the cold ionospheric plasma (cf. Figure 1). In part of the circuit the current is field-aligned. For this field-aligned current to flow from the ionosphere to the magnetosphere a large potential drop is required. This is a consequence of the magnetic mirroring of the electrons carrying most of the current. Normally the plasma must be quasi-neutral, otherwise excessively high electric fields would be generated. However, Lennartsson finds that quasi-neutrality is possible in most of the plasma only if the potential makes a sudden jump in the part of the loop carrying upward field-aligned currents. Lennartsson identifies this potential jump with a double layer.

### 3. Observational evidence of double layers in space

#### 3.1 Studies of the pitch-angle distribution of auroral electrons

About ten years after Alfvén's suggestion of double layers in the ionosphere-magnetosphere of the Earth, the first measurements indicating the existence of such layers were performed. By means of a rocket probe reaching a height of about 250 km Albert and Lindstrom (1970) studied the pitch-angle distribution of electrons in the ionosphere above a visible aurora (angular resolution  $\approx 0.5^\circ$ ). At heights ranging from 180 km to 240 km they found that the flux of electrons (with energies peaked around 10 keV) exhibited several troughs and peaks in the pitch angle interval  $\approx 77^\circ$ - $103^\circ$ . Albert and Lindstrom interpreted the flux variations as being caused by ionospheric double layers. Their arguments were as follows: Assume that a precipitating electron is spiralling around the magnetic field lines of strength,  $B_1$ , at a pitch angle of,  $\alpha_1$  and with the energy  $W_1$  when a double layer of potential drop,  $\phi_{DL}$ , is encountered (see Figure 4a). When the electron passes the double layer it gains the energy,  $e\phi_{DL}$ , so that the total energy of the electron below the double layer is

$$W_0 = W_1 + e\phi_{DL} \quad . \quad (1)$$

Under the assumption that the magnetic moment of the electron is conserved

$$\mu = \frac{W_\perp}{B} = \text{const.} \quad , \quad (2)$$

we then have

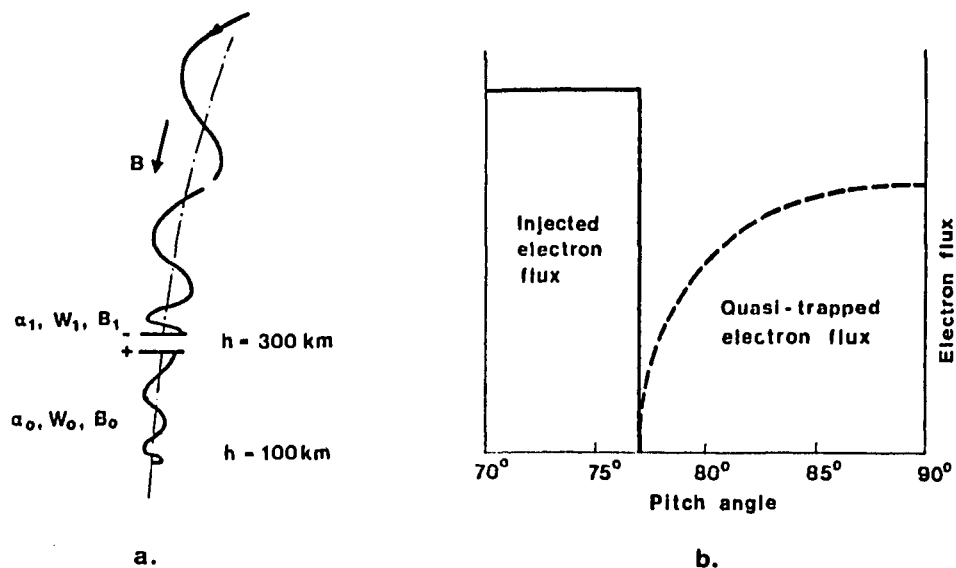


Fig.4.(a) Schematic picture of an electron spiralling down the magnetic field,  $B$ . At an altitude of about 300 km, where the pitch angle and energy of the electron are  $\alpha_1$  and  $W_1$  respectively, the electron encounters a double layer which accelerates it. At some position below the double layer the pitch angle and energy are  $\alpha_0$  and  $W_0$  respectively. (b) Idealized picture of the pitch angle distribution of electrons below a double layer. The injected electrons, which have passed the double layer, have pitch angles only below a certain limit (in this example  $77^\circ$ ). In the interval between this limit and  $90^\circ$  quasi-trapped electrons are found (after Albert and Lindstrom, 1970).

$$\frac{W_1 \sin^2 \alpha_1}{B_1} = \frac{W_0 \sin^2 \alpha_0}{B_0} \quad (3)$$

where  $B_0$  is the strength of the magnetic field and  $\alpha_0$  is the pitch angle of the electron at the position of the rocket below the double layer. From Equations (1) and (3) we find

$$\sin^2 \alpha_0 = \frac{B_0}{B_1} \left(1 - \frac{e\phi_{DL}}{W_0}\right) \sin^2 \alpha_1 \quad (4)$$

Equation (4) shows that the pitch angle,  $\alpha_0$ , has a maximum value  $\alpha_{0 \max}$ . Putting  $\alpha_1 = 90^\circ$  we get

$$\sin^2 \alpha_{c \max} = \frac{B_0}{B_1} \left(1 - \frac{e\phi_{DL}}{W_0}\right) \quad (5)$$

Hence, it is clear that there must be a region of void in the interval  $\alpha_{0 \max} < \alpha_0 < 90^\circ$  as regards the injected electron flux (see Figure 4b).

An important effect of the double layer is to lower the magnetic mirror point of the precipitating electrons. As a result of this, enhanced scattering of the electrons will take place. Some of the scattered electrons are quasi-trap-

ped in a region limited by the mirror point and the double layer. The quasi-trapped electrons are found in the pitch-angle interval  $\alpha_{0 \max}$  to  $90^\circ$  (see Figure 4b). Albert and Lindstrom identified the experimentally observed troughs in the pitch-angle distribution with the flux minimum at  $\alpha_{0 \max}$  shown in Figure 4b.

If we differentiate Equation (5) and eliminate  $e\phi_{DL}$  we obtain

$$\frac{B_0}{B_1} = \sin^2 \alpha_{0 \max} + W_0 \frac{\partial}{\partial W_0} (\sin^2 \alpha_{0 \max}) \quad (6)$$

Inserting the observed variation of  $\alpha_{0 \max}$  with  $W_0$  into this equation Albert and Lindstrom could determine the value of  $B_0/B_1$  and, hence, the level at which the double layer occurred. By means of Equation (5) the potential drop,  $\phi_{DL}$ , could furthermore be settled. Albert and Lindstrom found that fits to the experimental data indicated the presence of three double layers at altitudes of about 250, 270, and 280 km. The potential drops derived for these layers were 80, 160, and 160 V respectively.

### 3.2 Whirling motion of auroral irregularities

Indications for the presence of double layers above the auroral zone has also been given by Carlqvist and Boström (1970). Using TV-recordings made from the northern hemisphere they studied the motion of auroral irregularities near the magnetic zenith. Occasionally the irregularities were seen to stream in opposite directions giving the impression of elongated whirls. The sense of rotation was counter-clockwise and the duration of the phenomenon amounted to a few seconds only. The corresponding velocities were in the range  $4\text{--}20 \text{ km s}^{-1}$  and the width of the region in which the streaming could be seen was about 10 km. Carlqvist and Boström suggested that the whirling motions observed might be caused by magnetospheric double layers. They considered a model of a thin current slab containing a double layer and carrying magnetic-field-aligned currents upwards from the ionosphere to the magnetosphere (see Figure 5). Inside the double layer the equipotential surfaces are densely packed while crossing the magnetic field lines. Outside the layer the equipotential surfaces must be mainly parallel to the magnetic field because of the high parallel conductivity of the ambient plasma (Block, 1969). It is furthermore assumed that the surfaces are bent upwards as a result of the short-circuiting effect of the lower ionosphere. Hence, there is an electric field directed inwards towards the centre of the current slab in the plasma above the double layer. This electric field, together with the magnetic field, gives rise to drift motions of the plasma,  $\underline{v}_d = \underline{E} \times \underline{B}/B^2$ , above the layer. The drift motions, which are oppositely directed in both halves of the slab, are projected downwards on the ionosphere by means of the electrons accelerated in the double layer. Hence, the ionosphere acts as the screen of a cathode ray tube on which the motions of irregulari-

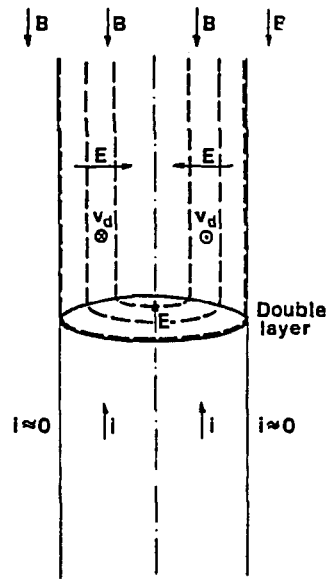


Fig.5. Schematic cross-section of a current slab containing a double layer. The equipotentials (dashed curves) are bent upwards and hence there are drift motions,  $\vec{v}_d = \text{ExB}/B^2$ , in the plasma above the double layer. Inhomogeneities in this plasma are projected downwards as moving auroral irregularities by means of the electrons accelerated in the double layer.

ties in the plasma above the double layer can be observed.

From the observed velocities of the auroral irregularities and the width of the streaming region it was possible to estimate the potential drop across the double layer. Using the values quoted above a potential drop of about 1-5 kV was obtained.

Assuming the current direction in the slab to correspond to an electron aurora the sense of rotation of the auroral irregularities, as seen from below, should be counter-clockwise in the northern hemisphere just as found from the TV-recordings. In the southern hemisphere the sense of rotation should be the opposite. Such a change of the sense of rotation with the sign of the latitude has in fact been detected by Hallinan and Davis (1970). When studying a great number of small-scale auroral structures called curls they found that these structures, as seen from below, rotated counter-clockwise in the northern hemisphere and clockwise in the southern hemisphere.

It should be noticed that the observations of the whirling auroral irregularities do not prove the existence of magnetospheric double layers. The observations only indicate that there are strong electric fields present above the moving auroral forms observed. These electric fields might in principle be generated by some other mechanism such as, for instance, anomalous resistivity. There are, however, good arguments that speak in favour of the double layer as the cause of the electric fields. The double layer should for instance accelerate an electron flux downwards producing a fairly monoenergetic peak. Such electron fluxes are often observed in connection with auroral arcs. The anomalous resistivity should primarily give rise to a strong local heating of the magnetospheric plasma.

### 3.3 Barium plasma experiments

During the last decade additional measurements have been performed which sup-

port the idea that double layers occur in the magnetosphere. Thus Wescott *et al.* (1976a,b) and Haerendel *et al.* (1976) have studied electric fields in the magnetosphere by means of artificially injected barium plasmas. During the second of two barium plasma experiments (the Skylab beta experiment) Wescott *et al.* found that the barium plasma first formed one streak which drifted magnetically eastward. About 15 minutes after injection the streak was observed to brighten and to split into multiple streaks above an altitude of  $h \approx 5500$  km (see Figure 6). The various streaks drifted apart with high velocities ( $15 \text{ km s}^{-1}$  at 9000 km altitude corresponding to a perpendicular electric field,  $E_{\perp} \approx 50 \text{ mV m}^{-1}$ ), and after some five minutes they had diffused and could no longer be detected. All that remained was the original streak truncated near  $h = 7600$  km. It is to be noticed that below an altitude of about 5500 km the streak did not split up or show any appreciable variation of intensity. From the upward motion of the truncated streaks it was concluded that the barium ions had gained an energy of at least 34 eV (from  $\approx 11$  eV to  $> 45$  eV) parallel to the magnetic field.

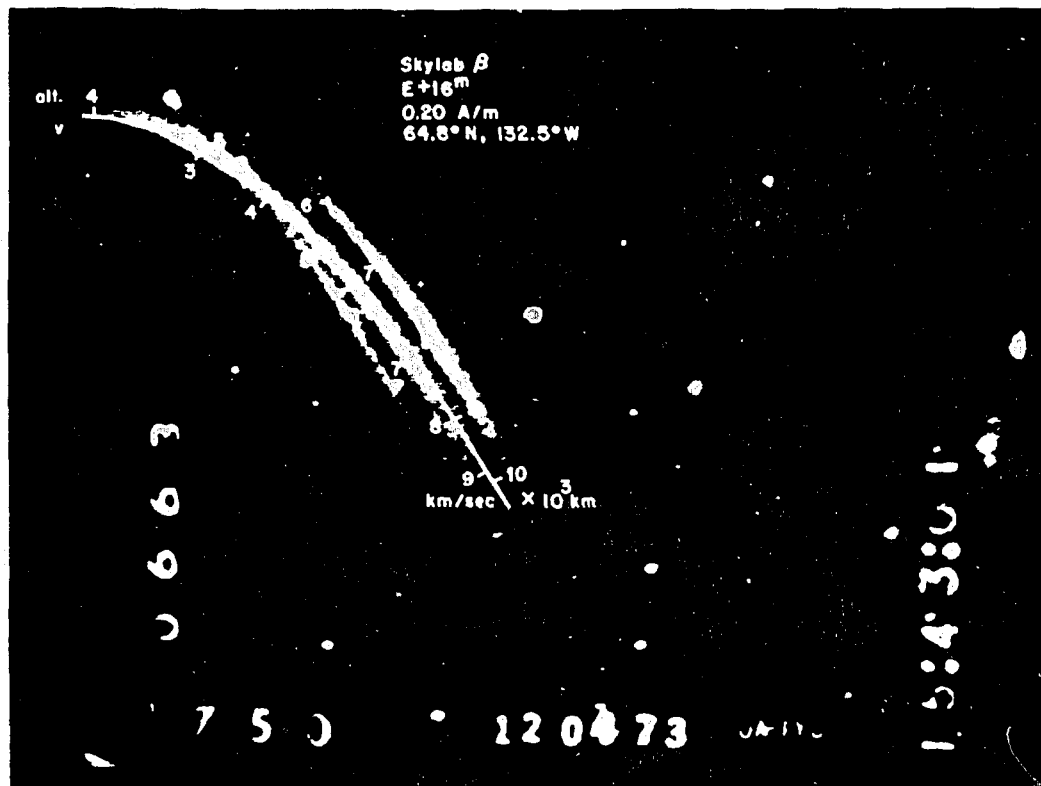


Fig.6. TV-frame of barium streaks at 16 minutes after injection (Wescott *et al.*, 1976). The superimposed solid curve represents a theoretically derived magnetic field line. To obtain a good fit it was assumed that there existed a field-aligned upward sheet current of  $0.2 \text{ A m}^{-1}$ , oriented magnetically east-west. Altitudes are shown on one side of the curve instantaneous streaming velocities on the other. Notice the lack of low-altitude continuation of the streaks on both sides of the main streak.

The injection of the barium plasma took place at the expansive phase of a magnetic substorm when the AE index was about 400  $\gamma$ . At the time of the splitting the projection of the flux tube of the streak on the 100 km level coincided with the poleward boundary of a diffuse aurora. The boundary was interpreted to be an eastward-drifting omega band (Akasofu, 1974). Comparison of the appearance of the streak and the appearance of theoretically calculated magnetic field lines showed that a good fit could be obtained only if there was an upward field-aligned sheet current of the magnitude  $\approx 0.2 \text{ A m}^{-1}$  present south of the streaks (or downward north of the streaks).

Wescott et al. proposed that their observational results could be interpreted in terms of a double layer according to either of the models shown in Figures 7a and 7b. In Figure 7a the solid curves represent the equipotential surfaces in and around a double layer as suggested by Block (1972b)(cf. Figure 3) while in Figure 7b the solid curves represent the equipotential surfaces as given by Swift et al. (1976). In both the figures the potential gradient is directed away from the axis of symmetry. The dashed-dotted lines illustrate the schematic location of the barium flux tube. If it is assumed that the double layer occurred at an altitude of about 5500 km these models may explain the rapid drift motion of the upper part of the barium streak and the upward acceleration of the barium ions. Furthermore, there should be no or little drift motion below the double layer.

By means of two similar barium plasma experiments Haerendel et al. (1976) investigated the electric fields in the magnetosphere under relatively quiet magnetic conditions. In the first of these experiments the barium plasma was injected along the magnetic field lines from an altitude of about 600 km. The

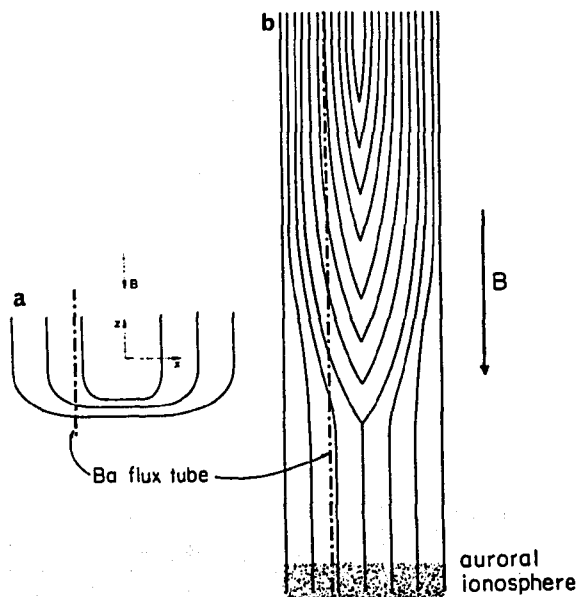


Fig.7 (a) Equipotentials in and around a double layer situated in a current sheet (Block, 1972b). (b) Equipotential model for an auroral arc (Swift et al., 1976). In both pictures the dashed-dotted lines represent the position of the barium flux tube (Wescott et al., 1976).

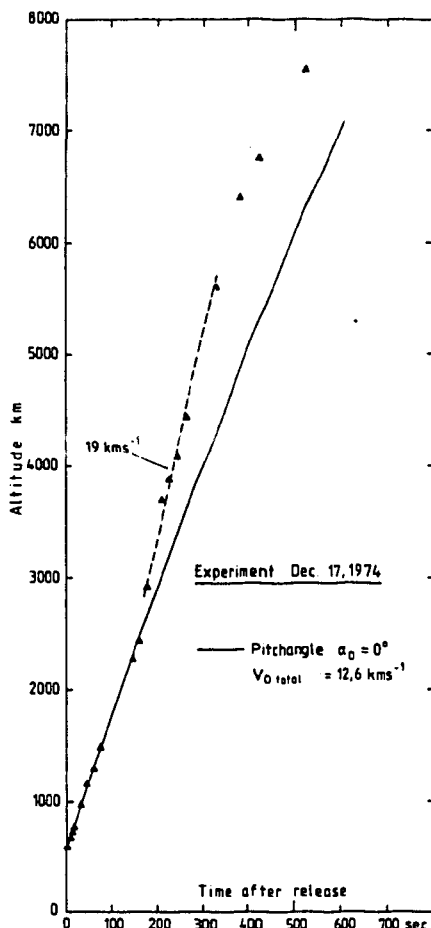


Fig.8. Observed upward motion of the upper tip of the barium ion jet (filled triangles) on Dec.17, 1974. The solid curve shows the adiabatic path of an ion with initial velocity  $12.6 \text{ km s}^{-1}$  parallel to the magnetic field while the dashed line represents a velocity of  $19 \text{ km s}^{-1}$ . The deviation of the data from an extrapolation of the dashed line at altitudes above  $\approx 6000 \text{ km}$  is due to decreasing brightness of the jet (Haerendel et al., 1976).

altitude of the upper tip of the barium jet was registered and is shown versus time in Figure 8. Here the solid line represents the theoretically calculated adiabatic motion of the barium ions (i.e. motion only governed by the Lorentz and gravitational forces) when released with the actually observed initial speed. As is evident from the figure the barium ions followed the adiabatic path quite well below an altitude of  $\approx 2500 \text{ km}$ . However, above this altitude there is a strong deviation from the adiabatic path with the particles moving upwards with a substantially increased velocity. The increase of the velocity corresponds to a gain of energy of the barium ions of  $190 \text{ eV}$ . At the time of the acceleration of the barium jet only a diffuse red aurora was observed in the area of interest. No auroral arc was visible underneath the barium jet.

In the second experiment the barium jet consisting of two major streaks (the splitting into these had occurred immediately after injection) was first found to follow an adiabatic path (the injection angle was  $180^\circ - 41^\circ = 139^\circ$  with respect to the direction of the magnetic field). About 11.5 minutes after injection one of the streaks started to move upwards with a much enhanced speed (see Figure 9 upper part). When the acceleration started the tip of the streak had reached an altitude of  $\approx 7500 \text{ km}$ . Despite of observational diffi-

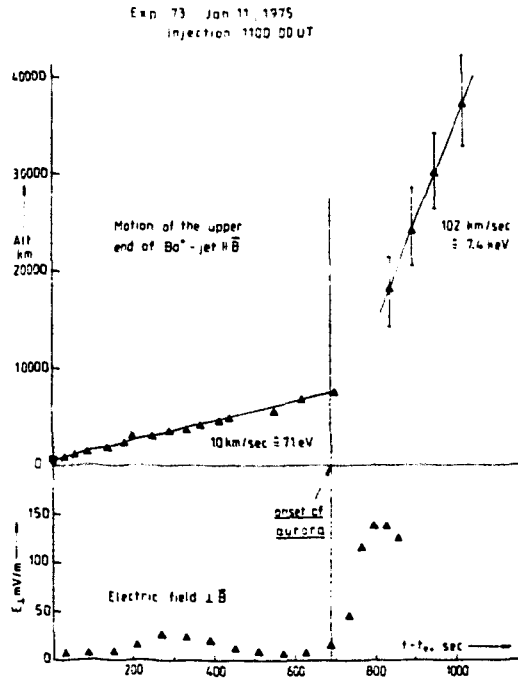


Fig.9. (Upper part) Observed upward motion of the upper tip of the barium jet (filled triangles) on Jan.11, 1975. At a height of  $\approx 7500$  km the ions were accelerated to a velocity of about  $100 \text{ km s}^{-1}$  corresponding to an energy gain of  $\approx 7.3$  keV. (Lower part) Transverse electric field observed at a height of 260 km and projected downwards along the magnetic field lines on the 100 km level (Haerendel *et al.*, 1976).

culties it could be concluded that the speed increased by roughly one order of magnitude from a value near  $10 \text{ km s}^{-1}$  before the acceleration up to  $\approx 100 \text{ km s}^{-1}$  after. This increase of the velocity corresponds to a free fall of the barium ions through a potential drop of  $\approx 7.3$  keV. At the same time as the acceleration of the jet took place a low-altitude barium cloud, that had settled at a height of  $\approx 260$  km, was activated showing a sudden increase of the transverse electric fields from  $\approx 15 \text{ mV m}^{-1}$  to  $\approx 140 \text{ mV m}^{-1}$  (see Figure 9, lower part).

During most of the first phase of the experiment no auroral arcs were observed in the neighbourhood of the magnetic field lines occupied by the barium jet. However, at the onset of the upward acceleration of the barium ions, 11.5 minutes after injection, bright auroral arcs appeared in the general area of the projected jet.

Haerendel *et al.* were not able to conclude whether the electric fields that accelerated the barium ions upwards were caused by double layers, plasma turbulence or other mechanisms. The main reason for this was that the integration time of the TV-pictures showing the streaks was too long to permit a determination of whether the potential drops were sharp or more distributed.

### 3.4 Satellite measurements

Further evidence for the occurrence of double layers in the magnetosphere comes from direct (*in situ*) measurements of the electric field made on board the S3-3 satellite (Mozer *et al.*, 1977 ; Temerin *et al.*, 1982). Mozer *et al.* found that when the satellite crossed the auroral zones at alti-

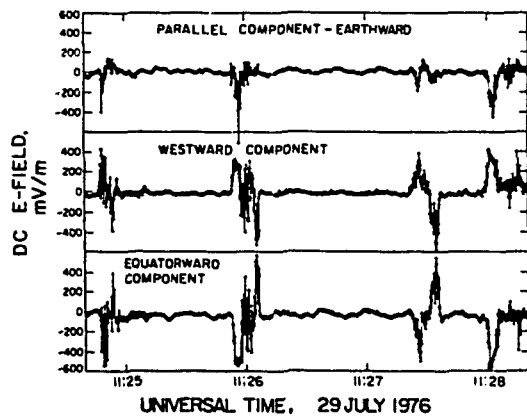


Fig.10. One of the best examples of large electric fields measured on board the S3-3 satellite (Mozer *et al.*, 1977). Both parallel and perpendicular components of several hundred  $\text{mV m}^{-1}$  were recorded. Unfortunately one of the electric field detectors was saturated in the event near 11:28.

tudes in the range, 2000-8000 km, strong electric fields of up to  $\approx 0.5 \text{ V m}^{-1}$  occasionally occurred. The electric fields were predominantly oriented perpendicular to the magnetic field, but sometimes the parallel component could be as large as or larger than the perpendicular components (see Figure 10). In the events shown by Figure 10 the parallel electric field is of the order of several hundred  $\text{mV m}^{-1}$  and directed away from Earth.

The enhanced electric fields were generally detected in limited regions having an extension of up to a few tens of kilometres along the path of the satellite. In such regions the perpendicular component could switch from one direction to the reverse with a number of spikes superimposed. However, usually the double-structure of the electric field pattern was not so clear as in Figure 10. The typical potential drops estimated from the measured electric field were of the order of a few kilovolts. In the general area surrounding the region of enhanced electric field it was mostly observed large magnetic-field-aligned currents ( $> 10^{-6} \text{ A m}^{-2}$ ), electrostatic waves (identified as ion-cyclotron waves), and upflowing ions with energies of a few kilovolts.

Mozer *et al.* interpreted their observational results in terms of oblique double layers (or electrostatic shocks as they call them) similar to the oblique double layer studied theoretically by Swift (1975). This kind of layer strongly depends on the presence of a magnetic field and has a thickness of several ion gyro-radii. Later Shawhan *et al.* (1978) have pointed out that the intense electric fields observed might equally well be due to ordinary double layers of the same type as those shown in Figures 5 and 7a.

Recently Temerin *et al.* (1982) have drawn attention to new results of the electric field measurements made on board the S3-3 satellite. The measurements reveal two types of structures which primarily appear in the parallel component of the electric field,  $E_{\parallel}$ . First there are structures denoted DL (see Figure 11) which predominantly consist of one polarity. The polarity is such as to accelerate ions upwards and electrons downwards. Secondly, there

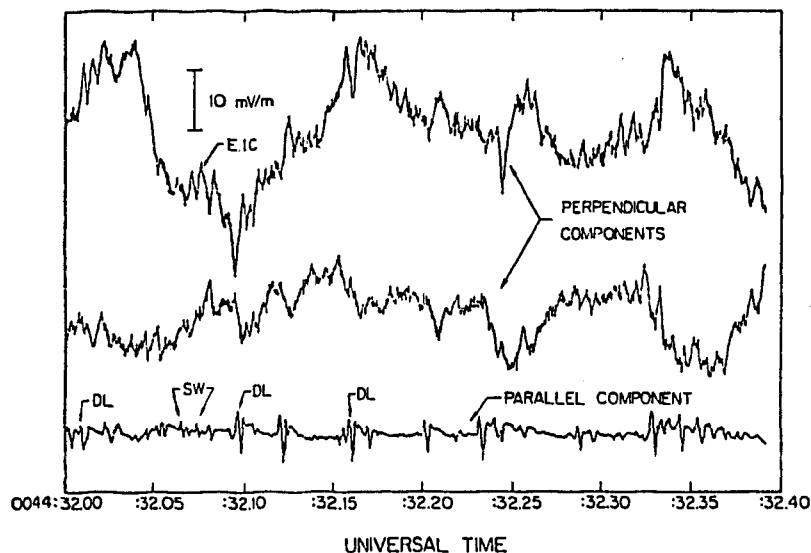


Fig.11. Perpendicular and parallel electric field components (ordinate) measured on board the S3-3 satellite during a 0.4 second time interval on Aug.11, 1976 and at an altitude of 6030 km (Temerin *et al.*, 1982).

are structures denoted SW (see Figure 11) consisting of two opposite polarities of approximately equal magnitude. Both the DL and SW structures of  $E_{\parallel}$  are characterized by an amplitude typically not greater than  $15 \text{ mV m}^{-1}$  and a duration of about 2-20 ms. As may be seen from Figure 11 the structures of  $E_{\parallel}$  have little or no correspondence in the perpendicular components. These latter components chiefly reveal electrostatic ion cyclotron waves and low frequency noise. Thus it is clear that the DL and SW structures differ appreciably from the electric field measurements reported earlier by Mozer *et al.* (1977).

The DL and SW structures were mainly observed in the dusk sector of the auroral zone at altitudes above 6000 km. Here, events consisting of 10 to 400 separate DL and SW structures were fairly common. The typical spatial scale of the events corresponded to  $\approx 1^{\circ}$  invariant latitude. In the general region where the events occurred there were upward-directed field-aligned currents with a current density of  $\approx 10^{-7} \text{ A m}^{-2}$ , intense beams of upward moving 0.5 keV ions, and large fluxes of downgoing 0.5 keV electrons. Associated with the events were also electrostatic ion-cyclotron waves and a depletion of the electron density.

Temerin *et al.* interpreted the DL structures as being caused by double layers and the SW structures as being due to solitary waves. From rather uncertain estimates of the difference of the onset times of the DL structures measured by two sets of double probes (the error was of the same magnitude as the quantities measured) Temerin *et al.* claimed that the velocity of the double layers along the magnetic field lines and relative to the spacecraft was  $\gg 50 \text{ km s}^{-1}$ . Combining this velocity with a typical duration of the DL structures of 4 ms they found that the length scale of the double layer parallel to the magnetic field was  $\gg 200 \text{ m}$ . Hence, with a parallel component of the electric field,  $E_{\parallel} \approx 10 \text{ mV m}^{-1}$  the potential drop across each of the double layers should be

of the order of a few volts or more.

Temerin *et al.* also found that during an event the DL structures occupied approximately 5% of the total time. Since in the structures  $E_{\parallel} \approx 10 \text{ mV m}^{-1}$ , this implies that the average parallel electric field was  $\approx 0.5 \text{ mV m}^{-1}$ . Such an electric field, distributed over an altitude interval of  $\approx 1000 \text{ km}$ , would give a potential drop of 0.5 kV corresponding to the particle energies observed.

Temerin *et al.* suggested that many small double layers in series, distributed along a magnetic field line, might account for kilovolt potential drops and for acceleration of auroral particles.

#### 4. Conclusions

The observations described in Section 3 clearly demonstrate that strong electric fields, with both parallel and perpendicular components of up to at least  $0.5 \text{ V m}^{-1}$ , exist in the ionosphere and magnetosphere of the Earth. It has been found that these fields can give rise to potential drops as large as about seven kilovolts. In some cases it has also been possible to establish that the potential drops are limited to fairly small distances along the magnetic field lines. Shawhan *et al.* (1978) and Goertz (1979) have pointed out that the double layer seems to be the only mechanism that is capable of producing the strongest electric fields observed ( $> 100 \text{ mV m}^{-1}$ ). Taking this argument and all the observational material reviewed above into account we must conclude that there is now very strong evidence for the existence of double layers in the ionosphere and magnetosphere.

It may be of some interest to compare the various observations indicating ionospheric and magnetospheric double layers in order to see in what respects they are similar and in what respects they differ. If we first consider the electric field, which is the quantity most carefully measured, we find that it varies within wide limits. Both the parallel component and the perpendicular component of the field cover the interval  $\approx 1\text{-}1000 \text{ mV m}^{-1}$  (see Table I). Table I reveals that also the time periods during which the electric fields are observed and the total potential drops inferred vary considerably in between different observations. Thus the time periods range from a few milliseconds to about one minute while the potential drops range from some volt to many kilovolts. Further, the altitudes at which the potential drops occur are found in the interval  $h \approx 250\text{-}8000 \text{ km}$ .

Although the quantities discussed above are subject to large spreads the various experimental results also exhibit several common features. In all cases where it has been possible to estimate the predominant direction of the parallel electric field it has been such as to accelerate electrons downwards and positive ions upwards. Furthermore, enhanced magnetic-field-aligned cur-

Table I

References	Electric fields measured	Total potential drops inferred	Height of potential drops	Time during which electric field is observed	Association with auroras
Albert and Lindstrom, 1970		$\Delta\phi \approx 80 \text{ V}$ $\Delta\phi \approx 160 \text{ V}$ $\Delta\phi \approx 160 \text{ V}$	$h \approx 250 \text{ km}$ $h \approx 270 \text{ km}$ $h \approx 280 \text{ km}$		Visible aurora
Carlqvist and Boström, 1970	$E_{\perp} \approx 0.2-1 \text{ Vm}^{-1}$ projected on $h \approx 100 \text{ km}$	$\Delta\phi \approx 1-5 \text{ kV}$		A few seconds	Evening aurora
Wescott et al., 1976	$E_{\perp} \approx 50 \text{ mVm}^{-1}$ at $h \approx 9000 \text{ km}$	$\Delta\phi > 34 \text{ V}$	$h \approx 5500 \text{ km}$	Of the order of minute	Boundary of diffuse aurora: Omega band
Haerendel et al., 1976		$\Delta\phi \approx 190 \text{ V}$	$h \approx 2500 \text{ km}$		Diffuse red aurora
- " -	$E_{\perp} \approx 140 \text{ mVm}^{-1}$ at $h \approx 260 \text{ km}$	$\Delta\phi \approx 7.3 \text{ kV}$	$h \approx 7500 \text{ km}$		Bright auroral arcs
Mozer et al., 1977	$E_{\perp} \approx 0.5 \text{ Vm}^{-1}$ $E_{\parallel} \approx 0.5 \text{ Vm}^{-1}$ at $h \approx 2000-8000 \text{ km}$	$\Delta\phi \approx 3 \text{ kV}$	$h \approx 2000-8000 \text{ km}$	0.1-10 s	In the auroral zone
Temerin et al., 1982	$E_{\parallel} \approx 15 \text{ mVm}^{-1}$ $E_{\perp} \ll E_{\parallel}$ at $h \approx 6000-8000 \text{ km}$	$\Delta\phi \gtrsim 2 \text{ V}$	$h \approx 6000-8000 \text{ km}$	2-20 ms	- " -

rents have often been observed in connection with parallel electric fields. Another common feature of the observations is that the electric fields recorded mostly seem to be positively correlated with auroral activity (and/or the auroral zones).

From what has been said above we can infer that the various observations are qualitatively rather similar but quantitatively very dispersed. This indicates that double layers having different properties are present in the ionospheric and magnetospheric plasmas. It is possible that the observations displayed in Table I may be divided into two or more distinct groups, each representing double layers having roughly the same parameter values. Whether such a division has any physical significance has, however, to await further investigations.

#### Acknowledgements

I wish to thank Professor C.-G. Fälthammar for reading the manuscript and for giving valuable comments.

#### References

- Akasofu, S.-I.: 1969, *Nature* 221, 1020.
- Akasofu, S.-I.: 1974, *Space Sci. Rev.* 16, 617.
- Albert, R.D. and Lindstrom, P.J.: 1970, *Science* 170, 1398.
- Alfvén, H.: 1958, *Tellus* 10, 104.
- Alfvén, H.: 1977, *Rev. Geophys. Space Phys.* 15, 271.
- Alfvén, H.: 1978, *Astrophys. Space Sci.* 54, 279.
- Alfvén, H.: 1981, *Cosmic Plasma*, Reidel Publ. Co., Dordrecht, Holland.
- Alfvén, H. and Carlqvist, P.: 1967, *Solar Phys.* 1, 220.
- Armstrong, J.C. and Zmuda, A.J.: 1970, *Trans, AGU* 51 (4), 405.
- Babič, M. and Torvén, S.: 1974, TRITA-EPP-74-02, Dept of Plasma Phys., Royal Inst. of Tech., Stockholm, Sweden.
- Belova, N.G., Galeev, A.A., Sagdeev, R.Z., and Sigov, Yu.S.: 1980, *JETP Lett.* 31, 518.
- Block, L.P.: 1969, Rep. No. 69-30, Depts of Electron and Plasma Phys., Royal Inst. of Tech., Stockholm, Sweden. Paper presented at the Ninth Int. Conf. on Phenomena in Ionized Gases, Bucharest, Rumania, September, 1969.
- Block, L.P.: 1972a, in B.M. McCormac (ed.), *Earth's Magnetospheric Processes*, Reidel Publ. Co., Dordrecht, Holland, p. 258.
- Block, L.P.: 1972b, *Cosmic Electrodynamics* 3, 349.
- Block, L.P.: 1975, in B. Hultqvist and L. Stenflo (eds.), *Physics of the Hot Plasma in the Magnetosphere*, Plenum Press, New York, London, p. 229.
- Block, L.P.: 1978, *Astrophys. Space Sci.* 55, 59.
- Carlqvist, P.: 1969, *Solar Phys.* 7, 377.
- Carlqvist, P.: 1979, *Solar Phys.* 63, 353.

- Carlqvist, P. and Boström, R.: 1970, *J. Geophys. Res.* 75, 7140.
- Cloutier, P.A., Anderson, H.R., Park, R.J., Vondrak, R.R., Spiger, R.J., and Sandel, B.R.: 1970, *J. Geophys. Res.* 75, 2595.
- Crawford, F.W. and Freeston, I.L.: 1963, Vie Conférence Internationale sur les Phénomènes d'Ionisation dans les Gas, Paris, Vol.I, p. 461.
- DeGroot, J.S., Barnes, C., Walstead, A.E., and Buneman, O.: 1977, *Phys. Rev. Letters* 38, 1283.
- Fälthammar, C.-G.: 1977, *Rev. Geophys. Space Phys.* 15, 457.
- Fälthammar, C.-G.: 1978, *J. Geomagn. Geoelectr.* 30, 419.
- Frank, L.A. and Ackerson, K.L.: 1971, *J. Geophys. Res.* 77, 4116.
- Goertz, C.K.: 1979, *Rev. Geophys. Space Phys.* 17, 418.
- Goertz, C.K. and Joyce, G.: 1975, *Astrophys. Space Sci.* 32, 165.
- Gurnett, D.A.: 1972, in E.R. Dyer (ed.), Critical Problems in Magnetospheric Physics, Inter-Union Committee on Solar-Terrestrial Physics, National Academy of Sciences, Washington, D.C., p. 123.
- Haerendel, G., Rieger, E., Valenzuela, A., Föppl, H., Stenbaek-Nielsen, H.C., and Wescott, E.M.: 1976, in European Programmes on Sounding-Rocket and Balloon Research in the Auroral Zone, Rep. ESA-SP115, European Space Agency, Neuilly, France.
- Hallinan, T.J. and Davis, T.N.: 1970, *Planet. Space Sci.* 18, 1735.
- Kan, J.R., Lee, L.C., and Akasofu, S.-I.: 1979, *J. Geophys. Res.* 84, 4305.
- Lennartsson, W.: 1978a, TRITA-EPP-78-08, Dept of Plasma Phys., Royal Inst. of Tech., Stockholm, Sweden.
- Lennartsson, W.: 1978b, *J. Geomagn. Geoelectr.* 30, 463.
- Meng, C.-I.: 1978, *Space Sci. Rev.* 22, 223.
- Mozer, F.S., Carlson, C.N., Hudson, M.K., Torbert, R.B., Parady, B., Yatteau, J., and Kelley, M.C.: 1977, *Phys. Rev. Letters* 38, 292.
- Raadu, M.A. and Carlqvist, P.: 1981, *Astrophys. Space Sci.* 74, 189.
- Sato, N.: 1982, in the present volume.
- Sato, T. and Okuda, H.: 1980, *Phys. Rev. Lett.* 44, 740.
- Sato, T. and Okuda, H.: 1981, *J. Geophys. Res.* 86, 3357.
- Schönhuber, M.J.: 1958, Quecksilber-Niederdruck-Gasentladungen, Lachner, München.
- Shawhan, S.D.: 1976, *J. Geophys. Res.* 81, 3373.
- Shawhan, S.D., Goertz, C.K., Hubbard, R.F., Gurnett, D.A., and Joyce, G.: 1975, in V. Formisano (ed.), The Magnetospheres of Earth and Jupiter, Reidel Publ. Co., Dordrecht, Holland, p. 375.
- Shawhan, S.D., Fälthammar, C.-G., and Block, L.P.: 1978, *J. Geophys. Res.* 83, 1049.
- Smith, R.A. and Goertz, C.K.: 1976, *J. Geophys. Res.* 83, 2617.
- Swift, D.W.: 1975, *J. Geophys. Res.* 80, 2096.
- Swift, D.W., Stenbaek-Nielsen, H.C., and Hallinan, T.J.: 1976, *J. Geophys. Res.* 81, 3931.
- Temerin, M., Cerny, K., Lotko, W., and Mozer, F.S.: 1982, submitted for publication to *Phys. Rev. Lett.*

- Torvén, S.: 1979, in P.J. Palmadesso and K. Papadopoulos (eds.), Wave Instabilities in Space Plasmas, Astrophysics and Space Science Book Series, Reidel Publ. Co., Dordrecht, Holland, p. 109.
- Torvén, S. and Babić, M.: 1975, in J.G.A. Hölscher and D.C. Schram (eds.), Proc. 12th Int. Conf. on Phenomena in Ionized Gases, American Elsevier Publ. Co., New York, p, 124.
- Torvén, S. and Babić, M.: 1976, IEE 4th Int. Conf. on Gas Discharges, Swansea, Conf. Publ. No 143, p. 323.
- Torvén, S. and Lindberg, L.: 1980, J. Phys. D: Appl. Phys. 13, 2285.
- Vondrak, R.R., Anderson, H.R., and Spiger, R.J.: 1969, Trans AGU 50, 663.
- Wagner, J.S., Tajima, T., Kan, J.R., Leboeuf, J.N., Akasofu, S.-I., and Dawson, J.M.: 1980, Phys. Rev. Lett. 45, 803.
- Wescott, E.M., Stenbaek-Nielsen, H.C., Davis, T.N., and Peek, H.M.: 1976a, J. Geophys. Res. 81, 4487.
- Wescott, E.M., Stenbaek-Nielsen, H.C., Hallinan, T.J., Davis, T.N., and Peek, H.M.: 1976b, J. Geophys. Res. 81, 4495.
- Zmuda, A.J., Martin, J.H., and Heuring, F.T.: 1966, J. Geophys. Res. 71, 5033.
- Zmuda, A.J., Heuring, F.T., and Martin, J.H.: 1967, J. Geophys. Res. 72, 1115.

## FORMATION OF DOUBLE LAYERS ON AURORAL FIELD LINES

R. Lysak, W. Lotko, M. Hudson, and E. Witt

Space Sciences Laboratory, University of California  
Berkeley, CA 94720 U. S. A.

In contrast to the situation in laboratory plasmas and computer simulations, double layers in naturally occurring plasmas exist far from the imposed boundary conditions. Consequently, their formation and dynamics involve an interplay between microscopic and macroscopic plasma conditions. In this context, it is of interest to consider the nature of double layers which occur in a plasma environment where particle populations of radically different origin mix, where the macroscopic dynamics cause temporal variations in the local plasma parameters, and where a state of stationary plasma turbulence may persist well beyond the double layer lifetime. Such an environment occurs at several thousand kilometer altitudes over the Earth's auroral zone.

Observations of double layers on auroral field lines were first made from the polar orbiting S3-3 satellite (Temerin *et al.*, 1982). These structures are observed in conjunction with electrostatic ion cyclotron waves in regions of upflowing ion beams. Double layers are seen in the component of the electric field parallel to the background magnetic field as asymmetric pairs of oppositely directed electric fields, with the strongest field pointing away from the earth, as opposed to solitary wave structures in which a symmetric pair of electric field spikes is seen.

The observed double layers exhibit characteristics similar to those seen in computer simulations with current-driven boundary conditions (Sato and Okuda, 1981; Kindel *et al.*, 1981) in that  $e\phi/T_e \sim 1$ , the double layer width is  $50 \lambda_D$  and the separation between adjacent double layers is  $\sim 1000 \lambda_D$ . These properties are in contrast with double layers observed in simulations (*e.g.*, Hubbard and Joyce, 1979) and laboratory experiments (Quon and Wong, 1976) in which a potential is imposed and double layers with  $e\phi/T_e \gg 1$  are formed.

One consistent feature of both solitary waves and double layers in the auroral zone is the observation of a parallel electric field pointing toward the ionosphere preceding a field pointing away from the ionosphere. This indicates that the structures must be either positive polarity pulses propagating downward, or negative polarity pulses propagating upward. The second possibility is generally favored since computer simulations (Sato and Okuda, 1980, 1981; Hudson and Potter, 1981; Kindel *et al.*, 1981) have

observed that double layers form at the locations of negative polarity solitary waves. Time stationary ion holes having negative polarity have been described analytically by Schamel and Bujarbarua (1980), Hasegawa and Sato (1982), and Hudson *et al.* (1982). In addition, Lotko and Kennel (1981, 1982) have shown that negative polarity ion-acoustic solitons are favored in the auroral plasma (see also Buti, 1980), and are more easily amplified than the positive polarity soliton (Lotko, 1982; Lotko and Kennel, 1982).

Despite the similarity of the observed structures with those found in simulation, the physical environment is quite different. The most obvious difference is that, while computer runs are generally made by imposing carefully chosen boundary conditions, in the auroral zone the current is determined by macroscopic dynamics. The energy which is dissipated by particle acceleration in the double layers must be provided by a generator region, usually taken to be in the plasma sheet (Rostoker and Boström, 1976) or on the flanks of the magnetosphere (Sonnerup, 1980). Alfvén waves generated in this region carry current toward the ionosphere on time scales of about one minute, which is the Alfvén travel time along an auroral field (Lysak and Carlson, 1981). Thus, auroral zone currents can be considered constant on the time scales of double layer evolution ( $1000 \omega_{pe}^{-1} \sim 20$  msec for  $n = 10 \text{ cm}^{-3}$ ). The large perpendicular electric fields on auroral field lines (Mozer *et al.*, 1980) which are associated with ion beam and double layer regions (Mozer and Temerin, 1982) constitute a transmission line to carry the Alfvén wave energy from the generator to the double layer region.

When the plasma sheet acts as a current generator, it has been shown that intense, narrow-scale perpendicular electric fields can be formed (Lysak and Dum, 1982). In this situation, microscopic current-driven simulations in which an external circuit restores the current to its initial value (Sato and Okuda, 1981) are appropriate. On the other hand, when the outer magnetosphere acts as a voltage generator, the current level is determined by the microscopic dynamics (*i.e.*, the effective resistivity of the field line). In this case, simulations in which the current is given as an initial value and allowed to decay (*e.g.*, Sato and Okuda, 1980; Hudson and Potter, 1981) may be more realistic.

In addition to differences in boundary conditions, the plasma composition in computer simulations differs from that in the auroral zone. While computer simulations are generally initialized with single Maxwellian populations, the auroral zone is non-Maxwellian, even in the equilibrium state. The plasma in regions where double layers are observed arises basically from

two sources, the plasma sheet and ionosphere. While ionospheric populations are generally cold ( $< 10$  eV), the plasma sheet is quite hot (0.1-5 keV). The presence of multi-component ion and electron populations leads to the possibility of new nonlinear normal modes of the plasma. In particular, in addition to the usual positive polarity ion acoustic soliton, Lotko and Kennel (1981, 1982) have found a negative polarity ion acoustic mode which can exist when the cold electron density is less than a third of the cold ion density (see also Buti, 1980). This mode is distinct from the ion hole solution of Schamel and Bujarbarua (1980), in that it propagates near the ion acoustic speed rather than the ion thermal speed. It exhibits the usual property of ion acoustic solitons, that the velocity increases with increasing amplitude, as opposed to the ion hole which slows down. This property clearly identifies the negative polarity spikes in the simulations of Sato and Okuda (1981) and Kindel *et al.* (1981) as ion holes rather than rarefactive ion acoustic solitons.

It cannot yet be stated conclusively which mode is responsible for the solitary waves observed on satellites, since it is difficult to determine the propagation velocity experimentally. Thus, one must resort to theoretical arguments. The formation of ion hole modes on auroral field lines may be inhibited by scattering of ions by ion cyclotron waves. In unmagnetized two-dimensional simulations (DeGroot *et al.*, 1977; Kindel *et al.*, 1981), double layer formation is inhibited by scattering due to ion acoustic waves which can disrupt the ion hole. In the auroral zone, the ion beam can generate ion cyclotron noise, which can scatter the ions. On the other hand, the negative polarity ion acoustic soliton does not depend on trapping of ions for its existence (although it can be modified by trapping). Here, the only requirement is the presence of two electron populations with different temperatures and a small cold electron density. This mode can also be generalized to oblique propagation in a magnetized plasma (Witt, 1982), whereas no such generalization of ion hole modes is yet available.

The suppression of cold electron density on auroral field lines can be accomplished by a large scale upward pointing parallel electric field. Such a field can be present if plasma sheet ions and electrons have different pitch angle anisotropies (Chiu and Cornwall, 1980), or if turbulence is present on the auroral field line (Lysak and Dum, 1982; and references therein). In either case, the upward pointing field will reflect ionospheric electrons and accelerate the ionospheric ions into a field-aligned beam, setting up the conditions under which negative polarity modes and double

layers can form.

In conclusion, auroral double layers do exhibit many characteristics similar to those in current-driven simulations, but arise under conditions quite different from those in simulation systems. The presence of plasma sources in the ionosphere and plasma sheet with different temperatures allows for a negative polarity ion acoustic mode in addition to the ion hole mode observed in current-driven simulations. This mode may be more stable against the cross-field scattering of ions which can destroy ion hole formation, but it does require a suppression of cold electrons, which can be accomplished by a large-scale parallel electric field below the double layer region.

#### References

1. Buti, B., Ion-acoustic holes in a two-electron temperature plasma, Phys. Lett., 76A, 251, 1980.
2. Chiu, Y. T. and J. M. Cornwall, Electrostatic model of a quiet auroral arc, J. Geophys. Res., 85, 543, 1980.
3. DeGroot, J. S., C. Barnes, A. E. Walstead, and O. Buneman, Localized structures and anomalous dc resistivity, Phys. Rev. Lett., 38, 1283, 1977.
4. Hasegawa, A. and T. Sato, Existence of a negative potential solitary-wave structure and formation of a double layer, Phys. Fluids, 25, 632, 1982.
5. Hubbard, R. F. and G. Joyce, Simulation of auroral double layers, J. Geophys. Res., 84, 4297, 1979.
6. Hudson, M. K. and D. W. Potter, Electrostatic shocks in the auroral magnetosphere, in Physics of Auroral Arc Formation (edited by S.-I. Akasofu and J. R. Kan), AGU Monograph, 25, p. 260, 1981.
7. Hudson, M. K., W. Lotko, I. Roth, and E. Witt, Solitary waves and double layers on auroral field lines, submitted to J. Geophys. Res., 1982.
8. Kindel, J. M., C. Barnes, and D. W. Forslund, Anomalous dc resistivity and double layers in the auroral ionosphere, in Physics of Auroral Arc Formation (edited by S.-I. Akasofu and J. R. Kan), AGU Monograph, 25, p. 296, 1981.
9. Lotko, W., Reflection dissipation of an ion-acoustic soliton, submitted to Phys. Fluids, 1982.
10. Lotko, W. and C. F. Kennel, Stationary electrostatic solitary waves in the auroral plasma, in Physics of Auroral Arc Formation (edited by S.-I. Akasofu and J. R. Kan), AGU Monograph, 25, p. 437, 1981.

11. Lotko, W. and C. F. Kennel, Spiky ion acoustic waves in the collisionless auroral plasma, submitted to J. Geophys. Res., 1982.
12. Lysak, R. L. and C. W. Carlson, Effect of microscopic turbulence on magnetosphere-ionosphere coupling, Geophys. Res. Lett., 8, 269, 1981.
13. Lysak, R. L. and C. T. Dum, Dynamics of magnetosphere-ionosphere coupling including turbulent transport, submitted to J. Geophys. Res., 1982.
14. Mozer, F. S., C. A. Cattell, M. K. Hudson, R. L. Lysak, M. Temerin, and R. B. Torbert, Satellite measurements and theories of low altitude auroral particle acceleration, Space Sci. Rev., 27, 155, 1980.
15. Mozer, F. S. and M. Temerin, Solitary waves and double layers as the source of parallel electric fields in the auroral acceleration region, Proceedings of the Nobel Symposium, Kiruna, Sweden, 1982.
16. Quon, B. H. and A. Y. Wong, Formation of potential double layers in plasma, Phys. Rev. Lett., 37, 1393, 1976.
17. Rostoker, G. and R. Boström, A mechanism for driving the gross Birkeland current configuration for the auroral oval, J. Geophys. Res., 81, 235, 1976.
18. Sato, T. and H. Okuda, Ion acoustic double layers, Phys. Rev. Lett., 44, 740, 1980.
19. Sato, T. and H. Okuda, Numerical simulations on ion acoustic double layers, J. Geophys. Res., 86, 3357, 1981.
20. Schamel, H. and S. Bujarbarua, Solitary plasma hole via ion vortex distribution, Phys. Fluids, 23, 2498, 1980.
21. Sonnerup, B. U. Ö., Theory of the low-latitude boundary layer, J. Geophys. Res., 85, 2017, 1980.
22. Temerin, M., K. Cerny, W. Lotko, and F. S. Mozer, Observations of double layers and solitary waves on auroral zone field lines, Phys. Rev. Lett., 48, 1175, 1982.
23. Witt, E., A general formulation for exact nonlinear solitary and periodic ion acoustic waves in a magnetoplasma, submitted to J. Geophys. Res., 1982.

SPACE OBSERVATIONS RELEVANT TO LABORATORY DOUBLE LAYERS, SHOCKS  
AND SOLITONS — THE PLASMAPAUSE AND HIGH LATITUDE HOLES

H. Kikuchi

Nihon University, College of Science and Technology, Tokyo  
and Nagoya University, Institute of Plasma Physics, Nagoya, Japan

ABSTRACT

The problem of "Double Layers and Electrostatic Shocks" is of current interest to laboratory and space plasma physicists. First of all, general properties of double layers are outlined, based upon a fluid model related to the classic but basic Langmuir and Bohm conditions and laboratory experiments recently performed. Moving on to a main topic of double layers in space, two examples of rather stable, stationary double layers in space are presented, namely the plasmopause and high-latitude plasma holes. The plasmopause is thought to be an ion-acoustic type of stationary double layer which is steepened during the main phase of a storm. In the recovery phase, it tends to possess a distinct oscillating structure just inside the plasmopause, the so-called plasmopause-associated irregularities or ducts that have been observed by the OGO satellite. With further increasing dispersion and/or decreasing dissipation, the first waves of this structure tend to convert to solitons but with oscillating tail. In this case, the leading solitons may form the double or multiple plasmopause which has been observed occasionally during the post-storm recovery or on the dusk side. Another example of stationary double layers in space would be high latitude holes that were originally found by the OGO-6 satellite. The locations of the  $> 30$  keV electron trapping boundary and precipitation, the electric field and convective flow reversals and the polar cap boundary all fall into the HLH region which is also well correlated with ELF and VLF activity, exhibiting enhancements in broad-band emissions. In particular, the *d-c* electric field reversal in the HLH region forms paired stationary double layers or electrostatic shocks. When instabilities develop by enhancements in field-aligned currents or ion beams, the HLH tends to create small-scale, time-dependent double layers that are thought to be the electrostatic shocks observed from the S3-3 satellite. Lastly, going back to basic problems of double layers, summarized are a number of still controversial questions and indicated are some problems to be solved in the future from the laboratory side.

Summary of Panel Discussion at the "Symposium on Double Layers"  
at Risø National Laboratory, Roskilde, Denmark

The Symposium has demonstrated the great progress in our understanding of Double Layers (DL) made during the last few years but also the problems that still remain to be solved.

Theoretical progress has come largely through application of soliton theory and through use of numerical simulations which have inspired and checked new theoretical ideas.

Experimentally, new advanced techniques have been developed. It is now possible to study the dynamics of DL-formation by measuring potential profiles and velocity distributions with a hundred microsecond intervals, as explained in the talks by Sato, Stenzel and others. DL:s in new geometries, especially in magnetic fields with mirrors or local inhomogeneities have been investigated.

Observationally, the recent results from the S3-3 satellite in polar orbit have for the first time established the existence of DL:s on auroral geomagnetic field lines. As shown in the poster paper by Lysak et al. there is not one single big DL above the aurora but a series, perhaps hundreds, of weak layers with a large total potential drop in agreement with ideas published ten years ago.

The panel discussion focussed on still remaining problems. Dr Torvén discussed pre-sheaths, i.e. transitions between the DL and adjoining plasmas. Dr Birdsall discussed the possible existence of a critical length for the pre-sheaths or for formation of a DL. Both simulations and experiments indicate thresholds for instabilities (at virtual cathodes and anodes enclosing the DL) associated with a normalizing length related to the plasma frequency and beam velocity. Dr Schamel suggested that the electron transit time through a pre-sheath may be of the same order as the ion transit time through the DL.

The problem of DL formation was also discussed. According to Dr Schamel it appears that even during strongly time-dependent trapping processes there is a tendency to approach steady state structures containing phase-space holes. That might imply that the formation process can be described in terms of a succession

of nearly steady state solutions.

Experiments and observations in space indicate that the formation of a DL begins with the growth of a soliton which later, supposedly through some dissipation mechanism, develop into the DL. This was discussed by Dr Lysak. Dr Schamel classifies the DL according to the existence or non-existence of positive or negative potential humps at the corresponding sides of the DL. In space there seem to be negative humps associated with DL:s grown out of negative solitons. What physics determines which kind of DL will be formed?

The DL stability presents a very difficult problem. No energy principle known today is applicable and a normal mode analysis gives a nonlocal eigenvalue problem involving integration along curved particle orbits (Schamel).

Other difficult problems posed and to some extent commented on during the panel discussion were:

- a) What is the role of the boundary conditions in numerical simulations?
- b) How can inhomogeneities, e.g. in the magnetic field, influence the formation and stabilization of DL:s? Particles trapped between the DL and a magnetic mirror do seem to play a role, e.g. above the aurora.
- c) The external circuit is clearly of importance. No good quantitative analysis exists today. This problem is particularly difficult for DL:s occupying only a small fraction of an extended plasma.
- d) What is the role of ionization for stabilization of the plasmas on each side of the DL? Experiments indicate that some supply of fresh plasma is necessary although the ionization length can be much larger than the DL thickness. In space above the aurora, where virtually no ionization occurs, fresh plasma can be supplied by  $\underline{E} \times \underline{B}$  -drift from outer space.

Thanks are due to all those who contributed to the discussions, in particular the panel members, Drs C.K. Birdsall, R.L. Lysak, H. Schamel and S. Torvén.

Lars Block

## AUTHOR INDEX

	Page		Page
Alexandroaie, D.	237	Mohan, M.	55
Armstrong, R.J.	47, 159	Mravlag, E.	205
Birdsall, C.K.	84	Nakamura, Y.	153
Block, L.P.	280	Nambu M.	77
Borovsky, J.E.	249	Nishihara, K.	41
Bujarbarua, S.	40, 77	Pécseli, H.L.	47, 147
Callebaut, D.K.	96	Popa, G.	205, 213
Carlqvist, P.	71, 255	Raadu, M.A.	60, 65
Chan, C.	170	Rasmussen, J.J.	147, 199
Fujita, H.	193, 209	Saeki, K.	199
Gekelman, W.	181	Sakagami, H.	41
Hasegawa, A.	41	Sanduloviciu, M.	205, 231, 237, 243
Hatakeyama, R.	141, 199, 219	Sato, N.	116, 141, 199, 209, 219
Hershkowitz, N.	170	Schamel, H.	13, 40
Hollenstein, C.	187	Schrittwieser, R.	141, 199
Hudson, M.	274	Sekar, A.N.	55
Iizuka, S.	199	Silevitch, M.B.	60
Jovanović, D.	90, 147	Skøelv, Å	159
Joyce, G.	249	Stenzel, R.L.	153, 181
Kanazawa, T.	141	Suzuki, Y.	219
Kaw, P.K.	55	Takeda, Y.	225
Kawai, Y.	209	Talaskan, S.	243
Kikuchi, H.	279	Taniuti, T.	41
Lafon, J.-P.J.	107, 113	Thomsen, K.	147
Laframboise, J.G.	78	Torvén, S.	59
Lindberg, L.	164	Trulsen, J.	47, 159
Lonngren, K.E.	170	Wild, N.	181
Lotko, W.	274	Witt, E.	274
Lynov, J.P.	147	Yagura, S.	193, 209
Lysak, R.	274	Yamada, E.	193, 209
Michelsen, P.	147, 199	Yamagiwa, K.	225

## LIST OF PARTICIPANTS

H. Amemiya  
 Inst. of Physical and  
 Chemical Research  
 2-1 Hirosawa  
 Wakoshi, Saitama  
 Japan

I. Axnäs  
 Dept. of Plasma Physics  
 Royal Institute of Technology  
 S-10044 Stockholm  
 Sweden

P.J. Barret  
 Dept. of Physics  
 University of Natal  
 Durban, Natal 4001  
 South Africa

C.K. Birdsall  
 EEE Dept.  
 University of California  
 Berkeley, CA 94720  
 U. S. A.

L.P. Block  
 Dept. of Plasma Physics  
 Royal Institute of Technology  
 S-10044 Stockholm  
 Sweden

J.E. Borovsky  
 Los Alamos National Laboratory  
 Los Alamos  
 New Mexico 87545  
 U. S. A.

N. Brenning  
 Dept. of Plasma Physics  
 Royal Institute of Technology  
 S-10044 Stockholm  
 Sweden

S. Bujarbarua  
 Phys. Dept.  
 Dibrugarh University  
 Dibrugarh 786004 Assam  
 India

D. Callebaut  
 Phys. Dept. U.I.A.  
 University of Antwerp  
 B-2610 Antwerp  
 Belgium

P. Carlqvist  
 Department of Plasma Physics  
 Royal Institute of Technology  
 S-10044 Stockholm  
 Sweden

C.T. Chang  
 Physics Department  
 Risø National Laboratory  
 DK-4000 Roskilde  
 Denmark

T. Chang  
 Center for Space Research  
 and Physics Dept.  
 MIT  
 Cambridge, MA 02139  
 U. S. A.

G. Chanteur  
 CNET/DRPE  
 38-40 Rue de Général Leclerc  
 F-92131 Issy Les Moulineaux  
 France

N. D'Angelo  
 Danish Space Research Institute  
 Lundtoftevej 7  
 DK-2800 Lyngby  
 Denmark

K.B. Dysthe  
 University of Tromsø  
 I.M.R.  
 Postboks 953  
 N-9001 Tromsø  
 Norway

C. Hollenstein  
 CRPP  
 Ecole Polytechnique Fédéral  
 21, Avenue des Bains  
 CH-1007 Lausanne  
 Switzerland

T. Honzawa  
 Dept. of Elec. Engineering  
 Utsunomiya University  
 Ishii-machi 2753  
 Utsunomiya 321  
 Japan

P. Høeg  
 Danish Space Research Inst.  
 Lundtoftevej 7  
 DK-2800 Lyngby  
 Denmark

I.B. Iversen  
 Danish Space Research Inst.  
 Lundtoftevej 7  
 DK-2800 Lyngby  
 Denmark

V.O. Jensen  
 Physics Dept.  
 Risø National Laboratory  
 DK-4000 Roskilde  
 Denmark

D. Jovanović  
 Institute of Physics  
 P.O. Box 57  
 YU-11000 Beograd  
 Yugoslavia

J.-P. J. Lafon  
 Observatoire de Paris-Meudon  
 F-92190 Meudon  
 France

J.G. Laframboise  
 Physics Dept.  
 York University  
 Toronto  
 Canada M 33 1P3

L. Lindberg  
 Dept. of Plasma Physics  
 Royal Inst. of Technology  
 S-10044 Stockholm  
 Sweden

K. Lonngren  
 Dept. of Engineering  
 The University of Iowa  
 Iowa City, Iowa 52242  
 U .S. A.

J.P. Lynov  
 Physics Dept.  
 Risø National Laboratory  
 DK-4000 Roskilde  
 Denmark

R. Lysak  
 Space Sciences Laboratory  
 University of California  
 Berkeley, CA 94720  
 U. S. A.

P. Michelsen  
 Physics Dept.  
 Risø National Laboratory  
 DK-4000 Roskilde  
 Denmark

K. Mima  
 Inst. of Laser Engineering  
 Osaka University  
 2-1 Yamadagaoka, Suita  
 Osaka 565  
 Japan

T. Neubert  
 Danish Space Research Inst.  
 Lundtoftevej 7  
 DK-2800 Lyngby  
 Denmark

H.L. Pécseli  
 Physics Dept.  
 Risø National laboratory  
 DK-4000 Roskilde  
 Denmark

F. Primdahl  
 Danish Space Research Inst.  
 Lundtoftevej 7  
 DK-2800 Lyngby  
 Denmark

M. Raadu  
 Dept. of Plasma Physics  
 Royal Inst. of Technology  
 S-10044 Stockholm  
 Sweden

J.J. Rasmussen  
 Physics Dept.  
 Risø National Laboratory  
 DK-4000 Roskilde  
 Denmark

C.W. Roberson  
Naval Research Laboratory  
Washington, D.C. 20375  
U. S. A.

K. Rypdal  
University of Tromsø  
I.M.R.  
Postboks 853  
N-9001 Tromsø  
Norway

N. Sato  
Dept. of Elect. Engineering  
Tohoku University  
Sendai 980  
Japan

H. Schamel  
Inst. for Theoretical Physics  
Ruhr University Bochum  
D-4630 Bochum 1  
FRG.

R. Schrittwieser  
Inst. for Theoretical Physics  
University of Innsbruck  
A-6020 Innsbruck  
Austria

M.B. Silevitch  
Dept. of Elect. Engineering  
North Eastern University  
Boston, MA 02115  
U. S. A.

Å. Skøelv  
University of Tromsø  
Postboks 953  
N-9001 Tromsø  
Norway

R.A. Smith  
Plasma Physics Division  
Science Applications, Inc.  
1710 Goodridge Drive, McLean  
Virginia 22102  
U. S. A.

L. Song  
Royal Inst. of Technology  
Dept. of Plasma Physics  
S-10044 Stockholm  
Sweden

Y. Sonoda  
Dept. of Energy Conversion  
Graduate School of Sciences  
Kyushu University  
Fukuoka 812  
Japan

F. Spangslev  
Danish Space Research Inst.  
Lundtoftevej 7  
DK-2800 Lyngby  
Denmark

R. Stenzel  
Dept. of Physics  
University of California  
Los Angeles, CA 90024  
U. S. A.

H. Sugai  
Dept. of Elect. Engineering  
Nagoya University  
Nagoya  
Japan

M. Weenink  
Group on Plasma Physics  
Eindhoven University of Techn.  
P.O.B. 513  
N-5600 MB Eindhoven  
The Netherlands

Y. Takeda  
Dept. of Physics  
College of Science and Techn.  
Nihon University  
Kanda, Surugadai  
Chiyoda-Ku, Tokyo 101  
Japan

S. Yagura  
Dept. of Eletr. Engineering  
Faculty of Science and Eng.  
Saga University  
Honjo-machi 1  
Saga 840  
Japan

K. Thomsen  
Physics Dept.  
Risø National Laboratory  
DK-4000 Roskilde  
Denmark

S. Torvén  
Dept. of Plasma Physics  
Royal Inst. of Technology  
S-10044 Stockholm  
Sweden

I. Tsukabayashi  
Nippon Inst. of Technology  
Miyashiro-cho  
Saitama-ken  
Japan

R.K. Varma  
Physical Research Laboratory  
Navrangpura  
Ahmedabad 380009  
India

**Sales distributors:**

**Jul. Gjellerup, Sølvgade 87,  
DK-1307 Copenhagen K, Denmark**

**Available on exchange from:**

**Risø Library, Risø National Laboratory,  
P. O. Box 49, DK-4000 Roskilde, Denmark**

**ISBN 87-550-0862-3  
ISSN 0106-2840**